
Doctoral Dissertations

Student Theses and Dissertations

Spring 2011

A geological and geophysical study of the Tendaho Graben in the Afar Depression, Ethiopia: insights into transitional continental rifting

David Lee Bridges

Follow this and additional works at: https://scholarsmine.mst.edu/doctoral_dissertations



Part of the [Geology Commons](#), and the [Geophysics and Seismology Commons](#)

Department: Geosciences and Geological and Petroleum Engineering

Recommended Citation

Bridges, David Lee, "A geological and geophysical study of the Tendaho Graben in the Afar Depression, Ethiopia: insights into transitional continental rifting" (2011). *Doctoral Dissertations*. 2020.
https://scholarsmine.mst.edu/doctoral_dissertations/2020

This thesis is brought to you by Scholars' Mine, a service of the Missouri S&T Library and Learning Resources. This work is protected by U. S. Copyright Law. Unauthorized use including reproduction for redistribution requires the permission of the copyright holder. For more information, please contact scholarsmine@mst.edu.

**A GEOLOGICAL AND GEOPHYSICAL STUDY OF THE TENDAHO GRABEN
IN THE AFAR DEPRESSION, ETHIOPIA: INSIGHTS INTO TRANSITIONAL
CONTINENTAL RIFTING**

by

DAVID LEE BRIDGES

A DISSERTATION

**Presented to the Faculty of the Graduate School of the
MISSOURI UNIVERSITY OF SCIENCE AND TECHNOLOGY**

In Partial Fulfillment of the Requirements for the Degree

DOCTOR OF PHILOSOPHY

In

GEOLOGY & GEOPHYSICS

2011

Approved by

Mohamed G. Abdelsalam, Co-advisor

Stephen S. Gao, Co-advisor

Fransica Oboh-Ikuenobe

Kelly H. Liu

Kevin Mickus

ABSTRACT

A detailed magnetic and gravity study across the Tendaho Graben (the Red Sea propagator within the Afar Depression, Ethiopia) revealed features that can best be interpreted as a continental rift undergoing oceanization. This NW-trending extensional structure is ~50 km wide and it is confined within well-developed NW-trending border faults that deform the 2 km thick and ~ 2 Ma basaltic flows of the Afar Stratoids. The age of the basaltic flows becomes progressively younger inward from the border faults until it reaches ~30,000 years close to the rift axis. The central part of the Tendaho Graben is characterized by a 10 km wide magnetic trough, the central part of which is dominated by a narrow zone (~3 km) of a relatively elevated magnetic anomaly that coincides with a linear region of hydrothermal activity. This magnetic geometry is similar in dimension and magnitude to that observed from magnetic stripes of typical mid-ocean ridges.

Forward modeling of the magnetic data (combined with geochronological data) shows that the basaltic rocks within the magnetic trough were crystallized after 0.78 Ma under normal magnetic polarity. The width of the magnetic trough (10 km) and the age of basaltic rocks (<0.78 Ma) indicate a spreading rate of ~ 0.64 cm/year. However, to achieve the ~50 km width of the Tendaho Graben which started opening ~2.0 Ma, a 1.64 cm/year spreading rate is needed between 1.6 and 0.78 Ma. This suggests that the spreading rate with Tendaho Graben is slowing down and extension within Afar is accommodated somewhere else. A new model is proposed for the evolution of the Tendaho Graben based on fieldwork, the newly acquired magnetic data and geochronology.

ACKNOWLEDGMENTS

I would like to extend a great gratitude to my co-advisors, Drs. Mohamed G. Abdelsalam and Stephen S. Gao, for their never ending patience and direction in developing my research abilities. Dr. Mohamed G. Abdelsalam has been a source of inspiration and encouragement for me. Dr. Stephan S. Gao has been guiding my graduate studies since my M.Sc. at Kansas State University and has provided me with unending help and advice since then. I will never forget the lively conversations with Dr. Kevin Mickus and his large contribution of potential field knowledge to my project. I would also like to thank the rest of my advisory committee, Drs. Fransica Oboh-Ikuenobe and Kelly H. Liu for their input, advice and patience in my research.

I would also like to thank Dr. John P. Hogan for his wonderful advice and encouragement while at Missouri S&T. I would like to thank the Department of Geology and Geophysics for hosting my studies and for the Ratcliff funding for my teaching assistantship appointments. I would also like to thank Statoil ASA for funding my fieldwork and my research assistantships. I would also like to thank H. Carrie Bender for our endless discussions and rants from Afar, Ethiopia to Rolla. Finally, I would like to thank my two sons, David and Justin, and my parents for being with me all these years as I pursued my academic ambitions and providing their never ending support.

TABLE OF CONTENTS

	Page
ABSTRACT	iii
ACKNOWLEDGEMENTS	iv
LIST OF ILLUSTRATIONS	viii
LIST OF TABLES	xi
 SECTION	
1. INTRODUCTION	1
1.1. OVERVIEW	1
1.2. PUBLICATION STATUS	1
2. GEOLOGY OF THE AFAR DEPRESSION	3
2.1. GEOLOGY	3
2.2. POTENTIAL FIELD WORK	7
2.3. TECTONICS	11
2.3.1. The Danakil Block	11
2.3.2. The Ali-Sabieh Block	13
2.3.3. The East-Central Block	13
2.3.4. The Manda Hararo-Gobaad Rift	14
2.3.5. The Asal-Manda Inakir Rift	15
2.3.6. The Sabure-Hertale-Adado Rift	15
3. TENDAHO GRABEN	17
3.1. PREVIOUS WORK	17
3.2. GEOLOGY	17
3.3. PETROLOGY AND GEOCHEMISTRY	21

3.4. GEOPHYSICAL WORK	23
3.5. SERDO EARTHQUAKE SEQUENCE OF 1969	26
3.6. DABBAHU RIFTING EPISODE OF 2005	31
4. METHODOLOGY	37
4.1. MAGNETIC DATA ACQUISTION	37
4.2. DATA REDUCTION	43
4.3. MAGNETIC INTERPRETATION	46
4.4. ANOMALY ENHANCMENT	47
4.4.1. Reduction to Pole	49
4.4.2. Analytic Signals and Total Derivative	53
4.5. FORWARD MODELING	56
4.6. EFFECT OF MAGNETIC REMENANCE ON MODELING	62
4.7. GRAVITY SURVEY	70
5. RESULTS	72
5.1. PROFILES	72
5.2. 2D DATA	74
5.3. ANOMALY ENHANCEMENT	76
5.4 FORWARD MODELING	82
5.5 GRAVITY SURVEY	88
6. DISCUSSION	90
6.1 LINEAR MAGNETIC BODIES	90
6.2 MAGNETIC STRIPES	95
6.3 REVISED EVOLUTION OF THE TENDAHO GRABEN	97

7. CONCLUDING REMARKS	102
7.1. CONCLUSIONS	102
7.2. FUTURE WORK	103
APPENDIX	104
BIBLIOGRAPHY	194
VITA	208

LIST OF ILLUSTRATIONS

Figure	Page
2.1. Regional plate kinematics of the Afar Depression.	4
2.2. Bouguer gravity anomalies of the Afar Depression (Mickus et al., 2007).	8
2.3. Project MAGNET flight paths and profiles (Girdler 1970).	9
2.4. Topographic relief map of the Afar Depression with important structures.	12
3.1. General geology of the Tendaho Graben.	18
3.2. Tendaho geochemistry data.	22
3.3. Station locations (red dots) of the Aquater magnetic and gravity field study within the TG.	24
3.4. Serdo tectonic map overview (Gouin 1979).	27
3.5. Surface geology of the Serdo area after the 1969 earthquake (Gouin 1979).	29
3.6. Overview of Dabbahu section of the Manda Harraro Rift (Ebinger et al., 2008).	32
3.7. Seismicity associated with the Dabbahu rifting events from 2005 to 2009 (Ebinger et al., 2010).	36
4.1. Workflow for the acquisition and reduction of the magnetic data.	38
4.2. Magnetometers used in collecting the magnetic data.	39
4.3. Cartoon showing how proton precession magnetometers work (Reynolds, 1997).	40
4.4. Simplified schematic of a cesium optically-pumped magnetometer (Reynolds, 1997).	41
4.5. The location of the magnetic data (red lines) collected in 2008.	42
4.6. The location of the magnetic data (blue lines) collected in 2009/10.	43

4.7. Diurnal variation over 9 days during the 2008 field season in Afar.	44
4.8. The IGRF magnetic field 2005 Epoch.	45
4.9. Magnetic interpretation workflow used in this study.	47
4.10. The effects of RM on a simple polyhedron.	63
5.1. High density magnetic profiles across the Tendaho Graben.	72
5.2. The main and south high density magnetic profiles (red and blue, respectively) plotted with magnetic profiles from the Aquater data (orange and green).	73
5.3. SRTM map of the Tendaho Graben with the magnetic profile lines plotted in corresponding colors to those of Figure 5.2.	73
5.4. Total-field magnetic anomaly map of the Ayrobera geothermal field.	74
5.5. Ayrobeara geothermal field gravity stations marked by red triangles.	75
5.6. Bouguer gravity anomaly profile W-E across the Ayrobeara geothermal field.	76
5.7. Reduction-to-pole of the main magnetic profile.	77
5.8. Analytic signals of the main magnetic profile.	78
5.9. Total derivative or amplitude of the analytic signal of the main magnetic profile.	79
5.10. Total-field magnetic anomaly map of the study area that will be used to demonstrate subsequent anomaly transformations.	80
5.11. Reduction-to-pole of Aquater data.	81
5.12. Directional derivative of Aquater data.	81
5.13. Total derivative of Aquater data.	82
5.14. Main profile forward model across the Tendaho Graben.	84
5.15. Simple block model that illustrates the significant role of magnetic polarity across the Tendaho Graben.	85
5.16. North forward modeled profile (Orange line on Figure 5.3).	86

5.17. South forward modeled profile (Blue line on Figure 5.3).	87
5.18. Gravity stations (red triangles) collected during the winter 2008 field campaign.	88
5.19. Profile of Bouguer gravity anomalies across the Tendaho Graben.	89
5.20. Forward model of the Bouguer gravity anomaly profile across the Tendaho Graben roughly coincident with the high resolution magnetic profile.	89
6.1. Comparison of the Tendaho Graben, Sheba oceanic spreading center and Manda Inakir Rift (Gulf of Aden propagator) magnetic profiles.	90
6.2. Observed and modeled gravity and magnetic profiles scaled together for easy comparison.	92
6.3. Geothermal sublimation features and fossil fumaroles in the Ayrobeara geothermal field.	93
6.4. Two-dimensional gravity forward model across the Tendaho Graben roughly coincident with the high density magnetic profile.	94
6.5. Magnetic lineations of Afar and their relative ages (Barberi and Varet, 1977).	96
6.6. Geochronologic data as a function of distance from the rift axis.	97
6.7. Proposed Evolution of the Tendaho Graben.	99

LIST OF TABLES

Table	Page
5.1. Final susceptibilities, remnant magnetization intensities, declinations and inclinations used for the Tendaho Graben forward model.	84

1. INTRODUCTION

1.1. OVERVIEW

The Afar Depression in Ethiopia is unique in that all stages of continental rifting transitioning to sea-floor spreading are observable on land. This work focuses on the Tendaho Graben, which hosts the termination of the Red Sea propagator. A dense magnetic survey was completed to study the crustal structure of the Tendaho Graben (TG). Linear magnetic bodies that follow the central axis of the Tendaho Graben were found. A detailed gravity survey across the TG provides supporting evidence that significant high-density mafic bodies have been emplaced along the central axis of the graben. Geochronologic research from other workers found younging volcanics toward the center of the graben. The magnetic profiles, supported with a complementary gravity profile, suggests that concentrated dike emplacement has occurred in the middle of the graben analogous to the type that may be responsible for seafloor spreading.

This work provides insights into the nature of tectonic extension across transitional continental rifts. The TG records a change from mechanically maintained extension to magma maintained extension. The upper crustal structure of TG is studied. A revised structural evolution of the TG from initiation ~2.0 Ma to present is proposed.

1.2. PUBLICATION STATUS

Deliverables for this work includes a paper submitted to the journal *Nature* titled “Magnetic stripes of a transitional continental rift in Afar”, another paper to be submitted to *Journal of Geophysical Research* titled, “A geological and geophysical study of the Tendaho Graben, Ethiopia, Afar: Insights into transitional continental rifting” and a third

manuscript yet to be prepared on a comparison of extensional styles of the Tendaho and Dobi Grabens as part of a post-doctoral study. It is anticipated that more publications will follow as part of the post-doctoral work.

2. GEOLOGY OF THE AFAR DEPRESSION

2.1. GEOLOGY

The Afar Depression is a triangular shaped depression that covers ~200,000 km² (Beyene and Abdelsalam, 2005). It is situated between the Nubian, Arabian and Somali tectonic plates (Figure 2.1). It is bounded to the west by the Ethiopian Plateau to the west, the Danakil Alps (Danakil Block) to the northeast and the Somalia Plateau to the southeast. The Ali-Sabieh Block lies to the east separating Afar from the Gulf of Aden. The depression itself is punctuated by deep grabens, shield volcanoes and axial volcanism. The western margin is a N-S escarpment exceeding 2000 m relief in places. From the ridgeline of the Ethiopian Escarpment to the Afar lowland, elevation drops from 3000-2500 m to 800–100 m (Mohr, 1983b). Marginal basins of 5 km wide and up to 30 km long can be found along the escarpment (Beyene and Abdelsalam, 2005). The Somali Escarpment drops down in a similar fashion with the marginal blocks tilted inward towards the depression. The Danakil Block to the northeast has topography that reaches as high as ~2130 m above sea level (Beyene and Abdelsalam, 2005). The Ali-Sabieh block is a subtle northward extension of the Somalia Plateau.

Sedimentary lowland plains characterize the central part of the depression. The Danakil Depression, in northern Afar, is the lowest basin some 120 m below sea level. The central part of Afar is flanked by the Tendaho Graben to the west and the Danakil Block to the east. This region is characterized by deep grabens (Beyene and Abdelsalam, 2005). The southwestern part of Afar hosts the continuation of the Main Ethiopian Rift until it joins the Tendaho Graben at the Tendaho-Gobaad Discontinuity.

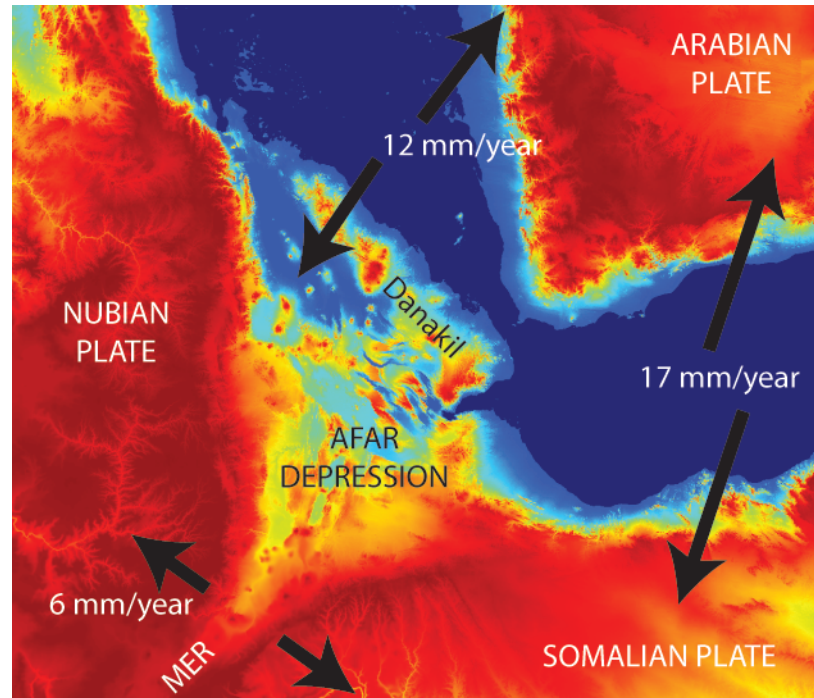


Figure 2.1. Regional plate kinematics of the Afar Depression. Black arrows show movement direction of plates. MER stands for Main Ethiopian Rift. Kinematic data are from Chu and Gordon (1998).

The geological units of the Afar can be divided into four main groups (Varet, 1978): 1) Neoproterozoic crystalline rocks, Mesozoic sedimentary rocks and Eocene-Miocene basement rocks; 2) Miocene igneous rocks; 3) Pliocene volcanic rocks; and 4) Quaternary volcanic and sedimentary rocks. The Arabian-Nubian Shield covers a large area in the region. The Neoproterozoic crystalline rocks represent part of the Arabian-Nubian shield (Abdelsalam and Stern, 1996) and occupy the periphery of the depression. These rocks are overlain by the Mesozoic sedimentary rocks which primarily consist of Jurassic age sandstone and limestone and Cretaceous sandstone (Beyene and Abdelsalam, 2005). It is important to note that none of the Neoproterozoic rocks are found within the Afar Depression, suggesting that they either do not exist there or they are covered by

Pliocene and Quaternary volcanics and sediments (Beyene and Abdelsalam, 2005). Eocene-Miocene flood basalts cover the Mesozoic sedimentary rocks on both the Ethiopian and Somali Plateaus. A few exposures of ~ 25 - 15 Ma flood basalts can be found within the depression in the Gulf of Tadjura and on the Ali-Sabieh Block (Beyene and Abdelsalam, 2005).

Some Alkaline and per-alkaline granites can be found in direct contact with the Neoproterozoic crystalline rocks, Jurassic sandstones and older Trap Series basalts (Varet, 1978). Younger Miocene igneous rocks within the Afar Depression include the Mabla and Dalha Series. The Mabla series consist mainly of rhyolites and ignimbrites erupted along N-S vents (Varet, 1978; Vellutini, 1990). The Dalha Series is a basaltic sequence up to ~ 800 m in thickness and locally interbedded with rare detrital sedimentary rocks and ignimbrites (Varet, 1978). The Pliocene-Pleistocene Stratoid series covers most of the Afar Depression. It records much of the recent tectonic activities in the depression. It covers 2/3 of the depression and reaches a thicknesses of up to 1500m (Barberi et al., 1974; Varet, 1978). The recent Quaternary volcanics mainly follow the axial valleys of the active spreading centers. These are dominantly large shield volcanoes and fissure basalts, from axial centers, along with a subordinate amount of rhyolitic pyroclastic material (Tefera et al., 1996). Lacustrine deposits are the dominant sedimentary rocks (Beyene and Abdelsalam, 2005). The major episodes of active volcanism can be summarized following Vellutini (1990) into: 1) Trap Series basalts > 25 Ma, 2) two phases of significant rhyolitic volcanism between 25 - 19 Ma and 14 - 9.5 Ma, 3) thick basaltic flows erupted between 9 - 1 Ma and 4) recent fissure basalt flows in elongated linear bodies < 1 Ma.

The idea of a mantle plume for the origin of the voluminous outpouring of continental flood basalts (~30 Ma) has been well examined. The evolution of Sr, Nd, and Pb isotopes from an ancient heterogeneous source to a HIMU (high μ) mantle component, supports the plume hypothesis (Vidal et al., 1991). The highest HIMU signatures ($^{87}\text{Sr}/^{86}\text{Sr} \sim 0.7035$, $^{206}\text{Pb}/^{204}\text{Pb} \sim 19.2$) are found in the young lavas of the Gulf of Aden propagator (Deniel et al., 1994). Deniel et al. (1994) proposed a model of a mantle diapir (Afar Mantle Plume) thermally eroding the subcontinental lithosphere. As extension increased, a greater component of HIMU is recorded with depleted mantle being detected in the most recent volcanics < 4 Ma. The Ethiopian Plateau flood basalts have been extensively studied (e.g. Pik et al., 1998; 1999; 2006). Pik et al. (2006) used $^3\text{He}/^4\text{He}$ signatures combined with Sr - Nd - Pb isotopic tracers in Miocene to Plio-Quaternary alkaline lavas in East Africa to suggest that two different plumes have affected the region since ~ 30 Ma. They proposed a deep-seated plume, perhaps at the core-mantle boundary, to be responsible for the ~30 Ma flood basalts characterized by a high ^3He signature and a shallow mantle upwelling distinct from the main Afar plume. The shallow upwelling is localized within the African Plate under the uplifted and rifted swells.

The nature of the lithosphere beneath the Afar Depression is debatable as it exhibits both continental and oceanic affinities. Models vary from typical oceanic crust (McKenzie et al., 1970) to an intermediate crust composed of stretched continental crust compensated by magmatic activity (Cochran, 1981; Kazmin and Byakov, 2000). Berckhemer (1975), using refraction seismology, suggested that the crustal thickness decreases from 38 km to 16 km from the Ethiopian Plateau to Djibouti. He also

interpreted an oceanic crust beneath Djibouti but a more transitional crust for the rest of Afar based on a V_p velocity of 6.6 - 6.8 km/s for the crust. The transitional nature of the Afar crust was further supported by Makris and Ginzburg (1987) when they reevaluated older seismic refraction profiles and gravity data and concluded that the Afar crust was very thin transitional crust with low seismic velocities between those typically found for continental and oceanic crust. They estimated a thickness of 26 km in central Afar that gradually decreases towards the Red Sea to ~ 14 km. Joffe and Garfunkel (1987) determined an amount of extension (β) for the Afar Depression to be ~ 1.8 . Mohr (1989) compared the extension rate for Afar with that of the Red Sea and interpreted it to mean that the Afar crust must have a high density of dike injection ($\sim 65\%$) to maintain its calculated extension. Makris and Ginzburg (1987) assumed that the transitional crust was homogenous. Mohr (1989) argued the case that the diking could be highly concentrated (e.g. beneath the propagators) thereby having areas of 'neo-oceanic' and narrow (< 200 km) zones of continental lithosphere.

2.2. POTENTIAL FIELD WORK

The first systematic gravity investigation in the Afar Depression was undertaken by Makris et al. (1975) who compiled approximately 4,000 gravity stations in Ethiopia, Djibouti and Eritrea to produce a Bouguer gravity anomaly map. The gravimetric field is closely correlated with the morphological features of the Afar Depression (Figure 2.2). The highest mountain ranges had the smallest Bouguer gravity anomaly of ~ 260 mGal. The greatest Bouguer gravity anomaly (> 15 mGal) is associated with the Red Sea along

the northeast coast. Many gravity surveys have been conducted in the Main Ethiopian Rift such as Cornwall et al. (2006) and Mickus et al. (2007).

The first major magnetic survey in Afar was conducted by U.S. Project Magnet in 1966 (Girdler, 1970). The survey consisted of 8 profiles parallel to the southwestern Red Sea shore with an average spacing of 90 km and one profile perpendicular (Figure 2.3).

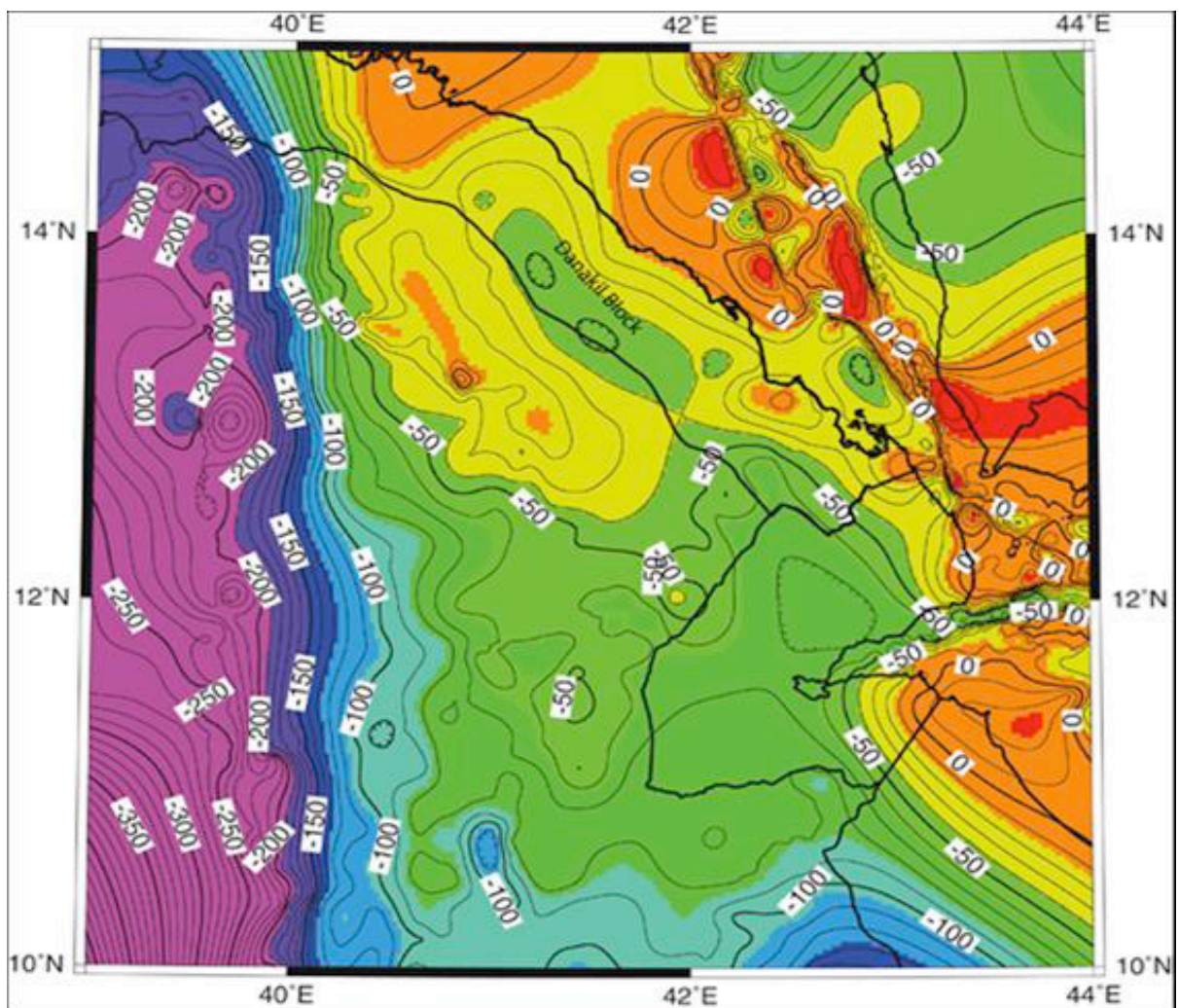


Figure 2.2. Bouguer gravity anomalies of the Afar Depression (Mickus et al., 2007). Contour interval is 10 mGal.

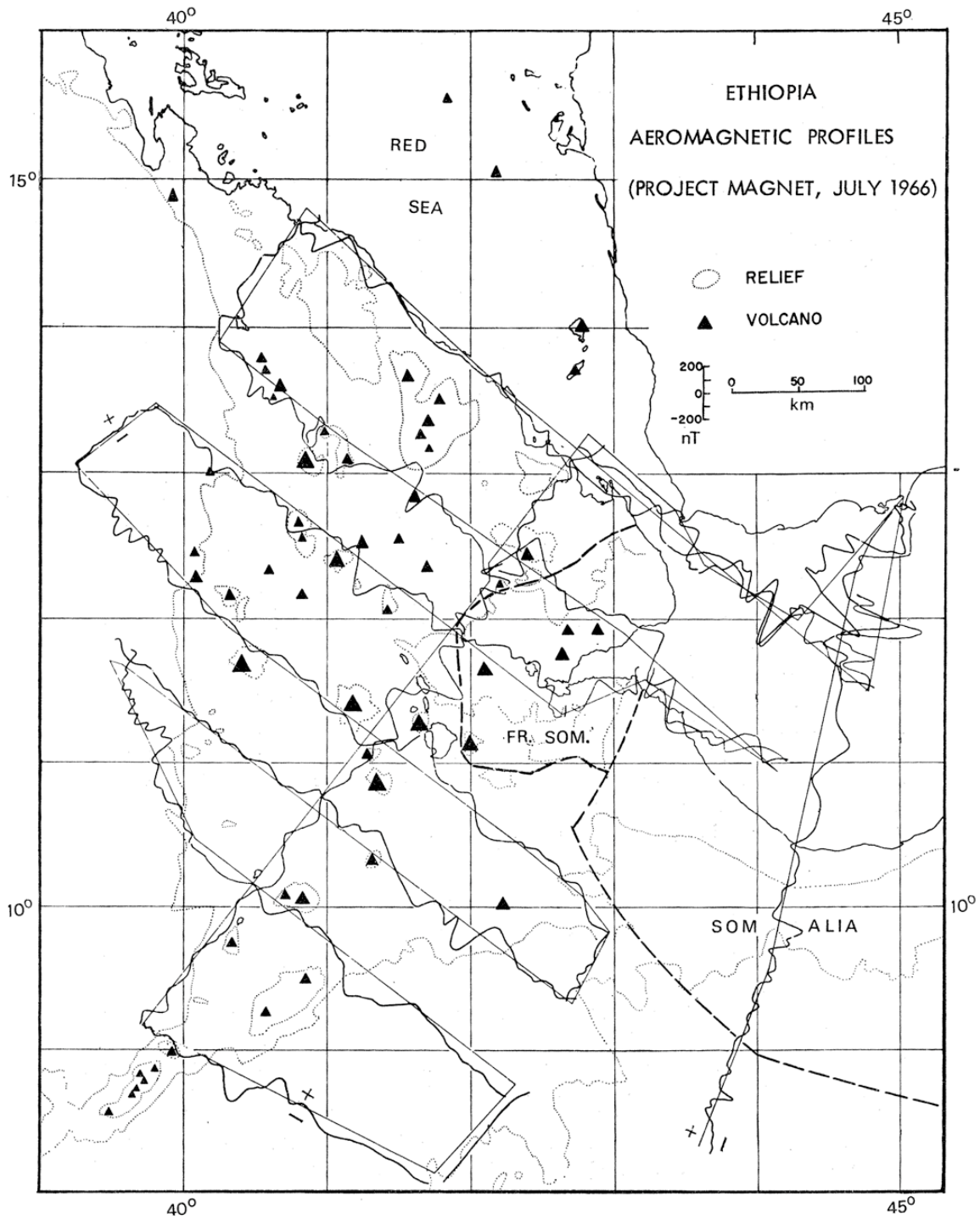


Figure 2.3. Project MAGNET flight paths and profiles (Girdler, 1970).

The flight height increased from the Red Sea towards inland. The survey revealed significant long wavelength anomalies over the depression that was similar to those over the Gulf of Aden.

Based on the intriguing results of Project Magnet, Girdler (1970) planned a robust survey with line spacing of 10 km. The survey height was 1.83 km. Fifteen tie lines were flown. Overall ground position accuracy ranged from 0.5 km to 1 km. Girdler (1970) collected a total track of 24,000 km between February and April 1968. A Gulf Mark III fluxgate magnetometer was utilized for the survey. Two total anomaly maps were prepared using 12.5°N as the dividing latitude with a contour interval of 50 nT and 1:500,000 scale. The total field values ranged from > 500 nT to < -1000 nT. Girdler (1970) remarked that the features south of 12.5°N are more impressive than the ones to the north and trended NW instead of following the NNW Red Sea trend. The ones in the south are trending to the west where they intersected the N-S trending Ethiopian escarpment. Girdler never published the total magnetic anomaly map. Courtillot et al. (1980) flew the next regional magnetic survey in February 1977. Although their survey was restricted to the Republic of Djibouti and the surrounding areas of Ethiopia, they used denser 5 km flight line spacing at a 200 m flight height. They acquired a total of 54 N-S oriented lines and 9 cross or tie lines spaced 25 km apart. A small part of the western Gulf of Aden was flown at 600 m also. A cesium optically pumped magnetometer was used along with two base stations at Arta and Assa Gueyla. A total magnetic anomaly map was subsequently prepared. The map shows high amplitude (500 – 1000 nT peak-to-peak) short wavelength (10- 20 km) anomalies and low amplitude (<200 nT) and longer wavelength (40 – 50 km) anomalies. The former corresponds to oceanic anomalies while

the latter ones are more typical of continental type anomalies. Courtillot et al. (1980) referred to the second kind as “quiet” zone as they lie between the Gulf of Aden and the oceanic type anomalies on land.

2.3. TECTONICS

The Afar Depression is part of the East African Rift system, which is part of Afro-Arabian Rift System. This system extends from southern Africa, through the East African Rift System, Afar Depression, Red Sea, Dead Sea, through the Jordan Valley and terminates in Syria. The Red Sea, Gulf of Aden and Main Ethiopian Rift form a so-called rift-rift-rift triple junction between the Arabian, Nubian and Somalian Plates (Beyene and Abdelsalam, 2005). The major tectonic elements associated with the Afar Depression include the Dankil, Ali-Sabieh and East Central Blocks; the Manda Hararo-Gobaad, Asal-Manda Inakir; and the Sabure-Hertale-Adado rifts (Figure 2.4). A detailed description of the above elements follows.

2.3.1. The Danakil Block. The Danakil Block is ~ 500 km long and ~ 100 km wide with a mean elevation of ~ 400 m (Chu and Gordon, 1998; Collet et al., 2000; Courtillot et al., 1984; Eagles et al., 2002; Le Pichon and Francheteau, 1978; Manighetti et al., 2001; Souriot and Brun, 1992; Vellutini, 1990). It has been considered a horst, micro-plate or block that host pre-rift geologic units (Beyene and Abdelsalam, 2005). Manighetti (2001) proposed a date of ~20 Ma when the Danakil Block broke away from the Ethiopian plateau in a anticlockwise rotation. Le Pichon and Francheteau (1978) obtained a 30° rotation. This rotation has been accommodated by the westward propagation of the Gulf of Aden spreading ridge expressed as the Asal-Manda Inakir rift.

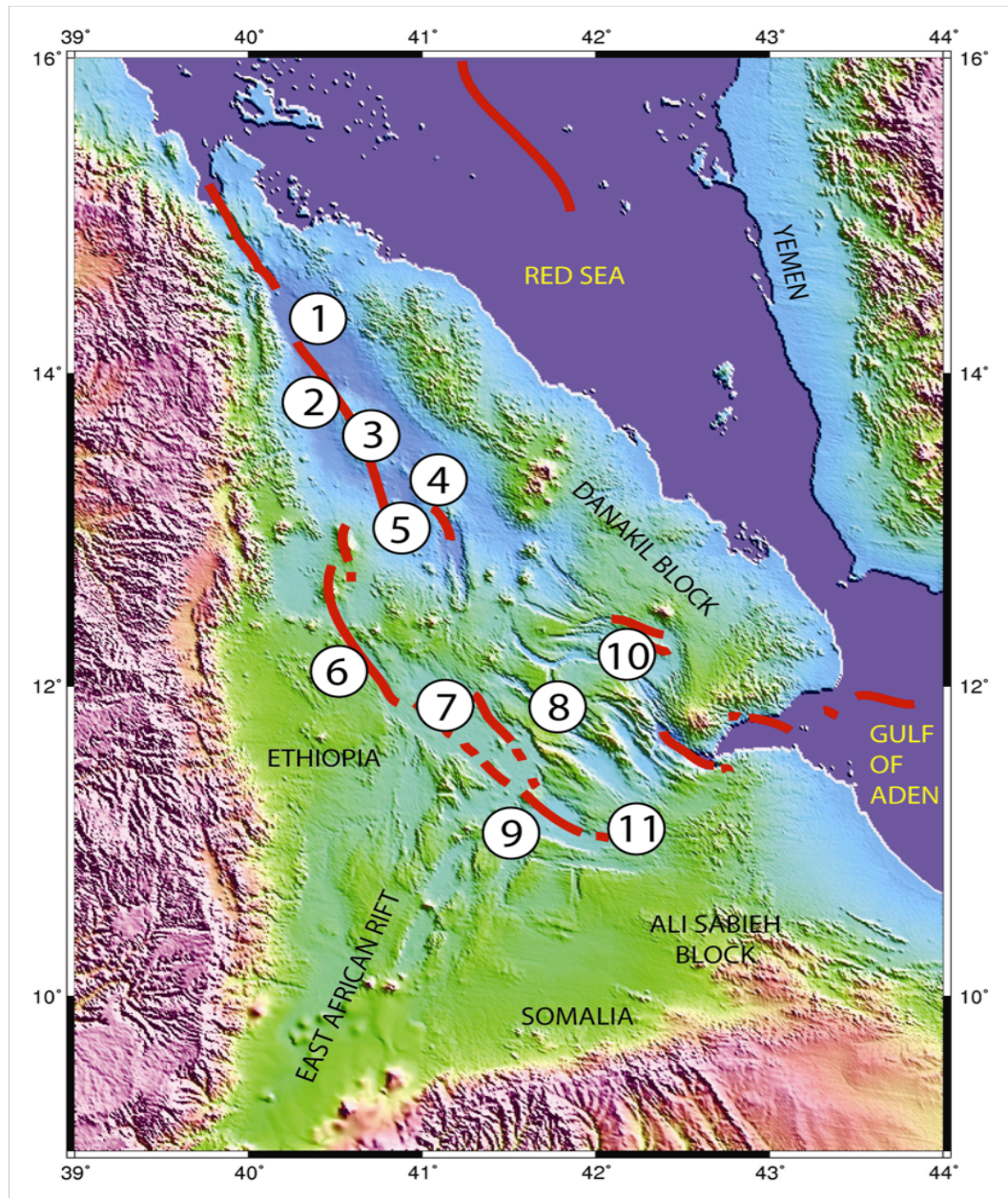


Figure 2.4. Topographic relief map of the Afar Depression with important structures. 1= Danakil Rift. 2= Red Sea Trend. 3=Erta Ale Volcano. 4=Alyata Volcano. 5=Tat Ale Volcano. 6= Manda Harraro - Gobaad Rift. 7= Awsa Plain. 8=Dobi Graben 9= Tendaho Gobaad Discontinuity. 10= Asal - Manda Inakir Rift. 11= Gulf of Aden Trend. After Beyene and Abdelsalam, 2005.

Sourotit and Brun (1992) proposed a 10° rotation for the Danakil Block in the last ~ 4 Ma.

They further argue that this rotation concentrated extension in the northern Afar, caused a

clockwise rotation in central Afar associated with diffuse extension, oblique extension in the Tajura area and dextral strike-slip faulting in southern Afar.

Collet et al. (2000) suggested a different model where the block behaves more independently and has experienced anti-clockwise rotation and sinistral strike-slip motion independent of the Nubian Plate. Eagles et al. (2002) argued that no dextral-strike-slip faulting is present near the Main Ethiopian Rift that would be predicted by the Collet et al. (2000) model. They proposed that the Danakil Block rotated clockwise slowly in response to the Nubian and Somalian Plates between ~ 11 Ma and ~ 3.2 Ma and accelerated rapidly since then possibly due to oceanic-type accretion within Afar. Lastly, Chu and Gordon (1998) used magnetic anomalies in the Red Sea to calculate an anticlockwise rotation of 1.22° per Ma with respect to the Nubian Plate.

2.3.2. The Ali-Sabieh Block. The Ali-Sabieh Block is generally considered the area that extends from the Somali Plateau towards the Afar Depression in the area of Aysha. This block was thought to have rotated $\sim 90^\circ$ clockwise in the course of 20 Ma concurrent with the Dankil Block in a “saloon door” fashion opening the Afar Depression (Manighetti et al., 2001). This is further supported by spatter cones that are aligned $\sim 90^\circ$ to the E-W Somalian Escarpment, along with sinistral strike-slip faults that have developed due to the clockwise rotation of the block.

2.3.3. The East-Central Block. This block is actually composed of several micro-blocks separated by deep graben structures. The block as a whole has rotated clockwise $\sim 11^\circ$ in the past 2 Ma due to a dextral shear couple caused by the Gulf of Aden propagator to the East and the Red Sea propagator to the west (Acton et al., 1991; Acton et al., 2000; Courtillot et al., 1984). Acton et al. (2000) suggested that the East

Central Block (ECB) rotation has ceased with rift localization within the Tendaho. This rotation has reactivated NW trending faults in a sinistral strike-slip manner in bookshelf-faulting mechanism (Courtilot, 1982; Courtilot et al., 1984; Courtilot et al., 1980; Manighetti et al., 2001; Sigmundsson, 1992; Tapponnier et al., 1990). A more plausible model called the “crank-arm” model was proposed by Souriot and Brun (1990).

According to this model, it is external forces such as movement of the Danakil Block that has caused the clockwise rotation. Recent geodesy and field work also supported this model more favorably. The individual microblocks have also rotated clockwise but at different rates ranging from 0° to 13° with respect to the Ali-Sabieh Block in the last ~ 1.8 Ma (Lahitte et al., 2003). The extension in the East Central Block is localized in major grabens such as the Dobi (Beyene and Abdelsalam, 2005).

2.3.4. The Manda Hararo-Gobaad Rift. The Red Sea spreading center expresses itself as the Manda Hararo-Gobaad rift on land. It intersects land at the Gulf of Zula near the Danakil Depression and continues south to Erta Ale subsequently splitting into the Tat Ale-Dader trend in the east and Alyata-Manda Hararo trend to the west (Beyene and Abdelsalam, 2005). The western branch probably stops at the Tat Ale axial range that extends into the Dadar Graben. The eastern branch continues southeastward to the Tendaho-Gobaad Discontinuity. Here the volcanism is young (~ 30) ka and represents the southern termination of the Red Sea propagator (Lahitte et al., 2001). The axial zones within the Danakil Depression are segmented into 50 – 80 km long volcanic ranges (Beyene and Abdelsalam, 2005). This is similar in morphology, spacing and size to second order non-transform offset segmentation of slow spreading mid-oceanic ridges

(Hayward and Ebinger, 1996). These ridges decrease in size to the rift-in-rift structures found in the Tendaho Graben (Tazieff et al., 1972).

2.3.5. The Asal-Manda Inakir Rift. The Gulf of Aden spreading center steps onto land at the Gulf of Tajura and is expressed as the Asal-Manda Inakir rift. It is bounded by the Danakil Block to the east and the East Central Block to the west. It trends NW after trending NE-SW in the Gulf of Tajura (Dauteuil et al., 2001). Rift propagation and spreading are dominant. Oceanic magnetic anomalies over the Aden ridge terminate at Lake Asal in a magnetic quiet zone (Courtilot et al., 1984). Rifting is episodic suggesting alternating extensional mechanisms, magma-assisted and mechanical stretching (Courtilot et al., 1984). Around 1 Ma, the Ghoubbet-Asal-Manda Inakir rift began to open (Courtilot et al., 1984).

2.3.6. The Sabure-Hertale-Adado Rift. The northern part of the Main Ethiopian Rift that propagates away from the Afar Depression is called the Sabure-Hertale-Adado rift (Beyene and Abdelsalam, 2005). This rift is characterized by segmented Miocene rift-in-rift basins (Beyene and Abdelsalam, 2005). The Adado rift is dextrally offset from the Hertale rift by the 35 km long Ayelu Amoissa lineament that parallels the Tendaho Graben (Beyene and Abdelsalam, 2005). These rift basins are typically ~20 km wide and ~60 km long magmatic segments that decrease systematically in size towards central Afar (Ebinger and Casey, 2001; Hayward and Ebinger, 1996). It is believed that these segments represent incipient spreading centers (Ebinger and Casey, 2001; Hayward and Ebinger, 1996; Manighetti et al., 1998).

The forces acting on these blocks and plates have been characterized as passive rifting or active rifting (Beyene and Abdelsalam, 2005). Passive forces are due to slab

pull of a subducted plate. Active forces of rifting would be asthenosphere pushing its way up due to mantle convection or a mantle plume. Passive rifting would occur in the order of rifting, uplift followed by volcanism. Active rifting would be the likely candidate if uplift occurred first, then volcanism followed by rifting. It is generally agreed that the Arabian-Nubian Shield was uplifted based on the volcanism that preceded it. According to Menzies et al. (2002), the events in Afar occurred in a volcanism, rifting and uplift order which fits neither model. It could be a combination of both hypotheses to explain what is observed in Afar. Hempton (1987) and Bohannon et al. (1989) describe the movement of the Arabian Plate away from the Nubian and Somalian plates as passive due to the closing of the Tethys Sea and the activity along the Zagros Orogenic Front. The separation of the Nubian and Somailian plates could be a secondary effect of a ~ 40 Ma plume (Gass, 1975) pushing the plates apart (Beyene and Abdelsalam, 2005).

3. TENDAHO GRABEN

3.1. PREVIOUS WORK

The Tendaho Graben (TG) was first studied in the 1930's by Dainelli (1943) who published 4 volumes that describe the geology of Eastern Africa. The first systematic research on the TG specifically, was started in 1970's and continued through the 1990's during the Tendaho Geothermal Project led by Aquater (1996a, b). Recent work has focused on the geochemistry (Barrat et al., 2003) and the tectonics of the graben (Abbate et al., 1995; Thurmond et al., 2006; Thurmond, 2007)

3.2. GEOLOGY

The TG is located in central Afar and terminates the NE extension of the MER structures. It is bounded to the east by the East Central Block and to the west by the marginal blocks created by normal faulting associated with the Ethiopian Plateau escarpment. The TG is an extension of the Manda Hararo rift segment to the northwest of the Goba Ad structure, a half-graben, to the southeast (Abbate et al., 1995) (Figure 2.8). The TG is the largest rift basin in the central Afar (Acocella et al., 2008). It is typically 50 km in width (Abbate et al., 1995) and extends a few hundred kilometers in the NW-SE direction. Its flanks primarily consist of Statoid basalts and younging axial volcanics toward the center of the graben (Kidane et al., 2003; Lahitte et al., 2003) (Figure 3.1). The floor consists of young volcanics in axial ranges and lacustrine deposits. The TG hosts historically active Karub and Dama Ali volcanoes (Simkin and Siebert, 1994). The relief from flanks to basin bottom is a few hundred meters however the sediment

thickness exceeds 1600m in places and could be much thicker based on data from the Tendaho Geothermal Project (Aquater, 1996a). Geochronological data suggests that the opening of TG was initiated as early as ~ 2.0 Ma (Acton et al., 1991; Acton et al., 2000). The youngest volcanics are found along the Manda Hararo rift axis at ~ 0.03 Ma (Lahitte et al., 2001). Just to the north of the TG a major dike injection event occurred in 2005 (Wright et al., 2006) along with active seismicity. A dike 60 km long and up to 8 m wide was emplaced (Wright et al., 2006).

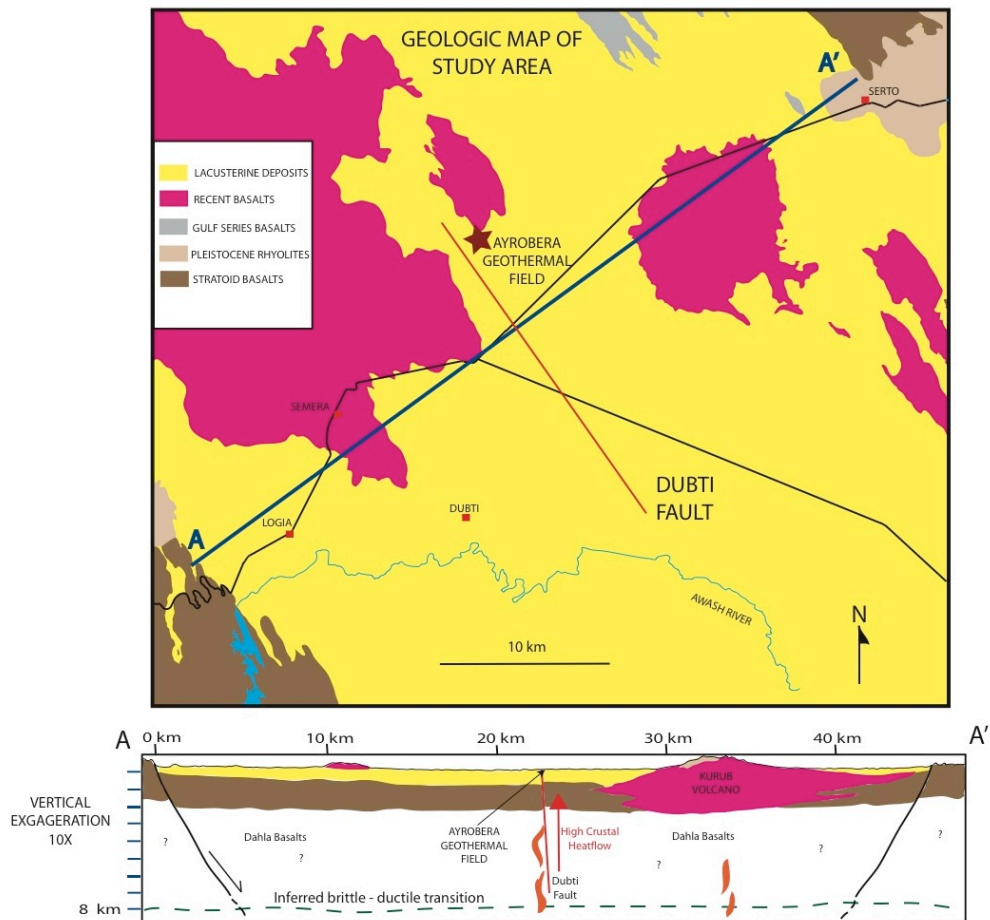


Figure 3.1. General geology of the Tendaho Graben. The red line shows the linear known extent of Dubti fault and associated hydrothermal activity. The maroon star marks the Ayrobera geothermal field mentioned in the text.

The TG is surrounded by NE and SW footwalls consisting of sub-horizontal Stratoid basalts dissected by NW-SE trending faults. These end with inward dipping blocks of Stratoids ~1 km wide that decrease in both displacement and rotation from 30° to 5° toward the graben axis giving syncline-like feature in a NW-SE orientation coincident with the rift axis (Acocella et al., 2008). The northeastern flank of TG exhibits a discontinuous flexural style that is well developed between Serdo and Gargori Bad 50 km to the southeast (Abbate et al., 1995). This style transitions to block-faulted, sub-horizontal structures in the graben. Slickensides indicate dip-slip movement in the area of Serdo; however the focal mechanism of an earthquake that occurred in 1969 shows a NW-oriented sinistral shear or NE-dextral shear (Gouin, 1979; Keebe et al., 1989; McKenzie et al., 1970). Field observations (Dakin et al., 1971; Gouin, 1979) support the NW-trending fault plane (Abbate et al., 1995).

The Manda Hararo rift in the TG exhibits open fissures and blocks that are elongated along the rift axis. The blocks vary in lengths from tens of kilometers to one kilometer (Abbate et al., 1995). The vertical throws are tens of meters with the exception of larger border faults (Abbate et al., 1995). This is similar to the Stratoid blocks located along the TG flanks, and other recent volcanics, which suggest that a mechanism deep under the rift is controlling their tectonic style rather than superficial activities (Abbate et al., 1995). The densely-spaced multitude of small-throw faults would suggest a thin brittle layer over a shallow soft layer (Abbate et al., 1995). This is supported by the abundant hydrothermal activity throughout the graben. To the southwest of Loggia, in the area of Alalo Bad, fossil and current evidence of hydrothermal activity are abundant. This could be associated with the major southwest border fault in the immediate vicinity. In this part

of the southwest flank, field evidence in the form of a few slickensides, suggest a dip slip motion and an absence of any strike-slip component (Abbate et al., 1995). Strike slip motion has been found not far away, 1 km north of Tendaho, at the contact between the southwest flank slope and basin floor in some siliceous veins created by hydrothermal activity (Abbate et al., 1995). A sinistral motion is suggested but multi phases of faulting are apparent and reflect only recent tectonics in the sediments.

The basin of TG primarily consists of alluvial and lacustrine plains with NW-SE elongated basalt outcrops. Ten km southwest of Karub, NW striking faults are present in the sediments indicated by aligned steaming grounds, fumaroles, hydrothermal deposits and faults steps (Abbate et al., 1995). Dextral shear, WNW-orientated, is indicated in the Gum' Atmali area by en echelon NNW-trending extensional fractures (Abbate et al., 1995).

Acocella et al. (2008) studied the structure of the Manda Hararo rift (Semera Plateau) in the TG in detail. The southern geomorphologic expression of this young rift is a basalt plateau (Semera Plateau) oriented NW-SE. It is dominantly recent axial basalts surrounded by lacustrine deposits and subordinate interbedded volcanics. The plateau itself is highly fractured by vertically displaced faults that are not expressed in the surrounding sediments. Acocella et al. (2008) divided the plateau into two domains, a mostly untilted domain to the west and a domain to the east characterized by NE-dipping blocks that decrease in dip to the east. The untilted domain is characterized by opposite facing, nearly vertical scarps with vertical displacements ~ 1 to 10 m high forming mini grabens. The eastern domain is much more complicated where the northeastern dipping blocks are interrupted by regularly spaced SW-dipping normal faults. Vertical

displacement is in the tens of meters and the grabens lack the extensional cracks found in the western domain. The overall characteristics surprisingly are quite similar to that observed at the margins of the TG (Acocella et al., 2008). This is similar to a rift-in-rift structure.

Lastly, thick (>1000 m) sequences of volcanics and sediments are present within TG and the young (~ 300 to 0.030 Ma) volcanics a few km east of Semera represent the current Manda Hararo rift axis (Lahitte et al., 2001). The antithetic nature of the fault blocks along with the topographical escarpments (>200 m) contribute to the ~ 1600 m vertical displacement of the TG (Acocella et al., 2008; Battistelli et al., 2002).

Acocella et al. (2008) used two different methods to estimate the extension across the TG. One uses the calculation of the β_d (~1.07 +/- 0.04) or stretching factor associated with tilted blocks (Jackson and White, 1989) and the other calculates β_t (~1.11) by using the initial crustal thickness and the current thickness of the crust. Acocella et al. (2008) obtained a mean β_{tot} of ~1.08. They came up with a total extension of ~3.6 mm/yr or 5 km for the TG in the last ~1.4 Ma. Schaefer (1975) determined a spreading rate of ~1.9 mm/yr for the TG; however, both Schaefer's and Acocella et al.'s rates are much too small to account for the observable 50 km width of the present TG assuming the initiation of TG at ~1.8 Ma. Using a crustal thickness of 15 km is an implausible parameter as most workers agree on a crustal thickness of 23 to 26 km for the TG region.

3.3. PETROLOGY AND GEOCHEMISTRY

The geochemistry of the TG has not been systematically studied with the exception of one peer-reviewed work and a couple of papers published in French. Barrat

et al. (2003) used major, trace and isotopic data to study the Quaternary basalts of the TG section of the Manda Hararo rift. They found that two types of basalts were erupted characterized by a more prevalent light rare earth element (LREE)-enriched type with a restricted range of $^{87}\text{Sr}/^{86}\text{Sr}$ ratios and the second type, a LREE-depleted type that is distinctly different from the N-MORB erupted by the Red Sea and Gulf of Aden spreading centers (Figure 3.2). The latter has also been reported for strongly LREE-depleted olivine tholeiites and picrites from Iceland (Barrat et al., 2003). A LREE-depleted component of the Afar plume could be responsible in the genesis of these basalts based on trace element, Sr and Nd systematics (Barrat et al., 2003). The former basalts display homogenous $^{143}\text{Nd}/^{144}\text{Nd}$ ratios, similar to other Quaternary basalts suggesting a similar mantle source.

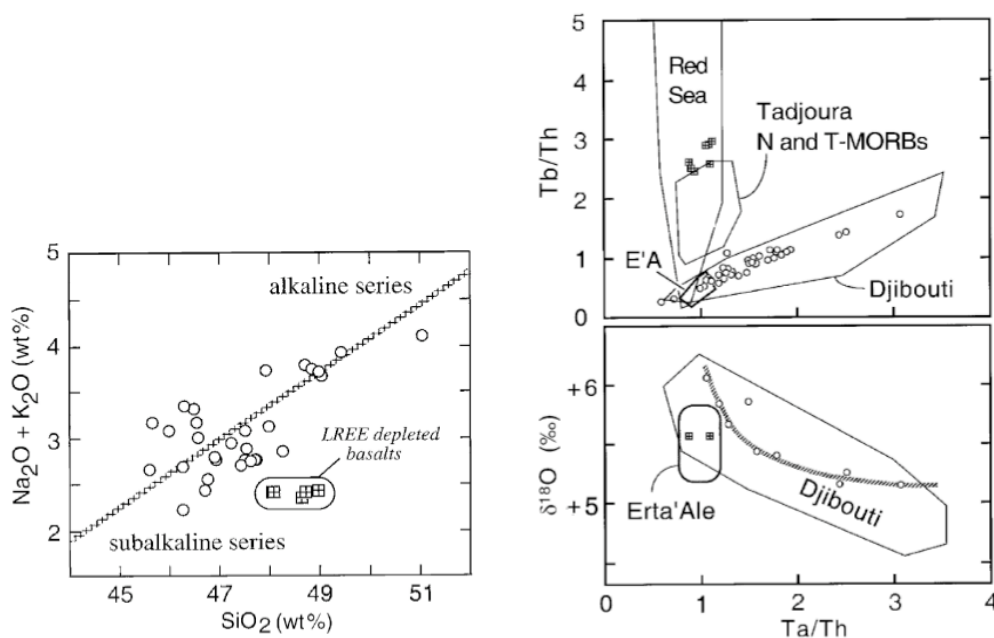


Figure 3.2. Tendamho geochemistry data. Left: Total alkalis vs. Silica Diagram Right: Tb/Th and $\delta^{18}\text{O}$ vs. Ta/Th (Barat et al., 2003).

Furthermore, the $\delta^{18}\text{O}$ values vary significantly between +5.15% and +6.1% and display strongly correlated Ta/Th ratios. Barrat et al. (2003) proposed that this is due to contamination from hydrothermally altered gabbroic cumulates. The Manda Hararo rift is unique in that it is the only place in the East African rift system that has both enriched-LREE basalts and depleted-LREE basalts.

In the northern Manda Harraro Rift, Barberi et al. (1975a) completed a thorough geochemical study of a basalt-pantellerite sequence from the Dabbahu volcano. This series can be explained entirely by crystal fractionation in shallow depths (Barberi et al., 1975a). Dabbahu basalts are olivine-tholeiites on a normative basis. Similar to other basaltic rocks of Afar, they are transitionally alkaline. The intermediate rocks are andesites and trachytes. Peralkaline rocks are also present. Evidence for crystal fractionation as the dominant process to produce the series include: 1) all rock types emanate from one volcanic structure with the intermediate and silicic rocks accounting for 10% of the total, 2) geochemical evidence in the form of linear correlation between pairs of residual trace elements and 3) Sr isotopic evidence (Barberi et al., 1975a).

3.4. GEOPHYSICAL WORK

The first systematic gravity study of the TG was part of the larger study of the Afar Depression by Makris et al. (1987) in the late 1960's. During the 70's -80's, Aquater conducted a high-density gravity survey for the Tendao geoelectric project (Figure 3.3). The area was centered on the Dubti geothermal field to the south of Semera. Bouguer gravity anomaly values in the TG range from -65 to -45 mGal. A pronounced gravity high \sim -50 mGal follows the Manda Harraro Rift axis.

The first magnetic survey to entirely cover the TG was completed by Girdler (1970). Six of the lines were flown in a (NW-SE) trend covering the TG along with 4 lines in a WNW-ESE orientation, neither sets favoring the NW-SE structures of the TG (perpendicular to strike being optimal). Despite this, some encouraging results came from the study. Barberi and Varet (1977) noticed that the magnetic anomalies were linear in the vicinity in the TG. The resolution of the survey was not adequate enough to interpret much information due to the lack of geochronologic and paleomagnetic data.



Figure 3.3. Station locations (red dots) of the Aquater magnetic and gravity field study within the TG.

The first systematic magnetic ground survey (1970's-1980's) was completed by Aquater as part of the Tendaho Geothermal Project. The stations are located in the same locations as the gravity stations (Figure 3.3). The mean station spacing is ~ 230 m and the

profiles follow the roads and form rectangular shapes parallel and orthogonal to the strike of the TG. The magnetic profiles perpendicular to strike across the TG verified the observations from the earlier aeromagnetic data that linear magnetic structures exist beneath the TG. A total-field anomaly (T_a) ranging from 400 to -600 nT is present and comparable in magnitude to those found in oceanic spreading centers. The large negative anomaly coincides with the Manda Hararo rift axis.

Berckhemer et al. (1975) completed the first seismic refraction study of TG in March 1972. Five deep refraction lines were run each 120 km to 250 km long, two of which have limited coverage of the TG north and east of Aysaita, about 40 km SE of Karub volcano. The major results are: 1) the crust under the TG has a transitional structure with a thickness of 26 km north of Aysaita, 2) an anomalous mantle is under TG with a $V_p = 7.3 - 7.6$ km/s with a depth of 26 km and a thickness of 26 – 35 km, 3) a majority of the crust has a V_p of 6.6 - 6.8 km/s and lastly, 4) a thin layer of $V_p = 6.0 - 6.3$ km/s highly attenuated silic upper crust exist under TG.

The first magnetotelluric study of TG was completed by Berktold et al. (1975) in the early 70's. They had three stations in the TG at Loggia, Serdo and Aysiata. They reported a resistivity of 500 (Ω m) in the uppermost part of the crust to 50 (Ω m) at a depth about 15 km. They interpret this to indicate a 60 °C/km geothermal gradient or 800 -1000 °C at a depth of 15 km beneath TG. In the 70's and 80's, Aquater completed a more comprehensive magnetotelluric survey. They imaged the upper few kilometers in detail to assess fluid mobility related to the geothermal project. They reported that the upper 8 m of the TG basin sediments have a resistivity of ~264 (Ω m). Relatively low resistivities (~ 1 to 8 Ω m) are found between 8 and 800 m. From 800 to 1400 m the

resistivity varies between 100 to $\sim 188 \Omega\text{m}$. The focus was primarily the sediments of the TG basin so a direct comparison of results with Beckett et al. (1975) is not possible.

No major tomographic work has focused on TG; however, new work by Gao et al. (2010) has detected a bilayer of anisotropy when imaging deeper into the mantle using SKS shear wave splitting techniques. A P-wave study by Benoit et al. (2006) imaged one profile across the TG and found P wave perturbations of $\sim 2\%$ indicative of warm upwelling asthenospheric material and possibly the presence of crustal melt beneath the rift axis.

3.5. SERDO EARTHQUAKE SEQUENCE OF 1969

In the morning of March 29, 1969, the small village of Serdo was shaken by an M_b 5.9 earthquake (Figure 3.4). Of the ~ 420 town's residents, 24 died and ~ 167 injured. Serdo is located near the northeast master fault of the TG some 10 km WNW of the Karub volcano (Figure 3.1). On April 5, another, even more powerful 6.2 M_b shock occurred that opened 3 faults 8 km east of Serdo. The WWSSN station at Addis Ababa recorded over 250 aftershocks, some of which reached 5.2 in M_b . This earthquake and its aftershocks revealed some of the tectonic nature of the TG and are important in understanding the overall tectonics of the rift.

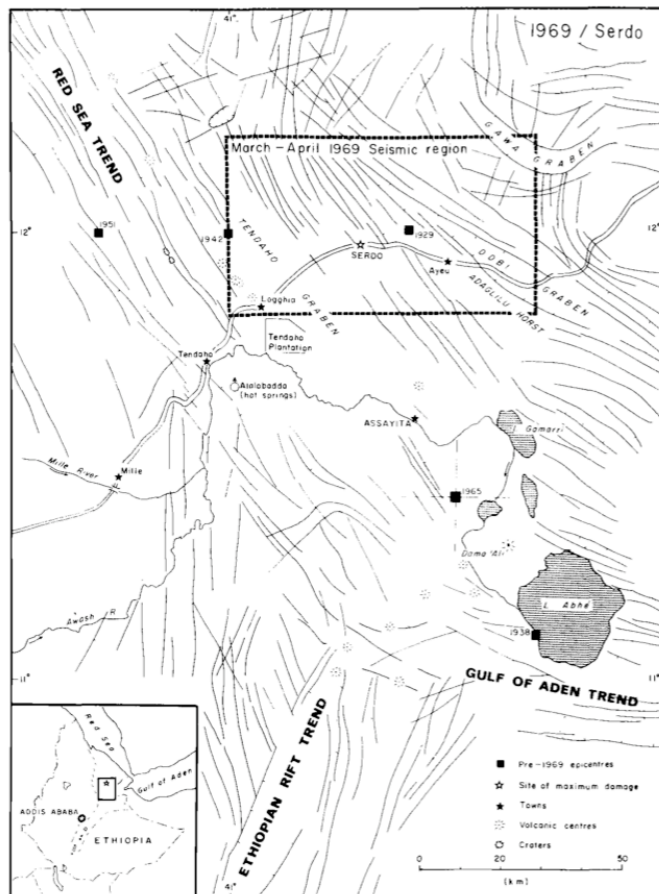


Figure 3.4. Serdo tectonic map overview (Gouin 1979).

Much of the material from this section is taken from Gouin (1979). The Serdo village had older stone masonry structures built by the company that built the Asseb-Combolcia road in the 30's. Serdo was built on fault block that is tilting to the southwest and strikes approximately $N40^{\circ}W$. Most of the town was located in the plain to the east of the block but certain structures were on top of the block, which consist of nearly vertically banded rhyolites. Historically the area has hosted active tectonics. On December 23, 1608, smoke was coming out of the ground east of Mt. Waraba (possibly Dami' Ali), near a lake in Aussa (possibly Lake Abhe). From March to midsummer,

1627, seismovolcanic activity occurred that reportedly killed 50 people in the village of Waraba. Between 1883 and 1965, six strong earthquakes occurred in the central Afar region. Seismologists have focused on 11 of the 250 foreshocks and aftershocks with a body-wave magnitude of 3.0 or greater. On April 4, one day before the largest shock, USAID officials made a low-altitude air survey of Serdo and could not find any surface manifestations of the March 29 shock. On April 5, an investigation team from Addis Ababa University, headed by Gouin headed to Serdo. They noticed that all the stone masonry structures were destroyed by the first shock. Residents reported feeling a sudden jerk to the NE. Vertically, a 60 cm offset was detected using vertical control benchmarks.

The April 5 shock caused many geological surface effects (Figure 3.5). Several cracks were observed on the highway (paved) up to 20 m long, 30 cm wide and up to 20 cm deep. All but two were parallel to the road. A culvert likely caused the one perpendicular to the road and the other located 5 km east of Serdo was orientated 10° with respect of the direction of the road. These cracks were controlled by the highway structure rather than tectonically except perhaps the last one. Two areas where cracks are likely related to tectonics are located 8 km east of Serdo and 500 m south of the village in the sediments of the Kurub plain. The cracks to the south of the town were located in an area 400 m long by 10 m wide with individual cracks 0.5 to 3 m long and 1-20cm wide and 15 – 20 cm deep. The entire area subsided by 20 – 25 cm. The general trend is $N40^{\circ}W$ and turns E-W at the NW end. These cracks formed from the 29 March trembler and likely due to compaction. The second set of cracks was associated with a fault that formed from the April 5 shock. Other cracks of noticeable attention were observed running through a kitchen and baking oven of the Tehame Tekle Hotal in Ayeu, 25 km

east of Serdo. It had a strike of N60-70W. Lastly some cracks appeared in the Tendaho Cotton Plantation and the most notable one cut through the structure of a fishpond at a N40W trend. The last two are associated with the April 5 shock.

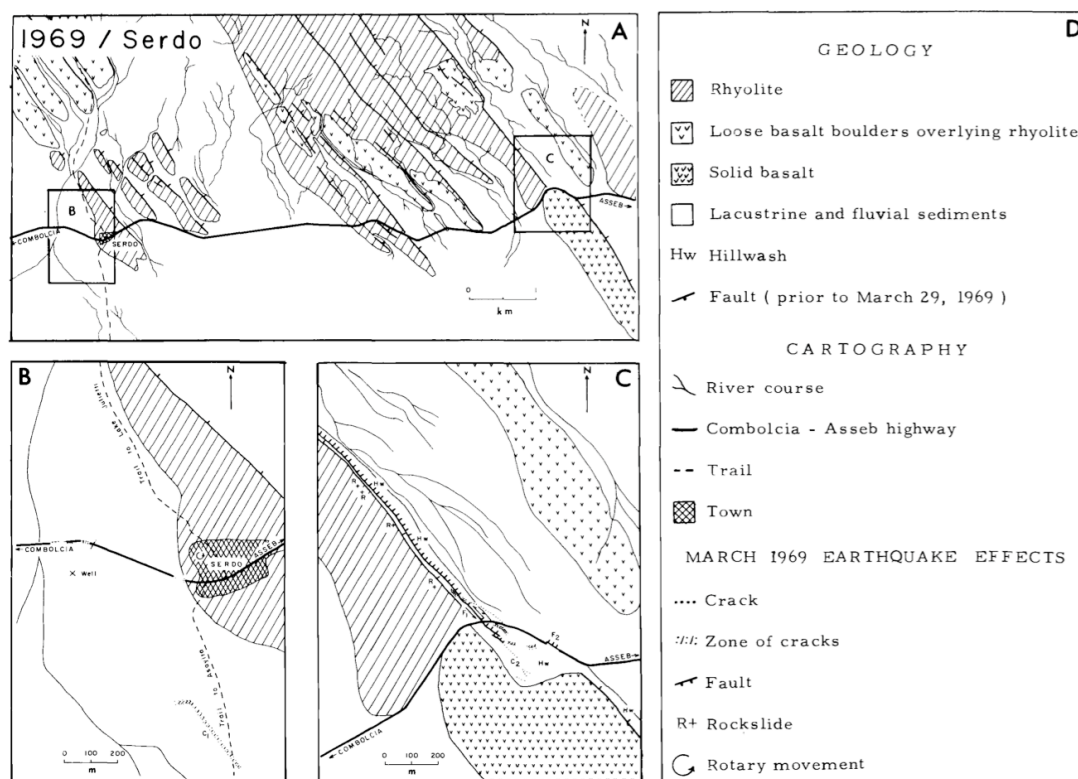


Figure 3.5. Surface geology of the Serdo area after the 1969 earthquake (Gouin (1979)).

Three faults were activated or created during the 1969 earthquake sequence. The first two are located near one another; about 8 km to the east of Serdo while the third one was 1 km further to the east than the other two. Fault one strikes N40°W, nearly perpendicular to the road and nearly parallel to a major fault scarp. It had a vertical displacement of 75 cm as measured in the road and exhibited a 50 cm sinistral

displacement. This fault could be traced for 100 m to the south of the road where it disappeared in the sediments and over 1 km to the north where it was lost in a talus slope. The second fault strikes N50°W and crosses the road 200 m east of the first fault described. It has a vertical displacement of 90-95 cm and no detectable strike-slip motion. The last fault is located 700 m to the east of the first fault and also has a strike of N50°W. This fault showed a small 10 cm sinistral displacement. All these faults were formed in the morning of the April 5 event.

In 1974, a microseismic network was created by the University of Durham and recorded usable data for 124 days. During the time, 400 local shocks were recorded. Epicenters were determined for 200 of the events and 25 had accurate depths. Most of the hypocenters were concentrated along the newly discovered faults 8 km east of Serdo. None of the events was deeper than 10 km. This could have implications for the location of the brittle-elastic depth. This depth would likely decrease towards the center of TG. Fault plane solutions computed by McKenzie (1970), Gouin (1979) and Fairhead and Girdler (1970) reveal two planes striking N63°E and N27°W with a 70° and 90° dip, respectively. Fairhead and Girdler (1970) were the only workers to choose the N63°E as the primary plane based on the ENE alignment of the larger earthquakes of the sequence and the suggested evidence of a ENE trending transform fault under the Bididi-Dubi volcanic line associated with the rotation of the Danakil Block away from the Nubian plate. Gouin (1979) argued that the general surface faulting pattern in the Serdo area does not agree with that interpretation.

Fairhead and Girdler (1970) calculated the b-value for the 12 epicenters while Dakin and Gouin (Dakin et al., 1971) used 251 events and ended up with similar results.

The mean value of ~ 0.75 is consistent with those found in other continental rifts. Another note to add is that the stress drop is low compared with that typical of intracontinent conditions where the crust is thicker. The stress drop is more consistent with that from a plate boundary.

According to Kebede et al., (1989) the similar waveforms for the 4 largest events suggest that the same fault plane was activated during the sequence. They argued for the ENE fault plane solution due to the proposed transform fault plane and all deformation takes place in a NE-SW fashion. Kebede et al. (1989) explained that the lower stress drop could be caused by a softer material below Serdo that likely exist beneath TG as a whole and perhaps even the entire central Afar.

3.6. DABBAHU RIFTING EPISODE OF 2005

The Dabbahu rifting episode of 2005 was a rare opportunity to observe oceanic spreading taking place subaerially. Similar episodes have been studied in Iceland and associated with the Gulf of Aden propagator in Afar in 1978. This event has been extensively studied with 9 peer-reviewed articles published at the time of this writing (2010). The evolution of geologic research from description to mechanics and now timescale studies exemplifies this event.

The Dabbahu rift is the ~ 60 km northern section of the Manda Hararo magmatic segment, part of the Red Sea propagator (Figure 3.6). The Dabbahu magmatic segment (DMS) is ~ 15 km wide (Rowland et al., 2007). The southern part of this magmatic segment terminates in the TG. This rift extends from the Dabbahu Volcano, for which the

rift was named, to the village of Semera on the Semera Plateau. It likely terminates in the sediment fill of the TG to the southeast of the Tendaho Plantation-Awash River.

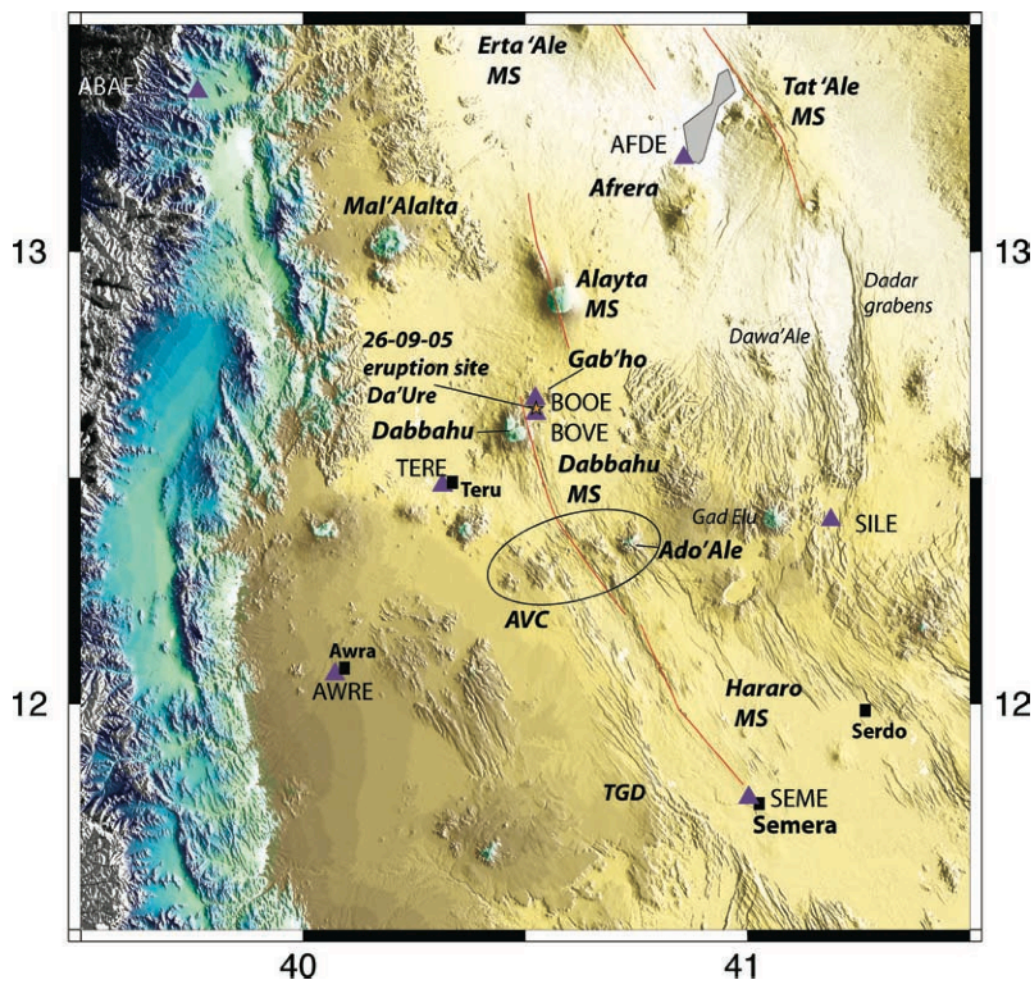


Figure 3.6. Overview of Dabbahu section of the Manda Harraro Rift (Ebinger et al., 2008). The red line marks the entire length of 2005 dike event.

From the area of Ado'Ale and to the south, the DMS trends NW-SE, and to the north, it trends in a more northerly direction. At its northern termination are numerous active volcanoes that include the Dabbahu and Gab' ho. The rift axis is composed of

chains of basaltic cones and fissure flows along with extensive fissural faulting (Wright et al., 2006). A well-defined axial valley extends from the southern flank of Dabbahu along the length of the DMS until it merges with the general lowering of the overall topography to the south. The DMS has an areal extent of $\sim 2000 \text{ km}^2$ and contains over 1200 distinct faults (Rowland et al., 2007). Faults have a mean strike of 333° but generally follow the strike of the rift axis except in the area of Ado' Ale where the rift axis bends southeastward. The faults are located generally within 7 km of the rift axis and commonly associated with fissures between the footwall and hanging wall blocks. Displacements are typically $< 20\text{m}$ horizontally and 1-3 m vertically within faults that are dominantly (60%) vertical (Rowland et al., 2007).

The chronology of the rifting episode is detailed in Ayele et al. (2007) and will be summarized here. The event was first known by the local inhabitants on September 9th or 10th by increasing seismicity. By 14th September, the seismicity increased to the point that the staff of the Addis Ababa observatory detected the activity. Larger shocks $> M 5$ started on September 20. These large shocks continued, 14 in all, until October 4th. On the morning of September 26th a large volcanic eruption started and was composed of silicic ash that created an umbrella cloud with an eruption column (Ayele et al., 2007). Earlier in the morning, a team from the Addis Ababa University was in the area 2 hours before the explosive vent opened up. It is located $\sim 5 \text{ km}$ ENE of the Dabbahu summit in an area called Da'Ure. The team observed degassing from the ground and newly formed fissures orientated N-S. The locals stated the ash cloud darkened the sky for three days but the actual extent of the eruption is not known. Ash fall was reported as far as 35 km to the southwest of the eruption vent in the village of Teru. The team returned in October

4th - 5th and found a N-S oriented fissure/crater 100 m at its widest and 60 m at its greatest depth. Intense degassing took place in which a loud noise was emanating. The smell of SO₂ extended 500 m from the fissure. The entire area was covered by silicic ash a few 10's of cm thick along with 2 - 3 m boulders thrown up to 20 m from the vent. The central part of the fissure had a small plug of effusive silicic lava (Ayele et al., 2007). Also of interest, is the number of recorded earthquakes reached a maximum of 45 per day on September 25th and decreased to one a day by October 1.

Several workers (Wright et al., 2006; Ayele et al., 2007; Grandin et al., 2009) used synthetic aperture RADAR interferometry (InSAR) to model the dike intrusion size. According to Wright et al. (2006) magma was injected as a dike nearly along the entire length of the DMS between the depths of 2 and 9 km and an average width of 3.5 m. They reported that a volume of 2.4 to 2.6 km³ is needed to accommodate the observed surface deformation. They used two sources beneath the Dabbahu and Gabho volcanoes based on radar interferometry detected deflation (0.5 km³). The Ayele et al. (2007) model is somewhat similar with the exception that their average width of the dike is ~5 m with the greatest width ~6 m. Their reported total volume is somewhat less (~1.6 km³) with a total deflation around Dabbahu ~0.4 km³. Grandin et al. (2009) report a 4.5 m average width dike, 65 km long and a ~1-2 km³ volume of magma was emplaced with a 0.5 km³ deflation beneath Dabbahu and Gabho volcanoes. A more plausible model is a dipping dike to west (towards the geomorphological rift axis) proposed by Barisin et al. (2009) using InSAR measurements and sub-pixel analysis of SPOT4 images. They conclude a total of 6 m of extension occurred. Other than the Dobbahu and Gabho volcanoes, Ayele et al. (2009) argued for a third magma injection point at Ado'Ale which

was the source for a majority of the magma that was emplaced. They also proposed a 15 - 30 cm/sec migration rate for the magma. The tectonic strain was not totally removed by the 2005 rifting episode as more dikes were emplaced in June and July 2006. Two dikes were emplaced, one on 17 June and the other 25 July (Keir et al., 2009) beneath the Ado'Ale volcanic complex. According to Keir et al., (2009) they were emplaced in 4-5 hour time frames. The June dike model suggests a max opening of 2.2 m and a volume of 0.12 km³ of magma injected while the July dike is ~1.1 m and 0.07, respectively. The June dike was longer (~ 10 km) and deeper (0-10 km) than the July dike, 9 km and 0-5 km, respectively. This activity is still ongoing (Figure 3.7).

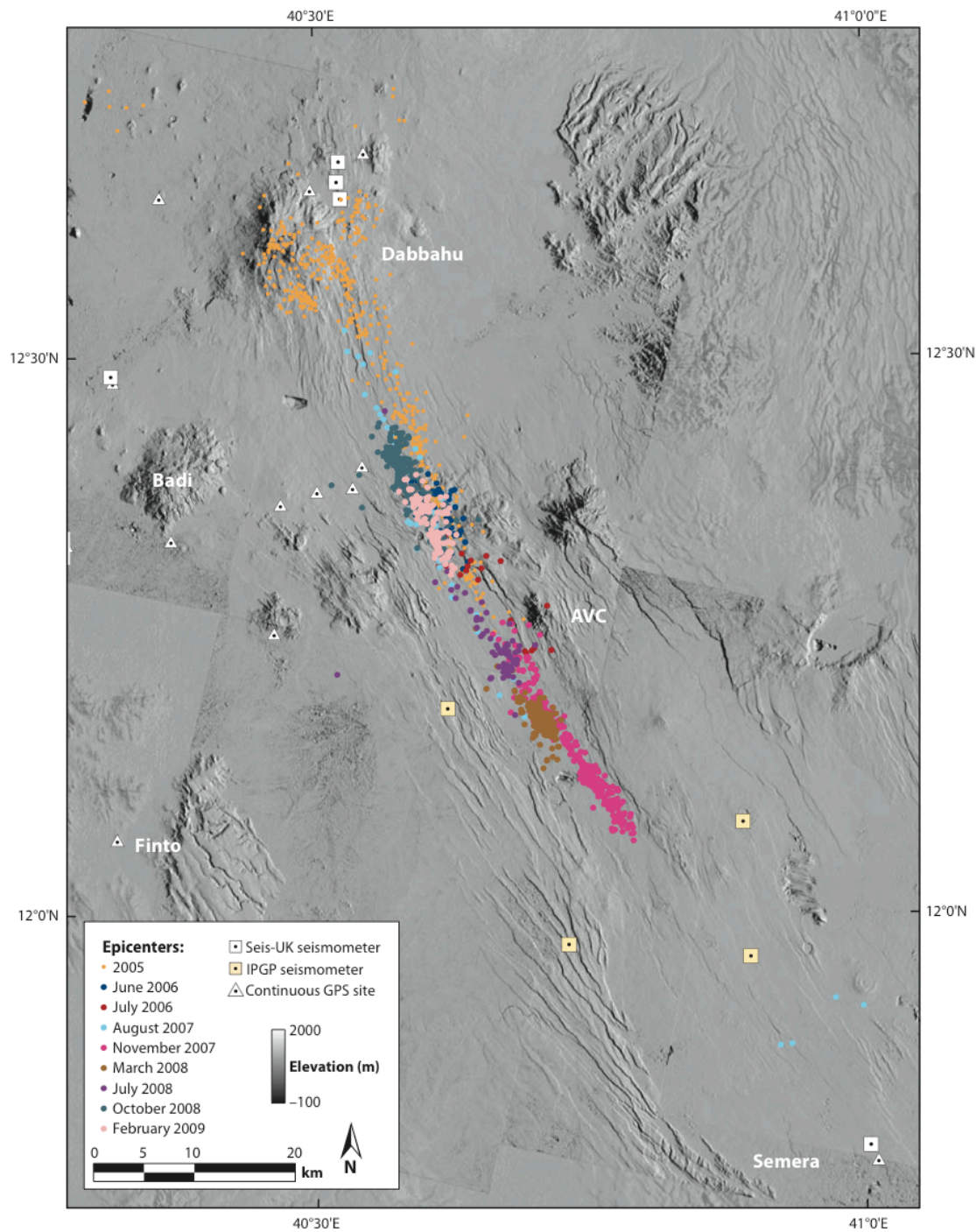


Figure 3.7. Seismicity associated with the Dabbahu rifting events from 2005 to 2009 (Ebinger et al., 2010).

4. METHODOLOGY

4.1. MAGNETIC DATA ACQUISITION

Magnetic data were collected in Afar during two field seasons, winter 2008 and winter 2009/2010. Figure 4.1 shows an outline of the general workflow for the acquisition and reduction of magnetic data into a data set suitable for interpretation. This chapter will roughly follow this workflow and subsequently provide a methodology for magnetic data interpretation.

A total of 846,901 magnetic measurements were obtained using a Geometrics G859 cesium optically pumped magnetometer (Figure 4.2). This instrument is mounted on a non-magnetic backpack and coupled with Novatel™ WAAS / EGNOS ready GPS. As a “walking” instrument, readings were set at 5 HZ and has a high sensitivity ~ 0.008nT/Hz RMS. Sensor direction corrections were necessary as surveying progressed due to low ambient magnetic field strength and optimum north sensor direction. A geometric G856 proton precession magnetometer (Figure 4.2) was used as a base station placed at the Semera Aquater geothermal camp. It has an accuracy of 0.5 nT and recorded the diurnal variation every 15 seconds. Proton-precession magnetometers, like the G-856, work by measuring the frequency of gyromagnetic rotation of hydrogen proton about the earth’s magnetic field. It uses a sensor field with a proton-rich liquid such as water or kerosene wrapped in wire. A charge is applied to the sensor causing the proton to align with the induced magnetic field. Then the charge is removed and the protons wobble back to the Earth’s magnetic field direction.

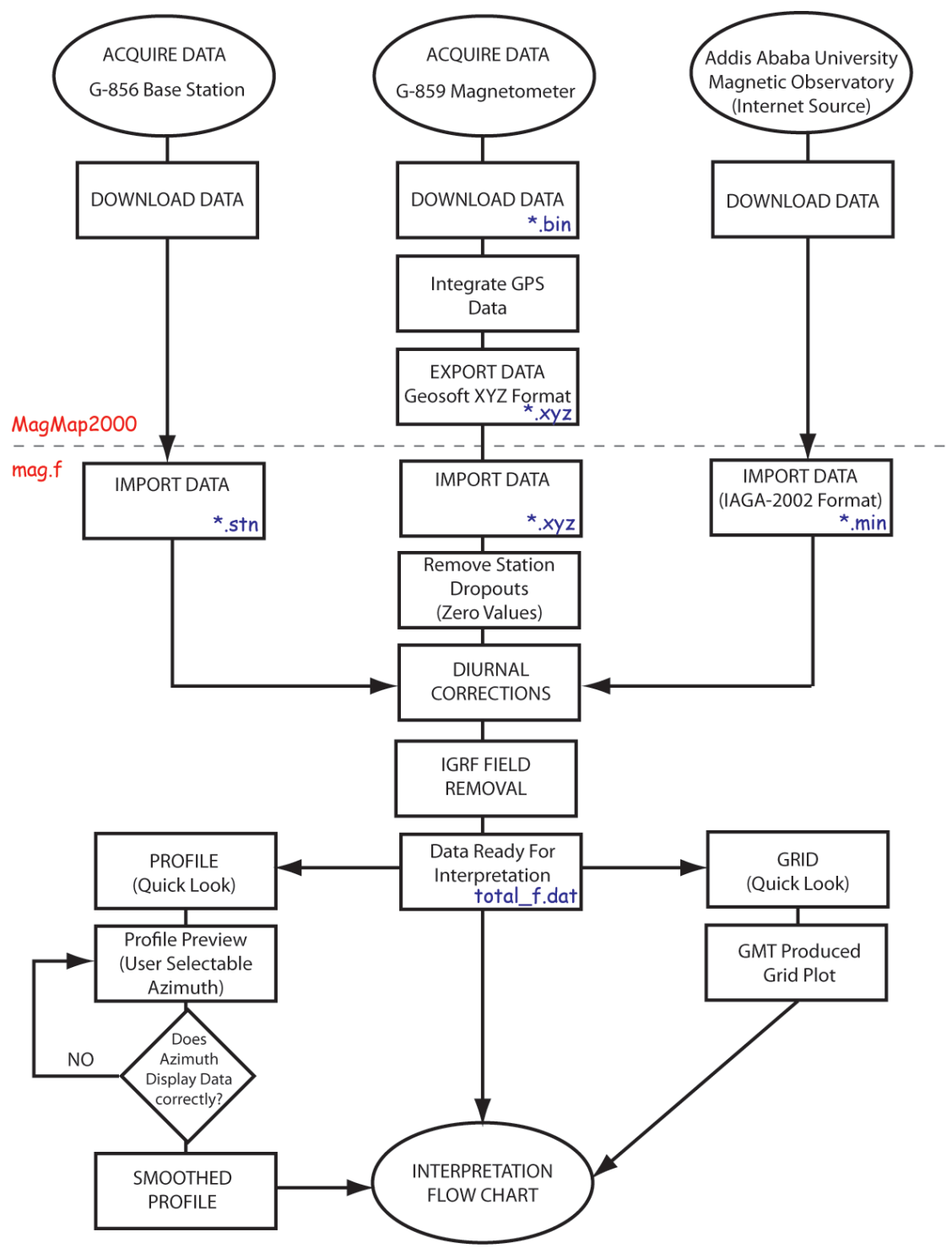


Figure 4.1. Workflow for the acquisition and reduction of the magnetic data. Purple text are associated file types. The gray dashed line separates the workflow based on the code used to process the steps.

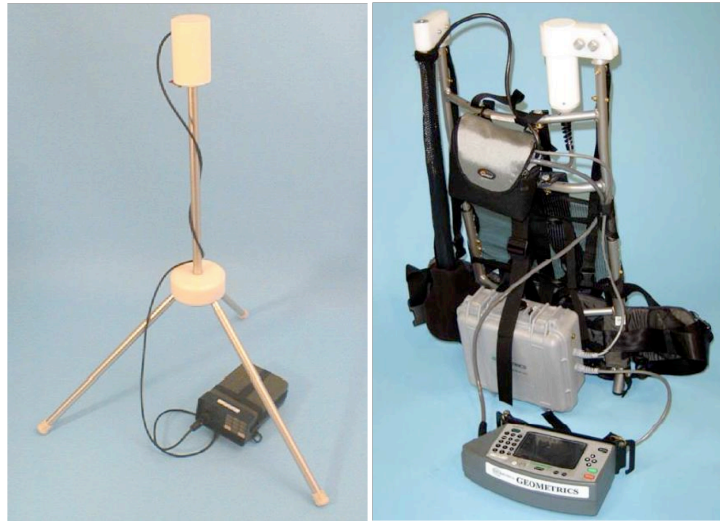


Figure 4.2. Magnetometers used in collecting the magnetic data. Left: Geometrics G856 proton precession magnetometer used as a base station. Right: Geometrics 859 cesium optically-pumped magnetometer used to collect the field data.

This frequency is directly proportional to the strength of the magnetic field that protons are in:

$$F = 2\pi\nu / \gamma_p \quad (1)$$

where ν is frequency and γ_p is a well-known constant called the gyromagnetic ratio of the proton (Figure 4.3). Orientation of the sensor is not important as it is measuring the total field strength unlike the fluxgate instrument. This instrument in general has a sensitivity of 10 nT and is the choice instrument for both ground and airborne surveys.

The Geometrics G-859 works by measuring precession of alkali vapors instead of hydrogen precession, in particular, cesium (Figure 4.4). Elements such as cesium, rubidium or sodium have a single electron in its outer shell that spin parallel or

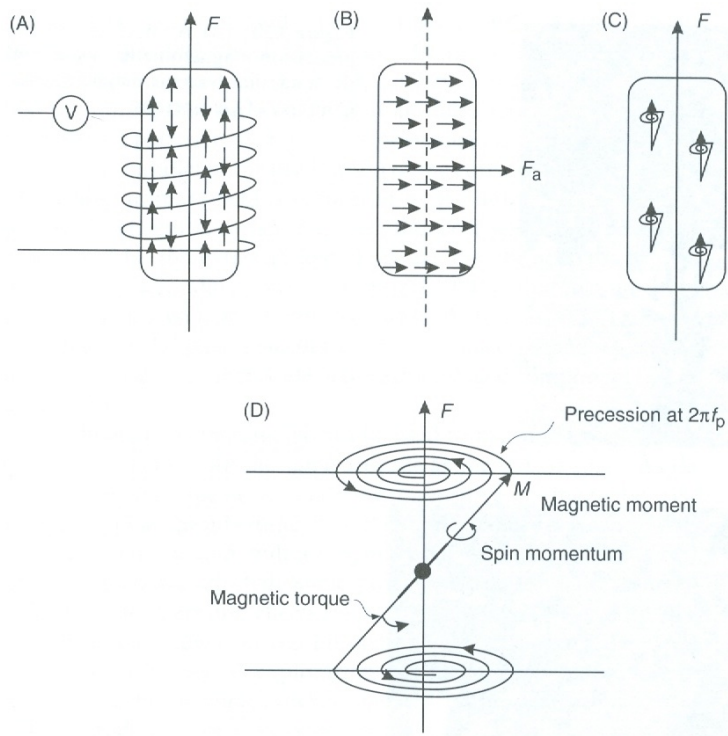


Figure 4.3. Cartoon showing how proton precession magnetometers work (Reynolds, 1997).

antiparallel to the Earth's magnetic field. A lamp irradiates the atoms and causes the outer electron to jump to the outer shell thereby in an excited state. As this occurs, the sample becomes increasingly transparent; this creates an increasing voltage in an optical sensor. This is called the pumping part due to pumping the ions up to the higher energy state. This occurs during the warm up period of the instrument. A radio frequency signal of appropriate energy that corresponds to the difference between the excited state and ground state of the atoms is applied. This cancels the pumping effect. Light from the lamp is circularly polarized and used to illuminate the sample located between the

photoelectric detector and lamp. The axis of this beam is aligned 45 degrees with respect to the Earth's field thereby causing the atom to precess at the Larmor frequency. At one

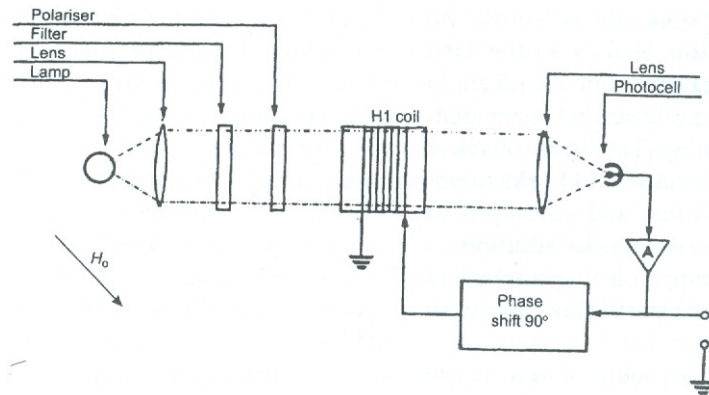


Figure 4.4. Simplified schematic of a cesium optically-pumped magnetometer (Reynolds, 1997).

half of the cycle, the atoms will be antiparallel with respect to the axis. This causes the intensity of the light to vary proportional to Larmor frequency. This is detected by the photocell, amplified and measured. The frequency is related by the following equation:

$$F = 2\pi\nu / \gamma_e \quad (2)$$

where γ_e is the gyromagnetic ratio of the electron (e.g. for Rb, the value $\gamma_e / 2\pi$ is $\sim 4.67\text{Hz/nT}$, for $F_e = 50,000$ is 233kHz) (Telford et al., 1990). This instrument can measure field variations as small as 0.01 nT .

During the 2008/2009 field season, a high resolution magnetic profile was obtained across the Tendaho Graben (TG), orthogonal to the prevailing NW-SE structures (287,608 measuring points) (Figure 4.5). A shorter profile was also obtained to the SE of the longer profile (58,818 measuring points). A 3d data set consisting of 51,312

stations were also collected at the Ayrobeara geothermal field (Figure 3.1.), located in the TG.

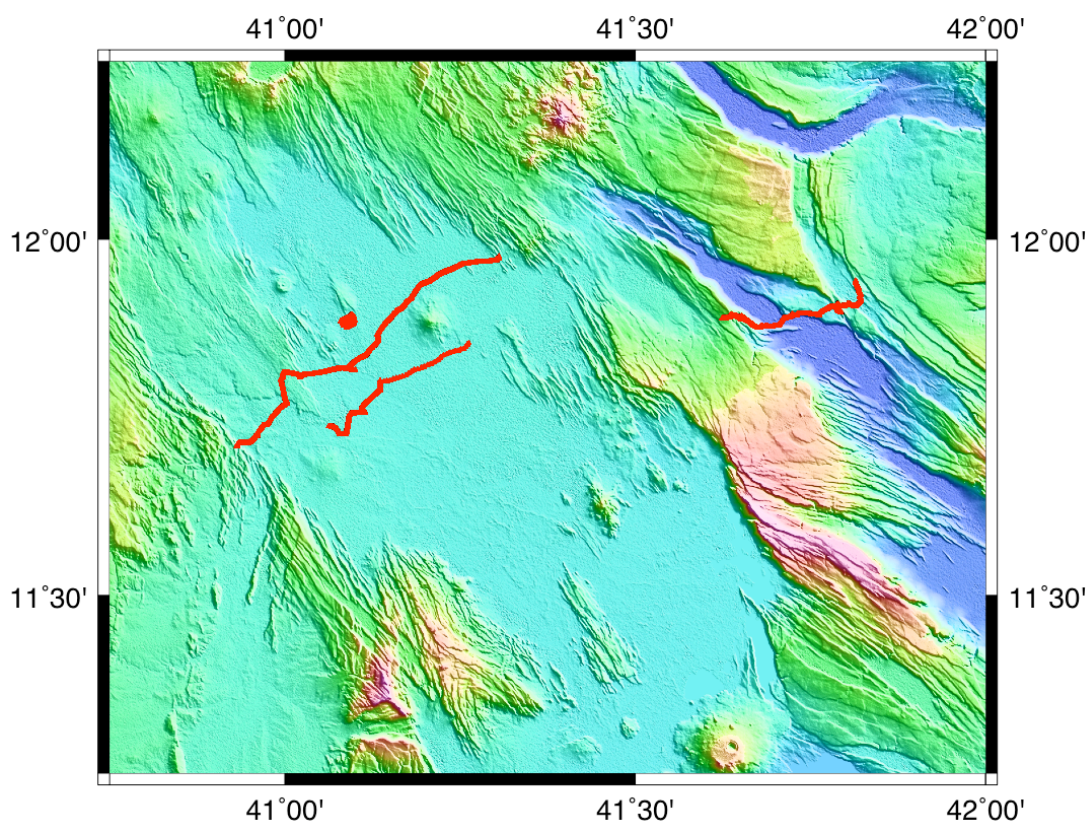


Figure 4.5. The location of the magnetic data (red lines) collected in 2008.

The winter 2009/2010 field campaign saw the collection of 383,504 measurements, primarily in the Dobi Graben (Figure 4.6). One day however, was spent collecting data along the northeast Tendaho footwall, following the Serdo-Erta Ale' road. Gravity and magnetic data were also obtained from an Aquater geophysical survey in 1980. A total of 2042 stations were measured with a proton precession magnetometer.

This data set is contaminated with surface noise and some had to be removed by hand.

(Figure 3.3)

The magnetometer data is downloaded to a laptop using the Magmap2000 software, provided by Geometrics, from both magnetometers and a USB port. The G859 data are synchronized with the GPS recorder data using the MagMap2000 software and are exported in Geosoft XYZ format for further processing (Figure 4.1).

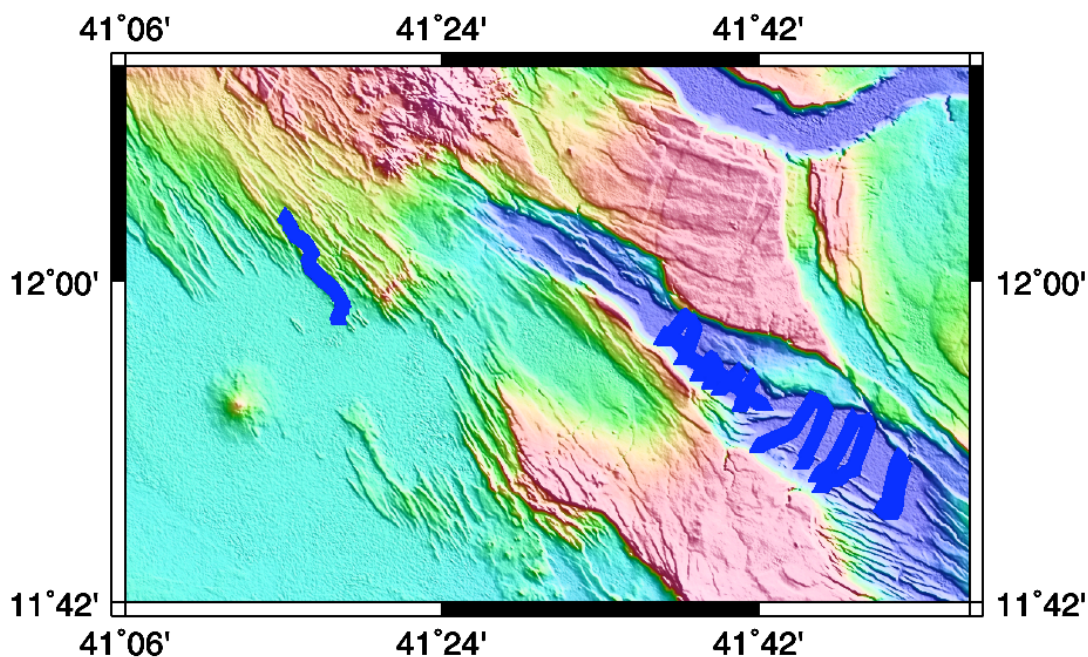


Figure 4.6. The location of the magnetic data (blue lines) collected in 2009/10. Data were also obtained from an Aquater geophysical survey in 1980.

4.2. DATA REDUCTION

The Geosoft XYZ data files are processed and reduced through a FORTRAN algorithm (mag.f), found in Appendix A. Data are initially imported by mag.f and data dropouts are removed. When the G859's sensor is not properly oriented in the ambient

magnetic field, the low field strength will cause a zero to be recorded at that point. All measurements of 0 are removed by the code.

A base station is used to correct for diurnal and erratic variations of the magnetic field. There is a daily variation of the geomagnetic field at a given location caused by charged particles in the ionosphere called diurnal variation. This effect must be removed from the total field data as it can vary the data by > 60 nT (Nabighian et al., 2005) (Figure 4.7). This is typically accomplished by have a base station in proximity to the survey area recording the variation. In the case another instrument is not available, one can always revisit stations and calculate the change for a given time period. The code `mag.f` averages all the base station readings for a single location and creates a datum.

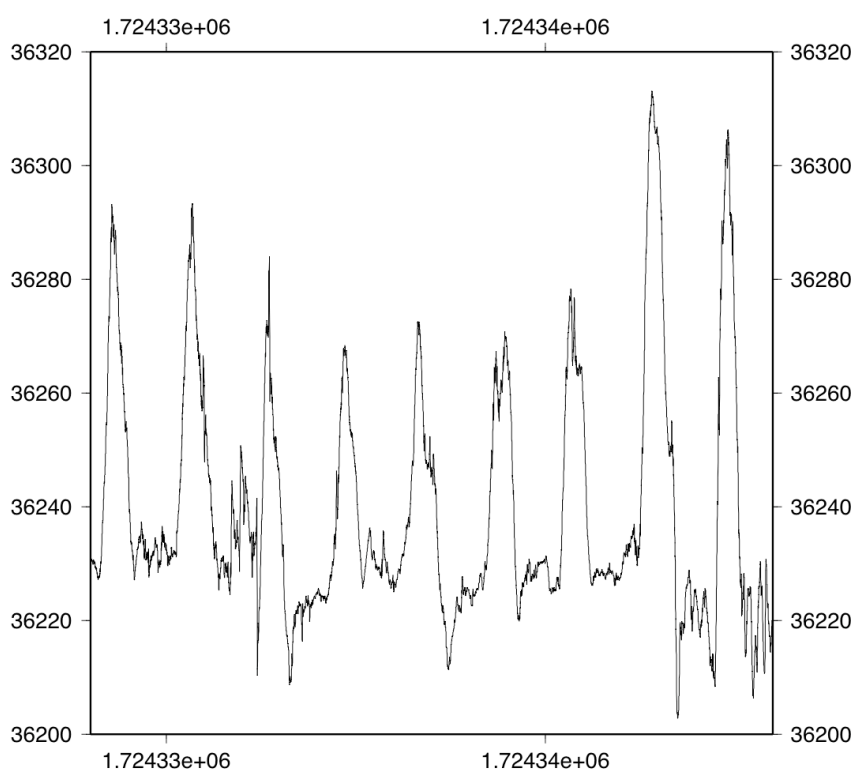


Figure 4.7. Diurnal variation over 9 days during the 2008 field season in Afar. The Y-axis is field strength and X-axis is seconds.

Next, it calculates the difference between the datum and each of the base station readings. Lastly, mag.f finds the closes two temporal corrections to a magnetic reading and adds an average of the differences to the magnetic reading thereby removing the diurnal effect.

The last correction that mag.f applies is the removal of the regional field. In areas like Afar where the regional field gradient is poorly resolved, this can best be done by removal of the IGRF (The International Geomagnetic Reference Field). IGRF is a spherical harmonic model of the Earth's geomagnetic field (Maus and Macmillan, 2005) due to the geodynamo effect (Figure 4.8). IGRF needs to be calculated every 5 years due to secular variation. Each of these "editions" is called an epoch (e.g. 2005).

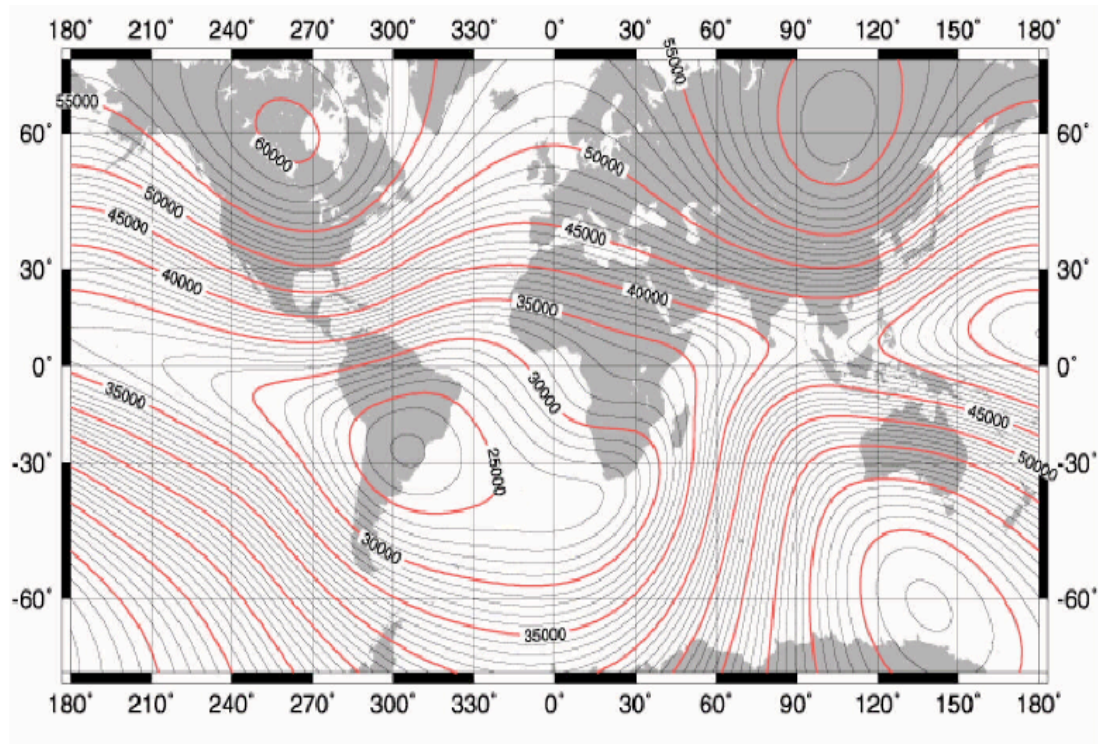


Figure 4.8. The IGRF magnetic field 2005 Epoch. From Geometrics Corp.

This field needs to be removed from total field data to produce the magnetic total field anomaly, T_a data. In equation form, T_a is defined as:

$$T_a = F_T - F_e \quad (3)$$

where F_T is the measured total field and F_e is the geomagnetic field produce by the Earth. This leaves the magnetic anomaly due to crustal sources of interest.

Elevation corrections are 0.03 gauss/m at the poles and 0.01 gauss/m at the equator (Telford et al., 1990) and thus can largely be ignored. The mag.f code produces ASCII text files of corrected magnetic data ready for interpretation by transformation or modeling. This data are commonly called total-field magnetic anomaly data.

4.3. MAGNETIC INTERPRETATION

After magnetic data are acquired and subsequently reduced, it is possible to transform or carry out modeling to explain the distribution of the data as to its relation to the crustal sources. Figure 4.9 summarizes the interpretation workflow completed or attempted for this study. Although, all methods of interpretation are not commonly used for any one particular study, it was attempted in this work to better understand magnetic potential fields.

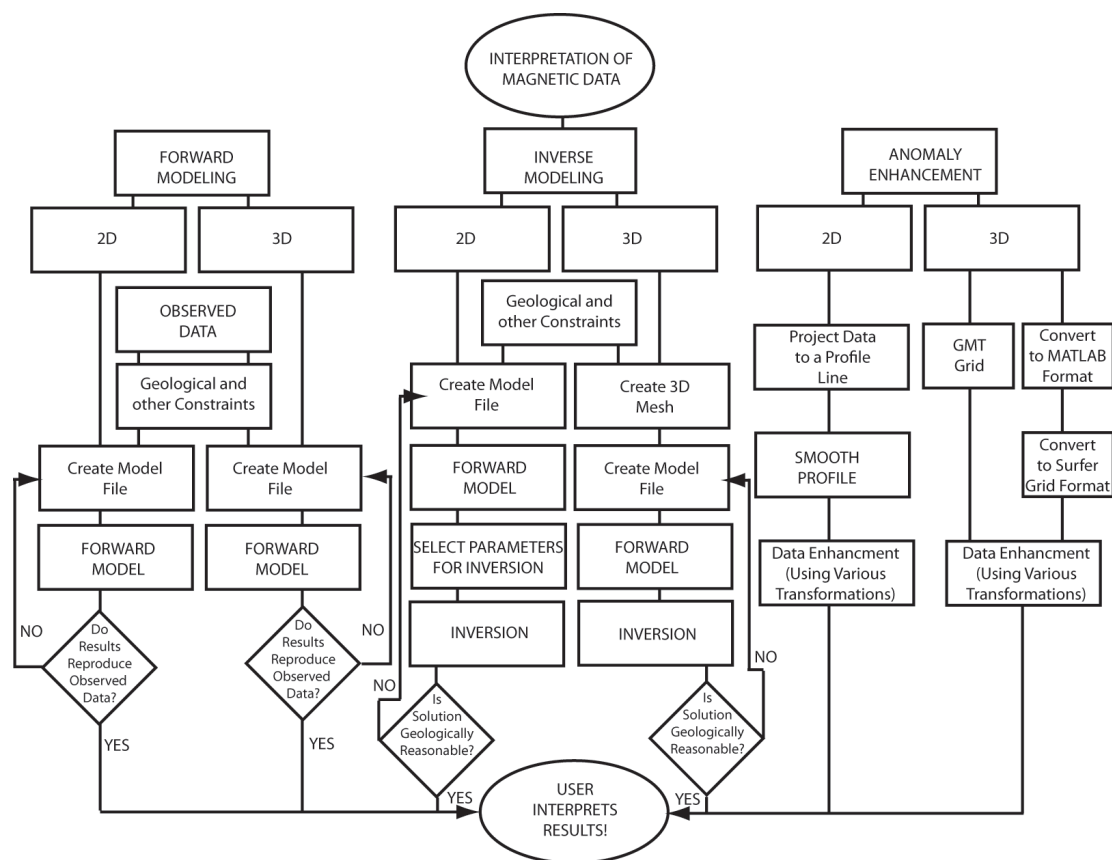


Figure 4.9. Magnetic interpretation workflow used in this study.

4.4. ANOMALY ENHANCEMENT

Anomaly enhancements generally can be applied to aid interpreting of any potential field such as gravity or magnetic. Transformations do not change the data only its form enabling easier interpretation. These transformations are typically applied to total-field magnetic anomaly data. The most often used transformations are wavelength filtering, polynomial trend-surfaces, continuation, directional derivatives, reduction to the pole (RTP), pseudogravity and analytic signal. Lastly, RTP and analytic signal will have their own subsections due to their importance in this work..

Upward continuation (UC) is a commonly used transformation. The concept was thoroughly explored by Henderson and Zietz (1949). The most common uses of the UC transformation is to match aeromagnetic datasets flown at different heights and as a filter to remove surface effects, or magnetic noise (e.g. common with ground surveys). This process moves the observation plane of a dataset further from the source to match another dataset collected at a higher elevation or altitude as though they were collected at same altitude thereby creating continuity between the two different datasets. According to Blakley (1995), a potential field can be calculated at any point within a region from the behavior of the field on a surface enclosing the region. No knowledge is required about the sources of the field, except that none may be located within the region. Basically the measured magnetization at a point can be recalculated at another spatial point relative to the source as long as that new point is not within the source itself. The original point must lie in a measured surface (e.g. plane) directly associated with source. A level surface to level surface UC is common when working with aeromagnetic data. The conditions for this transformation are that observation plane has to be horizontal with respect to the ground (source) and the continued plane some distance higher and parallel to the observation plane. The calculations for an uneven surface to level surface are a bit more complicated than the simple case above. Ground surveys will incorporate this type of UC to remove magnetic noise and bring out deeper structures and requires an inversion problem followed by a forward calculation procedure (Blakely, 1995). This method would also work for an uneven surface to uneven surface UC. The complementary transformation is a downward continuation but due to inherent stability problems in the calculations this transformation is not commonly used.

Directional derivatives are useful for finding trends and boundaries in potential field sources. Many magnetic interpretation programs solve for horizontal or vertical derivatives in the Fourier domain. The observations must be on a horizontal plane or UC to a horizontal plane. The following equations are for the x and y horizontal derivatives

$$\begin{aligned}\hat{f}\left[\frac{d^n\phi}{dx^n}\right] &= (ik_x)^n \hat{f}[\phi], \\ \hat{f}\left[\frac{d^n\phi}{dy^n}\right] &= (ik_y)^n \hat{f}[\phi],\end{aligned}\tag{4,5}$$

where \hat{f} is the Fourier transform, f is the potential field data (e.g. nT), n is the order of the derivative (e.g. $n=1$ is the first derivative), $I = \sqrt{-1}$ and k is the wave number.

Similarly the vertical derivative can be found by the following equation:

$$\hat{f}\left[\frac{\partial^n\phi}{\partial z^n}\right] = [k]^n \hat{f}[\phi]\tag{6}$$

notation is the same as horizontal derivatives. Blakely (1995) specifically mentions that the second vertical derivative helps resolve or accentuate shallow structures. Directional derivatives help to discerning edges and resolve any structural trend that may exist in the dataset.

4.4.1. Reduction to Pole. The reduction-to-pole or RTP transformation is typically the first to be applied to total-field magnetic anomaly data. Due to the dipolar nature of magnetic fields, the observed anomalies are often offset from the causative magnetic body. This is true for every place on Earth except the magnetic poles where all the magnetic force is vertical. The RTP transformation's goal is to reproduce the vertical directed magnetic field at other places throughout the world. This makes the interpretation much easier for the analyst. This is completed by rotating the magnetic

vector to a vertical position from a given declination and inclination. One of the first complications of this method is the presence of remnant magnetizing field directing the magnetic vector away from the inducing field direction. If the magnetization direction and strength can be obtained, this is not an issue.

Barnov (1957) introduced this method and its numerical calculation (Barnov and Naudy, 1964). This method causes anomalies of a few nT disappear at the same time enhancing the significant anomalies and make them appear more symmetric. Barnov and Naudy (1964) mentions the remanent magnetism issue briefly. The frequency domain operator is (Cooper and Cowan, 2005):

$$A'(u,v) = \frac{A(u,v)}{(\sin\theta + i\cos\theta\sin(\phi + \alpha))^2} \quad (7)$$

where $A(u,v)$ is the amplitude of the frequencies (u,v) , q and f are the geomagnetic inclination and declination, respectively and a is $\tan^{-1}(u,v)$. One problem with the above operator is that q and f must remain constant throughout the area being transformed. In regional studies, this can create problems. One way to get around this problem is to calculate the RTP at each grid point (Cooper and Cowan, 2005). If it is the case that variations of the field parameters are small, then the average of the perturbations can be used in an iterative algorithm that allows the crustal magnetism to vary continuously over a plane in the frequency domain (Arkani-Hamed, 1988). Cooper and Cowan (2005) introduces a method that this can be done in the space domain. They used the following Taylor series expansion:

$$RTP_{var} = RTP_{mean} + \Delta inc \frac{\partial RTP}{\partial inc} + 0.5\Delta inc^2 \frac{\partial^2 RTP}{\partial inc^2} + \Delta dec \frac{\partial RTP}{\partial dec} + 0.5\Delta dec^2 \frac{\partial^2 RTP}{\partial dec^2} + \dots \quad (8)$$

where RTP_{mean} is the data reduced to pole using the average geomagnetic field inclination and declination, Δinc is the difference between the inclination at a given point and the average inclination and Δdec is calculated similarly. The derivatives are calculated in the space domain. Cooper and Cowan (2005) have shown that the first two terms of the Taylor series is needed for an acceptable solution but this is dependent on the complexity of the field area. Another problem with the general RTP frequency domain operator is the case when the geomagnetic inclination (q) approaches zero causing a singularity. This is called the low latitude problem of the RTP. Li (2008) provides an excellent review of the subject and the methods proposed to solve this problem. In the frequency domain, Li (2008) provides a RTP operator in polar coordinates:

$$R(r,\theta) = R(\theta) = \frac{1}{[\sin(I) + i\cos(I)\cos(D - \theta)]^2} \quad (9)$$

where I and D are the inclination and declination of the geomagnetic field and q is the wavenumber direction. In the above equation, if I is zero or $D-q=+/-90$, either condition will result in the equation becoming singular. According to Li (2008), any inclination below 20 can be referred to as low latitude (RTP-L).

Macleoud et al., (1993), Macleoud et al.,(1993b) and Grant and Dodds (1972) addressed this problem by introducing a second inclination I' , that is used to control the amplitude of the operator at low latitudes

$$R(r,\theta) = R(\theta) = \frac{1}{[\sin(I') + i\cos(I)\cos(D - \theta)]^2} \quad (10)$$

I' is typically set to a higher inclination than the true inclination and selected by using the smallest values that produce acceptable results. More correction is needed with increasing presence or remanence.

The RTP-L algorithm of Phillips (1997) uses a azimuthal filter that smoothly tapers the RTP operator within a $\pm \beta$ relative to the direction of the inclination by the following:

$$S(\theta) = \sin^p \left(\frac{\pi |\theta - D \pm 90|}{2\beta} \right) \quad (11)$$

where p is the exponential power parameter that determines the falloff of the taper and in practice has a marginal effect on the RTP result.

Hansen and Pawlowski (1989) offer another approach to the RTP-L problem by utilizing a Weiner filter. This filter specifically attacks the declination parallel artifacts caused by the amplification of noise in the RTP operator. If we integrate the Weiner filter into the RTP, the following equation is the result:

$$W(k_x, k_y) = \frac{R^*(k_x, k_y)}{R^*(k_x, k_y)R(k_x, k_y) + \frac{N^2}{S^2(k_x, k_y)}} \quad (12)$$

where $R^*(k_x, k_y)$ is the complex conjugate of the routine RTP operator and $R(k_x, k_y) = R(\mathbf{q})$ (Li, 2008) and N^2 is the noise power. This filter does not account for the amplification of the noise in the declination direction; it only removes it. The energy-balance technique of Keating and Zerbo (1996) does. This method automates the estimation of the signal-to-noise ratio power ratio and by assuming noise is fractal when the power ratio is constant for all wavenumbers. The analysis angle (\mathbf{b}) and the analysis

radius (h as a percentage of the Nyquist wavenumber k_n) need to be specified by the user. Of the above four methods, Li (2008) argues that the energy-balance method with a fractal noise assumption is the best RTP-L operator. He suggests that fractal noise is a better approximation for real datasets than white noise used by the other filters.

Lastly, an inversion based RTP-L method has been introduced (Li and Oldenburg, 2001) that utilizes the wavenumber domain. It calculates the magnetic field at arbitrary magnetic latitudes from the vertical field at the pole is treated as the forward modeling process. This allows the RTP to be a simple inverse problem that can be solved by regularization. The solution to the inverse problem is found by minimizing a model global objective that imposes flatness and a desired spectral decay on the Fourier transform of the RTP field.

4.4.2. Analytic Signals and Total Derivative. The analytic signals method was introduced by Nabighian (1972) for two dimensional bodies. The only assumption is the bodies have uniform magnetization. This transformation creates a peak around the edges of the causative body. A simple assumption for the 2D case is that this causative body can be represented as a polygon. The analytic signal is based on the vertical and horizontal derivatives that are a potential function and a Hilbert transform pair. He also shows that in the 2D case, the transform is totally independent of magnetization direction. This means that remnant magnetism will not affect the transform unlike the RTP transform. Nabighan (1984) extends his ideas toward the 3D case where the horizontal derivative is replaced with two derivatives orthogonal to one another and includes the vertical derivative. It is important to realize that the above transformations are complex or vector quantities. Li (2006) points out a general misconception in the literature

regarding the analytic signal starting with Roest et al. (1992). Nabighian (1984) define the 3D analytic signal as:

$$A(x,y) = \left(\frac{\partial M}{\partial x} \hat{x} + \frac{\partial M}{\partial y} \hat{y} + i \frac{\partial M}{\partial z} \hat{z} \right) \quad (13)$$

where M is the potential field anomaly. Roest et al. (1992) point out that the above equation satisfies the requirement of a Hilbert transform pair. It is also important to note that the vertical derivative can be calculated when two orthogonal horizontal derivatives are known. They further introduce another transform called the 3D amplitude function.

This function is based on the above equation and is as follows:

$$|A(x,y)| = \sqrt{\left(\frac{\partial M}{\partial x}\right)^2 + \left(\frac{\partial M}{\partial y}\right)^2 + \left(\frac{\partial M}{\partial z}\right)^2} \quad (14)$$

This function has been mistakenly called the 3D analytic signal many times in the literature since its introduction instead of the correct, amplitude of the analytic signal or more commonly total derivative. Roest et al. (1992) make another mistake by stating that their 3-D analytic signal is not affected by magnetization direction. This is only true in the case of vertical contacts. According to Li (2006), assuming vertical contacts reduced the problem to the same as the 2D case. The amplitude of the analytic signal (from now on, called total derivative) has been used to calculate depth to sources and edge detection. In 2D case, the assumption for calculating analytic signal is that the observation plane is horizontal and for the 3D case a horizontal plane. When the observation plane (or horizontal) is not horizontal, the depth estimates fail considerably. Hsu et al. (1996) proposed an enhanced analytic signal method for depth determination that is largely independent of magnetization direction. The assumptions that this method requires can be quite unreasonable in a geologic sense such as the bottom surfaces of the bodies are

infinite and vertical contacts. The amplitude of the enhanced AS can be calculated for the n 'th derivative by the following:

$$|A_n(x,y)| = \sqrt{\left(\frac{\partial^n M}{\partial x^n}\right)^2 + \left(\frac{\partial^n M}{\partial y^n}\right)^2 + \left(\frac{\partial^n M}{\partial z^n}\right)^2} \quad (15)$$

Hsu et al. (1996) method calculates depth by using the ratio of the maximum total derivative to the maximum amplitude of the enhanced AS to the 2nd order

$$d = \sqrt{2} \times \frac{\sqrt{|A(x,y)|_{\max}}}{\sqrt{|A_2(x,y)|_{\max}}} \quad (16)$$

It is important to note that like the total derivative - amplitude of the enhanced AS method is dependent on the inclination and therefore has some sensitivity of the magnetization direction. The amplitude of the enhanced AS becomes smaller closer to the equator or when the body strikes parallel to magnetic north. Debeglia and Corpel. (1997) and Salem et al. (2002) also use ratios of the amplitude of the enhanced AS to calculate depth although their methods are slightly different. Another way to think about the total derivative, is that is the envelope of all the given profiles for all inclinations. It is this very property that Haney et al. (2003) examined the influence of magnetization of 3D sources on their resultant AS envelopes. This method also validates that the AS of 2D sources are not affected by magnetization direction. They demonstrate with their modeling the significance that magnetization direction has on total derivative and that a significant part of the asymmetry of the envelope can be removed by doing a half reduction to pole. A half reduction to pole can be done by using the known Earth's geomagnetic field in the RTP operator (the same as assuming no remanent magnetism is present).

4.5. FORWARD MODELING

Magnetic and gravity data are measurements of a potential field. These fields are a certain parameter over space and time. The physical parameter for magnetic data are mostly magnetic susceptibility in the case of the induced component of the total magnetic vector and in the case of gravity anomalies, density is the causative parameter. Forces can be expressed as fields (e.g. F for gravity and B for magnetics). It is possible to describe these fields as a vector and scalar. This description creates what is called field lines, which are lines of equal force. In magnetics, we call these flux lines. These could also be visualized as equipotential surfaces. It is possible to model these fields using a forward technique where the analyst has *a priori* information about the causative body and inversion modeling where *a priori* information is not needed.

The forward method is commonly completed in three steps. A causative body is at first modeled based on knowledge of the geology and geophysical intuition. Next, the anomaly of the body is calculated and compared with the anomaly of the observed data. Lastly, body parameters are changed to better fit the observed data and the process starts over until a satisfactory match is obtained between the predicted anomaly of the model and the observed data. Forward methods are necessary in most inversion algorithms as part of the iterative process to calculate misfit between the observed model and the model derived from inversion. Forward modeling can be explained best by starting with simple causative bodies such as a sphere. Talwani et al. (1959) developed a 2-D approach to forward modeling. The method works similar for both magnetics and gravity. I will use gravity as an example. Magnetic and gravity anomalies produced by different causative bodies sum together to produce the observed anomalies we

measured. Each body (e.g. gravity) has its own density, volume and depth. In a 2D sense we can approximate these as arbitrary shaped polygons. In the case for a sphere, it can have more mass or less mass than the surrounding medium. From a given observation point P , the gravitational effect on point P :

$$g = \frac{G(\Delta m)}{r^2} \quad (17)$$

where r is the distance from observation point P , Δm is the change in mass and G is the universal gravitational constant. In the case of gravity, density (ρ) is the most important parameter and thus defined as mass (m) per unit volume (V). The change in mass (Δm) is given by:

$$\Delta m = (\Delta \rho)V \quad (18)$$

After factoring in the volume (V) of the sphere, the equation becomes

$$\Delta g = \frac{4\pi R^3 G(\Delta \rho)}{3} \frac{1}{(x^2 + z^2)} \quad (19)$$

where Δg is the magnitude of the total attraction of the sphere at point P . Since we only want the vertical component, the same as what a gravimeter would measure we need to change the equation one more time to:

$$\Delta g_z = \frac{4\pi R^3 G(\Delta \rho)}{3} \frac{z}{(x^2 + z^2)^{3/2}} \quad (20)$$

where Δg_z is the anomaly in mGal produced by a sphere. This is a simple example of how forward modeling is done. In a practical problem we need to be able to do the same for any amount of arbitrary shaped polygons.

Instead of using a volume of a causative body, the surface integral will be used. This essentially treats each point on a surface as the causative body rather than using the central point inside the causative body. Both results are comparable. This method assumes that that the causative bodies have uniform density and susceptibility. So written in the form of the surface integral, the gravity and magnetic anomaly is given by:

$$\begin{aligned} B &= -\frac{1}{4\pi} \nabla_0 \int \frac{1}{r} \mathbf{J} \cdot \mathbf{n} \, ds \\ F &= -G\rho \int \frac{1}{r} \mathbf{a} \cdot \mathbf{n} \, ds \end{aligned} \quad (21,22)$$

where \mathbf{B} is the magnetic flux density, \mathbf{F} is the gravitational field, \mathbf{G} is the gravitational constant, \mathbf{X} is the gradient at a source point and r is the distance between source point and observation point \mathbf{P} (Coggon, 1976). Coggon transforms the x,y,z coordinate system to the u,v,w coordinate system to correspond with each face. \mathbf{V} is normal to the face, \mathbf{w} is positive in the down direction and \mathbf{u} is positive in the x direction thus the face lies in the $\mathbf{u-w}$ plane. The following equations relates the x,y,z coordinates to the u,w,z coordinates.

$$\begin{aligned} u &= x \cos \delta - y \sin \delta \\ v &= x \sin \delta \cos \psi - y \cos \delta \cos \psi + z \sin \psi \\ w &= -x \sin \delta \sin \psi - y \cos \delta \sin \psi + z \cos \psi \end{aligned} \quad (23,24,25)$$

For the contribution of one face of the polygon to the observed anomaly, the above equation is changed to:

$$\begin{aligned} B &= -\frac{1}{4\pi} \nabla_0 \int \frac{1}{r} J_u \, du \, dw \\ F &= -G\rho \int \frac{1}{r} \, du \, dw \end{aligned} \quad (26,27)$$

Solving the above integrals for magnetics and the vertical gravity, the following expressions for A are:

$$\begin{aligned}
A_{uu} &= -\sin \phi \cdot \cos \phi \cdot l_1 + \sin^2 \phi \cdot t_1 \\
A_{uv} &= -\sin \phi \cdot l_2 \\
A_{uw} &= -\sin^2 \phi \cdot l_1 - \sin \phi \cdot \cos \phi \cdot t_1 \\
A_{vu} &= A_{uv} \\
A_{vv} &= -t_2 \\
A_{vw} &= \cos \phi \cdot l_2 - l_3 \\
A_{wu} &= A_{uw} \\
A_{wv} &= A_{vw} \\
A_{ww} &= \sin \phi \cdot \cos \phi \cdot l_1 + \cos^2 \phi \cdot t_1 - t_3 \\
A_w &= -\alpha \cdot A_{wu} - \beta \cdot A_{wv} - \gamma \cdot A_{ww}
\end{aligned} \tag{28-37}$$

where:

$$\begin{aligned}
\alpha &= u - u_0, \beta = v - v_0, \gamma = w - w_0 \\
r &= (\alpha^2 + \beta^2 + \gamma^2)^{1/2}, T = 1/r \\
l_1 &= \ln(r - \beta) \\
l_2 &= \ln[r - (\gamma \cdot \sin \phi + \alpha \cdot \cos \phi)] \\
l_3 &= \ln(r - \alpha) \\
t_1 &= \text{arc tan} \left[\frac{\beta(\gamma \cdot \sin \phi + \alpha \cdot \cos \phi)}{r(\gamma \cdot \cos \phi - \alpha \cdot \sin \phi)} \right] \\
t_2 &= \text{arc tan} \left[\frac{\beta^2 \cdot \cos \phi + \gamma(\gamma \cdot \cos \phi - \alpha \cdot \sin \phi)}{-\beta \cdot r \cdot \sin \phi} \right] \\
t_3 &= \text{arc tan} \left[\frac{\alpha \cdot \beta}{\gamma \cdot r} \right]
\end{aligned} \tag{38-45}$$

The A expressions can directly replace the appropriate A^* variable below to extract the corresponding components of the magnetic field and vertical gravity.

$$\begin{aligned}
Bu &= \frac{1}{4\pi} J_v A_{uv}^* \\
Bv &= \frac{1}{4\pi} J_v A_{vv}^* \\
Bw &= \frac{1}{4\pi} J_v A_{wv}^* \\
Fu &= G\rho A_v^*
\end{aligned} \tag{46-49}$$

$$J_v = lJ_x + mJ_y + nJ_z \tag{50}$$

For each face of N sides, each A^* is given as the following sum:

$$A^* = \sum_{i=1}^N [A(u_i - u_0, v - v_0, w_i - w_0, \phi_i) - A(u_{i+1} - u_0, v - v_0, w_{i+1} - w_0, \phi_i)] \quad (51)$$

Again the subscripts of A^* correspond to those of A . Lastly, the components need to be converted back into their x, y, z coordinates using the equations below.

$$\begin{aligned} B_x &= B_u \cos \delta + B_v \sin \delta \cos \psi - B_w \sin \delta \sin \psi \\ B_y &= -B_u \sin \delta + B_v \cos \delta \cos \psi - B_w \cos \delta \sin \psi \\ B_z &= B_v \sin \psi + B_w \cos \psi \\ F_z &= F_v \sin \psi \end{aligned} \quad (52-55)$$

Singh and Gupta (2001) used the above formulas to write a MATLAB code to calculate the anomaly caused by an arbitrary polygon. The results are the same as much more computationally intensive modeling by volume. This method is used to produce the forward models of this study.

The forward modeling program used for the inversion algorithm uses volumes rather than faces to calculate magnetization. Below, the major differences of using volumes to forward model as compared to using faces is shown. In the case of susceptibilities typically found in Earth materials, the magnetization \vec{J} is proportional to the susceptibility as given in the following equation:

$$\vec{J} = \kappa \vec{H}_0 \quad (56)$$

where κ is susceptibility and \vec{H}_0 is the inducing magnetic field. \vec{H}_0 is equal to \vec{B}_0/μ_0 and \vec{B}_0 is the inducing field and μ_0 is the free space permeability. The following integral, with a dyadic Green's function, yields the anomalous field produced by the distribution of magnetization \vec{J} :

$$\vec{B}_a(\vec{r}) = \frac{\mu_0}{4\pi} \int_V \nabla \nabla \frac{1}{|\vec{r} - \vec{r}'|} \cdot \vec{J} dv. \quad (57)$$

where \vec{r} is the position of the observation point. V is the volume of the magnetization. This method divides the subsurface into discrete cubes and assigns a susceptibility to each of these volumes. Important for this method is that the subsurface model must be larger than the anomaly of interest to account for outside contributions or sources. It is important to remember that objects smaller than the cube size cannot be images. Lastly, increasing the resolution, by using smaller cubes increases the computational effort therefore these factors have to be balanced. The above location is valid for observation locations above the Earth's surface.

Using the assumption that the susceptibility in each cube is constant, the above equation can be written in matrix form:

$$\begin{aligned}\vec{B}_a &= \mu_0 \begin{pmatrix} T_{11} & T_{12} & T_{13} \\ T_{21} & T_{22} & T_{23} \\ T_{31} & T_{32} & T_{33} \end{pmatrix} \kappa \vec{H}_0 \\ &\equiv \mu_0 \kappa T \vec{H}_0\end{aligned}\tag{58}$$

where T_{ij} is given by

$$T_{ij} = \frac{1}{4\pi} \int_V \frac{\partial}{\partial x_i} \frac{\partial}{\partial x_j} \frac{1}{|\vec{r} - \vec{r}'|} dv, \quad i=1,3; j=1,3\tag{59}$$

where x_1 , x_2 , and x_3 represent x , y , and z , respectively. The expressions for T_{ij} for a cuboidal source can be found in Bhattacharyya (1964) and Sharma (1966) and will not be derived here. The matrix T is symmetric and its trace equal to -1 when the observation point falls in the cube and 0 when outside. Only 5 independent elements need to be calculated. Once T is calculated, the magnetic anomaly \vec{B}_a and its projection onto any direction of measurement is easily obtained by the inner product with the directional vector.

4.6. EFFECT OF MAGNETIC REMENANCE ON MODELING

Magnetic remanence may have a significant effect on modeling magnetic sources in certain regions. This effect is much more pronounced on inversion modeling than forward calculations. Recalling that permanent magnetization moves the measured vector from the Earth's inducing field to that of a sum of the two sources. Thus the measured total field or gradient can be significantly altered by the remnant component. Figure 4.10 shows the same polyhedron modeled with and without remnant magnetism. It is easily apparent this effect would have on an inversion algorithm as the two field appears as though they are from totally different bodies.

Morris et al. (2007) shows that Konigsberger ratios between 0.1 and 10 have the greatest effect on the total magnetic vector. Values greater than 10 essentially overwhelms the induced component and the effective magnetic vector aligns itself approximately in the same direction of the permanent magnetization field while Konigsberger ratios below 0.1 are dominated by the induced vector due to the lack of significant permanent magnetization. In continental settings, most authors except the latter case and assume significant magnetic remanence is not present in their study area and model their data. Recent works has shown this may no longer be an acceptable assumption in some tectonic situations. Morris et al. (2001) modeled E-W striking dike that was vertically orientated. They forward modeled a dike with varying remanence and fixing all other parameters. Their test revealed that the total anomaly calculated, would yield a dike with a varying dip. Here remanence totally changes the account of the inversion not to mention considerably changes the amplitude of the total magnetic

anomaly along the length of the dike. Remanence adds to the ambiguity or non-uniqueness problem that plagues potential field modeling.

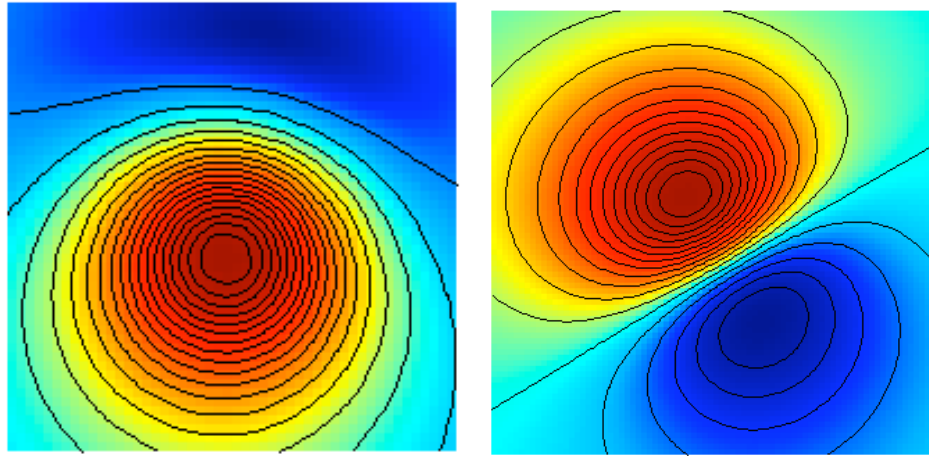


Figure 4.10. The effects of RM on a simple polyhedron. Left: A simple polyhedron modeled with inclination (Inc) of 70 degrees and declination (Dec) of 10 degrees in a 50,000 nT inducing field with no RM. Right: Same parameters as left figure except with the addition of a 5.0 A/m magnetization with a Rem. Inc of 10 degrees and Rem. Dec of 150 degrees.

Forward modeling by itself is usually not an issue as forward algorithms such as the one in the SAKI (Webring, 1985) package or the commonly used one by Singh and Gupta (2001) account for remanent magnetism as long as it is known and the user can supply it to the algorithm. The analyst needs to know if remanent magnetism is significant in their study area, and if multiple magnetization directions are possible (e.g. examination of more than one anomaly). There are three methods commonly used get around these inherent problems when working in a study area with $Q > 0.1$.

If the magnetization vector is known, this information can be supplied to the inversion algorithm and satisfactory results obtained. There have been several methods demonstrated in the literature to find remnant magnetization direction. The most obvious one of course is to collect orientated samples and measure the remanence and direction. This process can be expensive and collecting enough samples to represent the bulk area may not be possible (Morris et al., 2007; Shearer and Li, 2004). Another possibility is to use apparent polar wandering paths (APWP) if the age of the rock producing the anomaly is known. APWPs have been well studied and reliable catalogued up to 500 Ma for most continental regions (Morris et al., 2007).

Some Precambrian areas (e.g. the Canadian Shield) have been well studied too. Once the age of the magnetic producing body is measured or estimated, the appropriate APWP can be selected and provided a well-grounded estimate of the remnant magnetization vector of the anomaly. Dutra and Marangoni (2009) have successfully used this method in their study of an alkaline complex in Brazil.

Helbig's method was introduced by Lourenco and Morrison (1973), further refined by Phillips (2005), is based on the magnetic dipole moment by Helbig (1962) and the integral relations between the moments of a magnetic anomaly (Li et al., 2010). This method assumes a constant source direction throughout the anomalous body and produced by a compact body (Li et al., 2010). Three vectors are produced in which the inclination and declination can easily be found. The three orthogonal direction vectors are found by the following integrals,

$$\int_{-\infty}^{\infty} \int_{-\infty}^{\infty} xB_z(x,y)dx dy = -2\pi m_x,$$

$$\int_{-\infty}^{\infty} \int_{-\infty}^{\infty} yB_z(x,y)dx dy = -2\pi m_y,$$

$$\int_{-\infty}^{\infty} \int_{-\infty}^{\infty} xB_x(x,y)dx dy = -2\pi m_z, \quad (60,61,62)$$

where B_x , B_y , and B_z are the x, y, and z components of the magnetic anomaly (Li et al., 2010). This method can be problematic at low magnetic latitudes due to a half-reduction-pole is needed. A plus is that surveys are now being conducted that measure the three vector directions directly. This is especially more common recently in borehole measurements.

Haney and Li (2002) introduced a method for estimating magnetization direction by using multiscale edges of an anomaly derived from a continuous wavelet transform. This method only works in two directions and thus utilizes profiles. It utilizes two profiles orthogonal to one another in a N-S direction and E-W direction. An apparent inclination can be obtained from each profile. Using vector math, the inclination can be found using these two apparent inclinations.

Dannemiller and Li (2004, 2006) proposed a 3D method of using cross correlation between the vertical gradient and the total gradient of the RTP total magnetic field to find the magnetization direction. This is an extension of the 2D cross correlation method of Roest and Pilkington (1993) that used total gradient and pseudo-gravity. This method relies on the asymmetric nature of the vertical gradient and the RTP field and the total gradient of the same field. The cross correlation should be the greatest between the two fields when the correct inclination and declination used for the RTP calculation. It should be apparent that this method has additional difficulties for low magnetic surveys. Li et al.

(2010) has an excellent comparison between the Helbig's moment, wavelet multiscale edge and cross correlation methods using synthetic data and found that all three produced consistent and reliable estimates of magnetization direction. These methods are limited to single anomalies or more as long as all anomalies had the same magnetization direction.

For cases when more than one magnetization direction is present, estimating the individual magnetization direction may become impractical. Another possibility is to use magnetic transforms that are independent of magnetization direction or nearly so. If the forward modeling algorithm was changed to calculate the transformed quantity, effective susceptibility could be recovered. Paine et al. (2001) proposes a method using the analytic signal of the vertical integral (ASVI) and the vertical integral of the analytic signal (VIAS) transforms. These are applied to total magnetic anomaly data and have little relationship to magnetization direction. Of interest, they use the MAG3D (Li and Oldenburg, 1996) which inverts for susceptibility. The units for total anomaly are nT, while the units for the analytic signal transform is nT/m. The problem with most commonly used inversion algorithms such as MAG3D (Li and Oldenburg, 1996, 2003) is the forward modeling component. The authors acknowledge that ideally the forward modeling code of MAG3D should be changed but this is not possible due to MAG3D not being open code. Taking the vertical integral of the analytic signal transformations yields data in a form more consistent with total anomaly. These can be inverted to a certain degree using the traditional inversion algorithms. Paine et al. (2001) results using ASVI and VIAS, although better than inverting total magnetic anomaly data with remanence only produces marginal plausible geologic structures. According to Shearer and Li(2004) there are a number of theoretical difficulties associated with this method.

Shearer (2005) and Shearer and Li (2004) advanced Paine et al.'s (2001) ideas further using the total anomaly and total derivative transforms. They also create a forward modeling algorithm to fit their transformations. Their transformations are largely independent of magnetization direction and it is important to note that at this date, no one has found a 3D quantity that is totally independent of magnetization direction (Shearer and Li, 2004). Completing a half-reduction-to-pole and a subsequent total derivative transformation from total magnetic anomaly data that is directly inverted yields positive results. Shearer (2005), using synthetic models, suggest that the total amplitude transformation produced better results than the total gradient. She suggested this is due to the loss of low frequency content in the total gradient data. Total amplitude or amplitude of the anomalous magnetic field is defined as:

$$\begin{aligned} B &= \|\vec{B}_a\| \\ &= \sqrt{B_x^2 + B_y^2 + B_z^2} \end{aligned} \quad (63)$$

where B_x , B_y , and B_z are the three components of the magnetic field in a three dimensional Cartesian coordinate system (Shearer, 2005). The total gradient also erroneously known as 3d analytic signal is defined as

$$\begin{aligned} g &= \|\nabla B\| \\ &= \sqrt{\left(\frac{\partial B}{\partial x}\right)^2 + \left(\frac{\partial B}{\partial y}\right)^2 + \left(\frac{\partial B}{\partial z}\right)^2} \end{aligned} \quad (64)$$

where B is any given component of the total anomaly field (e.g. vertical anomaly) (Shearer, 2005). In the forward modeling routine of the inversion algorithm, Shearer (2005) implicitly assumes a nominal magnetization direction which is arbitrary and minimally affects the outcome of the forward modeling. The inversion scheme is similar,

for the most part to that of Li and Oldenburg (1996, 2003) except the use of three sensitivity matrices used for the forward modeling part instead of one. Again, it is important to point out the necessity of an assumed magnetization direction to facilitate the forward modeling part but it has little effect on the inversion. The obvious advantage for this method is little knowledge of the remnant magnetization is needed to successfully invert several anomalies at once, even with different magnetization directions.

The Shearer and Li (2004) method has its weaknesses as pointed out by Lelievre and Oldenburg (2009). Some error is introduced by the assumed magnetization direction in the forward modeling part. If the total gradient data was calculated instead of measured in the field with a gradiometer, significant error may be introduced into the inversion. They instead invert for a three-component subsurface magnetization vector instead of the scalar magnetic susceptibility parameter. The total magnetic vector (TMV) method is approached in a Cartesian framework and spherical formulation. This is done by changing the forward modeling part of the Li and Oldenburg (1996) inversion algorithm. The Cartesian formulation splits the magnetization into one component parallel to the Earth's field and two components perpendicular to the Earth's field. The three orthogonal directions, \hat{p} , \hat{s} , and \hat{t} with \hat{p} in the direction of the earth's field. Each cell has a vector \mathbf{m} called the Earth model vector and contains the three component of magnetization as shown

$$\mathbf{m} = [p, s, t]^T \quad (65)$$

where $\mathbf{p}=[p_1, \dots, p_m]$ and \mathbf{M} has length $3M$. This forward model works in units of effective susceptibility by dividing the three magnetization components by the amplitude of the Earth's inducing field \mathbf{H}_0 . For any j 'th cell the magnetization can be written as

$$\vec{J}_j = H_0 (p_j \hat{p} + s_j \hat{s} + t_j \hat{t}) \quad (66)$$

and the predicted data are calculated as

$$d^{pred} = G_p p + G_s s + G_t t. \quad (67)$$

The above equation can be simplified as

$$d^{pred} = G_{pst} m \quad (68)$$

where $G_{pst} = [G_p, G_s, G_t]$ (Lelievre and Oldenburg, 2009). In the spherical formulation, the Earth model vector has two angles and amplitude in each cell:

$$m = [a, \theta, \phi]^T \quad (69)$$

Lelievre and Oldenburg(2009) define the following Cartesian axes with + x northing, + y easting, and + z as down

$$\begin{aligned} \vec{u} &= J_x, \\ \vec{v} &= J_y, \\ \vec{w} &= J_z \end{aligned} \quad (70,71,72)$$

The following trigonometric expressions determine the Cartesian magnetization componets in the j 'th cell:

$$\begin{aligned} u_j &= a_j \cos(\theta_j) \cos(\phi_j), \\ v_j &= a_j \cos(\theta_j) \sin(\phi_j), \\ w_j &= a_j \sin(\theta_j) \end{aligned} \quad (73,74,75)$$

Like the Cartesian formulation the amplitude is used as an effective susceptibility.

Predicted data are calculated as

$$d^{pred} = G_u u + G_v v + G_w w. \quad (76)$$

The above equation is related to the sensitivity matrixes and simplified which yields

$$d^{pred} = G_{uvw} m \quad (77)$$

by defining

$$k = [u, v, w]^T \quad (78)$$

and

$G_{uvw} = [G_u, G_v, G_w]$. (Lelievre and Oldenburg, 2009).

4.7. GRAVITY SURVEY

Gravity data were also collected during the two winter field campaigns and processed by Kevin Mickus and his graduate students from Missouri State University. A brief methodology is prudent here for his work. A Lacoste and Romberg, model G gravimeter, on loan from the National Geospatial Imaging and Mapping Agency (NGA), was used to collect data. The position and elevation data for each station were determined by differential correction GPS methods with a Topcon GB-1000 dual frequency receiver. Positional data were collected for 15-20 minutes at each station. This data were corrected using GPS base stations ran by Eric Calais of Purdue University. The final positional accuracy was between 0.1 and 1.5 m for all stations.

Meter drift was corrected by using a local base station located at the Semera Aquater geothermal camp. This local station was tied to the absolute gravity station in Logia, part of the ISGN71 network. Using this base station allows for the data sets for both field campaigns to be merged together into one dataset along with additional data provided by the Ethiopian Geologic Survey and data from Aquater. The field data were corrected for Free-Air and Bouguer gravity corrections. The elevation data (recorded as ellipsoidal heights) were corrected to geoidal heights using a geoid created by NGA. A datum of mean sea level was used as a base for these elevations. A 2.67 gm/cc density

was used as a reduction density for the Bouguer gravity anomaly corrections. Lastly, terrain corrections were calculated using the 3D terrain correction algorithm from Oasis Montaj and a 90-m digital elevation model (DEM).

5. RESULTS

5.1. PROFILES

Inspection of the high resolution magnetic profiles perpendicular to strike of the Tendaho Graben (TG) suggests major linear magnetic bodies striking parallel with the major NW-SE structural elements of the area (Figures 5.1, 5.2, 5.3 and 5.4).

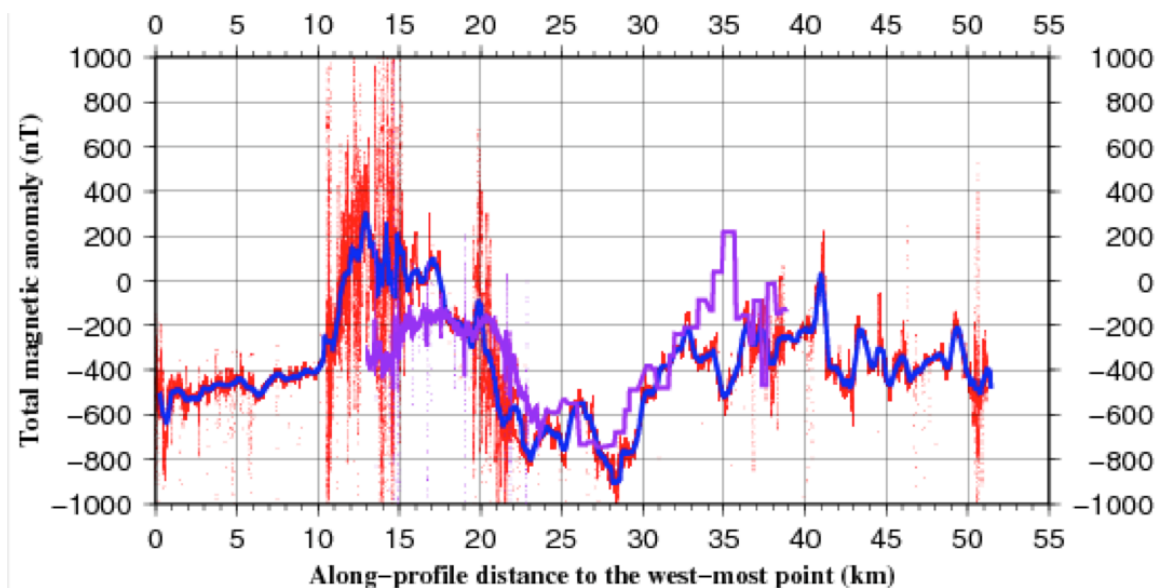


Figure 5.1. High density magnetic profiles across the Tendaho Graben. Red profiles are corrected data from the main profile, blue profiles are the data after smoothing to remove surface noise effects and the purple profile is the shorter south profile.

The central part of the TG is characterized by a 10 km wide magnetic trough, which exhibits a narrow zone (~3 km) of a relatively elevated magnetic anomaly that coincides with a linear region of hydrothermal activity (Figure 3.1) and follows the rift axis. Magnetic profiles from the 1980 Aquater data, provided by A. Alemu, exhibits the same characteristics (Figures 5.2, 5.3 and 5.4).

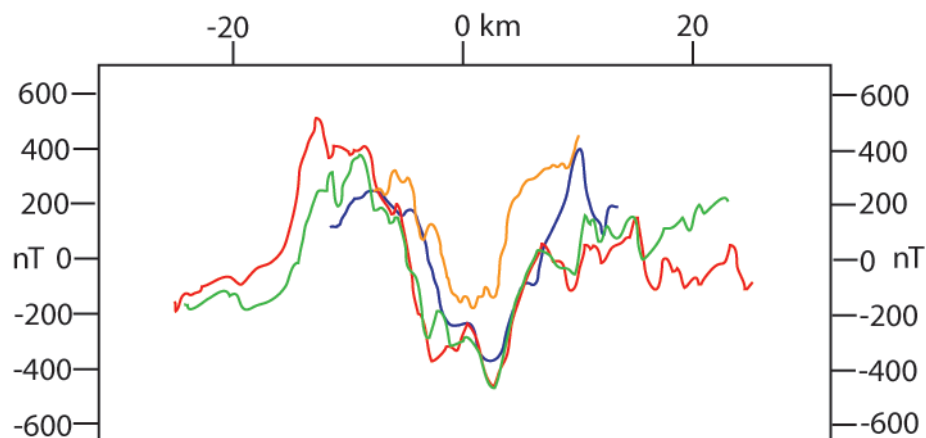


Figure 5.2. The main and south high density magnetic profiles (red and blue, respectively) plotted with magnetic profiles from the Aquater data (orange and green). The orange profile is referred to as the north profile in the text.

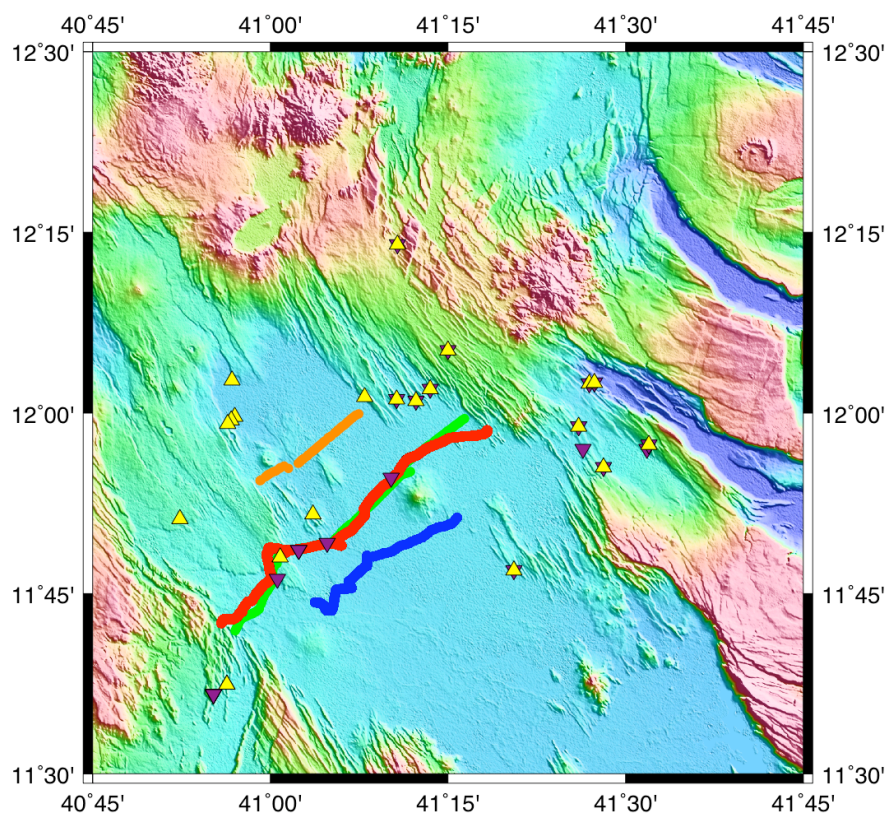


Figure 5.3. SRTM map of the Tendaho Graben with the magnetic profile lines plotted in corresponding colors to those of Figure 5.2. The purple inverted triangles are paleomagnetic sample locations (Kidane et al., 2003 and Acton et al., 2000), yellow triangles are geochronology sample locations (Kidane et al., 2003 and Lahitte et al., 2003).

5.2. 2D DATA

The Ayrobeara geothermal field is located near the known NW extant of the Dubti Fault structure (Figure 3.1) and associated hydrothermal activity. This area was used as a test for the 2D mapping abilities of the G859 magnetometer. Several profiles of total-magnetic field data were collected across the geothermal area (Figure 5.4). A narrow linear magnetic high (> 0 nT) was found surrounded symmetrically by significant magnetic lows < 1200 nT.

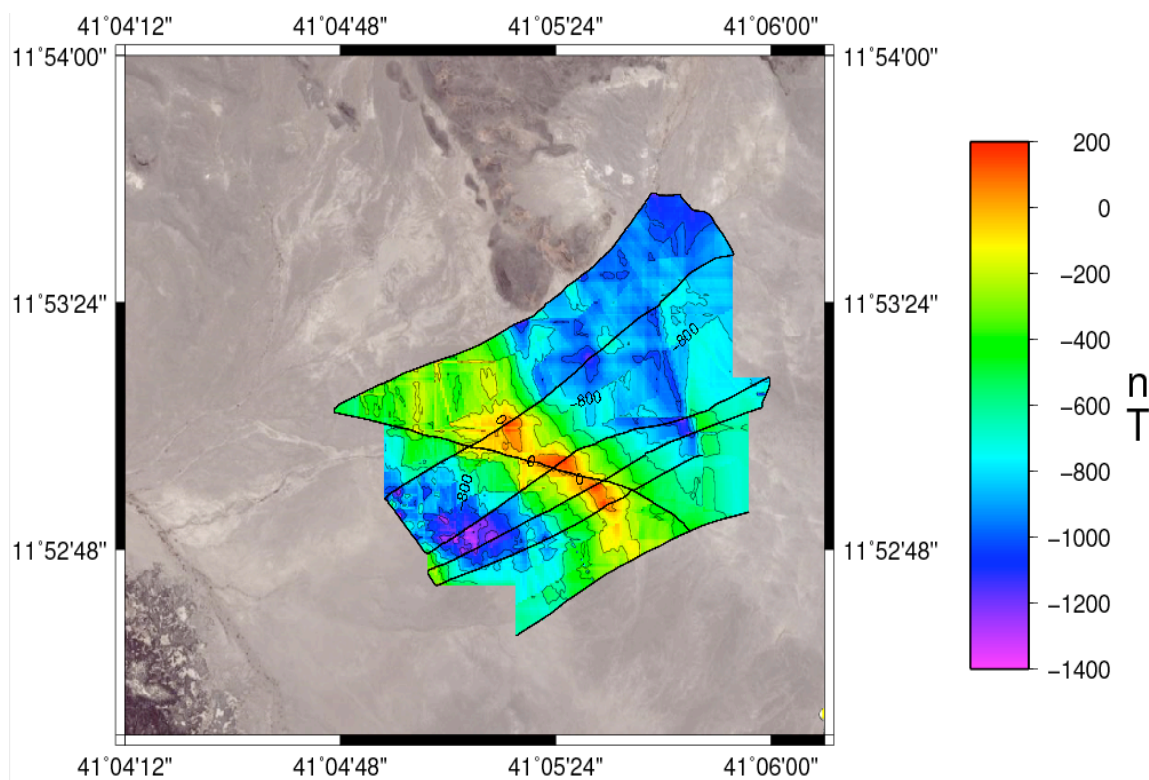


Figure 5.4. Total-field magnetic anomaly map of the Ayrobeara geothermal field. Black lines represent data locations. Contour interval is 200 nT.

A short, 20 station gravity profile, was measured across the Ayrobera geothermal field (Figure 5.5). It reveals a significant gravity low over a short horizontal distance. A low of ~ -55 mGal is found in the center of the area with symmetrical shoulders of ~ -51 mGal (Figure 5.6). This area also coincides with the small magnetic high that is present within the main rift axis trough (Figures 5.4 and 5.5).

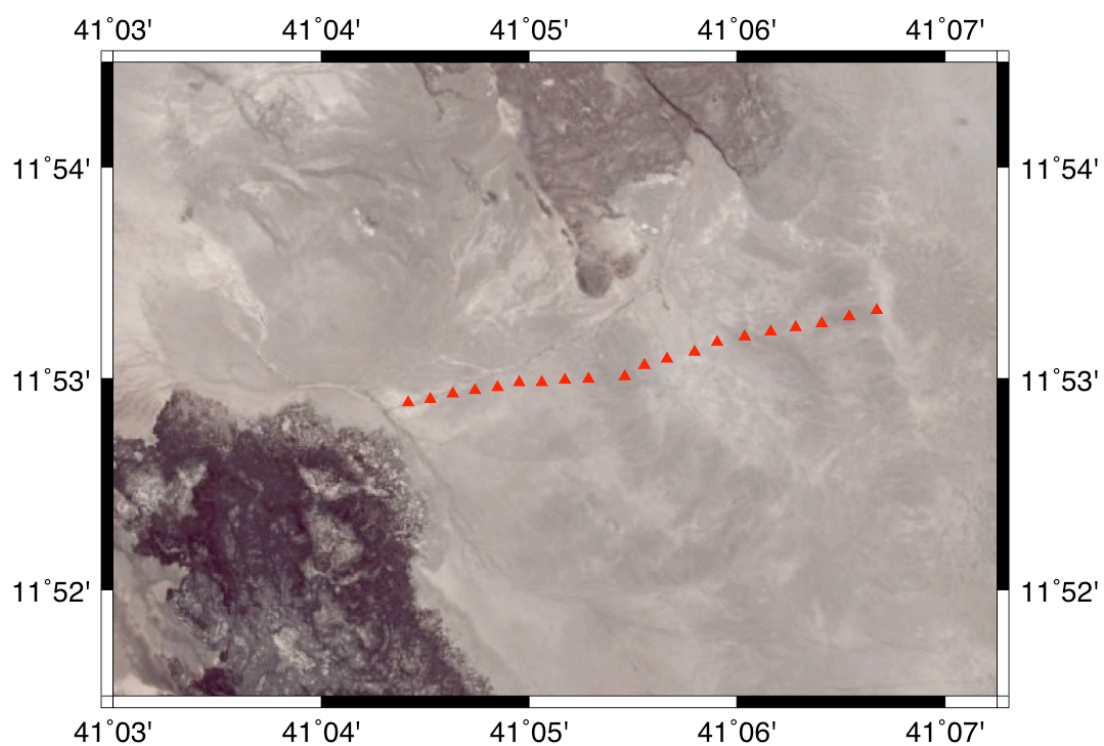


Figure 5.5. Ayrobera geothermal field gravity stations marked by red triangles.

Ayrobeara Geothermal Field

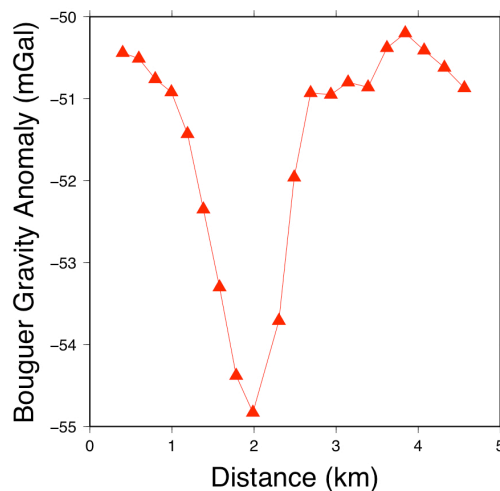


Figure 5.6. Bouguer gravity anomaly profile W-E across the Ayrobeara geothermal field. Red triangles are readings recorded at each station.

5.3. ANOMALY ENHANCEMENT

The three most useful transformations utilized for this study are the analytic signal, total gradient and directional derivative. The constant lithology, mainly basalt, of the TG and its footwalls, makes the interpretation of our study difficult in some cases. Typically the derivatives are useful for finding structures based on different lithologies or susceptibilities; however, in our study area, differences are most likely related to differences in the magnetization of the basalts.

The main profile reduction-to-pole (RTP) (Figure 5.7), nicely delineates the areas of positive and reversed polarity centered over their causative bodies. It is also important to note that magnetization direction does not influence RTP transformations of profile data. A 10 km wide peak of normal polarity dominates the central part of the graben. This could be the result of abundant diking occurring along the central axis of the TG. Another possibility is a significant increase in the susceptibility along the graben axis;

however, this is not likely as forward modeling shows that the remnant component of the observed total anomaly is much greater than the induced component that is dependent on susceptibility. Southwest of this magnetic high axis is 15 km wide zone of reverse polarity. A smaller 11 km wide reverse polarity zone is found to the NE of the central magnetic high axis. This zone exhibits a significantly less magnitude than the SW zone. The SW magnetic low zone is associated with the Semera Plateau which rises ~ 50 m above the surrounding sediment/lacustrine plain. Another possibility for the skewness between the reverse polarity shoulders is the $\sim 55^\circ$ azimuth of the profile (See Figure 5.3). These assumptions hold true in the case that central axis of the TG is behaving as a spreading center rather than the graben walls.

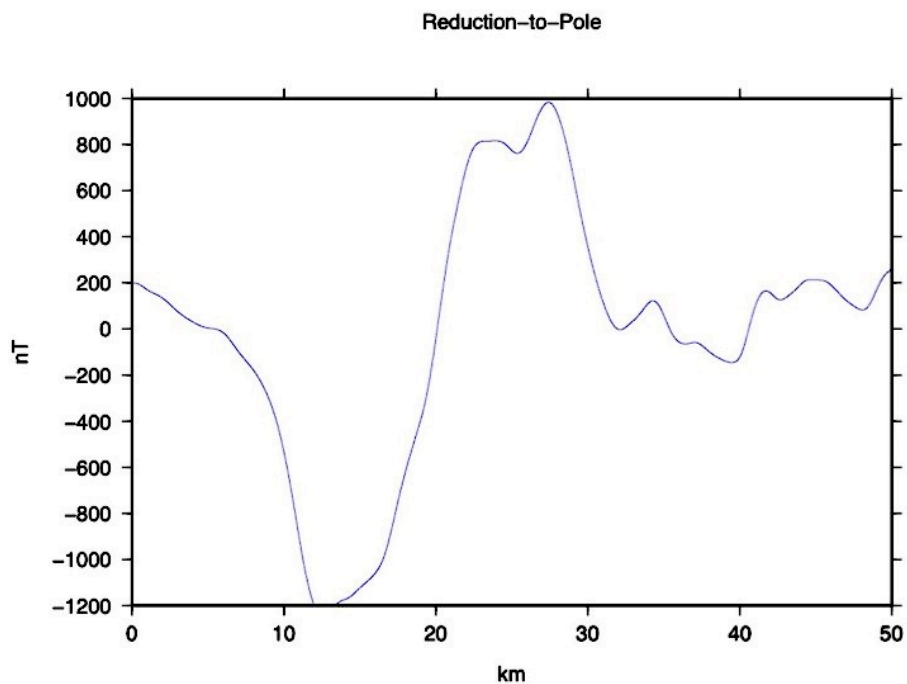


Figure 5.7. Reduction-to-pole of the main magnetic profile.

Analytic signals are commonly used as an edge detector with magnetic data. The edge can be a susceptibility, lithology or magnetization contrast caused by the presence of a body and/or structure. The analytic signals illustrates the contrasts between the large magnetic low possibly associated with the normal diking and two buried bodies to the NW centered around 37 and 45 km (Figure 5.8). These bodies are likely associated with the Karub Volcano. The local minima at ~ 26 km can be associated with local heat flow along the central axis of the graben and/or a fault. Aquater field work in the 70's and 80's located such a fault in drillholes. They also found high heat flow concentrated along this fault.

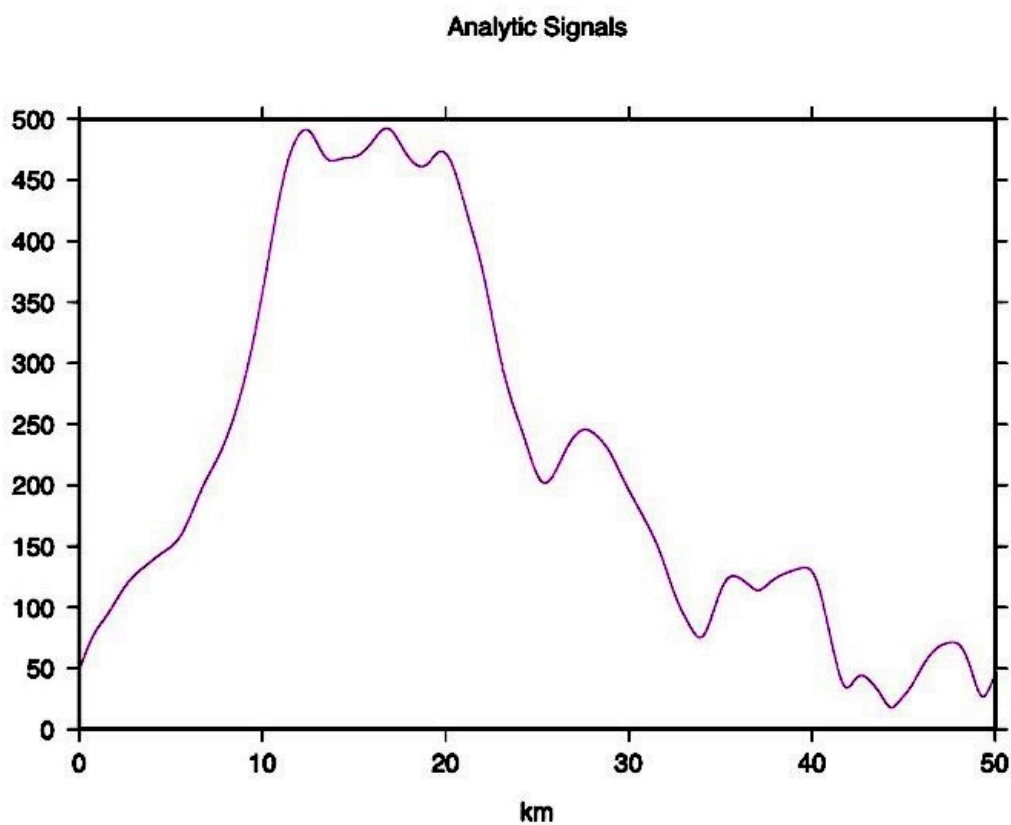


Figure 5.8. Analytic signals of the main magnetic profile.

Similar to the reduction-to-pole operator, total gradient (amplitude of the analytic signal) centers the peaks above the causative body (Figure 5.9). Unlike RTP, both positive and negative polarity anomalies are positive due to the square function in the transformation.

These enhancements have also been utilized in a spatial manner using the Aquater data. Despite the noise in the dataset, after upward continuing the data 500 m, the data cleaned up remarkably (Figure 5.10). This data was used for the subsequent transformations.

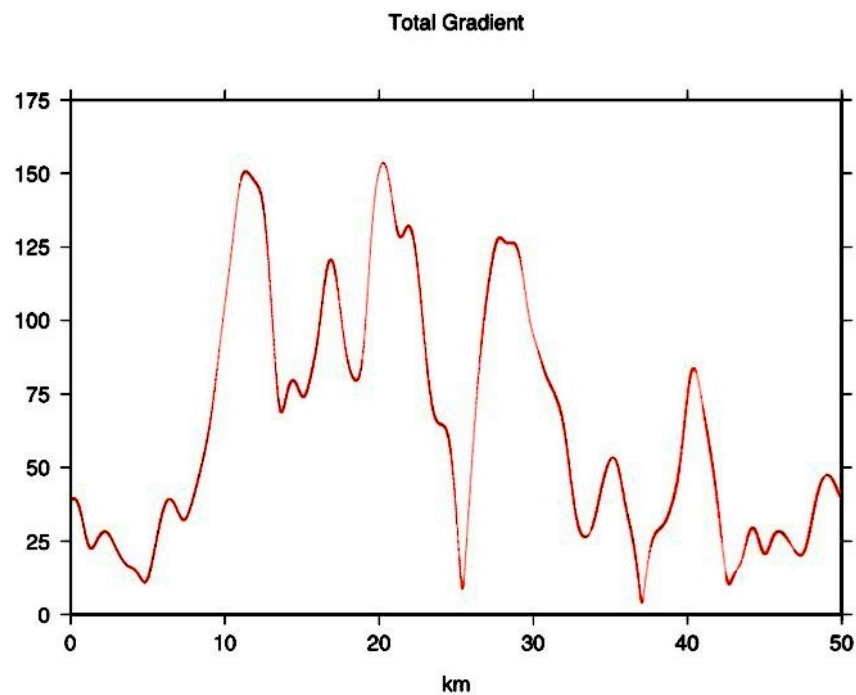


Figure 5.9. Total derivative or amplitude of the analytic signal of the main magnetic profile.

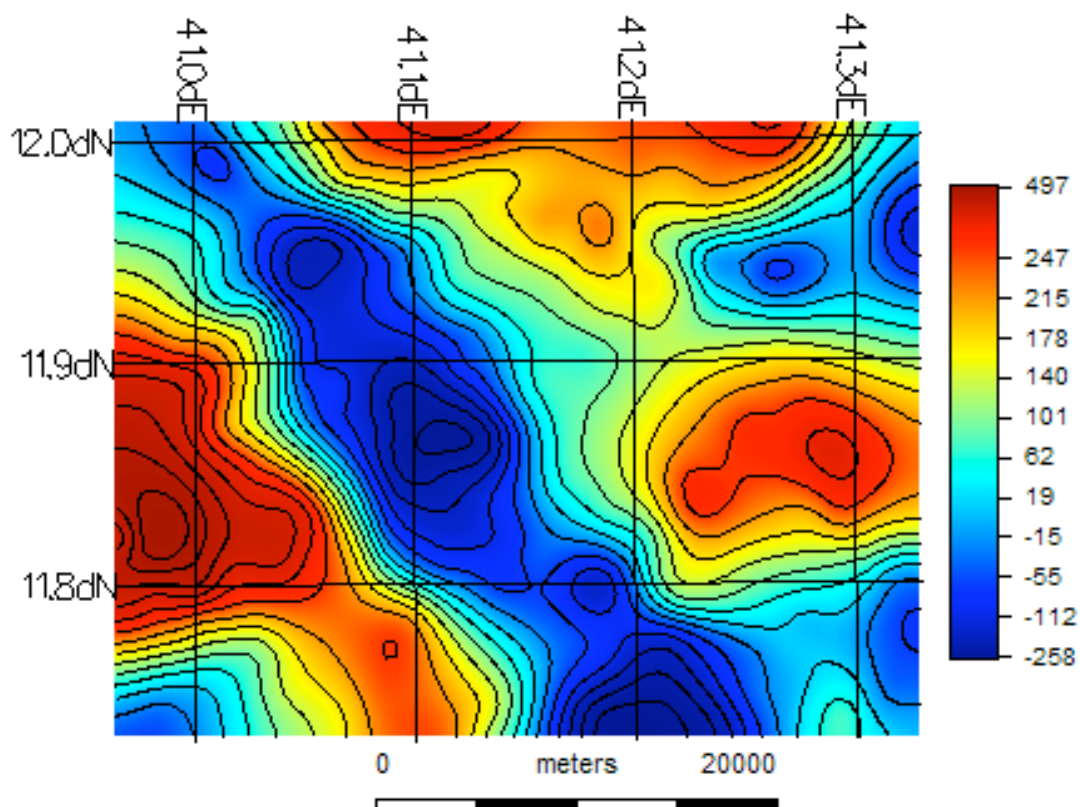


Figure 5.10. Total-field magnetic anomaly map of the study area that will be used to demonstrate subsequent anomaly transformations. The NW-SE trough of negative values corresponds to the main spreading axis of the Tendaho Graben between Semera and Karub Volcano (Figure 3.1). The units are nT (nanoTesla). The colorbar and geographic grid will be left off for easier viewing in Figures 5.11-5.13. Units will vary but the color blue will always represent more negative values (Figures 5.6 - 5.8). Contour interval is 40 nT.

Figure 5.11 illustrates the problem of the RTP operator at low latitudes. The anomalies are stretched out in the declination direction. Additionally, have significant magnetization that in some case differs significantly from that of the main field. RTP is practically useless in areas such as TG.

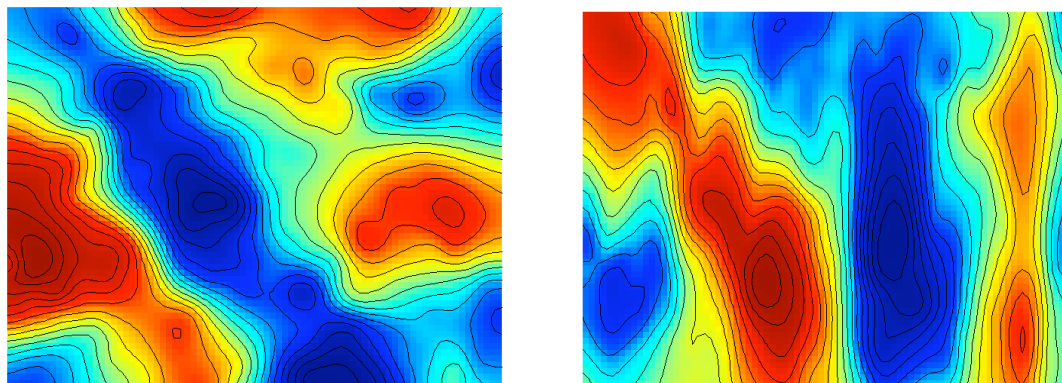


Figure 5.11. Reduction-to-pole of Aquater data. Left: Original data. Right: RTP-L still exhibiting elongation of features in the declination direction (2-degrees).

The structures in Afar and in particular the Tendaho Graben have well defined lineaments (NW-SW). Using directional derivative filters are useful for highlighting these structures. Figure 5.12 shows the results of a directional filter that was applied at an azimuth of 140° thus highlighting the magnetic features that follow the rift axis. The highest gradient follows the central rift axis.

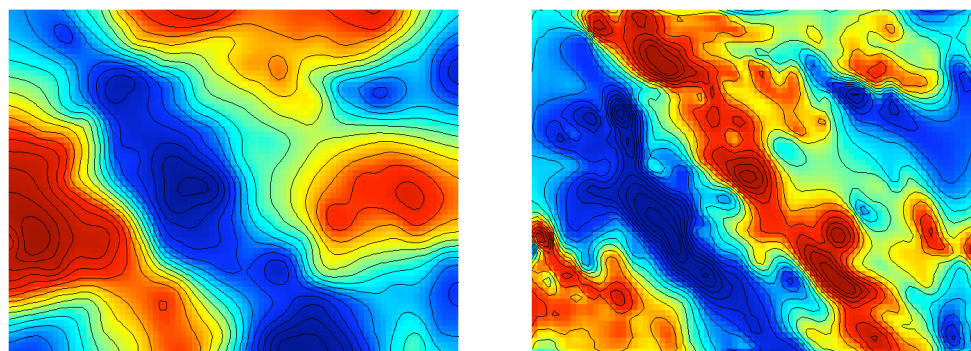


Figure 5.12. Directional derivative of Aquater data. Left: Original data. Right: Directional derivative at 50 degrees to highlight structures parallel to the Tendaho Graben.

Lastly, the total derivative transformation was tried because of its relative insensitivity to magnetization direction in order to move the anomalies over their causative sources. This transformation very well and clearly delineates the rift axis from its shoulders (Figure 5.13)

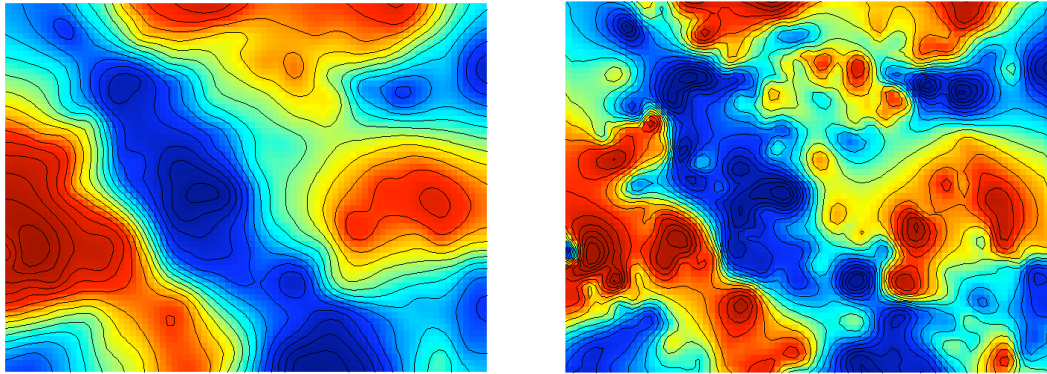


Figure 5.13. Total derivative of Aquater data. Left: Original data. Right: Total derivative.

5.4. FORWARD MODELING

Forward modeling of the total-field magnetic data is one method to explain the subsurface sources of the observed anomalies. For the TG area, one must include both the induced magnetic field and remnant magnetism (RM) in the model. A multitude of forward models using only induced magnetization were tried and none were able to even come close to reproducing the observed data.

One important parameter in the forward modeling is the presence of RM in the basalts of the TG. Although in most cases, RM is not a significant factor in most magnetic models, it can be significant in fine-grain rocks such as basalts that have a relatively high percentage of iron rich minerals such as magnetite and other ferromagnesian minerals. Typical oceanic basalt RM values have a mean of 8.6 A/m

(Courtilot et al., 1984). This can completely overprint the induced component and is the reason reverse polarity events are recorded in various lithologies is well documented. RM can be acquired many ways, however; igneous and some metamorphic rocks often acquire remanence by thermal cooling, also called natural remanence. This magnetization is usually permanent and is in the direction of the current geomagnetic field, of the ferric minerals as the temperature falls below the Curie temperature, typically 580 °C for magnetite. Rocks that are above the Curie temperature of the ferrous minerals that they contain, will not exhibit RM; this temperature depends on the principally on the chemical makeup of the magnetic minerals (Hunt et al., 1995). Thermal remanence can be reset by another heating event such as metamorphism. Remanence is most pronounced in small grain rocks such as basalts as compared to coarse grain gabbros (Hunt et al., 1995). RM more often than not decreases with age of the rocks as alteration, oxide development, and hydrothermal interactions react with the ferromagnesian minerals.

For the Afar Stratoid basalt, the range of RM intensity is between < 1 to 31 A/m with an average value of 4.65 A/m whereas the mean susceptibility in SI volume units is 0.02313 (Kidane et al., 1999). Parameters from Table 5.1 are used for the final forward models. The older Stratoid basalts were modeled with a RM intensity of 2.70 A/m and the younger axial rift volcanics with a RM of 5.70 A/m. These values are distributed similar to those observed over some oceanic spreading centers (Courtilot et al., 1984). The final forward model for the main profiles shows that a ~10 km wide stripe along the axis of the graben exhibits normal polarity (Figure 5.14). Larger shoulders of dominantly reverse polarity units surround the normal polarity strip.

Table 5.1 Final susceptibilities, remnant magnetization intensities, declinations and inclinations used for the Tendaho Graben forward model. Basalt susceptibility and remanent magnetization data are from Kidane (2003) and Acton (2000).

Unit	Suceptibility	Remnant (A/m)	Declination	Inclination
Sediments	0.00006	-	-	-
Fissure Basalts (N)	0.0230	2.70	1.46	16.8
Fissure Basalts (R)	0.0230	2.70	180	-14.4
Stratoid Basalts (R)	0.0230	2.70	175	-23
Recent Dikes (N)	0.0230	5.70	1.83	15
Upper Crust (R)	0.0126	2.00	169	-32.7

N=Normal Polarity R=Reverse Polarity

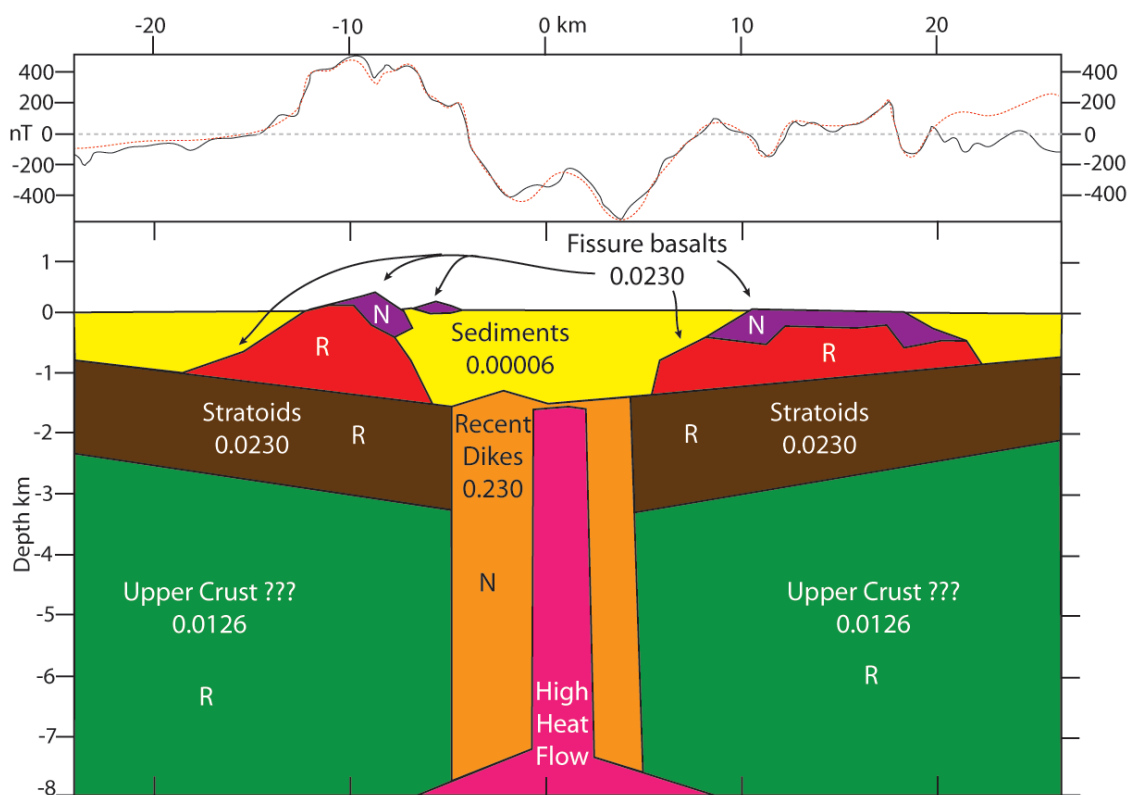


Figure 5.14. Main profile forward model across the Tendaho Graben. Above: Plot of observed total-field (black line) with calculated magnetic anomalies due to the model (red dashed).

An overly simplistic synthetic block model was created to validate the central diking interpretation (Figure 5.15). The large amplitude negative anomaly is the result of a ~ 10 km region of dominantly normal polarity intrusions and/or diking that is parallel to the rift axis. In equatorial regions, a normal polarity RM field roughly coupled with the inducing field produces a negative anomaly (Lillie, 1999). Conversely, reverse polarity RM, when overprinting the inducing field; will exhibit positive anomalies in equatorial regions (Lillie, 1999). The smaller area (~ 10 km) with respect to the dominant reversely polarized basalts suggests that the extensional rate of the TG is slowing. This simple model also explains the asymmetry of the reverse polarity shoulders due to profile azimuth.

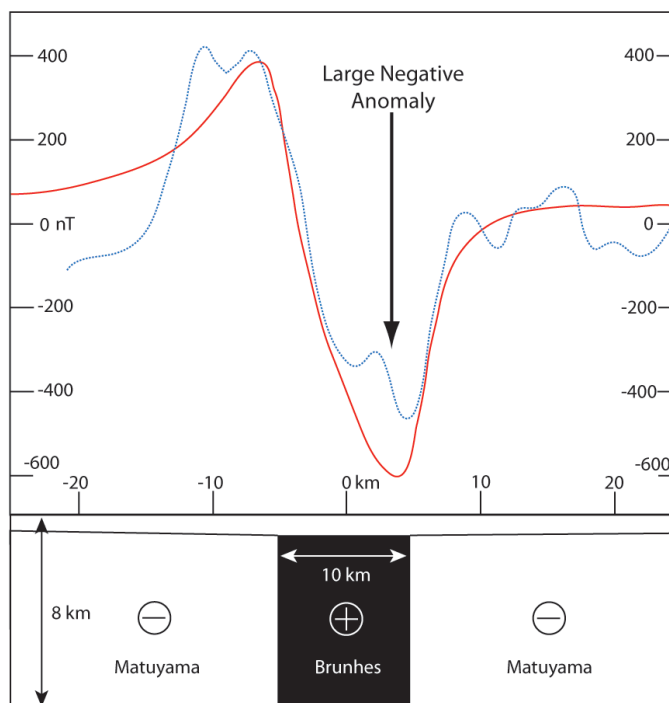


Figure 5.15. Simple block model that illustrates the significant role of magnetic polarity across the Tendaho Graben. Blue dashed line is the observed data and the red solid line is the model result. Matuyama and Brunhes are the last reversed and current magnetic chrons, respectively.

Two more profiles were modeled, one using the Aquater data for a north profile and the shorter high resolution profile for a south profile (Figures 5.2 and 53). Figures 5.16 & 5.17 show the results. The colors and corresponding susceptibilities are the same as those in Figure 5.14.

For the north profile, the amplitude of the anomalies are significantly less than those from the profiles to the south. The ~ 1 km wide of recent normal polarity diking is considerably less than then the 10 km width exhibited by the southern profiles. This suggests that the spreading rate is significantly slower or that this part of the magmatic segment is not currently active as compared to areas surrounding the two profiles to the south. It is likely in the transition between the active Dabbahu region just to the north and the active ridge axis in central and southern TG, that recent diking has not taken place.

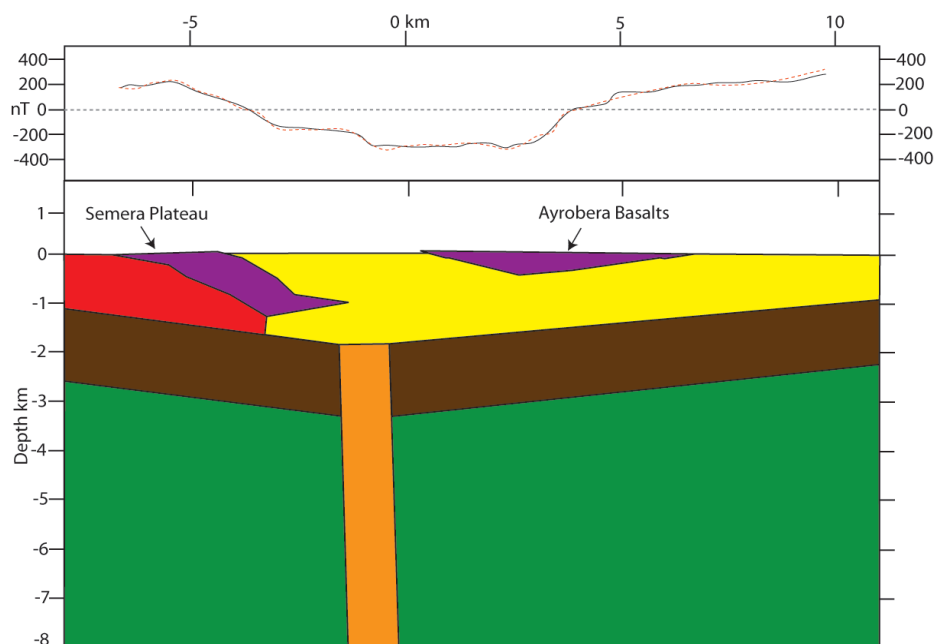


Figure 5.16. North forward modeled profile (Orange line on Figure 5.3). Colors and susceptibilities correspond to those of Figure 5.14. Black profile is observed data and red profile is predicted data.

The south profile exhibits a widening of the recent diiking area and a deepening of the lacustrine deposits. The lowering of the amplitude of the anomalies and increasing wavelengths support these observations. Based on other similar spreading centers found in Afar, this spreading segment likely extends further SE to the Dama 'Ali volcano near Lake Abhe. It should be noted that the recent basalts modeled interbedded in the lacustrine deposits could actually have many different spatial configurations and yield the same modeled data set. Despite their non-uniqueness, these interbedded basalts contribute little to deeper, longer wavelength structures.

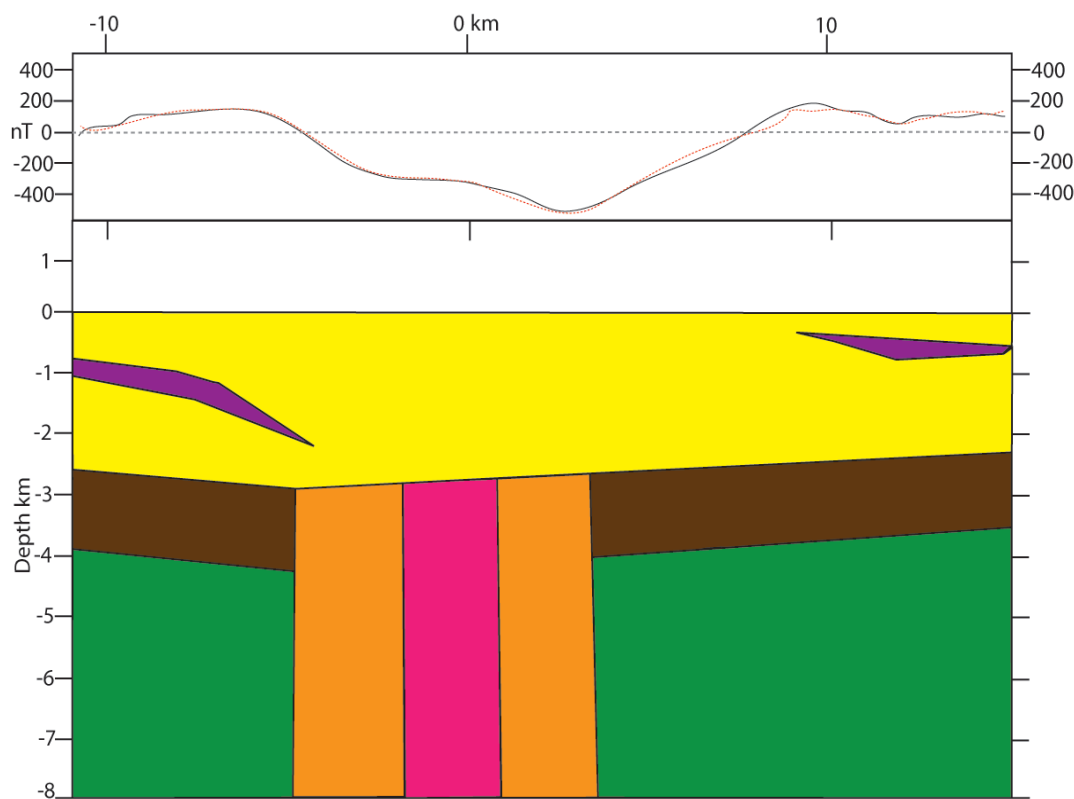


Figure 5.17. South forward modeled profile (Blue line on Figure 5.3). Colors and susceptibilities correspond to those of Figure 5.14. Black profile is observed data and red profile is predicted data.

5.5. GRAVITY SURVEY

A high-density Bouguer gravity anomaly profile was acquired that nearly coincides with the longer high resolution magnetic profile (Figures 5.3, 5.18 and 5.19). The gravity profile (Figure 5.19) shows a striking Bouguer gravity high in the center of TG, in spite of the fact that this part of the TG has the thickest lacustrine sediments, which would normally cause a Bouguer gravity anomaly low. Based on the magnetic data and other geophysical data, intrusion of denser mafic bodies could account for the observed Bouguer anomaly high. Forward modeling of the gravity profile, completed by Kevin Mickus with geological constraints provided by David Bridges, show that this gravity high can best be interpreted as an 8-10 km wide mafic body intruding along the central part of TG, a conclusion that is consistent with magnetic results (Figure 5.20).

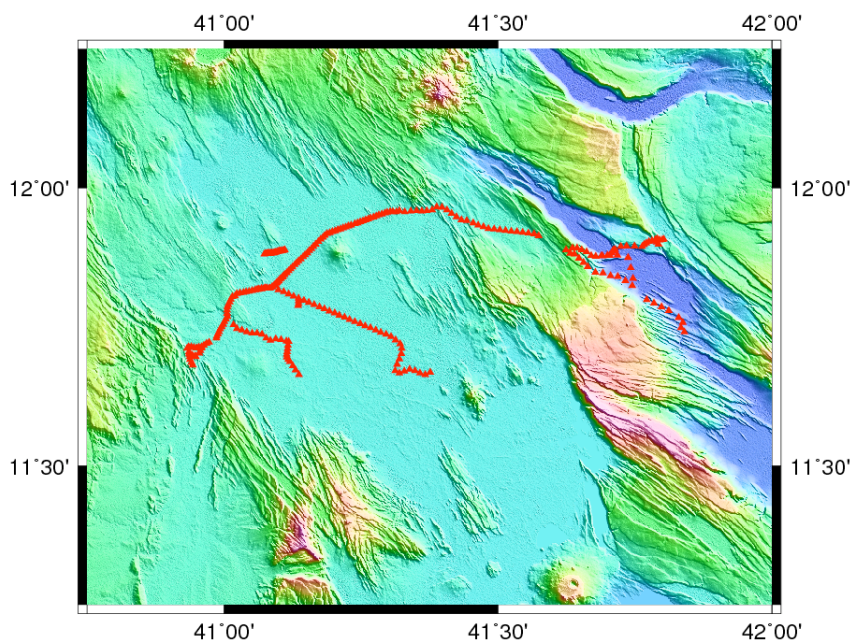


Figure 5.18. Gravity stations (red triangles) collected during the winter 2008 field campaign.

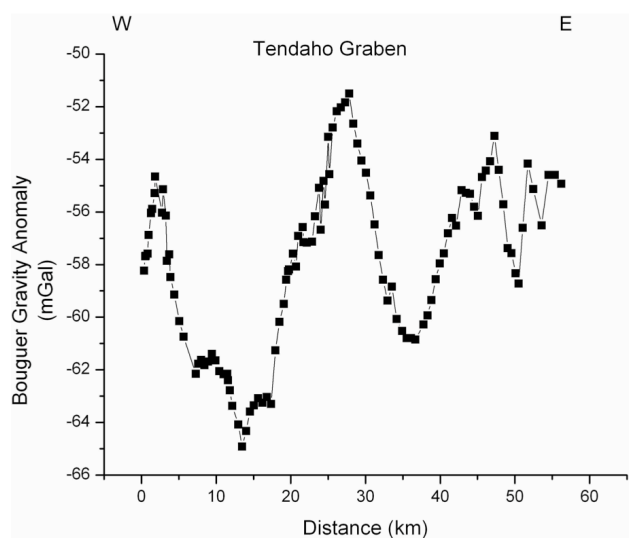


Figure 5.19. Profile of Bouguer gravity anomalies across the Tendaho Graben.

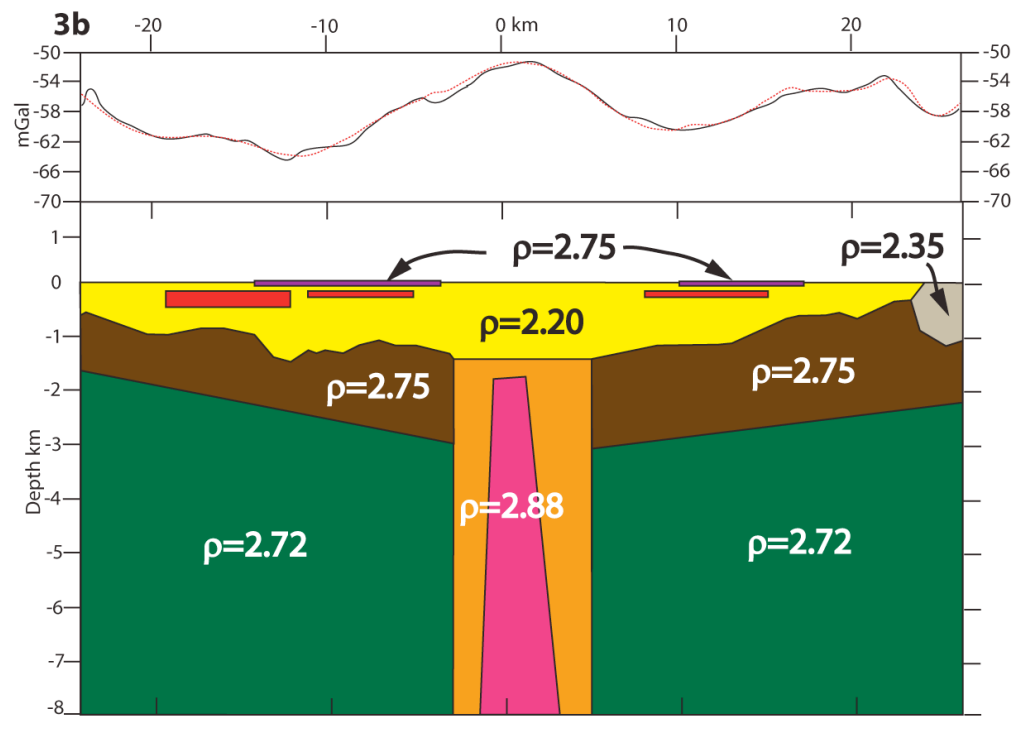


Figure 5.20. Forward model of the Bouguer gravity anomaly profile across the Tendaho Graben roughly coincident with the high resolution magnetic profile. The color scheme is the same as Figure 5.14 except the gray color represents rhyolite. Densities are gm/cc.

6. DISCUSSION

6.1 LINEAR MAGNETIC BODIES

The magnetic anomalies of the Tendaho Graben (TG) exhibit a geometry similar in dimension and magnitude to that observed from magnetic stripes of typical mid-ocean ridges and compare favorably with a nearby oceanic spreading center and its land version (Figure 6.1).

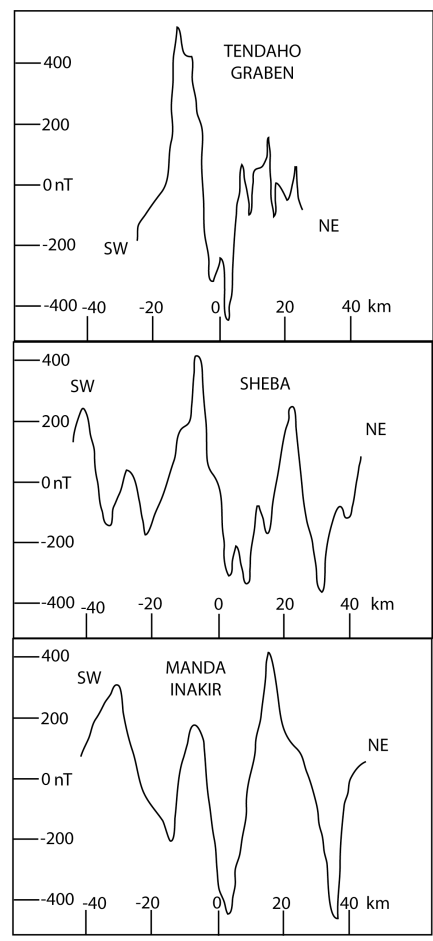


Figure 6.1. Comparison of the Tendaho Graben, Sheba oceanic spreading center and Manda Inakir Rift (Gulf of Aden propagator) magnetic profiles. Data for Sheba and Manda Inakir spreading centers are from Barberi and Varet (1977).

Applying a similar oceanic spreading geochronology technique to technique to the TG, it is possible to use the magnetic polarity changes to determine the mean spreading rate during the normal and reversed polarity periods. It is important to note that the spreading can be episodic or continuous and using magnetic geochronology produces a mean rather than an absolute extension rate. Based on the period of the present normal polarity chron (~ 0.78 km), a spreading rate of ~ 0.64 cm/yr is assumed using the 10 km width of dominantly normal polarity diking determined from forward modeling. From 1.8 Ma to 0.78 Ma, the geomagnetic field was dominantly reversed. Due to the much more heterogeneous nature of continental or transitional crust as compared to oceanic crust, the smaller chrons are likely to be lost in the high frequencies generated by shallow and surface features. To account for the ~ 50 km width of the TG, the spreading rate for this period has a mean of ~ 1.64 cm/yr. This agrees independently with Acocella et al. (2008) that the spreading rate of the Tendaho has drastically slowed since ~ 0.7 Ma.

The Bouguer gravity high coincides exactly with the magnetic trough (Figure 6.2). The gravity high is likely due to the active mafic diking along the current ridge axis in the last ~ 0.78 Ma. The high-resolution magnetic profiles provide a remarkable insight into the structure of the upper crust across the TG. The magnetic trough, that follows the ridge axis, exhibits a narrow 2-3 km zone of slightly elevated magnetic values that may be indicative of higher crustal heat flow.

These elevated magnetic anomalies also form a linear feature and was extensively surveyed in the Ayrobeara geothermal field. Aquater (1996a) argues for a nearly vertical fault that coincides with this zone called the Dubti Fault based on drillhole data (Aquater, 1996).

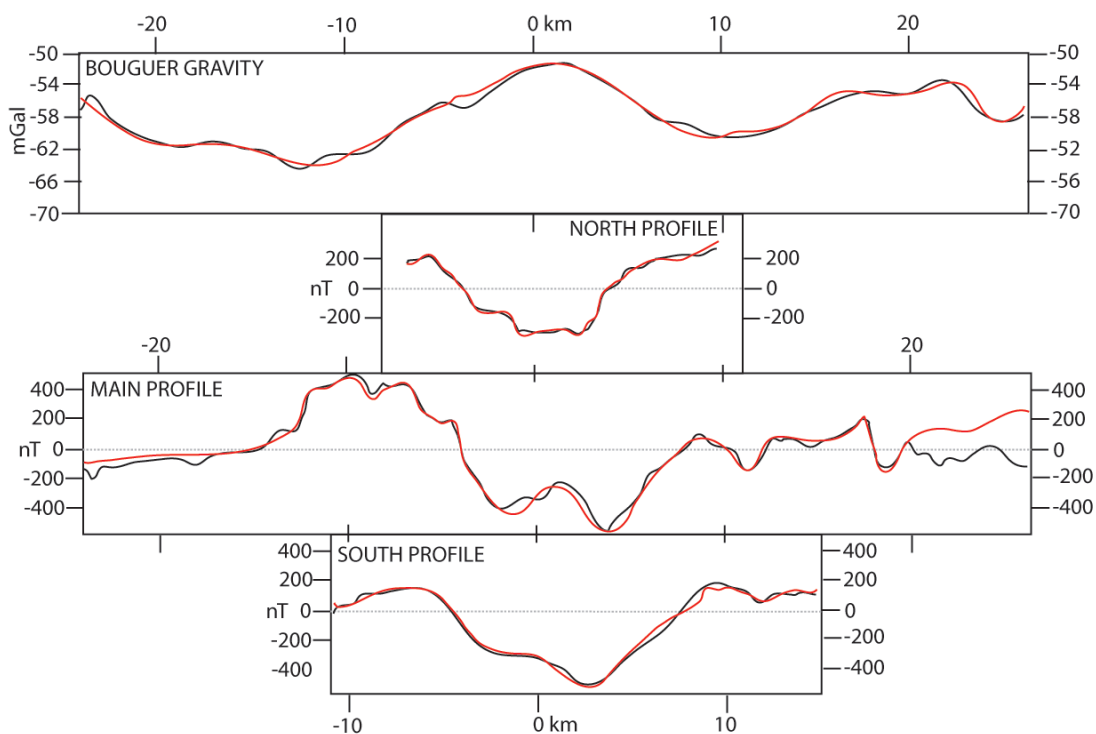


Figure 6.2. Observed and modeled gravity and magnetic profiles scaled together for easy comparison. Black profiles are observed data and red profiles are modeled data.

This is supported by surface manifestations of geothermal activity along the rift axis and geothermal exploratory well drilling (Aquater, 1996a). Near the Ayrobeara geothermal field, small versions of the chimneys that serve as hydrothermal vents typically found along mid oceanic ridges, are present (Figure 6.3). Based on the geothermal activity in the area, it is likely that the magnetic high is due to high crustal heat flow (Aquater, 1996a) associated with intense mafic diking present under the sediments and/or high heat flow concentrated along the Dubti Fault.



Figure 6.3. Geothermal sublimation features and fossil fumaroles in the Ayrobeara geothermal field.

Although thermal demagnetization of rocks due to the concentration of hydrothermal heat flow along the Dubti Fault is most likely the cause of the magnetic high, other possibilities are possible. A narrow sliver of reversely magnetized crust or dikes could cause the magnetic high; it is highly unlikely based on the likely large volume of normal magnetization crust surrounding it. The lack of large tectonic disturbances in the middle of a 50 km wide graben would likely preclude this possibility. The reason that a significant positive anomaly (>150 nT) exists in the Ayrobeara geothermal field is a mystery. Thermal demagnetization alone could not create such an anomaly. This anomaly would have to result from tectonic thinning likely related to the normal dip-slip Dubti Fault and/or demagnetization caused by alteration of the basalts.

Acocella et al. (2008) suggest that the young TG was a source of the voluminous Afar Stratoid basalts that dominate the surface geology of central Afar and reports a mean age of $\sim 1.8 \pm 0.1$ Ma for the basalts, this roughly coincides with the opening of the TG. This massive outpouring of basalts waned by ~ 0.8 Ma. Paleomagnetic work suggests this activity could have occurred in episodes rather than a long-term continuous event (Acton et al., 2000). Nonetheless, the spreading rate slowed down ~ 0.8 Ma due to the lack of a magmatic source and/or the transfer of extensional strain to the east, perhaps to the Gulf of Aden propagator or within the East Central Block. A conceptual model is proposed of an upper crust that has been extensively modified by diking and intrusions during the emplacement of the Stratoids and subsequently; as spreading continued, a 10 km zone of dominantly normal polarity dyking has been recording the past ~ 0.8 Ma of extension (Figure 6.4). The forward modeling of the magnetic and gravity data supports this model.

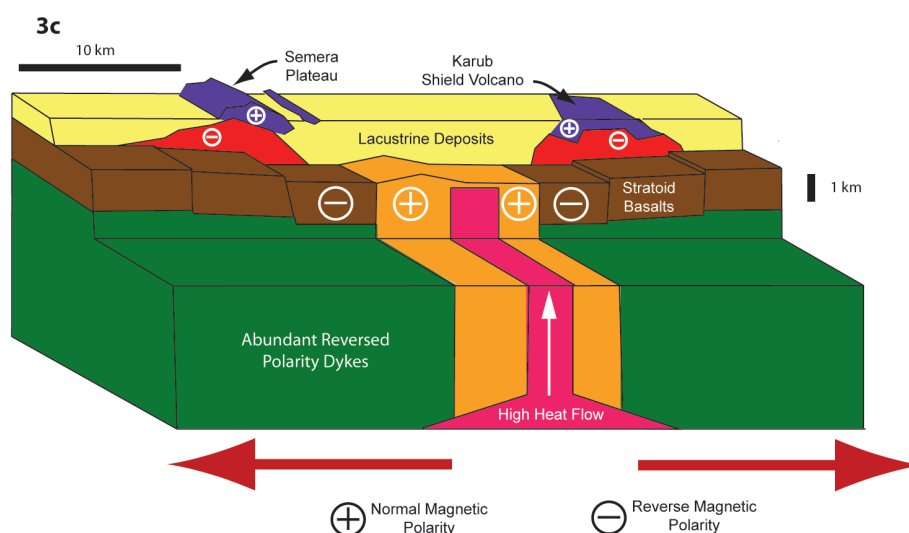


Figure 6.4. Two-dimensional gravity forward model across the Tendaho Graben roughly coincident with the high density magnetic profile. The color scheme is the same as Figure 5.14.

6.2. MAGNETIC STRIPES

The idea of magnetic stripes associated with the active magmatic segments in Afar is not new. Barberi and Varet (1977) argued their existence based on an aeromagnetic survey completed during the late 60's. They pointed to the existence of many linear magnetic anomalies associated with the Red Sea and Gulf of Aden propagators in the Afar (Figure 6.5). Barberi and Varet (1977) also argued the case for the existence of oceanic crust beneath these segments based on crustal thickness, gravity data, lack of any crustal xenoliths in the Afar volcanic rocks and geochemical data. They also suggested linear magnetic anomalies (stripes) typical of those associated with oceanic spreading centers exists in the area between the Asal and Abhe rifts. Lastly they concluded that the magnetic lineaments argues in western Afar cannot be matched with the magnetic timescale due to the lack of paleomagnetic and geochronologic data (Barberi and Varet, 1977). Evidence is provided here for the first time of magnetic stripes that can be correlated with the current geomagnetic timescale of Cande and Kent (1992). Hayward and Ebinger (1996) provide a conceptual model for the evolution of rift morphology from the onset of rifting to fully developed seafloor spreading for the MER and Afar. The areas of linear magnetic anomalies as shown by Barberi and Varet (1977) (Figure 6.4) correspond remarkably well with the middle and later stages of Hayward and Ebinger's (1996) model, the point at which smaller rifts are forming within the rift system. The TG is at this development stage and principally records the change from the Matuyama chron, reverse polarity, to the current Brunhes Chron. This provides insights into the extensional mechanism occurring at oceanic spreading centers.

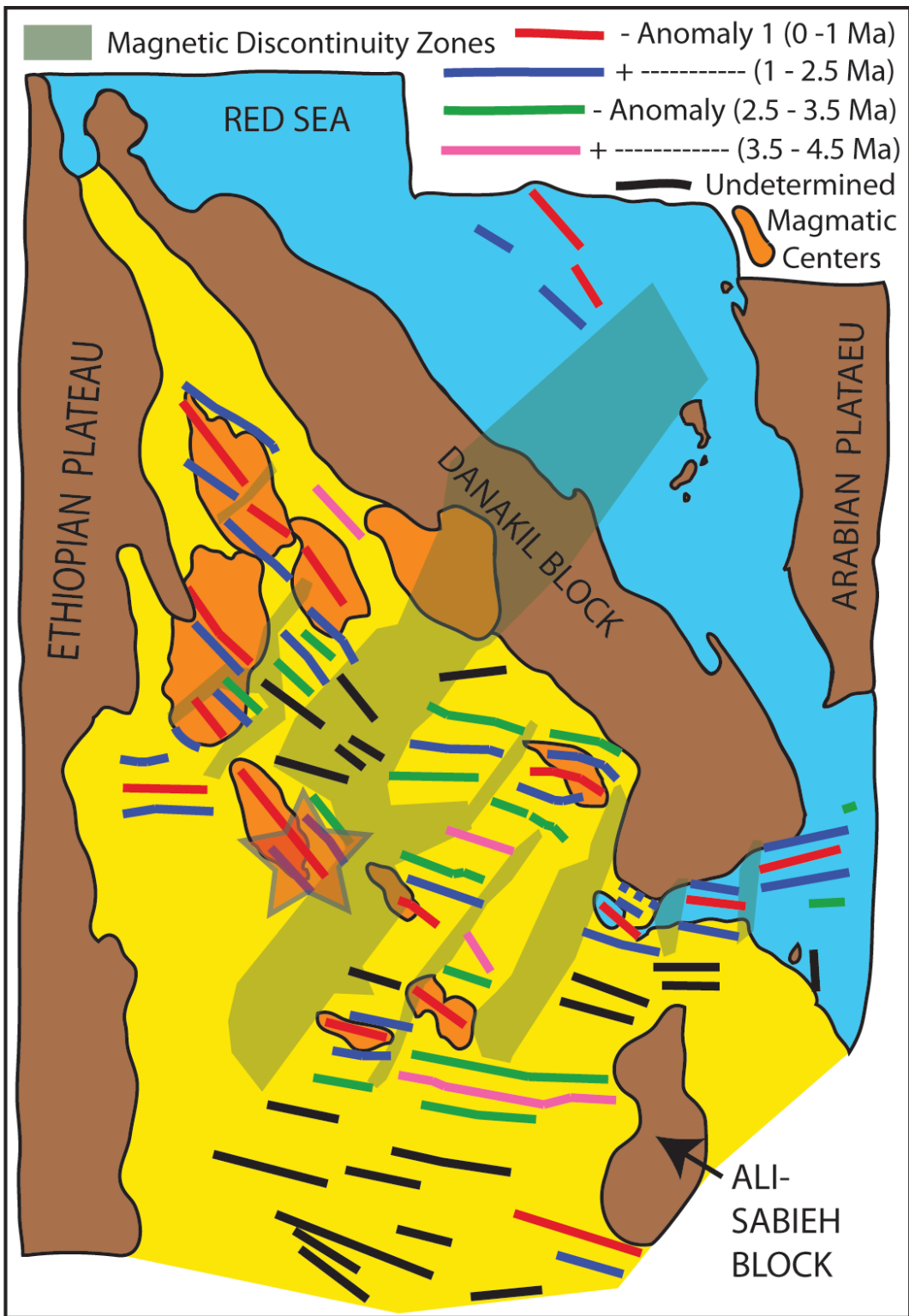


Figure 6.5. Magnetic lineations of Afar and their relative ages (Barberi and Varet, 1977). The magnetic discontinuity zones are characterized by low amplitude anomalies. The star is the location of the Tendaho Graben study area.

6.3. REVISED EVOLUTION OF THE TENDAHO GRABEN

The TG initiated ~2.0 Ma (Acton et al., 2000). This age of initiation is based on the age of the Stratoid Basalts and therefore serves only as a maximum age. TG is ~50 km wide and is the largest graben in central Afar. Normal faulting is dominant although some sinistral strike-slip is present (Abbate et al., 1995). The age of the Stratoid basalts and younger axial volcanics are progressively younger towards the middle of the graben (Figure 6.6). The graben is filled with lacustrine deposits which in some places are over 1.6 km thick (Abbate et al., 1995; Aquater, 1996a). The younger volcanics form a rift-in-rift structure.

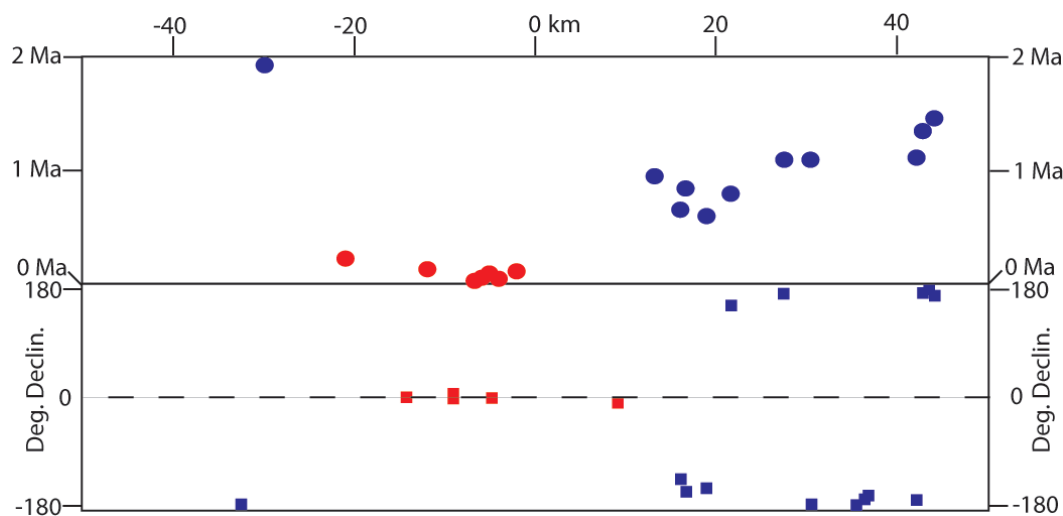


Figure 6.6. Geochronologic data as a function of distance from the rift axis. Locations for data are shown in Figure 5.3 as yellow triangles. Paleomagnetic declination with same horizontal projection. Blue points are reverse polarity and red points normal polarity. Data from Lahitte et al. (2003) and Kidane et al. (2003).

Several models for the evolution of the TG have been proposed (Acton et al., 1991; 2000; Thurmond, 2007 and Acocella et al., 2008). New data from this work has provided additional constraints, allowing for a more geological accurate model to be produced (Figure 6.7). Common to all models is the emplacement of the Stratoid Basalts between 3.5 and 0.6 Ma (Lahitte et al., 2003). Much of central Afar is covered by ~ 2 Ma Stratoids (Lahitte et al., 2003(Figure 6.7a).) and for all models this represents the initial formation deformed by the initiation of the TG.

Most of the previously mentioned models have the initiation of the TG ~ 1.8 Ma and are based on the Acton et al. (1991) model. Acton et al. (1990) arbitrarily chose 1.8 Ma, for the initiation of the TG due to Stratoid series blanketing all older formations and structures. Rotation of the East Central Block, that forms the NE footwall of the TG started ~ 2.0 Ma (Kidane et al., 2001). This would more likely be the correct initiation time of the TG and thereby the date chosen for the proposed model of this work.

The next event with an age control is the emplacement of the rhyolites presently near Serdo and to the W of Loggia (Figure 6.7c). Dating by Lahitte et al. (2003) reveals similar dates of emplacement (1.320 and 1.269 Ma). These silicic domes were likely emplaced when the TG was only 6.5 to 10 km wide. A modern analogue is the Imino Graben to the NE. The Dobe Graben, in the East Central Block, is another analogue that may be currently at the stage where the Tendaho Graben was around the emplacement of the rhyolites. The master faults of the graben were the focuses of melt ascent and emplacement. The previous models of Acton et al. (1991; 2000) and Thurmond (2007)

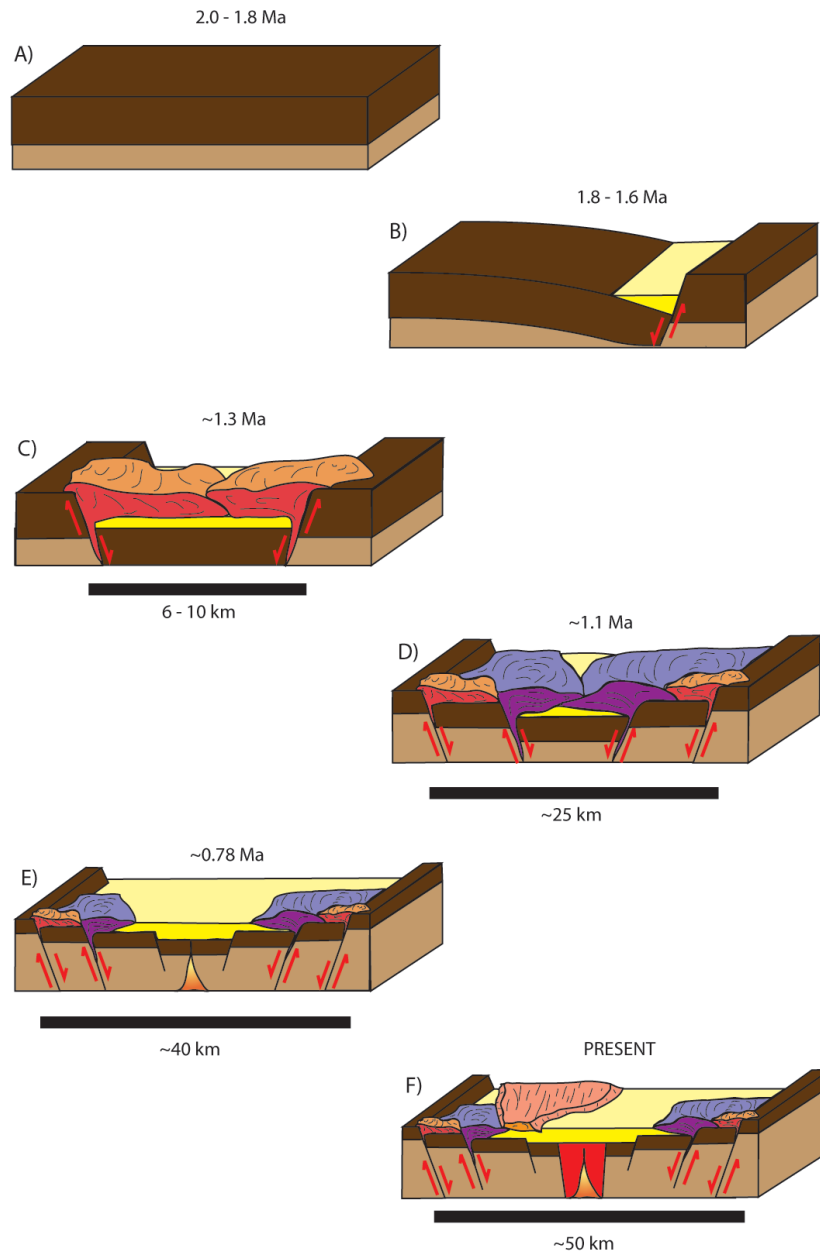


Figure 6.7. Proposed Evolution of the Tendaho Graben. A) Emplacement of Stratoid Basalts (dark brown) overlying unknown pre-Pleistocene surface (Light Brown). B) Continuing mechanical stretching creates a half graben to form along with sediment deposition. C) As extension continues, formation of a full graben along with high asthenospheric heat flow creates melts of rhyolitic composition that are emplaced along the master faults of the graben. D) The Tendaho Graben is now ~25 km wide and the Gulf Series basalts are emplaced again mainly focused along the crustal weakness zones create by normal faulting. E) Extension moves from the margins and border faults to the center of the graben and mechanical crustal thinning has been replaced by magmatic diking near the center of the graben. F). Present day scenario with ~ 10 km zone of dominantly normal polarity dikes.

have the rhyolites as precursors to rift initiation, however, this does not fit the geochronologic data. The large fissure flows of Gulf Series basalts were emplaced ~ 1.1 Ma (Lahitte et al., 2003) and filled the floor of the young TG (Figure 6.7d). These fissure basalts likely exploited syn-faulting that was occurring along the graben margins associated with the continuing extension of the upper crust.

The newly acquired magnetic data add an additional constraint in the proposed evolution of TG model. Around 0.78 Ma, accommodation of extension in the TG moved from the margins towards the center axis of the graben (Figure 6.7e). Due to the dominantly reversed polarity Stratoid blocks on the margins of this central axis, the exact transition time cannot be constrained with magnetic and field data alone. This transition from mechanically stretched crust to magma assisted extension could have occurred not long after the major pulse of Gulf Series basalts were emplaced. On the other hand, this transition could have happened after 0.78 Ma depending on the recent spreading rate of the Graben. Nonetheless, forward modeling has shown that a 10 km section of dominantly normal polarity dikes would fit the observed magnetic data (Figure 5.15). Based on regional spreading rates (e.g. Chu and Gordon, 1998), placing the initiation of diking around the change from the Mataysuma to Bhrunes chron (0.78 Ma) is appropriate.

The present TG width of ~ 50 km is the result of both brittle deformation and magma emplacement (Figure 6.7f). Diking and geothermal activity is concentrated in the center of the graben forming the Ayrobeara geothermal field in the NW to a large plantation to the SW. The Dubti Fault controls this activity. The extension rate of the TG has slowed considerably from 1.64 cm/yr from rift initiation to 0.78 Ma to 0.64 cm/yr

from 0.78 Ma to present. This would suggest that the extension across the central Afar Depression is being accommodated somewhere in the East Central Block or possibly the Gulf of Aden propagator. This evolution is unique in that it records the transition from mechanical stretching of the upper crust to a magma assisted extension regime.

7. CONCLUDING REMARKS

7.1. CONCLUSIONS

Magnetic data along with field data, geochronology and paleomagnetic data clearly document a subaerial version of the magnetic stripes more typically associated with oceanic spreading centers. The magnetic geometry is analogous in dimension and amplitude to that observed at oceanic spreading centers. The spreading rate of the Tendaho has decreased remarkably since ~ 0.8 signifying that extension within Afar is taking place further to the northeast, perhaps the currently active Gulf of Aden propagator. A revised structural evolution of the Tendaho Graben (TG) from initiation ~ 2.0 Ma to present is proposed.

The following is a summary of the major findings of this work:

- Linear magnetic bodies follow the strike of the TG.
- Gravity data suggests that the linear bodies are likely mafic dikes.
- The spreading rate of the TG has slowed significantly based on geomagnetic chronology.
- Evidence is provided in this work for the first time of subaerial magnetic stripes that can be correlated with the current geomagnetic timescale of Cande and Kent (1992).
- The TG evolution model suggested in this work is unique in that it records the transition from mechanical stretching of the upper crust to a magma assisted extension regime.

7.2. FUTURE WORK

Further work is possible to refine what stage of rift evolution could produce a magnetic signature consistent with those observed at oceanic spreading centers due to extension maintained by dyke emplacement. This would furthermore provide insights into the extension mechanisms that maintain established oceanic spreading centers.

APPENDIX

FORTRAN and MATLAB CODE GENERATED AND/OR USED FOR THIS STUDY

Main FORTRAN program that reduces the data, produces preliminary plots to aid the user in various selections and a final text file containing the IGRF removed and diurnally corrected data.

Makefile - to compile code on a Mac OSX 10.5 machine:

```
mag.app:mag.f
    g77 mag.f -o mag.app phrange.a minmax.o igrf10sub.o julday.o
```

Main program:

```
*****
*Mag 0.1.0 for reduction and transformation*
*of raw magnetic data!                      *
*(c) 2009 David L. Bridges                   *
*Missouri University of Science and Tech.  *
*****
```

```
PROGRAM MAG

PARAMETER (MAX=1000000,PI=3.14159265)

CHARACTER*100 PROF,CMD,MULTI,FILEI,DIR,NIN,BPATH,NINB
CHARACTER*30 FF,STN,BF,RES,RPA
REAL DIST,SLAT(MAX),SLONG(MAX),AZ2,MAXDIST,MAXMAG,MINMAG
&,DLAT,DLON,CLAT,CLON,COUNT3,ANG(MAX),LATCL(MAX),LONGCL(MAX)

&,LAT(MAX),LONG(MAX),ELEV(MAX),MAGFIELD(MAX),MAGB(MAX),MAGCL(MAX),
&ASPECT,SUMAVG,LATMIN,LATMAX,LONGMAX,LONGMIN,ELEVMIN,ELEVMAX,
&MAGD(MAX),SELEV(MAX),ELEVCL(MAX),MIM,MAM,DIST1(MAX),ANG1(MAX),
&DIST2(MAX),DIST3(MAX),DELTA,ETOS,STOE,DIST4(MAX),DL,V,ANG2(MAX),
&SDIST(MAX),SMAG(MAX),D1,D2,SSMAG,SSELEV,NN,SUMAVGB,DAVG,
&DCMAG(MAX),AZ,NEG
REAL*8 SEC(MAX),SECB(MAX),SECCL(MAX),TTIME(MAX),TTIMEB(MAX)
c &,TOTALT(MAX),TOTALTB(MAX)
INTEGER COUNT,
HOUR(MAX),MIN(MAX),MONTH(MAX),DAY(MAX),YEAR(MAX),
&HOURB(MAX),MINB(MAX),MONTHB(MAX),DAYB(MAX),YEARB(MAX),
&ISV,ITYPE,COUNT2,GRIDINC,HOURCL(MAX),NUMPTS,
&MINCL(MAX),MONTHCL(MAX),DAYCL(MAX),YEARCL(MAX),COUNT4,ZR,
&JLDAY(MAX),JLDAYB(MAX),NMPTMAX,COUNTER,fc
LOGICAL THERE
```



```
DOUBLE PRECISION ALT(MAX),COLAT(MAX),ELONG(MAX),DATE,X(MAX),
&Y(MAX),Z(MAX),F(MAX),TOTALTB(MAX),TOTALT(MAX),ELON1(MAX),
&ELAT1(MAX),ELON2(MAX),ELAT2(MAX),LONGDP(MAX),LATDP(MAX)
```

```
PRINT*, "
PRINT*, "
PRINT*, "
PRINT*, 'This program is for creating Magnetic Profiles for'
PRINT*, '2-D surveys or Total Anomaly Grids for 3-D surveys!'
PRINT*, "
PRINT*, 'Some required questions will be asked first, if you'
PRINT*, 'do not understand what the question is asking, a default'
PRINT*, 'value will be suggested. You can simply type the'
PRINT*, 'supplied default that is shown in the brackets'
PRINT*, "
PRINT*, 'It is my hope that this program will be useful to'
PRINT*, 'researchers wanting in-field data reduction and '
PRINT*, 'transformation along with general data inquiry'
PRINT*, 'analysis back in the lab/office. Dave L. Bridges'
PRINT*, "
PRINT*, "
10 PRINT*, "
PRINT*, "
PRINT*, 'Would you like an Profile Graph or Total Anomaly grid?'
PRINT*, 'PROFILE[P] or GRID [G] '
READ*, PROF

IF (PROF.eq.'P'.or.PROF.eq.'G') THEN
ELSE
    PRINT*,"
    PRINT*,"
    PRINT*,'I do not understand your answer!!!'
    GOTO 10
ENDIF

PRINT*,"
PRINT*,"
PRINT*, 'Where is the directory that contains your magnetic data?'
PRINT*, 'Enter the number [1] to use the current working'
PRINT*, ' directory'
15 FORMAT(A50)
READ(*,15) DIR

20 PRINT*,"
PRINT*,"
```

```

PRINT*, 'Do you have multiple data files? If so all data files '
PRINT*, 'MUST be in the directory entered previously'
PRINT*, '[Y or N]. Enter [Y] if single file is not located in'
PRINT*, 'current directory!'
READ*, MULTI
IF (MULTI.eq.'Y') THEN

DO j=1,100
  if(DIR(j:j).eq. ' ') THEN
    COUNTER=j-1
    GOTO 23
  ENDIF
ENDDO

23  CMD='ls '//DIR(1:COUNTER)//'/* > files.txt'
    CALL SYSTEM (CMD)

    ENDIF

    IF (MULTI.eq.'N'.or.DIR.eq.'1') THEN
24  PRINT*, "
    PRINT*, "
    PRINT*, 'What is the file name?'
    READ*, FILEI

    THERE=.FALSE.  !makes sure file is typed correctly!
    INQUIRE (FILE=FILEI,EXIST=THERE)
    IF(.NOT.THERE) GOTO 24

    ENDIF

    IF (MULTI.eq.'Y'.eqv.MULTI.eq.'N') THEN
    PRINT*, "
    PRINT*, "
    PRINT*, 'I do not understand your answer!!!'
    GOTO 20
    ENDIF

*****Time to read the data files into the program.
*****First the format for the geometrics format files.

IF (DIR.eq.'1') THEN
OPEN(6,file='files.txt') !Only used if current directory is selected
WRITE (6,*) FILEI
CLOSE(6)
ENDIF

```

*****The file type needs to be determined.

```

PRINT*,''
PRINT*,''
25 PRINT*, 'Data needs to be in one of three formats, Geosoft XYZ '
PRINT*, 'file format or a generic format.[No default]'
PRINT*, 'GEOMETRIC 859 [1]'
PRINT*, 'GEOMETRIC GRADIOMETER 858 [2]'
PRINT*, 'GENERIC FORMAT [3]'
READ*, FF

IF (FF.eq.'1') THEN

  open(11,file='files.txt')
  Do fc=1,1000
  READ(11,27,end=36) NIN
  PRINT 27, NIN
27  FORMAT (a100)
  OPEN(25,file=NIN)

  DO i=(count+1),MAX

    READ(25,30,END=35) LONG(i),LAT(i),ELEV(i),MAGFIELD(i),
    &  HOUR(i),MIN(i),SEC(i),MONTH(i),DAY(i),YEAR(i)
30  FORMAT (F13.10,1x,F13.10,5x,F8.3,3x,F9.3,1x,I2,1x,I2,1x,
    &  F5.2,2x,I2,1x,I2,1x,I2)

**** fixes 2009-2010 field data error!
  IF (DAY(i).gt.27.or.DAY(i).lt.4.) HOUR(i)=HOUR(i)-6
**** be sure to comment out if using for other projects!

  COUNT=COUNT+1
  ENDDO
35  CLOSE(25)
  ENDDO
36  CLOSE(11)
  PRINT*,''
  PRINT*,''
  PRINT 40, COUNT
40  FORMAT ('I have ingested ',I7, ' mag measurements!')
  ENDIF

IF(FF.eq.'2') THEN
  OPEN(11,file='files.txt')

```

```

Do fc=1,1000
READ(11,42,end=56) NIN
42 FORMAT (a50)
PRINT*,NIN
Open(25,file=NIN)
Do i=(COUNT+1),MAX
*   1   2   3   4   5   6   7   8   9   10  11  12  13
14  15  16  17  18  19
*1234567890123456789012345678901234567890123456789012345678901234
56789012345678901234567890123456789012345678901234567890123456789
0123456789012345678901234567890123456789012345678901234567890123
*
* -118.99498650 37.69873480 324122 4174263 2397 49450.85
49464.08 -638.78 49432.05 49432.05 -657.57 32.03 50089.625
15:34:19.60 2003/07/27
* -118.99498940 37.69873440 324122 4174263 2397 49445.02
49445.35 -644.60 49429.87 49429.87 -659.75 15.48 50089.624
15:34:20.10 2003/07/27

READ(25,45,END=55) LONG(i),LAT(i),ELEV(i),MAGFIELD(i)
45 FORMAT(2x,F13.8,1x,F12.8,28x,F4.0,6x,f8.2)

COUNT=COUNT+1
ENDDO

55 CLOSE(25)
ENDDO
56 CLOSE(11)
PRINT*,"
PRINT*,"
PRINT 60, COUNT

60 FORMAT ('I have ingested ', I7, ' mag measurements!')
ENDIF

IF(FF.eq.'3') THEN
OPEN (11,file='files.txt')
Do fc=1,1000
READ(11,63,end=70) NIN
PRINT*,NIN
63 FORMAT (a50)
OPEN(25,file=NIN)

*   1   2   3   4   5   6   7
*1234567890123456789012345678901234567890123456789012345678901234
567890

```

```
*41.3094 11.9542 36419 390.64 {GENERIC FORMAT}
```

```

Do i=1,MAX
  READ(25,*,END=65) LONG(i),LAT(i),MAGFIELD(i),ELEV(i)
  COUNT=COUNT+1
ENDDO

65  CLOSE(25)
    ENDDO
70  CLOSE(11)
    PRINT*,"
    PRINT*,"
    PRINT 75, COUNT
75  FORMAT ('I have ingested ', I7, ' mag measurements!')
    ENDIF

    IF (FF.eq.'1'.eqv.FF.eq.'2'.neqv.FF.eq.'3') THEN
      PRINT*,"
      PRINT*,'I do not understand your answer!'
      PRINT*,'Please enter 1, 2, or 3!'
      GOTO 25
    ENDIF

```

cThis section starts the inpput of the base station data

```

80  PRINT*,"
    PRINT*,"
    PRINT*,'Please enter the directory that contains the base'
    PRINT*,'data [Full Path]. Enter [N] if no file is available'
    PRINT*,'or data is already diurnally corrected. Enter [1]'
    PRINT*,'to use the current directory (Limited to one station!)'
    READ 81, BPATH
81  FORMAT(a50)

    IF (BPATH.eq.'N') GOTO 100

    DO J=1,100
      if(BPATH(j:j).eq. ' ') THEN
        COUNTER=j-1
        GOTO 83
      ENDIF
    ENDDO

83  CMD='ls '//BPATH(1:COUNTER)//'/* > bfiles.txt'
    CALL SYSTEM (CMD)

```

```

      IF (BPATH.eq.'1') THEN
84  PRINT*,"
      PRINT*,"
      PRINT*,'Please enter the name of the base station file to'
      PRINT*,'complete diurnal correction.'
      READ*,STN

      THERE=.FALSE.
      INQUIRE (FILE=STN,EXIST=THERE)
      IF(.NOT.THERE) GOTO 84

      OPEN (6,file='bfiles.txt')
      WRITE(6,*) STN
      CLOSE (6)
      ENDIF

      PRINT*,'What format is the data? '
      PRINT*,'Geometrics 856X [1]'
      PRINT*,'IAGA-2002 format [2]'
      READ*,BF
      SUMAVGB=0
      DAVG=0
      SUMAVG=0
      IF (BF.eq.'1') THEN
      OPEN (22,file='bfiles.txt')
      Do g=1,1000
      READ(22,86,end=92) NINB
      PRINT*,NINB
86  FORMAT (a50)

c   1   2   3   4   5
c123456789012345678901234567890123456789012345678901234567890
c0 36946.400   0.000 14:52:24.00 12/17/08 0
c0 36946.200   0.000 15:18:21.00 12/16/08 0
      OPEN(35,file=NINB)
      do j=(count2+1),max
      READ (35,90,END=91) MAGB(j),HOURLB(j),MINB(j),SECB(j),
&  MONTHB(j), DAYB(j), YEARB(j)
90  FORMAT(4x,F9.3,12x,I2,1x,I2,1x,F5.2,1x,I2,1x,
&  I2,1x,I2)
      COUNT2=COUNT2+1
      SUMAVGB=SUMAVGB+MAGB(j)
      ENDDO
91  CLOSE(35)

```



```

m=COUNT4
MAGCL(m)=MAGFIELD(l)
LONGCL(m)=LONG(l)
LATCL(m)=LAT(l)
ELEVCL(m)=ELEV(l)
PRINT*,ELEVCL(m)
HOURCL(m)=HOUR(l)
MINCL(m)=MIN(l)
SECCL(m)=SEC(l)
MONTHCL(m)=MONTH(l)
DAYCL(m)=DAY(l)
YEARCL(m)=YEAR(l)

ALT(m)=ELEV(l)/1000.0

IF (LAT(l).ge.0.0) COLAT(m)=90.0-LAT(l)
IF (LAT(l).lt.0.0) COLAT(m)=90.0+-1.0*LAT(l)
IF (LONG(l).le.180.0) ELONG(m)=LONG(l)
IF (LONG(l).lt.0.0) ELONG(m)=180.0+(180.0+LONG(l))

IF (YEAR(l).lt.50) DATE=YEAR(l)+2000
IF (YEAR(l).ge.50) DATE=YEAR(l)+1900

SUMAVG=SUMAVG+LATCL(m)

ENDIF
ENDDO

ZR=COUNT-COUNT4
SUMAVG=SUMAVG/COUNT4
ASPECT=COS(SUMAVG*(pi/180.0)) !for creating even spaced grids later
PRINT*,
PRINT*,
PRINT 110, ZR
110 FORMAT ('I have removed ',I6,' stations that had zero values!')
PRINT*,

CALL MINMAX(MAGCL,COUNT4,MIM,MAM)
IF (MAM-MIM.ge.3000) print*,'Your data may still have some data
&spikes!'

IF (BPATH.eq.'N') GOTO 200 !skips to IGRF if no base station data

cWe need to remove spikes

```


cTime for diurnal corrections!

cLet sync days using Julian days and total time in seconds for each day!
 cStations need to be organized by time also!

```

  Open(66,file='mag_sort.dat')
  DO n=1,COUNT4
  JLDAY(n)=JULDAY(MONTHCL(n),DAYCL(n),YEARCL(n))
  TTIME(n)=HOURL(n)*3600.0+MINCL(n)*60.0+SEC(n)
  TOTALT(n)=JLDAY(n)*1.0+TTIME(n)/(24.0*3600)
  WRITE(66,167) TOTALT(n),LONGCL(n),LATCL(n),ELEVCL(n),MAGCL(n),
  &HOURL(n),MINCL(n),SECCL(n),MONTHCL(n),DAYCL(n),YEARCL(n),JLDAY(n)
  &,TTIME(n),COLAT(n),ELONG(n)
167  FORMAT(F16.8,1x,F14.10,1x,F13.10,1x,F8.3,1x,F9.3,1x,I2,1x,I2,1x
  &,F5.2,1x,I2,1x,I2,1x,I2,1x,I7,1x,F8.0,1x,F13.10,1x,F13.10)
  ENDDO
  CLOSE(66)

  cmd='sort mag_sort.dat > fmag.dat'
  CALL SYSTEM (CMD)
  cmd='rm mag_sort.dat'
  CALL SYSTEM (CMD)

```

```

  OPEN(77,file='magb_sort.dat')
  DO o=1,COUNT2
  JLDAYB(o)=JULDAY(MONTHB(o),DAYB(o),YEARB(o))
  TTIMEB(o)=HOURB(o)*3600.0+MINB(o)*60.0+SECB(o)
  TOTALTB(o)=JLDAYB(o)*1.0+TTIMEB(o)/(24.0*3600)

  WRITE(77,178) TOTALTB(o),MAGB(o),HOURB(o),MINB(o),SECB(o),
  &MONTHB(o), DAYB(o), YEARB(o),JLDAYB(o),TTIMEB(o)
178  FORMAT(F15.7,1x,F9.3,1x,I2,1x,I2,1x,F5.2,1x,I2,1x,I2,1x,I7,1x,
  %1x,I7,F8.0)
  ENDDO
  CLOSE(77)

  cmd='sort magb_sort.dat > fbase.dat'
  CALL SYSTEM (CMD)
  cmd='rm magb_sort.dat'
  CALL SYSTEM (CMD)

```

cComplete diurnal correction
 cReopen Data

```

Open (81,file='fmag.dat')
DO op=1,COUNT4
READ (81,182) TOTALT(op),LONGCL(op),LATCL(op),ELEVCL(op),MAGCL(op)
&,HOURCL(op),MINCL(op),SECCL(op),MONTHCL(op),DAYCL(op),YEARCL(op),
&JLDAY(op),TTIME(op),COLAT(op),ELONG(op)
182  FORMAT(F16.8,1x,F14.10,1x,F13.10,1x,F8.3,1x,F9.3,1x,I2,1x,I2,1x
&,F5.2,1x,I2,1x,I2,1x,I2,1x,I7,1x,F8.0,1x,F13.10,1x,F13.10)
enddo
close(81)

```

```

OPEN (83,file='fbase.dat')
do oq=1,COUNT2
READ (83,184) TOTALTB(oq),MAGB(oq),HOURB(oq),MINB(oq),SECB(oq),
&MONTHB(oq),DAYB(oq), YEARB(oq),JLDAYB(oq),TTIMEB(oq)

```

cCorrect for AFAR 2008 data error

```

IF (DIR.eq.'Tendaho'.and.BPATH.eq.'Base') TOTALTB(oq)=TOTALTB(oq)
&-1

```

```

184  FORMAT(F15.7,1x,F9.3,1x,I2,1x,I2,1x,F5.2,1x,I2,1x,I2,1x,I7,1x,
%1x,I7,F8.0,1x)
ENDDO
CLOSE (83)
DAVG=SUMAVGB/COUNT2
PRINT*,TOTALT(1),TOTALTB(1),DAVG,ELEVCL(1)

```

cCaculate corrected final mag value!

```

i=0
j=0
OPEN (99,file='diurnal_cor.dat')
DO i=1,COUNT4
DO j=1,(COUNT2-1)
IF (TOTALT(i).ge.TOTALTB(j).and.TOTALT(i).le.TOTALTB(j+1)) THEN
DCMAG(i)=(MAGB(j)-SUMAVGB/COUNT2)
MAGD(i)=MAGCL(i)+DCMAG(i)
WRITE(99,187) TOTALT(i), DCMAG(i), MAGD(i), MAGCL(i)
187  FORMAT (F16.8,1x,f9.3,1x,f9.3,1x,f9.3)
IF (MOD(i,10000).eq.0) PRINT*,i
GOTO 190
ENDIF
ENDDO
190  CONTINUE
ENDDO
CLOSE (99)

```

c[200's] -- This section is for IGRF correction to create Total Field Data

```
200 PRINT*,"
  PRINT*,"
  PRINT*,'At this time, this program will use the IGRF v.10 to'
  PRINT*,'calculate total anomaly due to crustal sources. Future'
  PRINT*,'versions will allow the user to input a regional '
  PRINT*,'gradient provided by a local magnetic observatory for a'
  PRINT*,'better crustal magnetic field.'
```

cVariables needed for the IGRF subroutine

```
  ISV=0
  ITYPE=1

  IF (FF.eq.'3') THEN
    DATE=2000.0

    PRINT*,"
    PRINT*,"
250 PRINT*,'What year was your data collected in?'
    PRINT*,'Year must be in four digit format! [2000]'
    READ*,DATE

    IF (DATE.lt.1950) THEN
      PRINT*,'I cannot calculate the IGRF before 1950 or '
      PRINT*,'after 2010. Try again!'
      GOTO 250
    ENDIF
  ENDIF

  OPEN(99,file='total_f.dat')
  IF (BPATH.eq.'N') THEN
    DO k=1,COUNT4
      CALL IGRF10SYN (ISV,DATE,ITYPE,ALT(k),COLAT(k),ELONG(k),
        &X(k),Y(k),Z(k),F(k))
      WRITE(99,255) LONGCL(k),LATCL(k), MAGCL(k)-F(K), X(k),Y(k),Z(k),
        &F(k),ELEVCL(k)
255 FORMAT(f14.8,1x,f13.8,1x,f9.3,1x,f9.3,1x,f9.3,1x,f9.3,1x,f9.3,
  &f5.1)
    ENDDO
  ELSE ! For Diurnally corrected Data
    DO k=1,COUNT4
```

```

CALL IGRF10SYN (ISV,DATE,ITYPE,ALT(k),COLAT(k),ELONG(k),
&X(k),Y(k),Z(k),F(k))
WRITE(99,256) LONGCL(k),LATCL(k), MAGD(k)-F(K), X(k),Y(k),Z(k),
&ELEVCL(k)
256 FORMAT(f14.8,1x,f13.8,1x,f9.3,1x,f9.3,1x,f9.3,1x,f9.3,1x,f5.1)
ENDDO
ENDIF
CLOSE(99)

```

cLets find MIN and MAX of our coordinates, elevation, etc

```

CALL MINMAX (LONGCL,COUNT4,MIM,MAM)
LONGMIN=MIM
LONGMAX=MAM

CALL MINMAX (LATCL,COUNT4,MIM,MAM)
LATMIN=MIM
LATMAX=MAM

CALL MINMAX (ELEVCL,COUNT4,MIM,MAM)
ELEVMIN=MIM
ELEVMAX=MAM

IF (PROF.eq.'P') GOTO 300

IF (PROF.eq.'G') THEN
260 PRINT*,"
PRINT*,"
PRINT*,'What grid spacing would you like? Units are in meters!'
READ*, GRIDINC

```

cTime to create a GNT script file and execute it and use gv to view it!

```

OPEN (20, FILE='Tot_Mag_Grid.gmt')

WRITE(20,265) LONGMIN,LONGMAX,LATMIN,LATMAX,GRIDINC,ASPECT
265 FORMAT ('#!/bin/csh'//
& '//
& 'set lon1 = ', f9.2/
& 'set lon2 = ', f9.2/
& 'set lat1 = ', f9.2/
& 'set lat2 = ', f9.2/
& 'set a = ', I4,'e'/
& 'set aspect =', f9.2//)

WRITE(20,*) "awk '{print $1,$2,$3}' total_f.dat | blockmedian

```

```

&-R$lon1/$lon2/$lat1/$lat2 -I$a > total_bm.dat"
WRITE(20,*) "
WRITE(20,*) 'surface total_bm.dat -R -I$a -A$aspect
&-Gtotal_anomaly.grd'
WRITE (20,*)"
WRITE (20,*) 'grd2cpt total_anomaly.grd -Crainbow -Z > ta.cpt'
WRITE (20,*)"
WRITE (20,*) 'grdimage total_anomaly.grd -R -Cta.cpt -JM6i -B -K
& > total_anomaly.ps'
WRITE (20,*) "
WRITE (20,*) 'psxy total_f.dat -R -J -O -W0.1 -Sp >>
$total_anomaly.ps'

```

```
CLOSE (20)
```

```

CMD='chmod a+x Tot_Mag_Grid.gmt'
CALL SYSTEM (CMD)
CMD='Tot_Mag_Grid.gmt'
CALL SYSTEM (CMD)
CMD='gv total_anomaly.ps'
Call SYSTEM (CMD)
ENDIF

```

```

PRINT*,"
PRINT*,"
PRINT*,'Would you like to try another grid increment? [Y or N] '
READ*, RES
IF (RES.eq.'Y') THEN
GOTO 260
ELSE
GOTO 999
ENDIF

```

c300's selecting a profile to plot

cIt would be nice to have the prog show a graph with suggested profile directions

```

300 PRINT*,"
PRINT*,"

```

- c 180 will serve as West to East
- c FIND endpoints of line

```

DLAT=LATMAX-LATMIN
DLON=LONGMAX-LONGMIN
CLAT=(LATMAX+LATMIN)/2
CLON=(LONGMAX+LONGMIN)/2

```

```

OPEN(11,file='lines.dat')
do j=1,180
ELAT1(j)= CLAT+(DLAT/2)*sin(j*(pi/180))
ELON1(j)= CLON +(DLON/2) *cos(j*(pi/180))
ELAT2(j)= CLAT+(DLAT/2)*sin((j+180)*(pi/180))
ELON2(j)= CLON +(DLON/2) *cos((j+180)*(pi/180))
WRITE(11,*)ELON1(j),ELAT1(j)
WRITE(11,*)ELON2(j),ELAT2(j)
WRITE(11,366) '>'
366 FORMAT (a1)
CALL DISTAZ (event,ELAT2(j),ELON2(j),stname,ELAT1(j),ELON1(j)
&,DIST,DELTA ,STOE,ETOS)
COUNT3=COUNT3+1
DIST1(j)=DIST
ANG(j)=ETOS
ENDDO
CLOSE(11)

cmd='rm tmp.dat tmp1.dat pts.dat'
call system(cmd)

c Enter buffer zone around profile line to collect points

367 PRINT*,"
PRINT*,"
PRINT*,'Please enter how far from your profile you would like'
PRINT*,'to include data.[meters]
READ*,DL

377 OPEN(44,file='tmp.dat')
OPEN(66,file='pts.dat')
DO k=1,count3
NUMPTS=0
PRINT*,'DOING ANGLE ',k,AZ
DO l=1,COUNT4
LATDP(l)=LATCL(l)
LONGDP(l)=LONGCL(l)

IF (ANG(k).gt.270) THEN

CALL DISTAZ (event,ELAT1(k),ELON1(k),stname,LATDP(l),LONGDP(l),
&DIST,DELTA,STOE,ETOS)
ANG1(l)=ETOS
DIST2(l)=DIST
DIST3(l)=DIST2(l)*cos((ANG(k)*pi/180)-(ANG1(l)*pi/180))*-1

```

```
DIST4(l)=DIST2(l)*sin((ANG(k)*pi/180)-(ANG1(l)*pi/180))
ENDIF
```

```
IF (ANG(k).ge.0.and.ANG(k).lt.90) THEN
CALL DISTAZ (event,ELAT2(k),ELON2(k),stname,LATDP(l),LONGDP(l),
&DIST,DELTA,STOE,ETOS)
ANG1(l)=ETOS
```

```
DIST2(l)=DIST
DIST3(l)=DIST2(l)*cos((ANG(k)*pi/180)-(ANG1(l)*pi/180))
DIST4(l)=DIST2(l)*sin((ANG(k)*pi/180)-(ANG1(l)*pi/180))
```

```
ENDIF
```

```
IF (ANG(k).le.90) AZ2=ABS(ANG(k)-90.0)
IF (ANG(k).gt.270) AZ2=ANG(k)-180.0
IF (ABS(DIST4(l)).le.(DL/1000).and.(AZ+0.5).gt.AZ2.and.(AZ-0.5)
&.le.AZ2.and.TIME.eq.1) THEN
IF (DIST3(l).le.0) CONTINUE
```

```
IF (BPATH.eq.'N') THEN
WRITE(44,*) DIST3(l),MAGCL(l)-F(l),LONGCL(l),LATCL(l),
&ELEVCL(l),ANG(k)
IF (MAXMAG.le.(MAGCL(l)-F(l))) MAXMAG=MAGCL(l)-F(l)
IF (MINMAG.ge.(MAGCL(l)-F(l))) MINMAG=MAGCL(l)-F(l)
IF (MAXDIST.le.DIST3(l)) MAXDIST=DIST3(l)
ELSE ! Use diurnal corrections!
WRITE(44,*) DIST3(l),MAGD(l)-F(l),LONGCL(l),LATCL(l),
&ELEVCL(l),ANG(k)
IF (MAXMAG.le.(MAGD(l)-F(l))) MAXMAG=MAGD(l)-F(l)
IF (MINMAG.ge.(MAGD(l)-F(l))) MINMAG=MAGD(l)-F(l)
IF (MAXDIST.le.DIST3(l)) MAXDIST=DIST3(l)
```

```
ENDIF
```

```
ENDIF
```

```
IF (ABS(DIST4(l)).le.(DL/1000)) NUMPTS=NUMPTS+1
```

```
387 CONTINUE
```

```
ENDDO
```

```
IF (NUMPTS.ge.NMPTMAX) NMPTMAX=NUMPTS
```

```
IF (ANG(k).ge.270) THEN
```

```
ANG2(k)=ANG(k)-180.0
```

```
WRITE (66,*) ANG2(k),NUMPTS
```

```
ENDIF
```

```

WRITE (66,*) ANG(k),NUMPTS
ENDDO
CLOSE(44)
CLOSE(66)

```

```

cmd='sort -n tmp.dat > tmp1.dat'
call system(cmd)

```

```

IF (TIME.eq.1) GOTO 398

```

cTime to plot numpoints vs azimuth

```

PRINT*,''
PRINT*,'Select the profile azimuth you would like using the'
PRINT*,'supplied graph [0-180] Hint: Pick the largest peak for'
PRINT*,'best results!'
PRINT*,''
OPEN (77,file='points.gmt')
V=NMPTMAX/4.0
Write(77,395) NMPTMAX,V
395 FORMAT ('#!/bin/csh '//
&'//
&'set max = ',I9/
&'set v = ',F9.2/
&'//
&'psxy pts.dat -R0/180/0/$max -JX6i -W0.1 -St0.1
& -Ba20/$v > points.ps'//)
CLOSE(77)
CMD='chmod a+x points.gmt'
CALL SYSTEM (CMD)
CMD='points.gmt'
CALL SYSTEM (CMD)
CMD='gv points.ps'
CALL SYSTEM (CMD)
397 READ*,AZ
IF (AZ.lt.0.0.and.AZ.gt.180.0) THEN
PRINT*,'Your answer must be an number between between 0 and 180.'
PRINT*,'Please try again!'
GOTO 397
ENDIF
TIME=TIME+1
IF (TIME.eq.1) GOTO 377

```

ctime to plot the raw profile!

```

398 open(88,file='raw_profile.gmt')
WRITE(88,399) MAXDIST,MINMAG,MAXMAG

```



```

399 FORMAT('#!/bin/csh'//
    &"//
    &'set maxdist = 'f9.2/
    &'set minmag = 'f9.2/
    &'set maxmag = 'f9.2/
    &"//
    &'psxy tmp1.dat -R0/$maxdist/$minmag/$maxmag -W0.1 -B
    &-JX6i > raw_profile.ps'/)

```

```

CLOSE(88)

```

```

CMD='chmod a+x raw_profile.gmt'
CALL SYSTEM (CMD)

```

```

CMD='raw_profile.gmt'
CALL SYSTEM (CMD)

```

```

CMD='gv raw_profile.ps'
CALL SYSTEM (CMD)

```

```

PRINT*,"
PRINT*,"
PRINT*,'Would you like to plot another raw profile? [Y or N]'
READ*,RPA
IF (RPA.eq.'Y') THEN
TIME=0
GOTO 397
ENDIF

```

c400's creation of a smoothing window.

c Lets calculate average distance between measurements.

```

400 PRINT*,"
    PRINT*,"

    SUMAVG=0
    DO i=1,COUNT4-1
    CALL DISTAZ (EVENT,LATDP(i),LONGDP(i),STNAME,LATDP(i+1),
    &LONGDP(i+1),DIST,DELTA,STOE,ETOS)
    SUMAVG=DIST+SUMAVG
    ENDDO

    SUMAVG=SUMAVG/(COUNT4-1)
    PRINT*,'The average station spacing is: ',SUMAVG
    PRINT*,'How large would you like your smoothing window [meters]?'

```

```
READ*, DW
```

cI use a linear smoothing window but more robust algorithms can be added later!

```

OPEN(11,file='tmp1.dat')
OPEN(22,file='smooth.dat')
DO i=1,MAX
  READ(11,*,END=411) SDIST(i),SMAG(i),SLONG(i),SLAT(i),SELEV(i)
c  NEG=SDIST(1)
  ENDDO
411 CLOSE(11)

  DO j=1,(i-1)
  IF(MOD(j,1000).eq.0) PRINT*,'Doing window ',j,' of ',i-1
  D1=SDIST(j)
  D2=D1+DW/1000
  SSMAG=0.0
  SSELEV=0.0
  NN=0
  DO k=1,(i-1)
  IF (SDIST(k).ge.D1.and.SDIST(k).LT.D2) THEN
    NN=NN+1
    SSMAG=SSMAG+SMAG(k)
    SSELEV=SSELEV+SELEV(k)
  ENDIF
  ENDDO

  IF (NN.ge.1) WRITE (22,420) D1+(DW/1000), SSMAG/NN, SSELEV/NN

420 FORMAT(F15.10,1x,f10.3,1x,F15.10)
  ENDDO
  CLOSE(22)

```

c Time to plot the result!

```

OPEN (33,file='smooth_profile.gmt')
WRITE(33,430) MAXDIST,MINMAG,MAXMAG
430 FORMAT('#!/bin/csh'//
  &'//
  &'set maxdist = 'f9.2/
  &'set minmag = 'f9.2/
  &'set maxmag = 'f9.2/
  &'//
  &'psxy tmp1.dat -R0/$maxdist/$minmag/$maxmag -W0.1/255/0/0 -B
  &-JX6i -St0.05 -K > smooth_profile.ps'//
  &'psxy smooth.dat -R -W0.5/0/0/255 -O -J >> smooth_profile.ps'//)

```

CLOSE(33)

```
CMD='chmod a+x smooth_profile.gmt'
CALL SYSTEM (CMD)
CMD='smooth_profile.gmt'
CALL SYSTEM (CMD)
CMD='gv smooth_profile.ps'
CALL SYSTEM (CMD)
```

c500's reduction to pole

C I will use Blakely, 1996 for RTP and some other transformations.
c Data needs to be sequential from west to east and north to east.

```
999 STOP
END
```

Subroutines needed for mag.f (Main)

JULDAY - calculates Julian Date:

```
function julday(mm,id,iyyy)
  integer julday,id,iyyy,mm,igreg
  parameter (igreg=15+31*(10+12*1582))
  integer ja,jm,jy
  jy=iyyy
  if (jy.eq.0) pause 'julday: there is no year zero'
  if (jy.lt.0) jy=jy+1
  if (mm.gt.2) then
    jm=mm+1
  else
    jy=jy-1
    jm=mm+13
  endif
  julday=int(365.25*jy)+int(30.6001*jm)+id+1720995
  if (id+31*(mm+12*iyyy).ge.igreg) then
    ja=int(0.01*jy)
    julday=julday+2-ja+int(0.25*ja)
  endif
  return
end
```

c (c) copr. 1986-92 numerical recipes software p"kb.

MINMAX - finds minimum and maximum of a vector set:

```
SUBROUTINE MINMAX (X2,NX,MIN,MAX)
```

```
    PARAMETER(N=1000000)
```

```
    REAL MIN, MAX
```

```
    INTEGER NX
```

```
    REAL X2(N)
```

```
    MIN=X2(1)
```

```
    MAX=X2(1)
```

```
    DO J=1,NX
```

```
    IF (X2(J).lt.MIN) MIN=X2(J)
```

```
    IF (X2(J).gt.MAX) MAX=X2(J)
```

```
    ENDDO
```

```
    RETURN
```

```
    END
```

IGRF10SYN - code I converted to a subroutine that calculates the 10th generation IGRF field for a given location and elevation

```
subroutine igrf10syn (isv,date,itYPE,alt,colat,elong,x,y,z,f)
```

```
c
```

```
c This is a synthesis routine for the 10th generation IGRF as agreed
c in December 2004 by IAGA Working Group V-MOD. It is valid 1900.0 to
c 2010.0 inclusive. Values for dates from 1945.0 to 2000.0 inclusive are
c definitive, otherwise they are non-definitive.
```

```
c INPUT
```

```
c isv = 0 if main-field values are required
```

```
c isv = 1 if secular variation values are required
```

```
c date = year A.D. Must be greater than or equal to 1900.0 and
c less than or equal to 2015.0. Warning message is given
c for dates greater than 2010.0. Must be double precision.
```

```
c itype = 1 if geodetic (spheroid)
```

```
c itype = 2 if geocentric (sphere)
```

```
c alt = height in km above sea level if itype = 1
```

```
c = distance from centre of Earth in km if itype = 2 (>3485 km)
```

```
c colat = colatitude (0-180)
```

```
c elong = east-longitude (0-360)
```

```
c alt, colat and elong must be double precision.
```

```
c OUTPUT
```

```
c x = north component (nT) if isv = 0, nT/year if isv = 1
```

```
c y = east component (nT) if isv = 0, nT/year if isv = 1
```

```
c z = vertical component (nT) if isv = 0, nT/year if isv = 1
```

```
c f = total intensity (nT) if isv = 0, rubbish if isv = 1
```

```
c
```

c To get the other geomagnetic elements (D, I, H and secular
c variations dD, dH, dI and dF) use routines ptoc and ptocsv.
c
c Adapted from 8th generation version to include new maximum degree for
c main-field models for 2000.0 and onwards and use WGS84 spheroid instead
c of International Astronomical Union 1966 spheroid as recommended by IAGA
c in July 2003. Reference radius remains as 6371.2 km - it is NOT the mean
c radius (= 6371.0 km) but 6371.2 km is what is used in determining the
c coefficients. Adaptation by Susan Macmillan, August 2003 (for
c 9th generation) and December 2004.
c 1995.0 coefficients as published in igrf9coeffs.xls and igrf10coeffs.xls
c used - (Kimmo Korhonen spotted 1 nT difference in 11 coefficients)
c Susan Macmillan July 2005

c

implicit double precision (a-h,o-z)

dimension gh(3060),g0(120),g1(120),g2(120),g3(120),g4(120),

1 g5(120),g6(120),g7(120),g8(120),g9(120),ga(120),

2 gb(120),gc(120),gd(120),ge(120),gf(120),gg(120),

3 gi(120),gj(120),gk(195),gl(195),gm(195),gp(195),

4 p(105),q(105),cl(13),sl(13)

equivalence (g0,gh(1)),(g1,gh(121)),(g2,gh(241)),(g3,gh(361)),

1 (g4,gh(481)),(g5,gh(601)),(g6,gh(721)),(g7,gh(841)),

2 (g8,gh(961)),(g9,gh(1081)),(ga,gh(1201)),

3 (gb,gh(1321)),(gc,gh(1441)),(gd,gh(1561)),

4 (ge,gh(1681)),(gf,gh(1801)),(gg,gh(1921)),

5 (gi,gh(2041)),(gj,gh(2161)),(gk,gh(2281)),

6 (gl,gh(2476)),(gm,gh(2671)),(gp,gh(2866))

c

data g0/ -31543.,-2298., 5922., -677., 2905.,-1061., 924., 1121., 1900

1 1022.,-1469., -330., 1256., 3., 572., 523., 876., 1900

2 628., 195., 660., -69., -361., -210., 134., -75., 1900

3 -184., 328., -210., 264., 53., 5., -33., -86., 1900

4 -124., -16., 3., 63., 61., -9., -11., 83., 1900

5 -217., 2., -58., -35., 59., 36., -90., -69., 1900

6 70., -55., -45., 0., -13., 34., -10., -41., 1900

7 -1., -21., 28., 18., -12., 6., -22., 11., 1900

8 8., 8., -4., -14., -9., 7., 1., -13., 1900

9 2., 5., -9., 16., 5., -5., 8., -18., 1900

a 8., 10., -20., 1., 14., -11., 5., 12., 1900

b -3., 1., -2., -2., 8., 2., 10., -1., 1900

c -2., -1., 2., -3., -4., 2., 2., 1., 1900

d -5., 2., -2., 6., 6., -4., 4., 0., 1900

e 0., -2., 2., 4., 2., 0., 0., -6./ 1900

data g1/ -31464.,-2298., 5909., -728., 2928.,-1086., 1041., 1065., 1905

1 1037.,-1494., -357., 1239., 34., 635., 480., 880., 1905

2 643., 203., 653., -77., -380., -201., 146., -65., 1905

3 -192., 328., -193., 259., 56., -1., -32., -93., 1905
 4 -125., -26., 11., 62., 60., -7., -11., 86., 1905
 5 -221., 4., -57., -32., 57., 32., -92., -67., 1905
 6 70., -54., -46., 0., -14., 33., -11., -41., 1905
 7 0., -20., 28., 18., -12., 6., -22., 11., 1905
 8 8., 8., -4., -15., -9., 7., 1., -13., 1905
 9 2., 5., -8., 16., 5., -5., 8., -18., 1905
 a 8., 10., -20., 1., 14., -11., 5., 12., 1905
 b -3., 1., -2., -2., 8., 2., 10., 0., 1905
 c -2., -1., 2., -3., -4., 2., 2., 1., 1905
 d -5., 2., -2., 6., 6., -4., 4., 0., 1905
 e 0., -2., 2., 4., 2., 0., 0., -6./ 1905
 data g2/ -31354., -2297., 5898., -769., 2948., -1128., 1176., 1000., 1910
 1 1058., -1524., -389., 1223., 62., 705., 425., 884., 1910
 2 660., 211., 644., -90., -400., -189., 160., -55., 1910
 3 -201., 327., -172., 253., 57., -9., -33., -102., 1910
 4 -126., -38., 21., 62., 58., -5., -11., 89., 1910
 5 -224., 5., -54., -29., 54., 28., -95., -65., 1910
 6 71., -54., -47., 1., -14., 32., -12., -40., 1910
 7 1., -19., 28., 18., -13., 6., -22., 11., 1910
 8 8., 8., -4., -15., -9., 6., 1., -13., 1910
 9 2., 5., -8., 16., 5., -5., 8., -18., 1910
 a 8., 10., -20., 1., 14., -11., 5., 12., 1910
 b -3., 1., -2., -2., 8., 2., 10., 0., 1910
 c -2., -1., 2., -3., -4., 2., 2., 1., 1910
 d -5., 2., -2., 6., 6., -4., 4., 0., 1910
 e 0., -2., 2., 4., 2., 0., 0., -6./ 1910
 data g3/ -31212., -2306., 5875., -802., 2956., -1191., 1309., 917., 1915
 1 1084., -1559., -421., 1212., 84., 778., 360., 887., 1915
 2 678., 218., 631., -109., -416., -173., 178., -51., 1915
 3 -211., 327., -148., 245., 58., -16., -34., -111., 1915
 4 -126., -51., 32., 61., 57., -2., -10., 93., 1915
 5 -228., 8., -51., -26., 49., 23., -98., -62., 1915
 6 72., -54., -48., 2., -14., 31., -12., -38., 1915
 7 2., -18., 28., 19., -15., 6., -22., 11., 1915
 8 8., 8., -4., -15., -9., 6., 2., -13., 1915
 9 3., 5., -8., 16., 6., -5., 8., -18., 1915
 a 8., 10., -20., 1., 14., -11., 5., 12., 1915
 b -3., 1., -2., -2., 8., 2., 10., 0., 1915
 c -2., -1., 2., -3., -4., 2., 2., 1., 1915
 d -5., 2., -2., 6., 6., -4., 4., 0., 1915
 e 0., -2., 1., 4., 2., 0., 0., -6./ 1915
 data g4/ -31060., -2317., 5845., -839., 2959., -1259., 1407., 823., 1920
 1 1111., -1600., -445., 1205., 103., 839., 293., 889., 1920
 2 695., 220., 616., -134., -424., -153., 199., -57., 1920
 3 -221., 326., -122., 236., 58., -23., -38., -119., 1920

4 -125., -62., 43., 61., 55., 0., -10., 96., 1920
 5 -233., 11., -46., -22., 44., 18., -101., -57., 1920
 6 73., -54., -49., 2., -14., 29., -13., -37., 1920
 7 4., -16., 28., 19., -16., 6., -22., 11., 1920
 8 7., 8., -3., -15., -9., 6., 2., -14., 1920
 9 4., 5., -7., 17., 6., -5., 8., -19., 1920
 a 8., 10., -20., 1., 14., -11., 5., 12., 1920
 b -3., 1., -2., -2., 9., 2., 10., 0., 1920
 c -2., -1., 2., -3., -4., 2., 2., 1., 1920
 d -5., 2., -2., 6., 6., -4., 4., 0., 1920
 e 0., -2., 1., 4., 3., 0., 0., -6./ 1920
 data g5/ -30926., -2318., 5817., -893., 2969., -1334., 1471., 728., 1925
 1 1140., -1645., -462., 1202., 119., 881., 229., 891., 1925
 2 711., 216., 601., -163., -426., -130., 217., -70., 1925
 3 -230., 326., -96., 226., 58., -28., -44., -125., 1925
 4 -122., -69., 51., 61., 54., 3., -9., 99., 1925
 5 -238., 14., -40., -18., 39., 13., -103., -52., 1925
 6 73., -54., -50., 3., -14., 27., -14., -35., 1925
 7 5., -14., 29., 19., -17., 6., -21., 11., 1925
 8 7., 8., -3., -15., -9., 6., 2., -14., 1925
 9 4., 5., -7., 17., 7., -5., 8., -19., 1925
 a 8., 10., -20., 1., 14., -11., 5., 12., 1925
 b -3., 1., -2., -2., 9., 2., 10., 0., 1925
 c -2., -1., 2., -3., -4., 2., 2., 1., 1925
 d -5., 2., -2., 6., 6., -4., 4., 0., 1925
 e 0., -2., 1., 4., 3., 0., 0., -6./ 1925
 data g6/ -30805., -2316., 5808., -951., 2980., -1424., 1517., 644., 1930
 1 1172., -1692., -480., 1205., 133., 907., 166., 896., 1930
 2 727., 205., 584., -195., -422., -109., 234., -90., 1930
 3 -237., 327., -72., 218., 60., -32., -53., -131., 1930
 4 -118., -74., 58., 60., 53., 4., -9., 102., 1930
 5 -242., 19., -32., -16., 32., 8., -104., -46., 1930
 6 74., -54., -51., 4., -15., 25., -14., -34., 1930
 7 6., -12., 29., 18., -18., 6., -20., 11., 1930
 8 7., 8., -3., -15., -9., 5., 2., -14., 1930
 9 5., 5., -6., 18., 8., -5., 8., -19., 1930
 a 8., 10., -20., 1., 14., -12., 5., 12., 1930
 b -3., 1., -2., -2., 9., 3., 10., 0., 1930
 c -2., -2., 2., -3., -4., 2., 2., 1., 1930
 d -5., 2., -2., 6., 6., -4., 4., 0., 1930
 e 0., -2., 1., 4., 3., 0., 0., -6./ 1930
 data g7/ -30715., -2306., 5812., -1018., 2984., -1520., 1550., 586., 1935
 1 1206., -1740., -494., 1215., 146., 918., 101., 903., 1935
 2 744., 188., 565., -226., -415., -90., 249., -114., 1935
 3 -241., 329., -51., 211., 64., -33., -64., -136., 1935
 4 -115., -76., 64., 59., 53., 4., -8., 104., 1935

5 -246., 25., -25., -15., 25., 4., -106., -40., 1935
 6 74., -53., -52., 4., -17., 23., -14., -33., 1935
 7 7., -11., 29., 18., -19., 6., -19., 11., 1935
 8 7., 8., -3., -15., -9., 5., 1., -15., 1935
 9 6., 5., -6., 18., 8., -5., 7., -19., 1935
 a 8., 10., -20., 1., 15., -12., 5., 11., 1935
 b -3., 1., -3., -2., 9., 3., 11., 0., 1935
 c -2., -2., 2., -3., -4., 2., 2., 1., 1935
 d -5., 2., -2., 6., 6., -4., 4., 0., 1935
 e 0., -1., 2., 4., 3., 0., 0., -6./ 1935
 data g8/ -30654., -2292., 5821., -1106., 2981., -1614., 1566., 528., 1940
 1 1240., -1790., -499., 1232., 163., 916., 43., 914., 1940
 2 762., 169., 550., -252., -405., -72., 265., -141., 1940
 3 -241., 334., -33., 208., 71., -33., -75., -141., 1940
 4 -113., -76., 69., 57., 54., 4., -7., 105., 1940
 5 -249., 33., -18., -15., 18., 0., -107., -33., 1940
 6 74., -53., -52., 4., -18., 20., -14., -31., 1940
 7 7., -9., 29., 17., -20., 5., -19., 11., 1940
 8 7., 8., -3., -14., -10., 5., 1., -15., 1940
 9 6., 5., -5., 19., 9., -5., 7., -19., 1940
 a 8., 10., -21., 1., 15., -12., 5., 11., 1940
 b -3., 1., -3., -2., 9., 3., 11., 1., 1940
 c -2., -2., 2., -3., -4., 2., 2., 1., 1940
 d -5., 2., -2., 6., 6., -4., 4., 0., 1940
 e 0., -1., 2., 4., 3., 0., 0., -6./ 1940
 data g9/ -30594., -2285., 5810., -1244., 2990., -1702., 1578., 477., 1945
 1 1282., -1834., -499., 1255., 186., 913., -11., 944., 1945
 2 776., 144., 544., -276., -421., -55., 304., -178., 1945
 3 -253., 346., -12., 194., 95., -20., -67., -142., 1945
 4 -119., -82., 82., 59., 57., 6., 6., 100., 1945
 5 -246., 16., -25., -9., 21., -16., -104., -39., 1945
 6 70., -40., -45., 0., -18., 0., 2., -29., 1945
 7 6., -10., 28., 15., -17., 29., -22., 13., 1945
 8 7., 12., -8., -21., -5., -12., 9., -7., 1945
 9 7., 2., -10., 18., 7., 3., 2., -11., 1945
 a 5., -21., -27., 1., 17., -11., 29., 3., 1945
 b -9., 16., 4., -3., 9., -4., 6., -3., 1945
 c 1., -4., 8., -3., 11., 5., 1., 1., 1945
 d 2., -20., -5., -1., -1., -6., 8., 6., 1945
 e -1., -4., -3., -2., 5., 0., -2., -2./ 1945
 data ga/ -30554., -2250., 5815., -1341., 2998., -1810., 1576., 381., 1950
 1 1297., -1889., -476., 1274., 206., 896., -46., 954., 1950
 2 792., 136., 528., -278., -408., -37., 303., -210., 1950
 3 -240., 349., 3., 211., 103., -20., -87., -147., 1950
 4 -122., -76., 80., 54., 57., -1., 4., 99., 1950
 5 -247., 33., -16., -12., 12., -12., -105., -30., 1950

6 65., -55., -35., 2., -17., 1., 0., -40., 1950
 7 10., -7., 36., 5., -18., 19., -16., 22., 1950
 8 15., 5., -4., -22., -1., 0., 11., -21., 1950
 9 15., -8., -13., 17., 5., -4., -1., -17., 1950
 a 3., -7., -24., -1., 19., -25., 12., 10., 1950
 b 2., 5., 2., -5., 8., -2., 8., 3., 1950
 c -11., 8., -7., -8., 4., 13., -1., -2., 1950
 d 13., -10., -4., 2., 4., -3., 12., 6., 1950
 e 3., -3., 2., 6., 10., 11., 3., 8./ 1950
 data gb/ -30500., -2215., 5820., -1440., 3003., -1898., 1581., 291., 1955
 1 1302., -1944., -462., 1288., 216., 882., -83., 958., 1955
 2 796., 133., 510., -274., -397., -23., 290., -230., 1955
 3 -229., 360., 15., 230., 110., -23., -98., -152., 1955
 4 -121., -69., 78., 47., 57., -9., 3., 96., 1955
 5 -247., 48., -8., -16., 7., -12., -107., -24., 1955
 6 65., -56., -50., 2., -24., 10., -4., -32., 1955
 7 8., -11., 28., 9., -20., 18., -18., 11., 1955
 8 9., 10., -6., -15., -14., 5., 6., -23., 1955
 9 10., 3., -7., 23., 6., -4., 9., -13., 1955
 a 4., 9., -11., -4., 12., -5., 7., 2., 1955
 b 6., 4., -2., 1., 10., 2., 7., 2., 1955
 c -6., 5., 5., -3., -5., -4., -1., 0., 1955
 d 2., -8., -3., -2., 7., -4., 4., 1., 1955
 e -2., -3., 6., 7., -2., -1., 0., -3./ 1955
 data gc/ -30421., -2169., 5791., -1555., 3002., -1967., 1590., 206., 1960
 1 1302., -1992., -414., 1289., 224., 878., -130., 957., 1960
 2 800., 135., 504., -278., -394., 3., 269., -255., 1960
 3 -222., 362., 16., 242., 125., -26., -117., -156., 1960
 4 -114., -63., 81., 46., 58., -10., 1., 99., 1960
 5 -237., 60., -1., -20., -2., -11., -113., -17., 1960
 6 67., -56., -55., 5., -28., 15., -6., -32., 1960
 7 7., -7., 23., 17., -18., 8., -17., 15., 1960
 8 6., 11., -4., -14., -11., 7., 2., -18., 1960
 9 10., 4., -5., 23., 10., 1., 8., -20., 1960
 a 4., 6., -18., 0., 12., -9., 2., 1., 1960
 b 0., 4., -3., -1., 9., -2., 8., 3., 1960
 c 0., -1., 5., 1., -3., 4., 4., 1., 1960
 d 0., 0., -1., 2., 4., -5., 6., 1., 1960
 e 1., -1., -1., 6., 2., 0., 0., -7./ 1960
 data gd/ -30334., -2119., 5776., -1662., 2997., -2016., 1594., 114., 1965
 1 1297., -2038., -404., 1292., 240., 856., -165., 957., 1965
 2 804., 148., 479., -269., -390., 13., 252., -269., 1965
 3 -219., 358., 19., 254., 128., -31., -126., -157., 1965
 4 -97., -62., 81., 45., 61., -11., 8., 100., 1965
 5 -228., 68., 4., -32., 1., -8., -111., -7., 1965
 6 75., -57., -61., 4., -27., 13., -2., -26., 1965

7 6., -6., 26., 13., -23., 1., -12., 13., 1965
 8 5., 7., -4., -12., -14., 9., 0., -16., 1965
 9 8., 4., -1., 24., 11., -3., 4., -17., 1965
 a 8., 10., -22., 2., 15., -13., 7., 10., 1965
 b -4., -1., -5., -1., 10., 5., 10., 1., 1965
 c -4., -2., 1., -2., -3., 2., 2., 1., 1965
 d -5., 2., -2., 6., 4., -4., 4., 0., 1965
 e 0., -2., 2., 3., 2., 0., 0., -6./ 1965
 data ge/ -30220., -2068., 5737., -1781., 3000., -2047., 1611., 25., 1970
 1 1287., -2091., -366., 1278., 251., 838., -196., 952., 1970
 2 800., 167., 461., -266., -395., 26., 234., -279., 1970
 3 -216., 359., 26., 262., 139., -42., -139., -160., 1970
 4 -91., -56., 83., 43., 64., -12., 15., 100., 1970
 5 -212., 72., 2., -37., 3., -6., -112., 1., 1970
 6 72., -57., -70., 1., -27., 14., -4., -22., 1970
 7 8., -2., 23., 13., -23., -2., -11., 14., 1970
 8 6., 7., -2., -15., -13., 6., -3., -17., 1970
 9 5., 6., 0., 21., 11., -6., 3., -16., 1970
 a 8., 10., -21., 2., 16., -12., 6., 10., 1970
 b -4., -1., -5., 0., 10., 3., 11., 1., 1970
 c -2., -1., 1., -3., -3., 1., 2., 1., 1970
 d -5., 3., -1., 4., 6., -4., 4., 0., 1970
 e 1., -1., 0., 3., 3., 1., -1., -4./ 1970
 data gf/ -30100., -2013., 5675., -1902., 3010., -2067., 1632., -68., 1975
 1 1276., -2144., -333., 1260., 262., 830., -223., 946., 1975
 2 791., 191., 438., -265., -405., 39., 216., -288., 1975
 3 -218., 356., 31., 264., 148., -59., -152., -159., 1975
 4 -83., -49., 88., 45., 66., -13., 28., 99., 1975
 5 -198., 75., 1., -41., 6., -4., -111., 11., 1975
 6 71., -56., -77., 1., -26., 16., -5., -14., 1975
 7 10., 0., 22., 12., -23., -5., -12., 14., 1975
 8 6., 6., -1., -16., -12., 4., -8., -19., 1975
 9 4., 6., 0., 18., 10., -10., 1., -17., 1975
 a 7., 10., -21., 2., 16., -12., 7., 10., 1975
 b -4., -1., -5., -1., 10., 4., 11., 1., 1975
 c -3., -2., 1., -3., -3., 1., 2., 1., 1975
 d -5., 3., -2., 4., 5., -4., 4., -1., 1975
 e 1., -1., 0., 3., 3., 1., -1., -5./ 1975
 data gg/ -29992., -1956., 5604., -1997., 3027., -2129., 1663., -200., 1980
 1 1281., -2180., -336., 1251., 271., 833., -252., 938., 1980
 2 782., 212., 398., -257., -419., 53., 199., -297., 1980
 3 -218., 357., 46., 261., 150., -74., -151., -162., 1980
 4 -78., -48., 92., 48., 66., -15., 42., 93., 1980
 5 -192., 71., 4., -43., 14., -2., -108., 17., 1980
 6 72., -59., -82., 2., -27., 21., -5., -12., 1980
 7 16., 1., 18., 11., -23., -2., -10., 18., 1980

8 6., 7., 0., -18., -11., 4., -7., -22., 1980
 9 4., 9., 3., 16., 6., -13., -1., -15., 1980
 a 5., 10., -21., 1., 16., -12., 9., 9., 1980
 b -5., -3., -6., -1., 9., 7., 10., 2., 1980
 c -6., -5., 2., -4., -4., 1., 2., 0., 1980
 d -5., 3., -2., 6., 5., -4., 3., 0., 1980
 e 1., -1., 2., 4., 3., 0., 0., -6./ 1980
 data gi/ -29873., -1905., 5500., -2072., 3044., -2197., 1687., -306., 1985
 1 1296., -2208., -310., 1247., 284., 829., -297., 936., 1985
 2 780., 232., 361., -249., -424., 69., 170., -297., 1985
 3 -214., 355., 47., 253., 150., -93., -154., -164., 1985
 4 -75., -46., 95., 53., 65., -16., 51., 88., 1985
 5 -185., 69., 4., -48., 16., -1., -102., 21., 1985
 6 74., -62., -83., 3., -27., 24., -2., -6., 1985
 7 20., 4., 17., 10., -23., 0., -7., 21., 1985
 8 6., 8., 0., -19., -11., 5., -9., -23., 1985
 9 4., 11., 4., 14., 4., -15., -4., -11., 1985
 a 5., 10., -21., 1., 15., -12., 9., 9., 1985
 b -6., -3., -6., -1., 9., 7., 9., 1., 1985
 c -7., -5., 2., -4., -4., 1., 3., 0., 1985
 d -5., 3., -2., 6., 5., -4., 3., 0., 1985
 e 1., -1., 2., 4., 3., 0., 0., -6./ 1985
 data gj/ -29775., -1848., 5406., -2131., 3059., -2279., 1686., -373., 1990
 1 1314., -2239., -284., 1248., 293., 802., -352., 939., 1990
 2 780., 247., 325., -240., -423., 84., 141., -299., 1990
 3 -214., 353., 46., 245., 154., -109., -153., -165., 1990
 4 -69., -36., 97., 61., 65., -16., 59., 82., 1990
 5 -178., 69., 3., -52., 18., 1., -96., 24., 1990
 6 77., -64., -80., 2., -26., 26., 0., -1., 1990
 7 21., 5., 17., 9., -23., 0., -4., 23., 1990
 8 5., 10., -1., -19., -10., 6., -12., -22., 1990
 9 3., 12., 4., 12., 2., -16., -6., -10., 1990
 a 4., 9., -20., 1., 15., -12., 11., 9., 1990
 b -7., -4., -7., -2., 9., 7., 8., 1., 1990
 c -7., -6., 2., -3., -4., 2., 2., 1., 1990
 d -5., 3., -2., 6., 4., -4., 3., 0., 1990
 e 1., -2., 3., 3., 3., -1., 0., -6./ 1990
 data gk/ -29692., -1784., 5306., -2200., 3070., -2366., 1681., -413., 1995
 1 1335., -2267., -262., 1249., 302., 759., -427., 940., 1995
 2 780., 262., 290., -236., -418., 97., 122., -306., 1995
 3 -214., 352., 46., 235., 165., -118., -143., -166., 1995
 4 -55., -17., 107., 68., 67., -17., 68., 72., 1995
 5 -170., 67., -1., -58., 19., 1., -93., 36., 1995
 6 77., -72., -69., 1., -25., 28., 4., 5., 1995
 7 24., 4., 17., 8., -24., -2., -6., 25., 1995
 8 6., 11., -6., -21., -9., 8., -14., -23., 1995

9 9., 15., 6., 11., -5., -16., -7., -4., 1995
 a 4., 9., -20., 3., 15., -10., 12., 8., 1995
 b -6., -8., -8., -1., 8., 10., 5., -2., 1995
 c -8., -8., 3., -3., -6., 1., 2., 0., 1995
 d -4., 4., -1., 5., 4., -5., 2., -1., 1995
 e 2., -2., 5., 1., 1., -2., 0., -7., 1995
 f 75*0./ 1995
 data gl/ -29619.4,-1728.2, 5186.1,-2267.7, 3068.4,-2481.6, 1670.9, 2000
 1 -458.0, 1339.6,-2288.0, -227.6, 1252.1, 293.4, 714.5, 2000
 2 -491.1, 932.3, 786.8, 272.6, 250.0, -231.9, -403.0, 2000
 3 119.8, 111.3, -303.8, -218.8, 351.4, 43.8, 222.3, 2000
 4 171.9, -130.4, -133.1, -168.6, -39.3, -12.9, 106.3, 2000
 5 72.3, 68.2, -17.4, 74.2, 63.7, -160.9, 65.1, 2000
 6 -5.9, -61.2, 16.9, 0.7, -90.4, 43.8, 79.0, 2000
 7 -74.0, -64.6, 0.0, -24.2, 33.3, 6.2, 9.1, 2000
 8 24.0, 6.9, 14.8, 7.3, -25.4, -1.2, -5.8, 2000
 9 24.4, 6.6, 11.9, -9.2, -21.5, -7.9, 8.5, 2000
 a -16.6, -21.5, 9.1, 15.5, 7.0, 8.9, -7.9, 2000
 b -14.9, -7.0, -2.1, 5.0, 9.4, -19.7, 3.0, 2000
 c 13.4, -8.4, 12.5, 6.3, -6.2, -8.9, -8.4, 2000
 d -1.5, 8.4, 9.3, 3.8, -4.3, -8.2, -8.2, 2000
 e 4.8, -2.6, -6.0, 1.7, 1.7, 0.0, -3.1, 2000
 f 4.0, -0.5, 4.9, 3.7, -5.9, 1.0, -1.2, 2000
 g 2.0, -2.9, 4.2, 0.2, 0.3, -2.2, -1.1, 2000
 h -7.4, 2.7, -1.7, 0.1, -1.9, 1.3, 1.5, 2000
 i -0.9, -0.1, -2.6, 0.1, 0.9, -0.7, -0.7, 2000
 j 0.7, -2.8, 1.7, -0.9, 0.1, -1.2, 1.2, 2000
 k -1.9, 4.0, -0.9, -2.2, -0.3, -0.4, 0.2, 2000
 l 0.3, 0.9, 2.5, -0.2, -2.6, 0.9, 0.7, 2000
 m -0.5, 0.3, 0.3, 0.0, -0.3, 0.0, -0.4, 2000
 n 0.3, -0.1, -0.9, -0.2, -0.4, -0.4, 0.8, 2000
 o -0.2, -0.9, -0.9, 0.3, 0.2, 0.1, 1.8, 2000
 p -0.4, -0.4, 1.3, -1.0, -0.4, -0.1, 0.7, 2000
 q 0.7, -0.4, 0.3, 0.3, 0.6, -0.1, 0.3, 2000
 r 0.4, -0.2, 0.0, -0.5, 0.1, -0.9/ 2000
 data gm/ -29556.8,-1671.8, 5080.0,-2340.5, 3047.0,-2594.9, 1656.9, 2005
 1 -516.7, 1335.7,-2305.3, -200.4, 1246.8, 269.3, 674.4, 2005
 2 -524.5, 919.8, 798.2, 281.4, 211.5, -225.8, -379.5, 2005
 3 145.7, 100.2, -304.7, -227.6, 354.4, 42.7, 208.8, 2005
 4 179.8, -136.6, -123.0, -168.3, -19.5, -14.1, 103.6, 2005
 5 72.9, 69.6, -20.2, 76.6, 54.7, -151.1, 63.7, 2005
 6 -15.0, -63.4, 14.7, 0.0, -86.4, 50.3, 79.8, 2005
 7 -74.4, -61.4, -1.4, -22.5, 38.6, 6.9, 12.3, 2005
 8 25.4, 9.4, 10.9, 5.5, -26.4, 2.0, -4.8, 2005
 9 24.8, 7.7, 11.2, -11.4, -21.0, -6.8, 9.7, 2005
 a -18.0, -19.8, 10.0, 16.1, 9.4, 7.7, -11.4, 2005

```

b      -12.8, -5.0, -0.1, 5.6, 9.8, -20.1, 3.6, 2005
c      12.9, -7.0, 12.7, 5.0, -6.7, -10.8, -8.1, 2005
d      -1.3, 8.1, 8.7, 2.9, -6.7, -7.9, -9.2, 2005
e      5.9, -2.2, -6.3, 2.4, 1.6, 0.2, -2.5, 2005
f      4.4, -0.1, 4.7, 3.0, -6.5, 0.3, -1.0, 2005
g      2.1, -3.4, 3.9, -0.9, -0.1, -2.3, -2.2, 2005
h      -8.0, 2.9, -1.6, 0.3, -1.7, 1.4, 1.5, 2005
i      -0.7, -0.2, -2.4, 0.2, 0.9, -0.7, -0.6, 2005
j      0.5, -2.7, 1.8, -1.0, 0.1, -1.5, 1.0, 2005
k      -2.0, 4.1, -1.4, -2.2, -0.3, -0.5, 0.3, 2005
l      0.3, 0.9, 2.3, -0.4, -2.7, 1.0, 0.6, 2005
m      -0.4, 0.4, 0.5, 0.0, -0.3, 0.0, -0.4, 2005
n      0.3, 0.0, -0.8, -0.4, -0.4, 0.0, 1.0, 2005
o      -0.2, -0.9, -0.7, 0.3, 0.3, 0.3, 1.7, 2005
p      -0.4, -0.5, 1.2, -1.0, -0.4, 0.0, 0.7, 2005
q      0.7, -0.3, 0.2, 0.4, 0.6, -0.1, 0.4, 2005
r      0.4, -0.2, -0.1, -0.5, -0.3, -1.0/    2005
data gp/ 8.8, 10.8, -21.3, -15.0, -6.9, -23.3, -1.0, -14.0, 2007
1      -0.3, -3.1, 5.4, -0.9, -6.5, -6.8, -2.0, -2.5, 2007
2      2.8, 2.0, -7.1, 1.8, 5.9, 5.6, -3.2, 0.0, 2007
3      -2.6, 0.4, 0.1, -3.0, 1.8, -1.2, 2.0, 0.2, 2007
4      4.5, -0.6, -1.0, -0.8, 0.2, -0.4, -0.2, -1.9, 2007
5      2.1, -0.4, -2.1, -0.4, -0.4, -0.2, 1.3, 0.9, 2007
6      -0.4, 0.0, 0.8, -0.2, 0.4, 1.1, 0.1, 0.6, 2007
7      0.2, 0.4, -0.9, -0.5, -0.3, 0.9, 0.3, -0.2, 2007
8      0.2, -0.2, -0.2, 0.2, 0.2, 0.2, -0.2, 0.4, 2007
9      0.2, 0.2, 0.5, -0.3, -0.7, 0.5, 0.5, 0.4, 2007
a      115*0.0/    2007

c
c  set initial values
c
x  = 0.0
y  = 0.0
z  = 0.0
if (date.lt.1900.0.or.date.gt.2015.0) go to 11
if (date.gt.2010.0) write (6,960) date
960 format (' This version of the IGRF is intended for use up',
1      ' to 2010.0.!' values for',f9.3,' will be computed',
2      ' but may be of reduced accuracy!')
if (date.ge.2005.0) go to 1
t  = 0.2*(date - 1900.0)
ll = t
one = ll
t  = t - one
if (date.lt.1995.0) then
nmx = 10

```

```

nc = nmx*(nmx+2)
ll = nc*ll
kmx = (nmx+1)*(nmx+2)/2
else
nmx = 13
nc = nmx*(nmx+2)
ll = 0.2*(date - 1995.0)
ll = 120*19 + nc*ll
kmx = (nmx+1)*(nmx+2)/2
endif
tc = 1.0 - t
if (isv.eq.1) then
tc = -0.2
t = 0.2
end if
go to 2
c
1 t = date - 2005.0
tc = 1.0
if (isv.eq.1) then
t = 1.0
tc = 0.0
end if
ll = 2670
nmx = 13
nc = nmx*(nmx+2)
kmx = (nmx+1)*(nmx+2)/2
2 r = alt
one = colat*0.017453292
ct = cos(one)
st = sin(one)
one = elong*0.017453292
cl(1) = cos(one)
sl(1) = sin(one)
cd = 1.0
sd = 0.0
l = 1
m = 1
n = 0
if (itype.eq.2) go to 3
c
c conversion from geodetic to geocentric coordinates
c (using the WGS84 spheroid)
c
a2 = 40680631.6
b2 = 40408296.0

```

```

one = a2*st*st
two = b2*ct*ct
three = one + two
rho = sqrt(three)
r = sqrt(alt*(alt + 2.0*rho) + (a2*one + b2*two)/three)
cd = (alt + rho)/r
sd = (a2 - b2)/rho*ct*st/r
one = ct
ct = ct*cd - st*sd
st = st*cd + one*sd
c
3 ratio = 6371.2/r
rr = ratio*ratio
c
c computation of Schmidt quasi-normal coefficients p and x(=q)
c
p(1) = 1.0
p(3) = st
q(1) = 0.0
q(3) = ct
do 10 k=2,kmx
if (n.ge.m) go to 4
m = 0
n = n + 1
rr = rr*ratio
fn = n
gn = n - 1
4 fm = m
if (m.ne.n) go to 5
if (k.eq.3) go to 6
one = sqrt(1.0 - 0.5/fm)
j = k - n - 1
p(k) = one*st*p(j)
q(k) = one*(st*q(j) + ct*p(j))
cl(m) = cl(m-1)*cl(1) - sl(m-1)*sl(1)
sl(m) = sl(m-1)*cl(1) + cl(m-1)*sl(1)
go to 6
5 gmm = m*m
one = sqrt(fn*fn - gmm)
two = sqrt(gn*gn - gmm)/one
three = (fn + gn)/one
i = k - n
j = i - n + 1
p(k) = three*ct*p(i) - two*p(j)
q(k) = three*(ct*q(i) - st*p(i)) - two*q(j)
c

```



```

subroutine distaz (event,evlatt,evlonn,stname,slatt,
*stlonn,dist,delta,stoe,etos)
c
c----Computes distances and azimuths between a station and an
c epicenter on an ellipsoidal earth. Uses spherical-trigonometry
c solution with geocentric latitude.
c----Completely rewritten 04/87 to use Bruce Julian's routines,
c however, north and west still are positive here.
c PHIL SLACK: changed longitude to positive east.
c----"event": event location and date
c "stname": station name (same use as "event").
c ("event" and "stname" are not used in current version)
c----"evlatt": event latitude in decimal degrees.
c "evlonn": event longitude " " " .
c "slatt": station latitude " " " .
c "stlonn": station longitude " " " .
c----"dist": epicenter-station distance in kilometers assuming
c one degree is KMDG km (better algorithms exist).
c "delta": epicenter-station distance in degrees (should be
c fully accurate).
c "stoe": station-to-epicenter azimuth
c "etos": event-to-station azimuth
c
include 'stdparm'
include 'stdconst'
c
character*4 stname
character*1 event(19)
double precision evlatt,evlonn,slatt,stlonn
double precision latev,lonev,latst,lonst,del,az,bz,ggtoqc
real dist,delta,stoe,etos,sngl
c
c----Make coordinates radians, east-positive, and geocentric
c
latev=ggtoqc(evlatt*DRAD)
lonev=evlonn*DRAD
latst=ggtoqc(stlatt*DRAD)
lonst=stlonn*DRAD
c
c----calculate
call refpt (latev,lonev)
call delaz (latst,lonst,del,az,bz)
c
c----convert for output
delta=sngl(del*DDEG)
dist=delta*KMDG

```

```

    stoe=sngl(bz*DDEG)
    etos=sngl(az*DDEG)
c
    return
    end

```

Misc. utility programs for generating profile data for plotting with GMT

Date profile.f

*Program to create profile data from lat long profile

```

PROGRAM PROFILE

PARAMETER (MAX=10000000,PI=3.14159265)

CHARACTER*50 CMD
DOUBLE PRECISION DATA(MAX),DIST1(MAX),ANG1(MAX),ANG2(MAX),
&SMOOTH(MAX),PX1,PY1,PX2,PY2,LAT(MAX),LONG(MAX),TDIST(MAX),
&D1,D2,SSMAG,DISTMAX,DISTMIN,ELEV(MAX)

*Declare endpoints of profile (W to E)
PX1=40.932
PY1=11.711
PX2=41.302
PY2=11.971

OPEN(5,file='tpm.dat')

DO I=1,MAX
READ (5,*,end=111) LONG(I),LAT(I), DATA(I),ELEV(I)
PRINT*,LONG(I)
CALL DISTAZ(event,LAT(I),LONG(I),stname,PY1,PX1,DIST, DELTA,ANG
&,ETOS)
DIST1(I)=DIST
ANG1(I)=ANG
ENDDO

111 CLOSE(5)

CALL DISTAZ(event,PY2,PX2,stname,PY1,PX1,DIST,DELTA,ANG,ETOS)
DANG=ANG

OPEN(6,file='tpm.out')
DO J=1,I-1
IF (ANG1(J).ge.DANG) THEN
ANG2(J)=ANG1(J)-DANG
ELSE

```

```

ANG2(J)=DANG-ANG1(J)
ENDIF
TDIST(J)=COS(ANG2(J)*PI/180)*DIST1(J)
WRITE(6,*)TDIST(J),DATA(J),ELEV(J)
ENDDO

CLOSE(6)

CMD='sort -n tpm.out > tpmsort.out'
CALL SYSTEM (CMD)

END

```

profile.f

*Program to create profile data from lat long profile

```

PROGRAM PROFILE

PARAMETER (MAX=10000000,PI=3.14159265)

CHARACTER*50 CMD
DOUBLE PRECISION DATA(MAX),DIST1(MAX),ANG1(MAX),ANG2(MAX),
&SMOOTH(MAX),PX1,PY1,PX2,PY2,LAT(MAX),LONG(MAX),TDIST(MAX),
&D1,D2,SSMAG,DISTMAX,DISTMIN,ELEV(MAX)

```

*Declare endpoints of profile (W to E)

```

PX1=40.932
PY1=11.711
PX2=41.302
PY2=11.971

```

```

OPEN(5,file='profile_north.txt')

```

```

DO I=1,MAX
READ (5,*,end=111) LONG(I),LAT(I), DATA(I),ELEV(I)
PRINT*,LONG(I)
CALL DISTAZ(event,LAT(I),LONG(I),stname,PY1,PX1,DIST, DELTA,ANG
&,ETOS)
DIST1(I)=DIST
ANG1(I)=ANG
ENDDO

```

```

111 CLOSE(5)

```

```

CALL DISTAZ(event,PY2,PX2,stname,PY1,PX1,DIST,DELTA,ANG,ETOS)
DANG=ANG

OPEN(6,file='profile_north.out')
DO J=1,I-1
IF (ANG1(J).ge.DANG) THEN
ANG2(J)=ANG1(J)-DANG
ELSE
ANG2(J)=DANG-ANG1(J)
ENDIF
TDIST(J)=COS(ANG2(J)*PI/180)*DIST1(J)
WRITE(6,*)TDIST(J),DATA(J),ELEV(J)
ENDDO

CLOSE(6)

CMD='sort -n profile_north.out > profile_northsort.out'
CALL SYSTEM (CMD)

****time to smooth teh gravity data****Comment this section out for mag data
OPEN(7,file='pp_1sort.out')
OPEN(8,file='pp_1smooth.out')

DISTMAX=0
DISTMIN=10000000
DO L=1,I-1
READ(7,*) TDIST(L),DATA(L),ELEV(L)
IF (TDIST(L).ge.DISTMAX) DISTMAX=TDIST(L)
IF (TDIST(L).le.DISTMIN) DISTMIN=TDIST(L)
ENDDO

* DO K=3,I-4 !Set smooth window to 10 measurementnts for Addis data
* only or small n<500 data sets
* SMOOTH(K)=(DATA(K-2)+DATA(K-1)+DATA(K)+DATA(K+1)+DATA(K+2))/5.0
c DO K=5,I-6
c SMOOTH(K)=(DATA(K-4)+DATA(K-3)+DATA(K-2)+DATA(K-1)+DATA(K)+
c &DATA(K+1)+ DATA(K+2)+ DATA(K+3)+DATA(K+4)+DATA(K+5))/10.0
c WRITE(8,*) TDIST(K), SMOOTH(K), ELEV(K)
c ENDDO

c CLOSE(8)
CLOSE(7)

c smoothing for larger data n>500 stations
c set window size in km

```

```

WIN=1.0 !km

DO M=1,I-1
c  IF (MOD(M,1000).eq.0) PRINT*,'DOING WINDOW ',M,' OF ',I-1
    D1=TDIST(M)
    D2=D1+WIN/2.0
    SSMAG=0.0
    NN=0
    DO N=1,I-1
    IF (TDIST(N).ge.D1.and.TDIST(N).lt.D2) THEN
    NN=NN+1
    SSMAG=SSMAG+DATA(N)
    ENDIF
    ENDDO
c  PRINT*, TDIST(M),DISTMIN ,DISTMAX
    IF(TDIST(M).ge.(DISTMIN+WIN/2.0).and.TDIST(M).lt.(DISTMAX-WIN/2.0)
    &)WRITE(8,*) TDIST(M) ,SSMAG/NN ,ELEV(M)
    ENDDO
    CLOSE(8)

END

```

SAKI input files for 2D forward/inversion codes after Webring(1985). Example files are for the main profile across the Tendaho Graben

Parameter File

Final.param

&parms

mfile='simple.mod'

efield=36592, einc=9.083, edec=1.83

azmuth=54.5

&

```

## This parameter file uses the field values
## computed with the 'make_synthetic.param'
## parameter file. The field value files are
## renamed from gfield.out and hfield.out (program
## default names).
## hfile='final_h2b.obs'

```

Magnetic Observation File**Final h.obs**

2.26692034 -115.062263
2.76697485 -101.229581
3.26768692 -88.6024244
3.76789757 -79.9393218
4.26936207 -75.1309188
4.77016164 -74.6353415
5.2709825 -77.2135983
5.77147667 -77.5484552
6.27248008 -70.281395
6.77262204 -56.5715278
7.27295949 -42.7783343
7.77309774 -31.3650282
8.27392646 -17.3112638
8.7743031 9.9089442
9.27470579 55.1148167
9.77492227 110.116116
10.2751133 170.14442
10.7754801 237.777633
11.2793382 313.411219
11.7793488 384.49232
12.2802775 426.520263
12.7806821 421.283672
13.2810004 387.590679
13.7812202 362.549119
14.2813138 360.989337
14.7814283 376.505824
15.2822019 397.2161
15.7828962 411.572503
16.2835253 408.268594
16.7840164 379.145689
17.2845487 328.064127
17.7848768 271.531154
18.2854254 223.782311
18.7861076 181.170881
19.2864829 121.351961
19.786677 31.2922941
20.2871854 -69.1169128
20.7877339 -147.897873
21.2879448 -199.879097
21.7879897 -240.323612
22.2882554 -282.24812
22.7893654 -321.462292
23.2902645 -341.611859
23.7907562 -341.440404

24.2909818 -328.813818
24.7922857 -307.959351
25.2925439 -295.306871
25.7937553 -312.023291
26.2948953 -363.855653
26.7961026 -424.627259
27.2964225 -462.602739
27.7970169 -465.383935
28.2975078 -429.572053
28.7985672 -357.388843
29.298636 -264.42265
29.7994919 -173.269858
30.3001489 -96.4023607
30.8002071 -36.948303
31.3004753 7.57049362
31.8008355 31.7448315
32.3011235 31.7359093
32.8016592 11.1345497
33.3025847 -19.8898827
33.8026356 -47.9211314
34.3030687 -55.1920053
34.8042224 -34.0810541
35.304507 2.06596641
35.8052719 30.8177161
36.3062857 41.0332706
36.807091 38.9490677
37.3079891 38.5516246
37.8088806 48.4364406
38.3092186 64.8336208
38.8093215 82.1654744
39.3116783 93.8157069
39.8118859 87.4214184
40.3126087 49.8376677
40.8136613 -9.132243
41.314146 -55.1808889
41.8152037 -66.3354822
42.3160726 -52.3699985
42.8161055 -39.3243271
43.3164923 -41.6533676
43.8165373 -56.2946124
44.3174936 -70.9529331
44.8181107 -78.2831818
45.3186248 -77.6042319
45.8192904 -68.6870287
46.3193774 -51.8764773
46.8195955 -30.0593487

47.3201607 -8.88824266

Gravity Observation Files

final-g.obs

2.63908026 -57.0853370513
3.15031647 -57.8417562057
3.81928097 -59.0195889308
4.40139656 -59.692693791
6.02639611 -61.3637732006
6.34306692 -61.3228404059
6.74594114 -61.2758616292
7.22218341 -61.2151251201
7.70547935 -61.1658933817
8.20474269 -61.1781513125
8.70121016 -61.2675358956
9.21039875 -61.4297505868
9.79090272 -61.7732493349
10.3069621 -62.2319101286
10.6515757 -62.392422751
10.9952288 -62.7826915738
11.3774834 -63.1669868438
11.811767 -63.560993686
12.353584 -63.7395535321
12.8783831 -63.6844253609
13.4031115 -63.4048678561
13.9293069 -63.0869864458
14.5057771 -62.7825780301
15.0664613 -62.580068824
15.6470292 -62.2284653003
16.2013399 -61.5197480595
16.7519415 -60.5402479245
17.2928027 -59.3198671358
17.8885824 -58.496077698
18.1920078 -58.054828311
18.4354978 -57.7699115426
18.4354978 -57.7699115426
18.5809733 -57.6374218865
19.0769235 -57.2192045244
19.5021287 -56.9175426494
19.5021287 -56.9175426494
19.7548646 -56.7629097548
20.371159 -56.5203617219
20.4745814 -56.4906221485
20.4745814 -56.4906221485
20.9020325 -56.4150003503
21.0202423 -56.385601551

21.0202423 -56.385601551
21.4692759 -56.2745682295
21.6016358 -56.2580836829
21.6016358 -56.2580836829
22.0027475 -56.0528258491
22.2306811 -55.914826296
22.2306811 -55.914826296
22.5408648 -55.7030001341
22.7859429 -55.4682802499
22.7859429 -55.4682802499
23.1427587 -55.1283690475
23.3537099 -54.9136040617
23.3537099 -54.9136040617
23.7751732 -54.459814817
23.9424099 -54.0823762165
23.9424099 -54.0823762165
24.3631358 -53.5931896891
24.943301 -52.7389910667
25.4927554 -51.9304628648
26.0514152 -51.5148758963
26.5910329 -51.6616777421
27.152522 -52.0862366754
27.6924454 -52.6873802565
28.2598728 -53.2962404051
28.8327383 -54.0169218389
29.4327246 -55.1176515754
30.0026917 -56.0728283075
30.563311 -56.7198593635
31.147668 -57.5781518219
31.7357086 -58.2782938981
32.3208771 -58.7916716182
32.9635905 -59.1942662796
33.6950499 -59.8554325663
34.3104478 -60.1260916317
34.9162149 -60.3770242516
35.4704991 -60.4138751972
36.0268713 -60.2291018374
36.5689811 -59.888478823
37.087792 -59.439781158
37.6179249 -58.8662031167
38.1704803 -58.2267992983
38.7135242 -57.6050161705
39.2496194 -57.0558427642
39.7942828 -56.5365324844
40.3347645 -56.0854978769
40.8693662 -55.6149756475

41.6188189 -54.9791712851
 42.1831611 -54.8637974676
 42.7200976 -54.8344134666
 43.2489967 -54.8252269635
 43.7811519 -54.7512672028
 44.3027776 -54.5107419079
 44.8330993 -54.1689387785
 45.4043473 -53.9052517449
 45.9534469 -53.9616435669
 46.5353282 -54.4822403182
 47.1237341 -55.9039353663
 47.7032623 -57.0181254475
 48.2250455 -57.6058456578
 48.7537655 -57.9428385946
 49.1576478 -57.9819749551
 49.6957325 -57.5755455141
 50.3409813 -57.063401603
 51.0561394 -56.8773356994
 52.1623684 -56.6607767582
 53.080513 -55.8377436922
 53.8955581 -55.237301788
 54.7578842 -55.1125748485

Model File

Final.mod

-300 26 0 26 15 26 25 23 35 26 50 26 350 26 350 30
 -300 30 -300 20 0 20 16.6 20 33.4 20 50 20 350 20
 -300 8 0 8 20 8 30 8 50 8 350 8 23.5 2 26.5 2
 26.5 8 23.5 8 20 1.5 30 1.5 30 3.5 20 3.5 -300 2.5
 0 2.5 50 2.5 350 2.5 -300 0.5 0 0.5 50 0.5 350 0.5
 -300 0.001 0 0.001 13.75 0.001 5.6 0.8 16 0.5
 19.3 1.4 30 0.9 33 0.5 34.2 0.5 34.2 0.3 39 0.3
 39 0.5 41.6 0.5 42 0.9 31 1.4 33.1 0.001 40 0.001
 50 0.001 350 0.001 17 0.1 17 0.5 18.3 0.1

>>*bodies*<<

0.230 0.000000 0 0 0 0 0 <<*dikeheat*>>
 22 23 24 25 <<*dikeheat*>>
 0.23 0.000795775 0 0 0.005 9.1 1.83 <<*dikeM*>>
 26 27 28 19 24 23 22 25 18 29 <<*dikeM*>>
 0.011 0.000795775 0 0 0.0027 -32.7 169 <<*uc1*>>
 30 31 29 18 17 16 <<*uc1*>>
 0.011 0.000795775 0 0 0.0027 -32.7 169 <<*uc2*>>
 28 32 33 21 20 19 <<*uc2*>>
 0.230 0.000795775 0 0 0.0027 -32.7 169 <<*strat1*>>

```

34 35 41 43 26 29 31 30 <<*strat1*>>
0.230 0.000795775 0 0 0.0027 -14.4 180 <<*strat2*>>
27 52 51 36 37 33 32 28 <<*strat2*>>
-0.460 0.000000 0 0 0 0 <<*sed1*>>
38 39 40 41 35 34 <<*sed1*>>
-0.230 0.000795775 0 0 0.0020 -15 190 <<*semeraR*>>
41 40 42 58 43 <<*semeraR*>>
-0.460 0.0000000 0 0 0 0 <<*sed2*>>
57 53 45 44 52 27 26 43 58 59 <<*sed2*>>
-0.230 0.000795775 0 0 0.002700 -15 190 <<*karubR*>>
44 45 46 47 48 49 50 51 52 <<*karubR*>>
-0.230 0.000795775 0 0 0.00270 9.083 1.83 <<*karubN*>>
53 54 50 49 48 47 46 45 <<*karubN*>>
-0.460 0.0000000 0 0 0 0 <<*sed 3*>>
54 55 56 37 36 51 50 <<*sed 3*>>
-0.230 0.000795775 0 0 0.0027 9.083 1.83 <<*semeraN*>>
40 57 59 58 42 <<*semeraN*>>

```

MATLAB CODES

FORWARD MODELING SCRIPTS

mag3D.m – forward mag/grav 3D modeling routine of Singh, 2001 used to generate Tendaho 3D magnetic model.

```

%clear all
Gc= 6.6732e-3; % Universal Gravitational constant.
% trapezod % Change this filename to compute other models
% prisma;
multibodexpB

Nedges=sum(Face(1:Nf,1));
Edge=zeros(Nedges,8);
% Get edgelengths
for f=1:Nf
    indx=[Face(f,2:Face(f,1)+1) Face(f,2)];
    for t=1:Face(f,1)
        edgeno=sum(Face(1:f-1,1))+t;
        ends=indx(t:t+1);
        p1=Corner(ends(1),:);
        p2=Corner(ends(2),:);
        V=p2-p1;
        L=norm(V);
        Edge(edgeno,1:3)=V;

        Edge(edgeno,4)=L;
        Edge(edgeno,7:8)=ends;
    end
end

```

```

    end,
end
for t=1:Nf
    ss=zeros(1,3);
    for t1=2:Face(t,1) - 1;
        v1=Corner(Face(t,t1+2),:) - Corner(Face(t,2),:);
        v2=Corner(Face(t,t1+1),:) - Corner(Face(t,2),:);
        ss=ss+cross(v2,v1);
    end
    Un(t,:)=ss./norm(ss);
end
[X,Y]=meshgrid([s_end:stn_spcng:n_end],[w_end:prof_spcng:e_end]);
[npro nstn]=size(X);

if calgrv,
    Gx=zeros(size(X));
    Gy=Gx;
    Gz=Gx;
end

if calmag
    Hin=Hincl*pi/180;
    Dec=Decl*pi/180;
    cx=cos(Hin)*cos(Dec);
    cy=cos(Hin)*sin(Dec);
    cz = sin(Hin);
    Uh=[cx cy cz];
    H=Hintn .* Uh; % The ambient magnetic field
    Ind_magn=Susc.*H/(4*pi); % Induced magnetization
    Min=Mincl*pi/180;
    Mdec=Mdecl*pi/180;
    mcx=cos(Min) *cos(Mdec);
    mcy=cos(Min)*sin(Mdec);
    mcz=sin(Min);
    Um=[mcx mcy mcz];
    Rem_magn=Mstrength .* Um; % Remnant magnetization
    Net_magn=Rem_magn+Ind_magn; % Net magnetization
    Pd=(Un * Net_magn)'; % Pole densities
    Hx=zeros(size(X));
    Hy=Hx;
    Hz=Hx;
end

% Comments: Now, for each observation point do the following:
% For each face find solid angle;
% for each side find p,q,r, and add p,q,r of sides

```

```

% to get P,Q,R for the face;
% if calmag=1, find hx,hy,hz;
% if calgrv=1, find gx,gy,gz.
% Add the components from all the faces to get
% Hx,Hy,Hz and Gx,Gy,Gz at the station.
h=waitbar(0,'Working');
for pr=1:npro,
    for st=1:nstn
        opt=[X(pr,st) Y(pr,st) 0];
        fsign=zeros(1,Nf);
        Omega=zeros(1,Nf);
        for t=1:Ncor
            cor(t,:) = Corner(t,.)-opt;
        end % shift origin

        for f=1:Nf
            nsides=Face(f,1);
            cors=Face(f,2:nsides+1);
            Edge(:,5:6)=zeros(Nedges,2); % Clear record of integration
            indx=[1:nsides 1 2];
            for t=1:nsides
                crs(t,:)=cor(cors(t,:));
            end
            % Find if the face is seen from inside
            fsign(f)=sign(dot(Un(f,:),crs(1,:)));
            % Find solid angle W subtended by face f at opt
            dp1=dot(crs(indx(1),:),Un(f,:));
            dp=abs(dp1);
            if dp==0
                Omega(f)=0;
            end
            if dp~=0,
                W=0;
                for t=1:nsides
                    p1=crs(indx(t),:);
                    p2=crs(indx(t+1),:);
                    p3=crs(indx(t+2),:);
                    [ang,perp]=mangle(p1,p2,p3,Un(f,:));
                    %           fprintf('%f %f %d %d %f %f\n',...
                    %           [X(pr,st) Y(pr,st) f t ang perp]);
                    W=W+ang;
                end
                W=W-(nsides-2).*pi;
                Omega(f)= -fsign(f)*W;
            end
            indx=[1:nsides 1 2];

```

```

for t=1:nsides
    crs(t,:)=cor(cors(t,:);
end
% Integrate over each side, if not done, and save result
PQR=[0 0 0];
for t=1:nsides
    p1=crs(indx(t,:);
    p2=crs(indx(t+1,:);
    Eno=sum(Face(1:f-1,1))+t; % Edge number
    if Edge(Eno,6)==1
        I=Edge(Eno,5);
        V=Edge(Eno,1:3);
        pqr=I.*V;
        PQR=PQR+pqr;
    end
    if Edge(Eno,6)~=1 % in original manuscript there was a typo...
        chsgn=1; % if origin, p1 & p2 are on a st line
        if dot(p1,p2)./(norm(p1)*norm(p2))==1
            if norm(p1)>norm(p2) % and pi farther than p2
                chsgn=-1;
                psave=p1;
                p1=p2;
                p2=psave; % interchange p1,p2
            end,
        end
        V=Edge(Eno,1:3);
        L=Edge(Eno,4);
        L2=L*L;
        b=2*(dot(V,p1));
        r1=norm(p1);
        r12=r1*r1;
        b2=b/L/2;
        if (r1+b2 == 0),
            V= -Edge(Eno,1:3);
            b=2*(dot(V,p1));
            b2=b/L/2;
        end
        if (r1+b2 ~= 0),
            I = (1/L).* log((sqrt(L2 + b + r12) + L + b2)./(r1 + b2));
        end
        s=find((Edge(:,7)==Edge(Eno,8)) & (Edge(:,8) == Edge(Eno,7)));
        I=I*chsgn; % change sign of I if p1,p2 were interchanged
        Edge(Eno,5)=I;
        Edge(s,5)=I;
        Edge(Eno,6)=1;
        Edge(s,6)=1;
    end
end

```

```

    pqr=l.*V;
    PQR=PQR+pqr;
end,
end % From Omega,l,m,n,PQR, get components of field due to
% face f
l=Un(f,1);
m=Un(f,2);
n=Un(f,3);
p=PQR(1,1);
q=PQR(1,2);
r=PQR(1,3);
if calmag==1,
    hx=Pd(f)*(l*Omega(f)+n*q-m*r);
    Hx(pr,st)=Hx(pr,st)+hx;
    hy=Pd(f)*(m*Omega(f)+l*r-n*p);
    Hy(pr,st)=Hy(pr,st)+hy;
    hz=Pd(f)*(n*Omega(f)+m*p-l*q);
    Hz(pr,st)=Hz(pr,st)+hz;
end
if calgrv== 1,
    if dp~=0 % if distance to face is non-zero
        gx=-dens*Gc*dp1*(l*Omega(f)+n*q-m*r);
        Gx(pr,st)=Gx(pr,st)+ gx;
        gy=-dens*Gc*dp1*(m*Omega(f)+l*r-n*p);
        Gy(pr,st)=Gy(pr,st)+ gy;
        gz=-dens*Gc*dp1*(n*Omega(f)+m*p-l*q);
        Gz(pr,st)=Gz(pr,st)+ gz;
    end
end
end
end
waitbar(pr/npro,h);
end % end of faces, stns, profiles
close(h);
if calmag== 1
    Htot=sqrt((Hx+H(1,1)).^2 + (Hy+H(1,2)).^2 + (Hz+H(1,3)).^2);
    Dt=Htot-Hintn; % Correct change in Total field
    % Approx. change in Total field
    Dta=Hx.*cx+Hy.*cy+Hz.*cz;
end

what=Dta';

[XI,YI]=meshgrid([s_end:stn_spcng/5:n_end],[w_end:prof_spcng/5:e_end]);
fine=griddata(Y,X,what,YI,XI,'cubic');
pcolor(YI,XI,fine); hold on

```

```

[cs,h]=contour(YI,XI,fine,[-500:10:0 0:25:500],'k');
% [cs,h]=contour(YI,XI,fine,'k');

% clabel(cs,h,'FontSize',10,'Rotation',0,'LabelSpacing',250),

grid
hold off
axis xy
% axis equal tight
colormap
shading flat
colorbar
%xlabel(cb,'Hallo. ');
%set(get(cb,'YLabel'),'string','\deltaT in nT');

xlabel('x in m')
ylabel('y in m')
zlabel('Depth in m')

% grid on; box on;
% Corner(:,3)=-Corner(:,3);
ptch=patch('Vertices',Corner(:,[2 1 3]),'Faces',Face(:,2:5),...
'FaceVertexCData',jet(64),'FaceColor',[0.5 0.5 0.5]);
alpha(1);
view(3);

% exportfig(gcf,'magbild.png','Format','png',...
% 'Color','rgb','Renderer','painters','Resolution',150)

```

Needed function for mag3D.m

angle.m

```
function[ang, perp]=angle(p1, p2, p3, Un)
```

```

%Comments: Angle.m finds the angle between planes O-p1-p2
%and O-p2-p3, where p1,p2,p3 are coordinates of three points,
%taken in ccw order as seen from origin O. This is used by
%grvmag3d for finding the solid angle subtended by a poly-
%gon at the origin. Un is the unit outward normal vector to the
%polygon.

```

```

inout=sign(sum(Un .* p1)); % Check if face is seen from inside
x2=p2(1,1); y2=p2(1,2); z2=p2(1,3);
if inout>0 % seen from inside; interchange p1 and p3
x3=p1(1,1); y3=p1(1,2); z3=p1(1,3);
x1=p3(1,1); y1=p3(1,2); z1=p3(1,3);
elseif inout<0 % seen from outside; keep p1 and p3 as they are

```



```

x1=p1(1,1); y1=p1(1,2); z1=p1(1,3);
x3=p3(1,1); y3=p3(1,2); z3=p3(1,3);end
% Normals
n1=[(y2*z1-y1*z2) (x1*z2-x2*z1) (x2*y1-x1*y2)];
n2=-[(y3*z2-y2*z3) (x2*z3-x3*z2) (x3*y2-x2*y3)];
n1=n1./norm(n1); n2=n2./norm(n2);
perp =sum([x3 y3 z3].*n1);
% sign of perp is -ve if points p1 p2 p3 are in cw order
perp=sign(perp);r=sum((n1.* n2)); ang=acos(r); if perp<0
ang=2*pi-ang; end;if inout==0, ang=0; perp=1; end,
return

```

Example of input file for mag3D.m

karub.m

```

%model, g/cm3 .
calgrv=1; % Change to zero if gravity field is not required
calmag=1; % Change to zero if magnetic field is not required
Ncor=5; Hintn=36390; Hincl=7.63; Decl=1.21; Susc=0.023;
Mstrength=200; Mincl=13.4; Mdecl=-9;Nf=5;
%Comments: Corner is an array of x, y, z coordinates of cor-
%ners in meters, one in each row, in a right-handed system with
%x-axis northward, y-axis eastward, and z-axis downward. Cor-
%ners may be given in any order.
Corner =[19 32 -0.6;27 27 1; 11 27 1.9;11 37 1.5;27 37 0.09];
fht=1; dens=0.5;
% Add fht to depths of all corners
Corner(:,3)=Corner(:,3)+fht;
%Comments: In each row of Face, the first number is the number
%of corners forming a face; the following are row numbers of the
%Corner array with coordinates of the corners which form that
%face, seen in ccw order from outside the object. The faces may
%have any orientation and may be given in any order, but all
%faces must be included.
Face=zeros([5,5]); % Initialize a sufficiently large array
Face(1,1:5)=[4 2 3 4 5]; Face(2,1:5)=[3 1 3 4 0];
Face(3,1:5)=[3 1 4 5 0]; Face(4,1:5)=[3 1 2 3 0];
Face(5,1:5)=[3 1 5 2 0];
%Comments: Rectangular grid of stations for computing fields.
%Profiles are along the x -axis (north-south direction). All values
%are in meters.
s_end =0; % Starting value of x; south end of profiles
stn_spcng=0.5; % Stepsize in north direction; stn interval
n_end=30; % Last x; maximum north coordinate
w_end=0; % y value for westernmost profile
prof_spcng=0.5; % Profile spacing
e_end=40; % y value for easternmost profile

```

gm2d.m – 2d magnetic and gravity code used for forward modeling of profiles in this work from Singh, 2002

```

%With all distances in meters, model density in gm/cm3,
%ambient induction and remnant magnetization in gammas
%and magnetic susceptibility in cgs units, program gives
%gravity fields in milligals and magnetic fields in gammas.
X=(xbegin:stn_spcng:xend)';nstn=size(X);
if calgrv
Gc=6.6732e-3;%Universal gravitational constant
Fx=zeros(size(X)); Fz=Fx;
end
if calmag
Hx=zeros(size(X)); Hz=Hx;
Hin=Hincl*pi/180;Dec=Decl*pi/180;pfan=pfang*pi/180;
cx=cos(Hin)*cos(pfan-Dec); cz=sin(Hin);
Uh=[cx cz]; H=Hintn.*Uh; end
for body=1:nbody % pickup a body
if calgrv, dens=phyc(body,1);end
if calmag, Susc=phyc(body,2); Ms=phyc(body,3);
Mincl=phyc(body,4);Mdecl=phyc(body,5);
Ind_magn=Susc.*H; % Induced magnetization vector
Min=Mincl*pi/180; Mdec=Mdecl*pi/180;
mcx=cos(Min)*cos(pfan-Mdec);
mcz=sin(Min);Um=[mcx mcz];
Rem_magn=Ms.*Um; % Remnant magnetization vector
Net_magn=Rem_magn+Ind_magn; end%net magnetization
for stn=1:nstn % Pick up a station
obspt=[X(stn) 0];
nc=face(body,1); % No. of corners
for f=1:nc % Pick up a face
%Find the outward normal vectors for each of the facets
p1=Corner(face(body,f+1,:)-obspt;
if f==nc,p2=Corner(face(body,2,:)-obspt;
else,p2=Corner(face(body,f+2,:)-obspt;end
v2=p2-p1;Un1(f,:)=v2(2) -v2(1)];
Un(f,:)=Un1(f,:)/norm(Un1(f,:));
% Find if the face is seen from outside, or inside
dp=sum(Un(f,:).* p1);fsign=sign(dp);
dp1=abs(dp);r1=norm(p1); r2=norm(p2);
%Find solid angle
if dp1==0, Omega=-fsign*2*pi;
else,ua=p1./r1;ub=p2./r2;
rdot=sum(ua .* ub);ang=acos(rdot);
W=2*ang;Omega=-fsign*W; end

```

```

%Find line integral
Q=2*(log(r2/r1));
l=Un(f,1); n=Un(f,2);
%Now using Omega,l,n and Q, get hx,hz due to face f.
if calmag==1 & calgrv==1, % simultaneous calculation
Pd=sum(Un(f,:).*Net_magn); % surface pole-density
md=-Gc*dens*dp; % surface mass-density
hx=(l* Omega+n* Q);
hz=(n* Omega-l* Q);
Hx(stn)=Hx(stn)+Pd* hx;
Hz(stn)=Hz(stn)+Pd* hz;
Fz(stn)=Fz(stn)+md* hz;end
if calgrv==1 & calmag==0,%only gravity
md=-Gc*dens*dp; %surface mass-density
hz=(n* Omega - l* Q);
Fz(stn)=Fz(stn)+md* hz; end
if calmag==1 & calgrv==0,%only magnetic
Pd=sum(Un(f,:).*Net_magn);%surface pole-density
hx=(l* Omega+n* Q);
hz=(n* Omega-l* Q);
Hx(stn)=Hx(stn)+Pd* hx;
Hz(stn)=Hz(stn)+Pd* hz;end
end, end, end %end of faces, stations, bodies
if calmag==1,
Htot=sqrt((Hx+H(1,1)).^2+(Hz+H(1,2)).^2);
Dt=Htot-Hintn; %Correct change in Total field
Dta=Hx.*cx+Hz.*cz;end%Approx change in Total field

```

Example input file for gm2d.m #1

model.m

```

calgrv=1;%change to zero if gravity is not required
calmag=1;%change to zero if magnetic is not required
%if calmagD0 then the following four lines is omitted
Hintn=50000;%Ambient magnetic field intensity, gammas
Decl=10;%Declination,degrees,clockwise from north
Hincl=10;%Inclination,degrees,downward from horizontal
pfang=20;%azimuthCxaxis,degrees,clockwise from north,
fht=-5.0; %height of observation plane
nbody=1; %number of bodies
ncor=3; %Total number of polygon corners
%Corner is an array of (x, z) of polygon corners,
Corner=[8 8; 8 6; 11 6];Corner(:,2)=Corner(:,2)+fht;
%For each body, phyc,is a row vector containing
%density contrast in gm/cm3, susceptibility in cgs,
%strength of remnant magnetization in gamma,

```

```

%its inclination and declination in degrees.
phyc(1,1:5)=[.5 .001 0 0 0];
face=zeros(50,20);%Initialize the body faces
%For each body, face array contains no. of vertex in the
%polygon cross section, their indices in clockwise order.
face(1,1:4)=[3 1 2 3 ];
xbegin=0; %Starting x, start of profile
stn_spcng=1; %Stepsize, station interval
xend=20; %Last x, end of profile

```

Example input file for gm2d.m #2

Tendaho.m

```

calgrv=1;
calmag=1;
Hintn=36592;
Decl=1.8333;
Hincl=9.08333;
pfang=59.1;
fht=0;
nbody=11;
ncor=89;
Corner=[22035.3 1521.37; 25826.3 1418.80;26324.5 7572.65;24260.49 7333.33;23930.8
1623.932;23118.47 1538.462;21290.7 1572.65;21222.96 7213.675;17623.25 7741.379;
17629.14 1568.966;19970.57 1316.239;
33.8484 820.5128;17533.48 1572.65; 17542.31 3265.85; 33.8484 2324.786;
22983.08 1572.65;23863.13 1606.838;24242.83 7371.648;29989.7 8020.216;16148.65
8021.368; 21328.93 7245.506;21358.35 1623.932;
25894.04 1418.803;45966.89 769.2308;45966.15 2085.47;26073.58 3275.862;
0 2358.974;17533.48 3316.239; 17501.84 7765.376; 15883 7991.956;67.69684
7965.812;
26146.43 3316.239;41949.23 2393.162;44130.24 2239.316;45898.45 2153.846;46043.41
7965.812;30112.58 7982.758;26470.2 7574.86;
11745.4 -102.5641;12930.1 -102.5641;13776.31 222.222;14859.46 427.3504;15671.82
820.5128;16610.75 1505.749;4793.229 999.6268;7751.288 666.667;9240.618
290.5983;10662.25 0;
13951.43 -310.3448;15313.47 0;15677.7 275.8621;14893.3 410.2564;13810.15
205.1282;12930 -119.6581; 11846.95 -102.5641;10797.65 -51.28205;12388.52 -
170.9402;13313.47 -241.3793;
33186.9 256.4103;36453.27 290.5983;37991.9 221.6328;38779.98 600.9432;40557.02
480.2535;41781.45 480.2535;42087.56 652.6673; 42393.67 842.3225;26943.34
1367.521;27315.67 803.4188;29460 441.9393;32306.84 547.0085;
29628.4 410.2564;31656.36 -34.18803;36875.64 -1.716676;38832.23
17.24138;40150.85 293.1034;41757.91 448.2759;40763.06 431.0345;38794.7
551.7241;38096.4 171.4435;36194.26 258.0236;33148 222.2222; 32306.84 478.6325;
16813.83 -155.1724;17542.31 -86.2069;18068 -17.0942;17704.19 17.09402;17016.19
34.48276;16490.07 34.48276;15721.12 -34.48276];

```

```

phyc(1,1:5)=[0.5 0.0018303 570 15 1.83];
phyc(2,1:5)=[0.5 0.0018303 270 -32.7 169];
phyc(3,1:5)=[0.5 0.00 0 0 0];
phyc(4,1:5)=[0.5 0.0018303 270 -14.4 180];
phyc(5,1:5)=[0.5 0.001 200 -32.7 169];
phyc(6,1:5)=[0.5 0.001 200 -32.7 169];
phyc(7,1:5)=[0.5 0.0018303 500 -14.4 180];
phyc(8,1:5)=[0.5 0.0018303 270 9.08 1.83];
phyc(9,1:5)=[0.5 0.0018303 270 9.08 180];
phyc(10,1:5)=[0.5 0.0018303 270.3 9.08 1.83];
phyc(11,1:5)=[0.5 0.0018303 270.3 16.8 1.46];
face=zeros(50,20);
face(1,1:12)=[11 1 2 3 4 5 6 7 8 9 10 11];
face(2,1:5)=[4 12 13 14 15];
face(3,1:8)=[7 16 17 18 19 20 21 22];
face(4,1:5)=[4 23 24 25 26];
face(5,1:6)=[5 27 28 29 30 31];
face(6,1:8)=[7 32 33 34 35 36 37 38];
face(7,1:11)=[10 39 40 41 42 43 44 45 46 47 48];
face(8,1:11)=[10 49 50 51 52 53 54 55 56 57 58];
face(9,1:13)=[12 59 60 61 62 63 64 65 66 67 68 69 70];
face(10,1:13)=[12 71 72 73 74 75 76 77 78 79 80 81 82];
face(11,1:8)=[7 83 84 85 86 87 88 89];
xbegin=0;
stn_spcng=500;
xend=46000;

```

Misc. Utilities for magnetic transformations and data input and output
Gri2mat - converts Surfer grid files to MATLAB matrices. From (Gerovska and Arauzo-Bravo, 2006)

```

%=====
function [Mat,Str]=Gri2Mat(NamFil)
%=====
% Covert GS ASCII grid to Matlab file format
% OUTPUT
% Mat: Matrix with the data
% Str: Structure of data

% Open the file
pF=fopen(NamFil,'r');

% Read DSAA label
Lin=fgetl(pF);
Tok=strtok(Lin);
if ~strcmp('DSAA',Tok)
error(['The data file, ' NamFil ' is not in ASCII Grid File Format']);

```

```

end %if ~strcmp('DSAA',Tok)

% Read number of columns and rows
Lin=fgetl(pF);
[StrCol,StrRow]=strtok(Lin);
NumRow=str2num(StrRow);
NumCol=str2num(StrCol);

% Read the X coordinates (West-East)
Lin=fgetl(pF);
[StrXini,StrXend]=strtok(Lin);
Xini=str2num(StrXini);
Xend=str2num(StrXend);

% Read the Y coordinates (South-North)
Lin=fgetl(pF);
[StrYini,StrYend]=strtok(Lin);
Yini=str2num(StrYini);
Yend=str2num(StrYend);

% Read the Field Extrema
Lin=fgetl(pF);
[StrMin,StrMax]=strtok(Lin);
Min=str2num(StrMin);
Max=str2num(StrMax);

% Read the data
Mat=fscanf(pF,'%f',[NumCol,NumRow]);

% Transpose
Mat=Mat';

% Pack structure
Str.NumRow=NumRow;
Str.NumCol=NumCol;
Str.Xini=Xini;
Str.Xend=Xend;
Str.Yini=Yini;
Str.Yend=Yend;
Str.Min=Min;
Str.Max=Max;

% Close file -----
fclose(pF);

```

Mat2Gri – converts from Matlab matrice to Surfer ascii grid format

```

%=====
function Mat2Gri(NamFil,Mat,Str)
%=====
% Convert Matlab to GS ASCII grid file format
% INPUT
% NamFil: Name of the grid file
% Mat: Matrix with the data
% Str: Structure of data
% DSAA format
% ASCII grid files [.GRD] contain five header lines that provide
% information about the size and limits of the grid, followed by a list
% of Z values.
% The fields within ASCII grid files must be space delimited.
%
% The listing of Z values follows the header information in the file.
% The Z values are stored in row-major order starting with the minimum
% Y coordinate.
% The first Z value in the grid file corresponds to the lower left corner
% of the map.
% This can also be thought of as the southwest corner of the map, or,
% more specifically, the grid node of minimum X and minimum Y.
% The second Z value is the next adjacent grid node in the same row
% (the same Y coordinate but the next higher X coordinate).
% When the maximum X value is reached in the row,
% the list of Z values continues with the next higher row,
% until all the rows of Z values have been included.
%
% The general format of an ASCII grid file is:
%
% id The identification string DSAA that identifies the file as an ASCII
% grid file.
% nx ny nx is the integer number of grid lines along the X axis (columns)
% ny is the integer number of grid lines along the Y axis (rows)
% xlo xhi xlo is the minimum X value of the grid
% xhi is the maximum X value of the grid
% ylo yhi ylo is the minimum Y value of the grid
% yhi is the maximum Y value of the grid
% zlo zhi zlo is the minimum Z value of the grid
% zhi is the maximum Z value of the grid
% grid row 1
% grid row 2
% gridrow 3
% these are the rows of Z values of the grid, organized in row order.
% Each row has a constant Y coordinate.

```

```

% Grid row 1 corresponds to ylo and the last grid row corresponds to yhi.
% Within each row, the Z values are arranged from xlo to xhi.
% WARNING
% Every physical line is written along several lines in the file of a
% maximum of 10 columns
% The next line is separated by an empty line in the file
% Maximum number of columns per row

MaxCol=10;

% Unpack structure
Xini=Str.Xini;
Xend=Str.Xend;
Yini=Str.Yini;
Yend=Str.Yend;
Min=Str.Min;
Max=Str.Max;
NumRow=Str.NumRow;
NumCol=Str.NumCol;

% Open the file
pF=fopen(NamFil,'w');

% Write DSAA label
fprintf(pF,'DSAA\n');

% Write number of columns and rows
fprintf(pF,'%i %i\n',NumCol,NumRow);

% Write the X coordinates (West-East)
fprintf(pF,'%G %G\n',Xini,Xend);

% Write the Y coordinates (South-North)
fprintf(pF,'%G %G\n',Yini,Yend);

% Write the Field Extrema
fprintf(pF,'%G %G\n',Min,Max);

% Prepare the parameters for writing the data
% Calculate the number of file rows (nr) of every physical row

if NumCol<=MaxCol
    nr=1;
else % NumCol>MaxCol
    nr=ceil(NumCol/MaxCol);
    nclr=mod(NumCol,MaxCol); % Number of columns of the last row

```



```

if nclr==0

% If the number of columns is a multiple of MaxCol
% we increment artificially the number or rows in every physical row,
% since the number of colums in the las row is cero (is missing)
% in this case

nr=nr+1;
end % if nclr==0
end % if NumCol<=10

% Write data

for r=1:NumRow
c=0;
for j=1:nr-1
% Full columns
for k=1:MaxCol
c=c+1;
fprintf(pF,'%G ',Mat(r,c));
end % for k=1:MaxCol
fprintf(pF,'\n');
end % for j=1:nr-1
% Last row, with not full columns
for k=1:nclr
c=c+1;
fprintf(pF,'%G ',Mat(r,c));
end %for k=1:MaxCol
if nclr~=0
fprintf(pF,'\n');
end %if nclr~=0

% New line separating every group of lines

fprintf(pF,'\n');
end %for i=1:NumRow

% Close file -----
fclose(pF);

```

XYZ2Mat - generic conversion of xyz list to Matlab matrice

```

%=====
function [Mat,Str]=XYZ2Mat(NamFil)
%=====
% Converts XYZ to Matlab file format

```

```

% OUTPUT
% Mat: Matrix with the data
% Str: Structure of data

% Open the file
pF=fopen(NamFil,'r');

% Read the files
[Mat3,Count]=fscanf(pF,'%G',[3 inf]);

% Close file -----
fclose(pF);

Mat3=Mat3';
[NumRow0 NumCol0]=size(Mat3);
if NumCol0~=3
MesErr=['The data file: ' NamFil ' has ' num2str(NumCol0) ', instead of the required
3 columns for the XYZ format'];
error(MesErr);
end % if NumCol0~=3

% Look for the number of columns
Fin='n';
Yini=Mat3(1,2);
i=0;
NumCol=[];
while Fin=='n'
i=i+1;
yi=Mat3(i,2);
if yi~=Yini
Fin='y';
NumCol=i-1; % minus 1 because I discover in the next one
else % yi==Yini
if i==NumRow0
Fin='y';

% Strange case, vector matrix
NumCol=NumRow0;

end % if i==NumRow0
end % if y1~=yi
end % while Fin=='n'

% Calculate the number of rows
NumRow=NumRow0/NumCol;
if NumRow>floor(NumRow)

```

```

MesErr=['The data file: ' NamFil ', does not contain the regular grid required for the
XYZ format'];
error(MesErr);
end % if NumRow>ceil(NumRow)

```

```

% Calculate the rest of parameters
Xini=Mat3(1,1);
Yini=Mat3(1,2);
Xend=Mat3(end,1);
Yend=Mat3(end,2);
Min=min(Mat3(:,3));
Max=max(Mat3(:,3));

```

```

% Build the matrix
k=0;
for i=1:NumRow
for j=1:NumCol
k=k+1;
Mat(i,j)=Mat3(k,3);
end % for j=1:NumRow
end % for i=1:NumRow

```

```

% Pack structure
Str.NumRow=NumRow;
Str.NumCol=NumCol;

```

```

Str.Xini=Xini;
Str.Xend=Xend;

```

```

Str.Yini=Yini;
Str.Yend=Yend;

```

```

Str.Min=Min;
Str.Max=Max;

```

Mat2XYZ - converts Matlab matrices to XYZ format

```

%=====
function Mat2XYZ(NamFil,Mat,Str)
%=====
% Convert Matlab to XYZ file format (without blanks)
% INPUT
% NamFil: Name of the grid file
% Mat: Matrix with the data
% Str: Structure of data

```

```

ValGap=1.70141E+038;

```

```

% Unpack structure
Xini=Str.Xini;
Xend=Str.Xend;

Yini=Str.Yini;
Yend=Str.Yend;

Min=Str.Min;
Max=Str.Max;

NumRow=Str.NumRow;
NumCol=Str.NumCol;

% Open the file
pF=fopen(NamFil,'w');

% Increments
DelX=(Xend-Xini)/(NumCol-1);
DelY=(Yend-Yini)/(NumRow-1);

% Write data
for i=1:NumRow
y=Yini+(i-1)*DelY;
for j=1:NumCol
z=Mat(i,j);
if z~=ValGap
x=Xini+(j-1)*DelX;
fprintf(pF,'%G %G %G\n',x,y,z);
end % if z~=ValGap
end % for j=1:NumCol
end % for i=1:NumRow

% Close file -----
fclose(pF);

```

Arguments needed for the Surfer Grid and XYZ conversion codes

NamFil – The file name of the grid

Mat – the Matlab matrice

Str – a Matlab variable that contains the metadata of the gridfile or Matlab matrice

Str.Xini – first X value

Str.Xend – last X value

Str.Yini – first Y value

Str.Yend – last Y value

Str.Min – mininum z value

Str.Max – maximum z value

Str. NumCol – number of columns
 Str.NumRow – number of rows

Functions needed for the Surfer Grid and XYZ conversion codes

RecGap

```

%=====
function [Mat]=RecGap(Mat,ValGap,I,J)
%=====
% Recovers gaps with the blank values given in the variable ValGap
% Fill the gaps

NumGap=size(I,1);
for k=1:NumGap
i=I(k);
j=J(k);
Mat(i,j)=ValGap;
end % for i=1:NumGap

```

FinGap

```

%=====
function [Mat,I,J]=FinGap(Mat)
%=====
% Find gaps in a matrix (from GS ASCII grid format or XYZ format)
% OUTPUTS:
% MatFil : Matrix with filled blanks
% MatGap : Matrix with the positions of the blanks

ValGap=1.70141E+038;
FilGap=0;

% Find blanks
[I,J]=find(Mat==ValGap);

% Fill the blanks
% Mat(I,J)=FilGap;

NumGap=size(I,1);
for k=1:NumGap
i=I(k);
j=J(k);
Mat(i,j)=FilGap;
end % for i=1:NumGap

```

Code to find the magnitude transforms(Gerovska and Arauzo-Bravo, 2006)

MMATrans.m

```

% -----
%
% Copyright (c) 2006 by the Society of Exploration Geophysicists.
% For more information, go to http://software.seg.org/2006/0002 .
% You must read and accept usage terms at:
% http://software.seg.org/disclaimer.txt before use.
% -----
%
%
function mmatrans(varargin)

% 1. Name of the data file with its path
% 2. Type of data contained in the file
%   DT, It is necessary to supply two additional arguments
%   I, Inclination of geomagnetic field (in decimal degrees)
%   D, Declination of geomagnetic field (in decimal degrees)
%   Z, It is not necessary to supply additional arguments
% 3. Method to calculate the component derivatives
%   Spline
%   Fourier
% 4. Choose to extend or no the grid
%   Yes, Then supply the percentange with which to extend the grid
%   No
% 5. Type of output files (GS ASCII grid or XYZ)
% 6. Name of the directory in which to write the results
%   (if it does not exist, the results will be written
%   in the directory of the data file)
% AUTHORS: Daniela Gerovska and Marcos J. Arauzo-Bravo
% DATE   : August/2005

FilSep=filesep;

% Default configuration
Config.TypDat='DT';
Config.Inc=[];
Config.Dec=[];
Config.MetDer='Spline';
Config.ExtGri='y';
Config.Per=10;
Config.SavFor=''; % Save format

NumArg=nargin;
switch NumArg,

```

case 0,

%|<-From here-----till here>|

MesUse=...

```
[ 'Use:  MMATrans(Datafile,['-T',Inc,Dec,['-Z'],['-S'|'-F'],...
  '      ['-E',Per],['-G'|'-X'],['-D',Dir]
```

```
'Example: MMATrans("data.grd","-T","60","2","-F",...
  '      "-E","5","-X","-D","Results")
```

```
'      Calculates the MMA transformations of the GS ASCII grid file data.grd '
'      located in the current directory and containing total anomalous '
'      magnetic field values. The inclination of the geomagnetic vector is '
'      60 degrees, and the declination of the geomagnetic vector is 2 '
'      degrees. The magnetic components first order horizontal '
'      derivatives are calculated using Fourier transforms. The input data '
'      grid is extended with 5 percent the number of grid rows and columns '
'      in the respective directions with half a cosine function. The output '
'      files are saved in XYZ format in the directory Results. If such '
'      directory does not exist, it will be created.
```

<Input parameters>

```
'Datafile is the name of the file with the data in GS ASCII grid format '
' or XYZ format
```

```
'T: Indicates that the datafile contains total anomalous magnetic field. '
' In this case it is necessary to input the average values over the survey '
' area of the inclination and declination of the geomagnetic vector.
```

```
' Inc: Inclination (in decimal degrees, e.g. 2.75), only for total magnetic '
' field data.
```

```
' Dec: Declination (in decimal degrees), only for total magnetic field '
' data.
```

```
'Z: Indicates that the datafile contains the Za component of the anomalous '
' magnetic field.
```

```
' In this case it is not necessary to input the average value of the '
' inclination and the declination of the geomagnetic field.
```

```
'S: Uses beta splines to calculate the magnetic components first order '
' horizontal derivatives.
```

```
'F: Uses Fourier transforms to calculate the magnetic components first order '
' horizontal derivatives.
```

```
'E: Extends the data grid with the percentage that follows.
```

```
' Per: Numerical value of the percentage with which the data grid will be '
' extended.
```

```
'G: Indicates that the results will be saved in GS ASCII grid format.
```

```
'X: Indicates that the results will be saved in XYZ format.
```

```
'D: Indicates that the following string is the name of the directory in which '
' the results will be saved.
```

```
' Dir: The name of the directory, where the output files will be saved.
```

```
' By default this is the current directory. '];
```



```

return

end % if ~size(ver('splines'),1)
end % if strcmp(MetDer,'Splines')

% Test if the directory of the results exists
if ~isdir(DirRes)
    disp(['The output directory ' DirRes ' does not exist']);
    disp(['It will be created']);
    mkdir(DirRes);
end % if ~isdir(DirRes)

% Extension results
ExtRes=['.' SavFor];

% Read data
ReaFor=Ext;
switch ReaFor, % Read format
case '.grd', [Mat,Str]=Gri2Mat(NamFil);
case '.xyz', [Mat,Str]=XYZ2Mat(NamFil);
otherwise error(['Wrong data file extension: ' ReaFor '. It should be .grd or
.xyz.']);
end % switch ReaFor, Read format

% Find blanks
[Mat,RowGap,ColGap]=FinGap(Mat);
[NumRow,NumCol]=size(Mat);

% Dx: spacing in South-North direction
% Dy: spacing in West-East direction

Dx=(Str.Yend-Str.Yini)/(NumRow+1);
Dy=(Str.Xend-Str.Xini)/(NumCol+1);

% Check whether number of columns and rows is even
% If not, add 1 row or 1 col to make it even with the cos extension
% function

if rem(NumRow,2)~=0
    NumRowExt=NumRow+1;
else % rem(NumRow,2)==0
    NumRowExt=NumRow;
end % if rem(NumRow,2)~=0

if rem(NumCol,2)~=0
    NumColExt=NumCol+1;

```

```

else % rem(NumCol,2)==0

    NumColExt=NumCol;
end % if rem(NumCol,2)~=0

% Extend the matrix
Mat=ExtCos(Mat,NumRow,NumCol,NumRowExt,NumColExt);
switch TypDat,
case 'DT', LapDT(Mat,Dx,Dy,Inc,Dec,ExtGri,MetDer,Per);
case 'Z', LapZ(Mat,Dx,Dy,ExtGri,MetDer,Per);
otherwise error(['Wrong data type. It should be "-T" or "-Z".']);
end % if Data=='DT'

% Recover the transformations from files
% [T,R,Q,E,L] to the output formats
% Cut the resultant matrices to original size

FulNamT=[DirRes FilSep 'T' Nam];
load T;
T=RecMat(T,FulNamT,RowGap,ColGap,Str,SavFor);

% Save the final mat file in the results directory
eval(['save' ' ' FulNamT '.mat' ' ' 'T']);

% Delete the temporary mat file
delete('T.mat');

FulNamR=[DirRes FilSep 'R' Nam];
load R;
R=RecMat(R,FulNamR,RowGap,ColGap,Str,SavFor);

% Save the final mat file in the results directory
eval(['save' ' ' FulNamR '.mat' ' ' 'R']);

% Delete the temporary mat file
delete('R.mat');

FulNamQ=[DirRes FilSep 'Q' Nam];
load Q;
Q=RecMat(Q,FulNamQ,RowGap,ColGap,Str,SavFor);

% Save the final mat file in the results directory

```

```

eval(['save' '' FulNamQ '.mat' '' 'Q']);

% Delete the temporary mat file
delete('Q.mat');
FulNameE=[DirRes FilSep 'E' Nam];
load E;
E=RecMat(E,FulNameE,RowGap,ColGap,Str,SavFor);

% Save the final mat file in the results directory
eval(['save' '' FulNameE '.mat' '' 'E']);

% Delete the temporary mat file
delete('E.mat');
FulNameL=[DirRes FilSep 'L' Nam];
load L;
L=RecMat(L,FulNameL,RowGap,ColGap,Str,SavFor);

% Save the final mat file in the results directory
eval(['save' '' FulNameL '.mat' '' 'L']);

% Delete the temporary mat file
delete('L.mat');

```

Functions needed by MMATrans

RecMat

```

function Mat=RecMat(Map,NamFil,I,J,Str,SavFor)
%=====
% Recover original size
% and postprocessing the mat files

Map=Map(1:Str.NumRow,1:Str.NumCol);

% Calculate the extrema before the recovering the blanks
Min=min(min(Map));
Max=max(max(Map));

Str.Min=Min;
Str.Max=Max;

% Recover the blanks
% Fills the gaps with 1.70141E+038

ValGap=1.70141E+038;

```

```

Mat=RecGap(Map,ValGap,I,J);

% Save matrix data
NamFilExt=[NamFil '.' SavFor];
switch SavFor,
case 'grd', % GS ASCII grid format
    Mat2Gri(NamFilExt,Mat,Str);
case 'xyz', % XYZ format
    Mat2XYZ(NamFilExt,Mat,Str);
case "", % Default
    otherwise error(['Wrong output file extension: ' SavFor '. It should be grd or xyz.']);
end %switch SavFor,

% Postprocessing the mat files
% Fill the gaps of the mat files with NaN
ValGap=NaN;
Mat=RecGap(Map,ValGap,I,J);

```

ExtCos

```

%=====
function gExt=ExtCos(g,NumRow,NumCol,NumRowExt,NumColExt)
%=====
% Extension of the grid with half a cosine function
% Cosine taper right and upper side

s=0.5*(g(:,NumCol)+g(:,1));
r=0.5*(g(:,NumCol)-g(:,1));
lim=NumColExt-NumCol;
rlamb=lim+1;
arg=pi/rlamb;
for k=1:lim
    ge=s+r*cos(arg*k);
    g(:,NumCol+k)=ge;
end %for k=1:lim
g=g';

% Cosine taper upper side
s=0.5*(g(:,NumRow)+g(:,1));
r=0.5*(g(:,NumRow)-g(:,1));
lim=NumRowExt-NumRow;
rlamb=lim+1;
arg=pi/rlamb;
for k=1:lim
    ge=s+r*cos(arg*k);

```

```

g(:,NumRow+k)=ge;
end %for k=1:lim
gExt=g';

```

AnaOpt

```

%=====
function [Config,i]=AnaOpt(varargin,Config,i)
%=====
% Analyzes the command line input arguments
% 1. Name of the file with the data
% 2. Type of data contained in the file
% DT, It is necessary to supply two additional arguments
% I, Inclination
% D, Declination
% Z, It is not necessary to supply additional arguments
% 3. Method to calculate the component derivatives
% Spline
% Fourier
% 4. Choose to extend or not the grid
% Yes, Supply the percentenge with which to extend the grid
% No
% 5. Type of output files (GS ASCII grid or XYZ)
% 6. Name of the directory in which to write the results
% (if it does not exist, it will be created)

i=i+1;
Option=varargin{i};
NumCha=size(Option,2);

if NumCha<10
O1=Option(1,1);
if O1=='-'
O2=Option(1,2);
switch upper(O2),
case 'Z',
Config.TypDat='Z';
case 'T',
i=i+1;
Option=varargin{i};
Inc=Option;
Inc=str2num(Inc);
if isempty(Inc)
error(['The value for inclination, ' Option ', is not numeric.']);
end % if isempty(Inc)
if Inc<-90
error(['The value for inclination, ' Option ', is smaller than the minimum, -90.']);

```

```

end % if Inc>90
if Inc>90
    error(['The value for inclination, ' Option ', is bigger than the maximum, 90.']);
end % if Inc>90

i=i+1;
Option=varargin{i};
Dec=Option;
Dec=str2num(Dec);
if isempty(Dec)
    error(['The value for declination, ' Option ', is not numeric.']);
end % if isempty(Dec)
if Dec<-180
    error(['The value for declination, ' Option ', is smaller than the minimum, -180.']);
end % if Dec<-180
if Dec>180
    error(['The value for declination, ' Option ', is bigger than the maximum, 180.']);
end % if Dec>180

Config.TypDat='DT';
Config.Inc=Inc;
Config.Dec=Dec;
case 'S',
    Config.MetDer='Spline';
case 'F',
    Config.MetDer='Fourier';
case 'E',
    i=i+1;
    Option=varargin{i};
    Per=Option;
    Per=str2num(Per);
    if isempty(Per)
        error(['The value for extension, ' Option ', is not numeric.']);
    end % if isempty(Per)
    if Per<0
        error(['The value for extension, ' Option ', is smaller than the minimum, 0.']);
    end % if Per<0
    if Per>30
        error(['The value for extension, ' Option ', is bigger than the maximum, 30.']);
    end % if Per>30
    Config.Per=Per;

if Per>0
    Config.ExtGri='y';
else % Per<=0
    Config.ExtGri='n';
end

```

```

end % if Per>0

case 'G',
  Config.SavFor='grd';
case 'X',
  Config.SavFor='xyz';

case 'D',
  i=i+1;
  Option=varargin{i};
  Config.DirRes=Option;

end % switch O2,
else % if O1~='- '
  error(['Option ' Option ', no valid.']);
end % if O51=='-'
else % NumCha>=10
  error(['Option ' Option ', no valid.']);
end % if NumCha>1

```

LapDT.m and LapZ.m files are also needed by MMATrans.m

nsdcalc.m – code that creates a normalized standard deviation (NSTD), a new edge-detection filter for potential field data from Cooper and Cowan (2008)

```

% *****
% Copyright (c) 2008 by the Society of Exploration Geophysicists.
% For more information, go to http://software.seg.org/2008/0001 .
% You must read and accept usage terms at:
% http://software.seg.org/disclaimer.txt before use.
%
% Revision history:
% Original SEG version March 2008.
% *****
%
function nsd=nsdcalc(g,wsize,s)
% *****
% *** Normalised standard deviation analysis
% *** GRJ Cooper Jan'07
% *** For best results optimise the histogram of the output
% *** after processing is complete
% *** Tested using Matlab 2007b under Windows XP SP2
% *****
% *** grcooper@iafrica.com
% *** www.wits.ac.za/science/geophysics/gc.htm
% *****

```

```

% Inputs;
% g ; matrix of data for processing
% wsize ; window size for std calculation. Must be odd & >=3
% s ; size of smoothing window (odd numbers only)
% zero or negative values apply no smoothing
% *****
% Outputs
% nsd ; matrix of normalised variance values
% *****

disp('Processing...');

% Check for sensible values of window size for std calculation
wsize=abs(wsize); if wsize<3; wsize=3; end; wsize=1+2*floor(wsize/2);
warning off MATLAB:divideByZero;

% Smooth the data first if requested

if s>0;
    se=ones(s)/(s*s); g=conv2(g,se,'same');
end;

% Compute gradients

[nr,nc]=size(g); nmax=max([nr nc]); npts=2^nextpow2(nmax);
[dx,dy]=gradient(g); dz=vertical(g,npts,nc,nr,1);

% Compute windowed std of gradients
w2=floor(wsize/2);
dxv=zeros(nr,nc); dyv=zeros(nr,nc); dzv=zeros(nr,nc);
for I=w2+1:nr-w2;
    if I/20==floor(I/20); disp(I); end;
    for J=w2+1:nc-w2;
        wx=dx(I-w2:I+w2,J-w2:J+w2); dxv(I,J)=std(wx(:));
        wy=dy(I-w2:I+w2,J-w2:J+w2); dyv(I,J)=std(wy(:));
        wz=dz(I-w2:I+w2,J-w2:J+w2); dzv(I,J)=std(wz(:));
    end;
end;

% NSD

nsd=dzv./(dxv+dyv+dzv);
nsd=nsd(w2+1:nr-w2,w2+1:nc-w2);

% Display results

```



```
f=figure(1); clf;
set(f,'Name','NSD Data Analysis'); set(f,'NumberTitle','off');
ax(1)=subplot(1,2,1); imagesc(g); axis equal; axis tight; axis off; axis xy; title('Data');
ax(2)=subplot(1,2,2); imagesc(nsd); axis equal; axis tight; axis off; axis xy;
title('Normalised SD');
linkaxes(ax,'xy');
colormap(gray(256));
```

Functions needed by nsdcalc.m

vertical

```
function dz=vertical(data,npts,nc,nr,xint) % Compute vertical derivative
cdiff=floor((npts-nc)/2); rdiff=floor((npts-nr)/2);
data1=taper2spline(data,npts,nc,nr,cdiff,rdiff);
f=fft2(data1); fz=f;
wn=2.0*pi/(xint*(npts-1));
f=fftshift(f);
cx=npts/2+1; cy=cx;
for I=1:npts
    freqx=(I-cx)*wn;
    for J=1:npts
        freqy=(J-cy)*wn;
        freq=sqrt(freqx*freqx+freqy*freqy);
        fz(I,J)=f(I,J)*freq;
    end;
end;
fz=fftshift(fz); fzinv=ifft2(fz);
dz=real(fzinv(1+rdiff:nr+rdiff,1+cdiff:nc+cdiff));
```

taper2spline

```
function gt=taper2spline(g,npts,nc,nr,cdiff,rdiff)
% Merge edges to the value opposite using a cubic spline

gt=zeros(npts); gt(rdiff+1:rdiff+nr,cdiff+1:cdiff+nc)=g;
gp=g(:,1:3); [gpx1,junk]=gradient(gp); % sides
gp=g(:,nc-2:nc); [gpx2,junk]=gradient(gp);
x1=0; x2=(2*cdiff)+1;
x=[1 1 0 0;x1 x2 1 1; x1^2 x2^2 2*x1 2*x2; x1^3 x2^3 3*x1^2 3*x2^2];
for I=1:nr;
    y=[g(I,nc) g(I,1) gpx2(I,3) gpx1(I,1)];
    c=y/x;
    for J=1:cdiff;
        gt(I+rdiff,J)=c(1)+(J+cdiff)*c(2)+c(3)*(J+cdiff)^2+c(4)*(J+cdiff)^3;
        gt(I+rdiff,J+nc+cdiff)=c(1)+J*c(2)+c(3)*J^2+c(4)*J^3;
```

```

end;
end;

gp=g(1:3,:); [junk,gpx1]=gradient(gp); % top and bottom
gp=g(nr-2:nr,:); [junk,gpx2]=gradient(gp);
x1=0; x2=(2*rdiff)+1;
x=[1 1 0 0;x1 x2 1 1; x1^2 x2^2 2*x1 2*x2; x1^3 x2^3 3*x1^2 3*x2^2];
for J=1:nc;
y=[g(nr,J) g(1,J) gpx2(3,J) gpx1(1,J)];
c=y/x;
for I=1:rdiff;
gt(I,J+cdiff)=c(1)+(I+rdiff)*c(2)+c(3)*(I+rdiff)^2+c(4)*(I+rdiff)^3;
gt(I+rdiff+nr,J+cdiff)=c(1)+I*c(2)+c(3)*I^2+c(4)*I^3;
end;
end;

for I=rdiff+nr+1:npts; % Corners
for J=cdiff+nc+1:npts;
if (I-nr-rdiff)>(J-nc-cdiff); gt(I,J)=gt(I,nc+cdiff); else gt(I,J)=gt(nr+rdiff,J); end;
end;
end;

for I=1:rdiff;
for J=1:cdiff;
if I>J; gt(I,J)=gt(rdiff+1,J); else gt(I,J)=gt(I,cdiff+1); end;
end;
end;

for I=1:rdiff; % bottom right
for J=cdiff+nc+1:npts;
if I>(npts-J); gt(I,J)=gt(rdiff+1,J); else gt(I,J)=gt(I,cdiff+nc); end;
end;
end;

for I=rdiff+nr+1:npts; % top left
for J=1:cdiff;
if (npts-I)>J; gt(I,J)=gt(rdiff+nr,J); else gt(I,J)=gt(I,cdiff+1); end;
end;
end;

```

rtpvariable.m – code for applying reduction-to-pole over a regional data set from Cooper and Cowan(2005)

```

function varrrtp=rtpvariable(magc,incv);
% *****

```

```

% *** RTP with variable geomagnetic parameters
% *** Uses a Taylor series expansion in the space domain
% *** GRJ Cooper July 2002
% *****
% *** magc ; input data (even no of datapoints in each dir)
% *** incv ; dataset of field inc over dataset - must be exactly
% *** the same size as magc. If omitted then inc is specified only
% *** at the dataset corners, and interpolated from there
% *****
% *** Type rtpvariable with no input parameters for demo application
% *****

dtr=pi/180; azimuth=0;

% interpolate inc variation over dataset using linear polynomial
if nargin==0
    disp('Loading demo data');
    load rtpdemodata;
end;
[nr,nc]=size(magc);
if nargin<2 % Specify inc variation only at corners
    disp('Generating grid of inclination data from values at grid corners');
    a=zeros(4,3); yval=zeros(4,1);
    a(1,1)=1; a(1,2)=nr; a(1,3)=1; yval(1,1)=-30;
    a(2,1)=1; a(2,2)=nr; a(2,3)=nc; yval(2,1)=-30;
    a(3,1)=1; a(3,2)=1; a(3,3)=1; yval(3,1)=-90;
    a(4,1)=1; a(4,2)=1; a(4,3)=nc; yval(4,1)=-90;
    p=pinv(a)*yval;
    [xi,yi]=meshgrid(1:nc,1:nr);
    incv=p(1)+p(2)*yi+p(3)*xi;
end;
incv=incv*dtr; inc=incv(nr/2,nc/2); % inclination at centre of grid
nmax=max([nr nc]); npts=(2^nextpow2(nmax));
cdiff=floor((npts-nc)/2); rdiff=floor((npts-nr)/2);
disp('Computing rtp');
rtpdata=rtp(magc,npts,nr,nc,rdiff,cdiff,azimuth,inc);
save('rtp.mat','rtpdata')
incv=incv-inc;
disp('Computing dx1');
drtp1=taylorrtp1(magc,npts,nr,nc,rdiff,cdiff,azimuth,inc);
disp('Computing dx2');
drtp2=taylorrtp1(drtp1,npts,nr,nc,rdiff,cdiff,azimuth,inc);
disp('Computing dx3');
drtp3=taylorrtp1(drtp2,npts,nr,nc,rdiff,cdiff,azimuth,inc);
disp('Computing rtpvar');

```

```

varrrtp=rtpdata+drtp1.*incv+0.5*drtp2.*incv.^2+0.1666666*drtp3.*incv.^3; % 3
terms - modify as required
figure(1);
subplot(1,2,1); imagesc(magc); axis equal; axis tight; axis xy; title('Data'); axis off;
hold on; contour(magc,6,'k'); hold off;
subplot(1,2,2); imagesc((incv+inc)/dtr); axis equal; axis tight; axis xy;
title('Inclination Variation');
axis off; colorbar;
currfig=get(0,'CurrentFigure'); set(currfig,'numbertitle','off');
set(currfig,'name','RTP Datasets');
figure(2);
subplot(1,3,1); imagesc(drtp1); axis equal; axis tight; axis xy; title('1st Derivative');
axis off;
subplot(1,3,2); imagesc(drtp2); axis equal; axis tight; axis xy; title('2nd Derivative');
axis off;
subplot(1,3,3); imagesc(drtp3); axis equal; axis tight; axis xy; title('3rd Derivative');
axis off;
currfig=get(0,'CurrentFigure'); set(currfig,'numbertitle','off');
set(currfig,'name','RTP Derivatives');
figure(3);
subplot(1,2,1); imagesc(rtpdata); axis equal; axis tight; axis xy; title('After Standard
RTP'); axis off;
hold on; contour(rtpdata,6,'k'); hold off;
subplot(1,2,2); imagesc(varrrtp); axis equal; axis tight; axis xy; title('c) After
Differential RTP'); axis off;
hold on; contour(varrrtp,6,'k'); hold off;
colormap('jet');
currfig=get(0,'CurrentFigure'); set(currfig,'numbertitle','off');
set(currfig,'name','RTP with Variable Inclination Over Survey Area');

```

Functions need by rtpvariable.m

taylorrtp1

```
function drtp=taylorrtp1(magc,npts,nr,nc,rdiff,cdiff,azimuth,inc); % Rtp derivatives
```

```

dtheta=0.01; dtr=pi/180;
rtpdata1=rtp(magc,npts,nr,nc,rdiff,cdiff,azimuth,inc);
rtpdata2=rtp(magc,npts,nr,nc,rdiff,cdiff,azimuth,inc+dtheta);
drtp=(rtpdata2-rtpdata1)/dtheta;

```

rtp

```

function rtpdata=rtp(magc,npts,nr,nc,rdiff,cdiff,azimuth,inc);
gf=taper2d(magc,npts,nc,nr,cdiff,rdiff);
f=fft2(gf,npts,npts);
fx=f;

```

```
% Direction cosines
```

```

L=cos(azimuth)*cos(inc);
M=sin(azimuth)*cos(inc);
N=sin(inc);
wn=2.0*pi/(npts-1);
for I=1:npts/2
  for J=1:npts/2
    U=I*wn; V=J*wn;
    temp=U*U+V*V;
    temp1=L*U+M*V;
    temp2=N*N*temp-temp1*temp1;
    base=temp2*temp2+4.0*N*N*temp1*temp1*temp;
    Rpart=temp*temp2/base;
    Ipart=-2.0*N*temp1*(temp^1.5)/base;
    temp3=real(f(I,J));
    temp4=imag(f(I,J));
    fx(I,J)=real(Rpart*temp3-temp4*Ipart)+i*real(Rpart*temp4+Ipart*temp3);
    temp1=-L*U+M*V;
    temp2=N*N*temp-temp1*temp1;
    base=temp2*temp2+4.0*N*N*temp1*temp1*temp;
    Rpart=temp*temp2/base;
    Ipart=-2.0*N*temp1*(temp^1.5)/base;
    temp3=real(f(npts-I+1,J));
    temp4=imag(f(npts-I+1,J));
    fx(npts-I+1,J)=real(Rpart*temp3-temp4*Ipart)+i*real(Rpart*temp4+Ipart*temp3);

temp1=L*U-M*V;
temp2=N*N*temp-temp1*temp1;
base=temp2*temp2+4.0*N*N*temp1*temp1*temp;
Rpart=temp*temp2/base;
Ipart=-2.0*N*temp1*(temp^1.5)/base;
temp3=real(f(I,npts-J+1));
temp4=imag(f(I,npts-J+1));
fx(I,npts-J+1)=real(Rpart*temp3-temp4*Ipart)+i*real(Rpart*temp4+Ipart*temp3);

temp1=-L*U-M*V;
temp2=N*N*temp-temp1*temp1;
base=temp2*temp2+4.0*N*N*temp1*temp1*temp;
Rpart=temp*temp2/base;
Ipart=-2.0*N*temp1*(temp^1.5)/base;
temp3=real(f(npts-I+1,npts-J+1));
temp4=imag(f(npts-I+1,npts-J+1));
fx(npts-I+1,npts-J+1)=real(Rpart*temp3-
temp4*Ipart)+i*real(Rpart*temp4+Ipart*temp3);
end;
end;

```

```
fxinv=ifft2(fx); rtpdata=real(fxinv(1+rdiff:nr+rdiff,1+cdiff:nc+cdiff));
```

taper2d

```
function gf=taper2d(g,npts,nc,nr,cdiff,rdiff);
gf=zeros(npts); gf(rdiff+1:rdiff+nr,cdiff+1:cdiff+nc)=g;
for J=cdiff+1:cdiff+nc
for I=1:rdiff
gf(I,J)=gf(2*rdiff-I+1,J)*((1+sin(-pi/2+(I-1)*pi/rdiff))*0.5);
gf(npts-I+1,J)=gf(npts-2*rdiff+I,J)*((1+sin(-pi/2+(I-1)*pi/rdiff))*0.5);
end;
end;

for I=rdiff+1:rdiff+nr
for J=1:cdiff

gf(I,J)=gf(I,2*cdiff-J+1)*((1+sin(-pi/2+(J-1)*pi/(cdiff)))*0.5);
gf(I,npts-J)=gf(I,npts-2*cdiff+J)*((1+sin(-pi/2+(J-1)*pi/(cdiff)))*0.5);
end;
end;

for J=1:cdiff
for I=1:rdiff
gf(I,J)=gf(rdiff+1,J)*((1+sin(-pi/2+(I-1)*pi/(rdiff)))*0.5);
gf(npts-I,J)=gf(npts-rdiff,J)*((1+sin(-pi/2+(I-1)*pi/(rdiff)))*0.5);
end;
end;

for J=cdiff+nc:npts
for I=1:rdiff
gf(I,J)=gf(rdiff+1,J)*((1+sin(-pi/2+(I-1)*pi/(rdiff)))*0.5);
gf(npts-I,J)=gf(npts-rdiff,J)*((1+sin(-pi/2+(I-1)*pi/(rdiff)))*0.5);
end;
end;
```

The following functions are for creating the tilt derivatives and derivatives of such. From Cooper and Cowan(2006)

```
function tilt1(data,azi,thresh,map,trans,s);
% *****
% *** Tilt angle calculations
% *** GRJ Cooper 2005
% *** School of Geosciences, University of the Witwatersrand
% *** Johannesburg, South Africa
% *** cooper@geosciences.wits.ac.za
% *** www.wits.ac.za/science/geophysics/gc.htm
% *****
```

```

% *** Parameters
% *** data ; matrix of double to be filtered
% *** azi ; directional filter azimuth in degrees from East
% *** thresh; ; threshold for display of hyp tilt eg 70
% *** map ; colourmap to use eg 'jet'
% *** trans ; transparency for overlay of 2nd order tilt - 0<trans<1
% *** s ; size of smoothing matrix to use - must be odd
% *** input 0 for no smoothing
% *****
% *** NB Needs image processing toolbox for transparency overlay
warning off MATLAB:divideByZero;
dmin=min(data(:)); dmax=max(data(:)); dm=0.5*(dmin+dmax);
data(isnan(data))=dm; data(isinf(data))=dm;
if s>0
    se=ones(s)/(s*s); data=conv2(data,se,'valid'); % smooth
end;

[nr,nc]=size(data);
dtr=pi/180.0; azi=azi*dtr; thresh=thresh*dtr;
[dx,dy]=gradient(data); dxtot=sqrt(dx.*dx+dy.*dy);
nmax=max([nr nc]); npts=2^nextpow2(nmax);
dz=vertical(data,npts,nc,nr,1);
t1=atan(dz./dxtot);
th=real(atanh(dz./dxtot));
tdx=real(atan(dxtot./abs(dz)));

dx1=dx*cos(azi)+dy*sin(azi); % Standard directional derivative
dx2=dx*cos(azi+pi/2)+dy*sin(azi+pi/2);
dxz=sqrt(dx2.*dx2+dz.*dz); ta=atan(dx1./dxz); % Tilt directional derivative

% 2nd order Tilt angle
ts=t1;
if s<3 s=3; end; se=ones(s)/(s*s); s2=floor(s/2);
ts=conv2(t1,se,'same');
[dxs,dys]=gradient(ts);
dzs=vertical(ts,npts,nc,nr,1);
dxtots=sqrt(dxs.*dxs+dys.*dys);
t2=atan(dzs./dxtots);

% Plot results
figure(1); clf;
zm=mean(data(:)); zs=std(data(:)); zmax=zm+zs*2; zmin=zm-zs*2;
data(data>zmax)=zmax; data(data<zmin)=zmin;
subplot(1,1,1); imagesc(data); axis equal; axis tight; axis xy; axis off; title('Data');
colormap(jet(256));

```

```

figure(2);
subplot(1,1,1); imagesc(t1); axis equal; axis tight; axis xy; axis off; title('Standard
Tilt Angle');
save('tilt_ang.mat','t1')
colormap(gray(256));
figure(3); clf;
zm=mean(th(:)); zs=std(th(:)); zmax=zm+zs*2; zmin=zm-zs*2;
subplot(1,2,1); imagesc(th,[zmin zmax]); axis equal; axis tight; axis xy; axis off;
title('Hyperbolic Tilt Angle');
save('HTA.mat','th')
data2=data; zmax=max(data(:)); data2(th>thresh)=zmax;
subplot(1,2,2); imagesc(data2); axis equal; axis tight; axis xy; title('HTA Maximum
Overlain on Data');
save('HTA_max_over.mat','data2')
axis off; colormap(gray(256));
figure(4);
subplot(1,2,1); imagesc(t2); axis equal; axis tight; axis xy; axis off; title('2nd Order
Tilt Angle'); colormap(gray(256));
save('2nd_ord_tilta.mat','t2')
agray=mat2gray(data); inda=gray2ind(agray,256); clear agray;
mapstr=[map '(256)']; ms=colormap(mapstr);
RGB=ind2rgb(inda,ms); clear inda;
subplot(1,2,2); imagesc(RGB); axis equal; axis tight; axis xy;
hold on; h=imagesc(t2); axis equal; axis tight; axis off; axis xy; colormap('gray');
alpha(h,trans); hold off; title('Data with Overlain 2nd Order Tilt Angle');
figure(5); clf;
zm=mean(dx1(:)); zs=std(dx1(:)); zmax=zm+zs*3; zmin=zm-zs*3;
subplot(1,2,1); imagesc(dx1,[zmin zmax]); axis equal; axis tight; axis xy; axis off;
title('Directional Derivative');
save('Dir_derv.mat','dx1')
subplot(1,2,2); imagesc(ta); axis equal; axis tight; axis xy; axis off; title('Tilt Based
Directional Derivative');
save('Tilt_base_Dir_Derv.mat','ta')
colormap(gray(256));
figure(6); clf;
zs=std(dxtot(:)); zmax=3*zs;
subplot(1,2,1); imagesc(dxtot,[0 zmax]); axis equal; axis tight; axis xy; axis off;
title('Total Derivative');
save('tot_derv.mat','dxtot')
subplot(1,2,2); imagesc(tdx); axis equal; axis tight; axis xy; axis off; title('TDX');
save('TDX.mat','tdx')
figure(1);

```

Functions needed by Tilt1.m

vertical

```
function dz=vertical(data,npts,nc,nr,xint);
```



```

cdiff=floor((npts-nc)/2); rdiff=floor((npts-nr)/2);
data1=taper2d(data,npts,nc,nr,cdiff,rdiff);
f=fft2(data1); fz=f;
wn=2.0*pi/(xint*(npts-1));
f=fftshift(f);
cx=npts/2+1; cy=cx;
for I=1:npts
    freqx=(I-cx)*wn;
    for J=1:npts
        freqy=(J-cy)*wn;
        freq=sqrt(freqx*freqx+freqy*freqy);
        fz(I,J)=f(I,J)*freq;
    end;
end;

fz=fftshift(fz); fzinv=ifft2(fz);
dz=real(fzinv(1+rdiff:nr+rdiff,1+cdiff:nc+cdiff));

```

taper2d

```

function gf=taper2d(g,npts,n,m,ndiff,mdiff);
gm=mean(g(:));
gf=zeros(npts); gf(mdiff+1:mdiff+m,ndiff+1:ndiff+n)=g-gm;
for J=mdiff+1:mdiff+m
    for I=1:ndiff
        gf(I,J)=gf(I,J)*((1+sin(-pi/2+(I-1)*pi/ndiff))*0.5);
        gf(npts-I+1,J)=gf(npts-I+1,J)*((1+sin(-pi/2+(I-1)*pi/ndiff))*0.5);
    end;
end;

for I=ndiff+1:ndiff+n
    for J=1:mdiff
        gf(I,J)=gf(I,J)*((1+sin(-pi/2+(J-1)*pi/(mdiff)))*0.5);
        gf(I,npts-J)=gf(I,npts-J)*((1+sin(-pi/2+(J-1)*pi/(mdiff)))*0.5);
    end;
end;

for J=1:mdiff
    for I=1:ndiff
        gf(I,J)=gf(I,J)*((1+sin(-pi/2+(I-1)*pi/(ndiff)))*0.5);
        gf(npts-I,J)=gf(npts-I,J)*((1+sin(-pi/2+(I-1)*pi/(ndiff)))*0.5);
    end;
end;

for J=mdiff+m:npts
    for I=1:ndiff
        gf(I,J)=gf(I,J)*((1+sin(-pi/2+(I-1)*pi/(ndiff)))*0.5);
    end;
end;

```

```

gf(npts-I,J)=gf(npts-I,J)*((1+sin(-pi/2+(I-1)*pi/(ndiff)))*0.5);
end;
end;
for J=mdiff+m:npts % Corners
for I=ndiff+n:npts
gf(I,J)=gf(I,J)*cos((I-ndiff-n)*pi/(2*ndiff))*cos((J-ndiff-m)*pi/(2*mdiff));
end;
end;
for J=1:mdiff
for I=1:ndiff
gf(I,J)=gf(I,J)*cos((I-ndiff)*pi/(2*ndiff))*cos((J-ndiff)*pi/(2*mdiff));
end;
end;

for J=1:mdiff
for I=ndiff+n:npts
gf(I,J)=gf(I,J)*cos((I-ndiff-n)*pi/(2*ndiff))*cos((J-ndiff)*pi/(2*mdiff));
end;
end;
for J=mdiff+m:npts
for I=1:ndiff
gf(I,J)=gf(I,J)*cos((I-ndiff)*pi/(2*ndiff))*cos((J-ndiff-m)*pi/(2*mdiff));
end;
end;

```

Circular and radial tilt angle functions from Cooper and Cowan(2006)

TiltDr.m

```

function tiltDr(data,s);
% *****
% *** Circular and Radial Tilt angle
% *** GRJ Cooper 2005
% *** School of Geosciences, University of the Witwatersrand
% *** Johannesburg, South Africa
% *** cooper@geosciences.wits.ac.za
% *** www.wits.ac.za/science/geophysics/gc.htm
% *****
% *** s ; size of smoothing kernel, must be odd. Enter 0 for no smoothing

warning off MATLAB:divideByZero;
if s>0
se=ones(s)/(s*s); data=conv2(data,se,'valid'); % smooth
end;

[nr,nc]=size(data);
dmin=min(data(:)); dmax=max(data(:)); dm=0.5*(dmin+dmax);
data(isnan(data))=dm; data(isinf(data))=dm;

```

```

nmax=max([nr nc]); npts=2^nextpow2(nmax); rtd=180/pi;
[dx,dy]=gradient(data);
dz=vertical(data,npts,nc,nr,1);

figure(1);
zm=mean(data(:)); zs=std(data(:)); zmax=zm+zs*2; zmin=zm-zs*2;
data=mat2gray(data,[zmin zmax]);
azi=zeros(nr,nc);

figure(1);
subplot(1,1,1); imagesc(data); axis equal; axis tight; axis off; axis xy;
colormap(gray(256));
title('RIGHT click inside image to set centre location');
[c,r,P]=impixel; xpos=c(1); ypos=r(1);
for I=1:nr

    for J=1:nc
        xdif=(J-xpos); ydif=(I-ypos);
        azi(I,J)=atan2(ydif,xdif)-pi;
    end;
end;

dx1=-dx.*cos(azi)-dy.*sin(azi);
dx2=-dx.*cos(azi+pi/2)-dy.*sin(azi+pi/2);
dx1z=sqrt(dx1.*dx1+dz.*dz); t2=atan(dx2./dx1z);
dx2z=sqrt(dx2.*dx2+dz.*dz); t3=atan(dx1./dx2z);

figure(1);
subplot(1,1,1); imagesc(data); axis equal; axis tight; axis xy; title('Data'); axis off;
figure(2);
zm=mean(dx1(:)); zs=std(dx1(:)); zmax=zm+zs*2; zmin=zm-zs*2;

subplot(1,1,1); imagesc(dx1,[zmin zmax]); axis equal; axis tight; axis xy;
title('Directional Derivative'); axis off;
colormap(gray(256));
figure(3);
subplot(1,1,1); imagesc(t3); axis equal; axis tight; axis xy; axis off; title('Radial Tilt
Angle');
figure(4);
subplot(1,1,1); imagesc(t2); axis equal; axis tight; axis xy; axis off; title('Circular Tilt
Angle');
figure(5);
tr=atan(t3./abs(t2));
subplot(1,1,1); imagesc(tr); axis equal; axis tight; axis xy; axis off;
colormap(gray(256)); title('Radial Tilt Derivative Ratio');
figure(3);

```

Functions needed by TiltDr.m**vertical**

```

function dz=vertical(data,npts,nc,nr,xint);
cdiff=floor((npts-nc)/2); rdiff=floor((npts-nr)/2);
data1=taper2d(data,npts,nc,nr,cdiff,rdiff);
f=fft2(data1); fz=f;
wn=2.0*pi/(xint*(npts-1));
f=fftshift(f);
cx=npts/2+1; cy=cx;
for I=1:npts
    freqx=(I-cx)*wn;
    for J=1:npts
        freqy=(J-cy)*wn;
        freq=sqrt(freqx*freqx+freqy*freqy);
        fz(I,J)=f(I,J)*freq;
    end;
end;

fz=fftshift(fz); fzinv=ifft2(fz);
dz=real(fzinv(1+rdiff:nr+rdiff,1+cdiff:nc+cdiff));

```

taper2d

```

function gf=taper2d(g,npts,n,m,ndiff,mdiff);
gm=mean(g(:));
gf=zeros(npts); gf(mdiff+1:mdiff+m,ndiff+1:ndiff+n)=g-gm;
for J=mdiff+1:mdiff+m
    for I=1:ndiff
        gf(I,J)=gf(I,J)*((1+sin(-pi/2+(I-1)*pi/ndiff))*0.5);
        gf(npts-I+1,J)=gf(npts-I+1,J)*((1+sin(-pi/2+(I-1)*pi/ndiff))*0.5);
    end;
end;

for I=ndiff+1:ndiff+n
    for J=1:mdiff
        gf(I,J)=gf(I,J)*((1+sin(-pi/2+(J-1)*pi/(mdiff)))*0.5);
        gf(I,npts-J)=gf(I,npts-J)*((1+sin(-pi/2+(J-1)*pi/(mdiff)))*0.5);
    end;
end;

for J=1:mdiff
    for I=1:ndiff
        gf(I,J)=gf(I,J)*((1+sin(-pi/2+(I-1)*pi/(ndiff)))*0.5);
        gf(npts-I,J)=gf(npts-I,J)*((1+sin(-pi/2+(I-1)*pi/(ndiff)))*0.5);
    end;
end;

```

```

for J=mdiff+m:npts
for I=1:ndiff
gf(I,J)=gf(I,J)*((1+sin(-pi/2+(I-1)*pi/(ndiff)))*0.5);
gf(npts-I,J)=gf(npts-I,J)*((1+sin(-pi/2+(I-1)*pi/(ndiff)))*0.5);
end;
end;

for J=mdiff+m:npts % Corners
for I=ndiff+n:npts
gf(I,J)=gf(I,J)*cos((I-ndiff-n)*pi/(2*ndiff))*cos((J-ndiff-m)*pi/(2*mdiff));
end;
end;

for J=1:mdiff
for I=1:ndiff
gf(I,J)=gf(I,J)*cos((I-ndiff)*pi/(2*ndiff))*cos((J-ndiff)*pi/(2*mdiff));
end;
end;

for J=1:mdiff
for I=ndiff+n:npts
gf(I,J)=gf(I,J)*cos((I-ndiff-n)*pi/(2*ndiff))*cos((J-ndiff)*pi/(2*mdiff));
end;
end;

for J=mdiff+m:npts
for I=1:ndiff
gf(I,J)=gf(I,J)*cos((I-ndiff)*pi/(2*ndiff))*cos((J-ndiff-m)*pi/(2*mdiff));
end;
end;

```

createfigure.m – *creates a color figure from a Matlab matrice*

```
function createfigure(cdata1)
```

```

% Create figure
figure1 = figure('NumberTitle','off',...
    'Name','Figure');

% Create plot
subplot1 = subplot(1,2,1,'Visible','off','Parent',figure1,...
    'PlotBoxAspectRatio',[32 32 1],...
    'Layer','top',...
    'DataAspectRatio',[1 1 1]);
% Uncomment the following line to preserve the X-limits of the axes
% xlim(subplot1,[0.5 64.5]);

```

```

% Uncomment the following line to preserve the Y-limits of the axes
% ylim(subplot1,[0.5 64.5]);
box(subplot1,'on');
hold(subplot1,'all');

% Create image
image(cdata1,'Parent',subplot1,'CDataMapping','scaled');

% Create contour
contour(cdata1,'LineColor',[0 0 0],...
'LevelList',[-1.699 17.73 37.17 56.6 76.04 95.47],...
'Parent',subplot1);

```

analytic.m - calculates analytic signal

```

% *****
function An=analytic(g)

[nr,nc]=size(g); nmax=max([nr nc]); npts=2^nextpow2(nmax);
[dx,dy]=gradient(g); dz=vertical(g,npts,nc,nr,1);

An=dz+dy+dx

```

Functions need by analytic.m

vertical

```

function dz=vertical(data,npts,nc,nr,xint) % Compute vertical derivative

cdiff=floor((npts-nc)/2); rdiff=floor((npts-nr)/2);
data1=taper2spline(data,npts,nc,nr,cdiff,rdiff);
f=fft2(data1); fz=f;
wn=2.0*pi/(xint*(npts-1));
f=fftshift(f);
cx=npts/2+1; cy=cx;
for l=1:npts
    freqx=(l-cx)*wn;
    for J=1:npts
        freqy=(J-cy)*wn;
        freq=sqrt(freqx*freqx+freqy*freqy);
        fz(l,J)=f(l,J)*freq;
    end;
end;
fz=fftshift(fz); fzinv=ifft2(fz);
dz=real(fzinv(1+rdiff:nr+rdiff,1+cdiff:nc+cdiff));

```

taper2spline

```

function gt=taper2spline(g,npts,nc,nr,cdiff,rdiff)

```

```

% Merge edges to the value opposite using a cubic spline

gt=zeros(npts); gt(rdifff+1:rdifff+nr,cdifff+1:cdifff+nc)=g;
gp=g(:,1:3); [gpx1,junk]=gradient(gp); % sides
gp=g(:,nc-2:nc); [gpx2,junk]=gradient(gp);
x1=0; x2=(2*cdifff)+1;
x=[1 1 0 0;x1 x2 1 1; x1^2 x2^2 2*x1 2*x2; x1^3 x2^3 3*x1^2 3*x2^2];
for l=1:nr;
y=[g(l,nc) g(l,1) gpx2(l,3) gpx1(l,1)];
c=y/x;
for J=1:cdifff;
gt(l+rdifff,J)=c(1)+(J+cdifff)*c(2)+c(3)*(J+cdifff)^2+c(4)*(J+cdifff)^3;
gt(l+rdifff,J+nc+cdifff)=c(1)+J*c(2)+c(3)*J^2+c(4)*J^3;
end;
end;

gp=g(1:3,:); [junk,gpx1]=gradient(gp); % top and bottom
gp=g(nr-2:nr,:); [junk,gpx2]=gradient(gp);
x1=0; x2=(2*rdifff)+1;
x=[1 1 0 0;x1 x2 1 1; x1^2 x2^2 2*x1 2*x2; x1^3 x2^3 3*x1^2 3*x2^2];
for J=1:nc;
y=[g(nr,J) g(1,J) gpx2(3,J) gpx1(1,J)];
c=y/x;
for l=1:rdifff;
gt(l,J+cdifff)=c(1)+(l+rdifff)*c(2)+c(3)*(l+rdifff)^2+c(4)*(l+rdifff)^3;
gt(l+rdifff+nr,J+cdifff)=c(1)+l*c(2)+c(3)*l^2+c(4)*l^3;
end;
end;

for l=rdifff+nr+1:npts; % Corners
for J=cdifff+nc+1:npts;
if (l-nr-rdifff)>(J-nc-cdifff); gt(l,J)=gt(l,nc+cdifff); else gt(l,J)=gt(nr+rdifff,J); end;
end;
end;

for l=1:rdifff;
for J=1:cdifff;
if l>J; gt(l,J)=gt(rdifff+1,J); else gt(l,J)=gt(l,cdifff+1); end;
end;
end;

for l=1:rdifff; % bottom right
for J=cdifff+nc+1:npts;
if l>(npts-J); gt(l,J)=gt(rdifff+1,J); else gt(l,J)=gt(l,cdifff+nc); end;
end;
end;

```

```

for l=rdiff+nr+1:npts; % top left
for J=1:cdiff;
if (npts-l)>J; gt(l,J)=gt(rdiff+nr,J); else gt(l,J)=gt(l,cdiff+1); end;
end;
end;

```

totalderv.m - calculates total derivative for total field magnetic data

```
function Td=totalderv(g)
```

```

[nr,nc]=size(g); nmax=max([nr nc]); npts=2^nextpow2(nmax);
[dx,dy]=gradient(g); dz=vertical(g,npts,nc,nr,1);

```

```
Td=sqrt(dz.*dz+dy.*dy+dx.*dx)
```

Functions needed for totalderv.m

vertical

```
function dz=vertical(data,npts,nc,nr,xint) % Compute vertical derivative
```

```

cdiff=floor((npts-nc)/2); rdiff=floor((npts-nr)/2);
data1=taper2spline(data,npts,nc,nr,cdiff,rdiff);
f=fft2(data1); fz=f;
wn=2.0*pi/(xint*(npts-1));
f=fftshift(f);
cx=npts/2+1; cy=cx;
for I=1:npts
freqx=(I-cx)*wn;
for J=1:npts
freqy=(J-cy)*wn;
freq=sqrt(freqx*freqx+freqy*freqy);
fz(I,J)=f(I,J)*freq;
end;
end;
fz=fftshift(fz); fzinv=ifft2(fz);
dz=real(fzinv(1+rdiff:nr+rdiff,1+cdiff:nc+cdiff));

```

taper2spline

```
function gt=taper2spline(g,npts,nc,nr,cdiff,rdiff)
% Merge edges to the value opposite using a cubic spline
```

```

gt=zeros(npts); gt(rdiff+1:rdiff+nr,cdiff+1:cdiff+nc)=g;
gp=g(:,1:3); [gpx1,junk]=gradient(gp); % sides
gp=g(:,nc-2:nc); [gpx2,junk]=gradient(gp);
x1=0; x2=(2*cdiff)+1;
x=[1 1 0 0;x1 x2 1 1; x1^2 x2^2 2*x1 2*x2; x1^3 x2^3 3*x1^2 3*x2^2];
for I=1:nr;

```



```

y=[g(l,nc) g(l,1) gpx2(l,3) gpx1(l,1)];
c=y/x;
for J=1:cdiff;
gt(l+rdiff,J)=c(1)+(J+cdiff)*c(2)+c(3)*(J+cdiff)^2+c(4)*(J+cdiff)^3;
gt(l+rdiff,J+nc+cdiff)=c(1)+J*c(2)+c(3)*J^2+c(4)*J^3;
end;
end;

gp=g(1:3,:); [junk,gpx1]=gradient(gp); % top and bottom
gp=g(nr-2:nr,:); [junk,gpx2]=gradient(gp);
x1=0; x2=(2*rdiff)+1;
x=[1 1 0 0;x1 x2 1 1; x1^2 x2^2 2*x1 2*x2; x1^3 x2^3 3*x1^2 3*x2^2];
for J=1:nc;
y=[g(nr,J) g(1,J) gpx2(3,J) gpx1(1,J)];
c=y/x;
for l=1:rdiff;
gt(l,J+cdiff)=c(1)+(l+rdiff)*c(2)+c(3)*(l+rdiff)^2+c(4)*(l+rdiff)^3;
gt(l+rdiff+nr,J+cdiff)=c(1)+l*c(2)+c(3)*l^2+c(4)*l^3;
end;
end;

for l=rdiff+nr+1:npts; % Corners
for J=cdiff+nc+1:npts;
if (l-nr-rdiff)>(J-nc-cdiff); gt(l,J)=gt(l,nc+cdiff); else gt(l,J)=gt(nr+rdiff,J); end;
end;
end;

for l=1:rdiff;
for J=1:cdiff;
if l>J; gt(l,J)=gt(rdiff+1,J); else gt(l,J)=gt(l,cdiff+1); end;
end;
end;

for l=1:rdiff; % bottom right
for J=cdiff+nc+1:npts;
if l>(npts-J); gt(l,J)=gt(rdiff+1,J); else gt(l,J)=gt(l,cdiff+nc); end;
end;
end;

for l=rdiff+nr+1:npts; % top left
for J=1:cdiff;
if (npts-l)>J; gt(l,J)=gt(rdiff+nr,J); else gt(l,J)=gt(l,cdiff+1); end;
end;
end;

```

BIBLIOGRAPHY

- Abbate, E., Passerini, P., and Zan, L., 1995, Strike-slip faults in a rift area: a transect in the Afar Triangle, East Africa: *Tectonophysics*, v. 241, p. 67-97.
- Acocella, V., Abebe, B., Korme, T., and Barberi, F., 2008, Structure of the Tendaho Graben and Manda Hararo Rift: Implications for the evolution of the southern Red Sea propagator in central Afar: *Tectonics*, v. 27, p. TC4016.
- Acton, G.D., Stein, S., and Engeln, J.F., 1991, Block rotation and continental extension in Afar: a comparison to oceanic microplate systems: *Tectonics*, v. 10, p. 501-526.
- Acton, G.D., Tessema, A., Jackson, M., and Bilham, R., 2000, The tectonic and geomagnetic significance of paleomagnetic observations from volcanic rocks from central Afar, Africa: *Earth and Planetary Science Letters*, v. 180, p. 225-241.
- Anderson, R.N., Honnorez, J., Becker, K., Adamson, A.C., Alt, J.C., and et, a., 1982, DSDP hole 504B, the first reference section over 1 km through layer 2 of the oceanic crust: *Nature*, v. 300, p. 589-594.
- Aquater, 1996a, Tendaho Geothermal Project -final report, Volume 1, Aquater, p. 324.
- , 1996b, Tendaho Geothermal Project -final report, Volume 2, Aquater, p. 324.
- Arkani-Hamed, J., 1988, differential reduction-to-the-pole of regional anomalies: *Geophysics*, v. 53, p. 1592-1600.
- Ayele, A., Jacques, E., Kassim, M., Kidane, T., Omar, A., Tait, S., Nercessian, A., Chabalier, J.-B.d., and King, G., 2007, The volcano-seismic crisis in Afar, Ethiopia, starting September 2005: *Earth and Planetary Science Letters*, v. 255, p. 177-187.
- Ayele, A., Keir, D., Ebinger, C., Wright, T.J., Stuart, G.W., Buck, W.R., Jacques, E., Ogubazghi, G., and Sholan, J., 2009, September 2005 mega-dike emplacement in the Manda-Harraro nascent oceanic rift (Afar depression): *Geophysical Research Letters*, v. 36, p. L20306.
- Baksi, A.K., 1993, A geomagnetic polarity time scale for the period 0-17 Ma, based on $^{40}\text{Ar}/^{39}\text{Ar}$ plateau ages for selected field reversals: *Geophysical Research Letters*, v. 20, p. 1607-1610.
- Baksi, A.K., Hsu, V., McWilliams, M.O., and Farrar, E., 1992, Ar-40/Ar-39 dating of the Brunhes-Matuyama geomagnetic field reversal: *Science*, v. 256, p. 356-357.

- Ballard, R.D., and van Andel, T.H., 1977, Morphology and tectonics of the inner rift valley at lat. 36°50'N on the Mid-Atlantic ridge: *Geological Society of America Bulletin*, v. 88, p. 507-530.
- Barberi, F., Bonatti, E., Marinelli, G., and Varet, J., 1974, Transverse tectonic during the split of continent: Data from the Afar rift: *Tectonophysics*, v. 23, p. 17-19.
- Barberi, F., Ferrara, G., Santacroce, R., Treuil, M., and Varet, J., 1975a, A transitional basalt-pantellerite sequence of fractional crystallization, the Boina Centre (Afar Rift, Ethiopia): *Journal of Petrology*, v. 16, p. 22-56.
- Barberi, F., Ferrara, G., Santacroce, R., and Varet, J., 1975b, Structural evolution of the Afar triple junction, *in* Pilger, A., and Rosler, A., eds., *Afar Depression of Ethiopia*: Stuttgart, E. Schweizerbart'sche Verlagbuchhandlung, p. 38-54.
- Barberi, F., and Varet, J., 1977, Volcanism of Afar: Small-scale plate tectonics implications: *Geological Society of America Bulletin*, v. 88, p. 1251-1266.
- Barisin, I., Leprince, S., Parsons, B., and Wright, T., 2009, Surface displacements in the September 2005 Afar rifting event from satellite image matching: Asymmetric uplift and faulting: *Geophysical Research Letters*, v. 36, p. L07301.
- Barnov, V., 1957, A new method for interpretation of aeromagnetic maps: pseudo-gravimetric anomalies: *Geophysics*, v. 22, p. 359-383.
- Barnov, V., and Naudy, H., 1964, Numerical calculation of the formula of reduction to the magnetic pole: *Geophysics*, v. 29, p. 67-79.
- Barrat, J.A., Joron, J.L., Taylor, R.N., Fourcade, S., Nesbitt, R.W., and Jahn, B.M., 2003, Geochemistry of basalts from Manda Hararo, Ethiopia: LREE-depleted basalts in central Afar: *Lithos*, v. 69, p. 1-13.
- Battistelli, A., Yiheyis, A., Calore, C., Ferragina, C., and Abatneh, W., 2002, Reservoir engineering assessment of Dubti geothermal field, Northern Tendaho Rift, Ethiopia: *Geothermics*, v. 31, p. 381-406.
- Benoit, M.H., Nyblade, A.A., and VanDecar, J.C., 2006, Upper mantle P-wave speed variations beneath Ethiopia and the origin of the Afar hotspot: *Geology*, v. 34, p. 329-332.
- Berckhemer, H., Baier, B., Bartelsen, H., Behle, A., Burkhardt, H., Gebrande, H., Makris, J., Menzel, H., and Vees, R., 1975, Deep Seismic soundings in the Afar region and on the highland of Ethiopia, *in* Pilger, A., and Rosler, A., eds., *Afar Depression of Ethiopia, Proceedings of an International Symposium on the Afar Region and Rift Related Problems, Volume 1*: Stuttgart, Germany, E. Schweizerbart'sche Verlagbuchhandlung, p. 89-107.

- Berketold, A., Haak, V., and Angenheister, G., 1975, Magnetotelluric measurements in the Afar area, *in* Pilger, A., and Rosler, A., eds., Afar Depression of Ethiopia, Proceedings of an International Symposium on the Afar Region and Related Rift Problems, Bad Bergzabern, Germany, 1974, Volume 1: Stuttgart, Germany, E. Schweizerbart'sche Verlagsbuchhandlung, p. 66-79.
- Beyene, A., and Abdelsalam, M.G., 2005, Tectonics of the Afar Depression: A review and synthesis: *Journal of African Earth Sciences*, v. 41, p. 41-59.
- Bhattacharyya, B.K., 1964, Magnetic anomalies due to prism bodies with arbitrary magnetization: *Geophysics*, v. 29, p. 517-531.
- Blakely, R.J., 1995, *Potential Theory in Gravity & Magnetic Applications*: New York, Cambridge University Press.
- Bleil, U., and Peterson, N., 1983, Variations in the magnetization intensity and low-temperature titanomagnetite oxidation of ocean floor basalts: *Nature*, v. 301, p. 384-388.
- Bohannon, R.G., Naeser, C.W., Schmidt, D.L., and Zimmerman, R.A., 1989, The timing of uplift, volcanism, and rifting peripheral to the red sea; a case for passive rifting: *Journal of Geophysical Research*, v. 94, p. 1683-1701.
- Buck, W.R., 2006, The role of magma in the development of the Afro-Arabian Rift System, *in* Yirgu, G., Ebinger, C.J., and Maguire, P.K.H., eds., *The Afar Volcanic Province within the East African Rift System*, Volume 259: London, Geological society, p. 43-54.
- Cande, S.C., and Kent, D.V., 1976, Constraints imposed by the shape of marine magnetic anomalies on the magnetic source: *Journal of Geophysical Research*, v. 81, p. 4157-4162.
- , 1992, A new geomagnetic polarity time scale for the Late Cretaceous and Cenozoic: *Journal of Geophysical Research*, v. 97, p. 13917-13951.
- Chu, D., and Gordon, R.G., 1998, Current plate motions across the Red Sea: *Geophysical Journal International*, v. 135, p. 313-328.
- Cochran, J.R., 1981, Pre-sea floor spreading development of the Gulf of Aden: *Oceanologica Acta Supplement*, v. 4, p. 155-165.
- Coggon, J.H., 1976, Magnetic and gravity anomalies of polyhedra: *Geoexploration*, v. 14, p. 93-105.

- Collet, B., Taud, H., Parrot, J.F., Bonavia, F., and Chorowicz, J., 2000, A new kinematic approach for the Danakil Block using a digital elevation model representation: *Tectonophysics*, v. 316, p. 343-357.
- Cooper, G.R.J., and Cowan, D.R., 2005, Differential reduction to the pole: *Computers & Geosciences*, v. 31, p. 989-999.
- , 2006, Enhancing potential field data using filters based on local phase: *Computers & Geosciences*, v. 32, p. 1585-1591.
- , 2008, Edge enhancement of potential-field data using normalized statistics: *Geophysics*, v. 73, p. H1-H4.
- , 2009, Terracing potential field data: *Geophysical Prospecting*, v. 57, p. 1067-1071.
- Cordell, L., and McCafferty, A.E., 1989, A terracing operator for physical property mapping with potential field data: *Geophysics*, v. 54, p. 621-634.
- Cornwell, D.G., Mackenzie, G.D., England, R.W., Maguire, P.K.H., Asfaw, L.M., and Oluma, B., 2006, Northern Main Ethiopian Rift crustal structure from new high-precision gravity data, *in* Yirgu, G., Ebinger, C.J., and Maguire, P.K.H., eds., *The Afar Volcanic Province within the East African Rift System*, Volume 259: Special Publications: London, Geological Society, p. 307-321.
- Courtillot, V., 1982, Propogating rifts and continental breakup: *Tectonics*, v. 1, p. 239-250.
- Courtillot, V., Achache, J., Landre, F., Bonhommet, N., Montigny, R., and Feraud, G., 1984, Episodic spreading and rift propogation: new paleomagnetic and geochronologic data from the afar nascent passive margin: *Journal of Geophysical Research*, v. 89, p. 3315-3333.
- Courtillot, V., Galdeano, A., and Mouel, J.L.L., 1980, Propogation of an accreting Plate Boundary: A discussion of new aeromagnetic data in the Gulf of Tadjurah and southern Afar: *Earth and Planetary Science Letters*, v. 47, p. 144-160.
- Cox, A., and Doell, R.R., 1960, Review of paleomagnetism: *Geological Society of America Bulletin*, v. 71, p. 645-768.
- Dainelli, G., 1943, *Geologia Dell'Africa Orientale*, Volume 1: Rome, Centro Studi Per L'Africa Orientale Italiana, p. 464.
- Dakin, F.M., Gouin, P., and Searle, R., 1971, The 1969 earthquakes in Sardo (Ethiopia): *Bulletin of the Geophysical Observatory, Addis Ababa*, v. 13, p. 19-28.
- Dannemiller, N., and Li, Y., 2004, A new method for determination of magnetization direction, 74th Annual International Meeting, SEG.

- , 2006, A new method for determination of magnetization direction: *Geophysics*, v. 71, p. L69-L73.
- Dauteuil, O., Huchon, P., Quemeneur, F., and Souriot, T., 2001, Propagation of an oblique spreading center; the western Gulf of Aden: *Tectonophysics*, v. 332, p. 423-442.
- Debayle, E., Kennett, B., and Priestley, K., 2005, Global azimuthal seismic anisotropy and the unique plate-motion deformation of Australia: *Nature*, v. 433, p. 509-512.
- Debeglia, N., and Corpel, J., 1997, Automatic 3-D interpretation of potential field data using analytic signal derivatives: *Geophysics*, v. 62, p. 87-96.
- Deniel, C., Vidal, P., Coulon, C., Vellutini, P.-J., and Pigué, P., 1994, Temporal evolution of mantle sources during continental rifting: The volcanism of Djibouti (Afar): *Journal of Geophysical Research*, v. 99, p. 2853-2869.
- Dutra, A.C., and marangoni, Y.R., 2009, Gravity and magnetic 3D inversion of Morro do Engenho complex, Central Brazil: *Journal of South American Earth Sciences*, v. 28, p. 193-203.
- Eagles, G., Gloaguen, R., and Ebinger, C.J., 2002, Kinematics of the Dabakil Microplate: *Earth and Planetary Science Letters*, v. 203.
- Ebinger, C.J., and Casey, M., 2001, Continental breakup in magmatic provinces: An Ethiopian example: *Geology*, v. 29, p. 527-530.
- Fairhead, J.D., and Girdler, R.W., 1970, The seismicity of the Red Sea, Gulf of Aden and Afar Triangle: *Phil. Trans. Roy. Soc. Lond. A.*, v. 267, p. 49-74.
- Fowler, C.M.R., 2005, *The Solid Earth*: Cambridge, UK, Cambridge University Press, 685 p.
- Gass, I.G., 1975, Magmatic and tectonic processes in the development of the Afro-Arabian Dome, *in* Pilger, A., and Rosler, A., eds., *Afar Depression of Ethiopia, Proceedings of an International Symposium on the Afar area and Rift Related Problems, Bad Bergzabren, Germany 1974, Volume 1*: Stuttgart, Germany, E. Schweizerbart'sche Verlagsbuchhandlung, p. 10-18.
- Gee, J., and Kent, D.V., 1994, Variations in layer 2A thickness and the origin of the central anomaly magnetic high: *Geophysical Research Letters*, v. 21, p. 297-300.
- Gerovska, D., and Arauzo-Bravo, M.J., 2006, Calculation of magnitude magnetic transforms with high centrality and low dependence on the magnetization vector direction: *Geophysics*, v. 71, p. 121-130.

- Gerovska, D., Arauzo-Bravo, M.J., and Stavrev, P., 2004, Determination of the parameters of compact ferro-metallic objects with transforms of magnitude magnetic anomalies: *Journal of Applied Geophysics*, v. 55, p. 173-186.
- , 2009, Estimating the magnetization direction of sources from southeast Bulgaria through correlation between reduced-to-the-pole and total magnitude anomalies: *Geophysical Prospecting*, v. 57, p. 491-505.
- Girdler, R.W., 1970, An aeromagnetic survey of the junction of the Red Sea, Gulf of Aden and Ethiopian rifts-A preliminary report: *P. Transactions of the Royal Society of London*, v. 267.
- Girdler, R.W., and Peter, G., 1960, An example of the importance of natural remanent magnetization in the interpretation of magnetic anomalies: *Geophysical Prospecting*, v. 8, p. 474-483.
- Gouin, P., 1979, *Earthquake History of Ethiopia and the Horn of Africa*: Ottawa, Ont., International Development Research Centre.
- Grandin, R., Socquet, A., Binet, R., Klinger, Y., Jacques, E., de Chabalier, J.-B., King, G.C.P., Lasserre, C., Tait, S., Tapponnier, P., Delorme, A., and Pinzuti, P., 2009, September 2005 Manda Hararo-Dabbahu rifting event, Afar (Ethiopia): Constraints provided by geodetic data: *Journal of Geophysical Research*, v. 114, p. B08404.
- Grant, F.S., and Dodds, J., 1972, *MAGMAP FFT processing system development notes*, Paterson Grant and and Watson Limited.
- Haney, M.M., Johnston, c., Li, Y., and Nabighian, M.N., 2003, Envelopes of 2D and 3D magnetic data and their relationship to the analytic signal: preliminary results, 73rd Annual International Meeting, SEG, extended abstracts.
- Haney, M.M., and Li, Y., 2002, Total magnetization direction and dip from multiscale edges, *SEG Expanded Abstracts*, Volume 21, p. 735.
- Hansen, R.O., and Pawlowski, R.S., 1989, Reduction to the pole at low latitudes by Wiener filtering: *Geophysics*, v. 54, p. 1607-1613.
- Harrison, C.G.A., 1987, Marine magnetic anomalies-The origin of the stripes: *Annual Review of Earth and Planetary Sciences*, v. 15, p. 505-543.
- Hayward, N.J., and Ebinger, C.J., 1996, Variations in the along-axis segmentation of the Afar Rift system: *Tectonics*, v. 15, p. 244-257.
- Helbig, K., 1962, Some integrals of magnetic anomalies and thier relationship to the paramters of the disturbing body: *Zeitschrift fur Geophysik*, v. 29.

- Hempton, M.R., 1987, Constraints on Arabian Plate motion and extensional history of the Red Sea: *Tectonics*, v. 6, p. 687-705.
- Henderson, R.G., and Zietz, I., 1949, The upward continuation of anomalies in total magnetic intensity fields: *Geophysics*, v. 14, p. 517-534.
- Hoffman, K.A., 1981, paleomagnetic excursions, aborted reversals and transitional fields: *Nature*, v. 294, p. 67-68.
- Holmes, A., 1931, Radioactivity and earth movements: *Geological Society of Glasgow Transactions*, v. 18, p. 559-606.
- Hsu, S.-K., 1996, High-resolution detection of geologic boundaries from potential-field anomalies: an enhanced analytic signal technique: *Geophysics*, v. 61, p. 373-386.
- Joffe, S., and Garfunkel, Z., 1987, Plate kinematics of the circum Red Sea- a re-evaluation: *Tectonophysics*, v. 141, p. 5-22.
- Kazmin, V.G., and Byakov, A.F., 2000, Magmatism and crustal accretion in continental rifts: *Journal of African Earth Sciences*, v. 30, p. 555-568.
- Keating, P., and Zerbo, L., 1996, An improved technique for reduction to the pole at low latitudes: *Geophysics*, v. 61, p. 131-137.
- Kebede, F., Kim, W.-Y., and Kulhanek, O., 1989, Dynamic source parameters for the March-May 1969 Serdo earthquake sequence in central Afar, Ethiopia, deduced from teleseismic body waves: *Journal of Geophysical Research*, v. 94, p. 5603-5614.
- Keebe, F., Kim, W.-Y., and Kulhanek, O., 1989, Dynamic source parameters of the March-May 1969 Serdo earthquake sequence in Central Afar, Ethiopia, deduced from teleseismic body waves: *Journal of Geophysical Research*, v. 94, p. 5603-5614.
- Keir, D., Hamling, I.J., Ayele, A., Calais, E., Ebinger, C., Wright, T.J., Jacques, E., Mohamed, K., Hammond, J.O.S., Belachew, M., Baker, E., Rowland, J.V., Lewi, E., and Bennati, L., 2009, evidence for focused magmatic accretion at segment centers from lateral dike injections captured beneath the red Sea rift in Afar: *Geology*, v. 37, p. 59-62.
- Kendall, J.-M., Stuart, G.W., Ebinger, C.J., Bastow, I.D., and Keir, D., 2005, magma-assisted rifting in Ethiopia: *Nature*, v. 433, p. 146-148.
- Kidane, T., Carlot, J., Courtillot, V., Gallet, Y., Quidelleur, X., Gillot, P.Y., and Haile, T., 1999, Paleomagnetic and geochronological identification of the Reunion subchron in Ethiopian Afar: *Journal of Geophysical Research*, v. 104, p. 10405-10419.

- Kidane, T., Courtillot, V., Manighetti, I., Audin, L., Lahitte, P., Quidelleur, X., Gillot, P.-Y., Gallet, Y., Carlut, J., and Haile, T., 2003, New paleomagnetic and geochronologic results from Ethiopian Afar: Block rotations linked to rift overlap and propagation and determination of a ~2 Ma reference pole for stable Africa: *Journal of Geophysical Research*, v. 108, p. 2102.
- Kidd, R.G.W., 1977, The nature and shape of the sources of marine magnetic anomalies: *Earth and Planetary Science Letters*, v. 33, p. 3310-320.
- Lahitte, P., Coulie, E., Mercier, N., Kidane, T., and Gillot, P.-Y., 2001, Chronologie K-Ar et TL du volcanisme aux extremites sud du propagateur mer Rouge wn Afar depuis 300 ka: *Earth and Planetary Science Letters*, v. 332, p. 13-20.
- Lahitte, P., Gillot, P.-Y., Kidane, T., Courtillot, V., and Bekele, A., 2003, New age constraints on the timing of volcanism in central Afar, in the presence of propagating rifts: *Journal of Geophysical Research*, v. 108, p. 2123.
- Larson, R.L., and Chase, C.G., 1972, Late Mesozoic evolution of the western Pacific Ocean: *Geological Society of America Bulletin*, v. 83, p. 3627-3644.
- Le Pichon, X., and Francheteau, J., 1978, A plate-tectonic analysis of the Red Sea-Gulf of Aden area: *Tectonophysics*, v. 46, p. 369-406.
- Lelievre, P.G., and Oldenburg, D.W., 2009, A 3D total magnetization inversion applicable when significant, complicated remanence is present: *Geophysics*, v. 74, p. L21-L30.
- Lemma, Y., Hailu, A., Desissa, M., and Kalberkamp, U., 2010, Intergrated geophysical surveys to characterize Tendaho Geothermal Field in north eastern Ethiopia, *Proceedings World Geothermal Congress: Bali, Indonesia*.
- Li, X., 2006, Understanding 3D analytic signal amplitude: *Geophysics*, v. 71, p. L13-L16.
—, 2008, Magnetic reduction-to-the-pole at low latitudes: observations and considerations: *The Leading Edge*, p. 990-1002.
- Li, Y., and Oldenburg, D.W., 1996, 3-D inversion of magnetic data: *Geophysics*, v. 61, p. 394-408.
- , 2001, Stable reduction to the pole at the magnetic equator: *Geophysics*, v. 66, p. 571-578.
- , 2003, Fast inversion of large-scale magnetic data using wavelet transforms and a logarithmic barrier method: *Geophysical Journal International*, v. 152, p. 251-265.

- Li, Y., Shearer, S.E., Haney, M.M., and Dannemiller, N., 2010, Comprehensive approaches the 3D inversion of magnetic data affected by remanent magnetization: *Geophysics*, v. 75, p. L1-L11.
- Lillie, R.J., 1991, *Whole Earth Geophysics: An Introductory Textbook for Geologists & Geophysicists*: Upper Saddle River, New Jersey, USA, Pearson Education, 361 p.
- Lourenco, J.S., and Morrison, H.F., 1973, Vector magnetic anomalies derived from the measurements of a single component of the field: *Geophysics*, v. 38, p. 359-368.
- Macleod, I.N., Jones, K., and Dai, T.F., 1993a, 3-D Analytic signal in the interpretation of total magnetic field data at low magnetic latitudes: *Exploration Geophysics*, v. 24, p. 679-687.
- Macleod, I.N., Viera, S., and Chaves, A.C., 1993b, Analytic signal and reduction-to-the-pole in the interpretation of total magnetic field data at low latitudes, *Proceedings of the third international congress of the Brazilian Society of Geophysicists*.
- Maguire, P.K.H., Keller, G.R., Klemperer, S., Mackenzie, G.D., Keranen, K., Harder, S., O'Reilly, B., Thybo, H., Asfaw, L.M., Khan, M.A., and Amha, M., 2006, Crustal structure of the northern Main Ethiopian Rift from the EAGLE controlled-source survey; a snapshot of incipient lithospheric break-up, *in* Yirgu, G., Ebinger, C.J., and Maguire, P.K.H., eds., *The Afar Volcanic Province within the East African Rift System, Volume 259: Special Publications*: London, Geological Society, p. 269-291.
- Makris, J., and Ginzburg, A., 1987, The Afar Depression: transition between continental rifting and sea-floor spreading: *Tectonophysics*, v. 141, p. 199-214.
- Makris, J., Menzel, H., Zimmerman, J., and Gouin, P., 1975, Gravity field and crustal structure of north Ethiopia, *in* Pilger, A., and Rosler, A., eds., *Afar Depresion of Ethiopia, Proceedings of an International Symposium on the Afar Region and Related Rift Problems, Bad Bergzabern, Germany, 1974, Volume 1*: Stuttgart, Germany, E. Schweizerbart'sche Verlagsbuchhandlung, p. 416.
- Manighetti, I., Tapponnier, P., Courtillot, V., Gallet, Y., Jacques, E., and Gillot, P.-Y., 2001, Strain transfer between disconnected, propogating rifts in Afar: *Journal of Geophysical Research*, v. 106, p. 13613-13665.
- Manighetti, I., Tapponnier, P., Gillot, P.-Y., Jacques, E., Courtillot, V., Armijo, R., Ruegg, J.-C., and King, G., 1998, Propagation of rifting along the Arabia-Somalia plate boundary: Into Afar: *Journal of Geophysical Research*, v. 103, p. 4947-4974.

- Marinelli, G., and Tazieff, H., 1975, Introduction to the Volume on the Afar, *in* Pilger, A., and Rosler, A., eds., Afar Depression of Ethiopia, Proceedings of an International Symposium on the Afar Region and Related Rift Problems held in Bad Bergzabern, Germany, Volume 1: Stuttgart, Germany, E. Schweizerbart'sche Verlagsbuchhandlung, p. xvi-xix.
- Maus, S., and Macmillan, S., 2005, 10th generation International Geomagnetic Reference Field: EOS Transactions of the American Geophysical Union, v. 86, p. 159.
- McKenzie, D., Davis, D., and Molnar, P., 1970, Plate tectonics of the Red Sea and east Africa: *Nature*, v. 226, p. 243-248.
- Menzies, M.A., Klemperer, S.L., Ebinger, C.J., and Baker, J., 2002, Characteristics of volcanic rifted margins, *in* Menzies, M.A., Klemperer, S.L., Ebinger, C.J., and Baker, J., eds., Volcanic Rifted Margins: Special Paper: Boulder, Colorado, Geological Society of America, p. 1-14.
- Mickus, K.L., Tadesse, K., Keller, G.R., and Oluma, B., 2007, Gravity analysis of the main Ethiopian rift: *Journal of African Earth Sciences*.
- Miller, H.G., and Singh, V., 1994, Potential field tilt-a new concept for the location of potential field sources: *Journal of Applied Geophysics*, v. 32, p. 213-217.
- Milsom, J., 2003, *Field Geophysics: West Sussex, England*, John Wiley & Sons Ltd.
- Mohr, P., 1983a, Perspectives on the Ethiopian volcanic province: *Bulletin of Volcanology*, v. 46, p. 23-43.
- , 1983b, The Morton-Black hypothesis for the thinning of continental crust-revisited in western Afar: *Tectonophysics*, v. 94, p. 509-528.
- , 1989, Nature of the crust under Afar: new igneous, not thinned continental: *Tectonophysics*, v. 167, p. 1-11.
- Mohr, P.A., 1972, Regional significance of volcanic geochemistry in the Afar Triple Junction, Ethiopia: *Geological Society of America Bulletin*, v. 83, p. 213-222.
- Morris, B., Pozza, M., Boyce, J., and Leblanc, G., 2001, Enhancement of magnetic data by logarithmic transformation: *The Leading Edge*, p. 882-885.
- Morris, B., Uglade, H., and Thomson, V., 2007, Magnetic remanence constraints on magnetic inversion models: *The Leading Edge*, p. 960-964.
- Nabighian, M.N., 1972, The analytic signal of two-dimensional magnetic bodies with polygonal cross-section: its properties and use for automated anomaly interpretation: *Geophysics*, v. 37, p. 507-517.

- , 1984, Towards a three-dimensional automatic interpretation of potential field data via generalized Hilbert transforms: Fundamental relations: *Geophysics*, v. 49, p. 780-786.
- Nabighian, M.N., Grauch, V.J.S., Hansen, R.O., LaFehr, T.R., Li, Y., Peirce, J.W., Phillips, J.D., and Ruder, M.E., 2005, 75th Anniversary: The historical development of the magnetic method in exploration: *Geophysics*, v. 70, p. 33ND-61ND.
- Paine, J., Haederle, M., and Flis, M., 2001, Using transformed TMI data to invert for remanently magnetised bodies: *Exploration Geophysics*, v. 32, p. 238-242.
- Phillips, J.D., 1997, Potential-Field Geophysical Software for the PC, version 2.2, Open-File Report, U.S. Geological Survey, p. 30.
- , 2005, Can we estimate total magnetization directions from aeromagnetic data using Helbig's formulas: *Earth, Planets, and Space*, v. 57.
- Pik, R., Deniel, C., Coulon, C., Yirgu, G., Hofmann, C., and Ayalew, D., 1998, The northwestern Ethiopian Plateau flood basalts: Classification and spatial distribution of magma types: *Journal of Volcanology and Geothermal Research*, v. 81, p. 91-111.
- Pik, R., Deniel, C., Coulon, C., Yirgu, G., and Marty, B., 1999, Isotopic and trace element signatures of Ethiopian flood basalts: Evidence for plume-lithosphere interactions: *Geochimica et Cosmochimica Acta*, v. 63, p. 2263-2279.
- Pik, R., Marty, B., and Hilton, D.R., 2006, How many mantle plumes in Africa? The geochemical point of view: *Chemical Geology*, v. 226, p. 100-114.
- Qin, R., and Buck, W.R., 2008, Why meter-wide dikes at oceanic spreading centers?: *Earth and Planetary Science Letters*, v. 265, p. 466-474.
- Reynolds, J.M., 1987, *An Introduction to Applied and Environmental Geophysics*: West Sussex, England, John Wiley & Sons, 796 p.
- Reynolds, R.L., Rosenbaum, J.G., Hudson, M.H., and Fishman, N.S., 1990, Rock magnetism, the distribution of magnetic minerals in the Earth's crust, and aeromagnetic anomalies, *in* Hanna, W.F., ed., *Geologic Applications of Modern Aeromagnetic Surveys*: U.S. Geological Survey Bulletin, p. 24-45.
- Robinson, E.S., and Coruh, C., 1988, *Basic Exploration Geophysics*: New York, USA, John Wiley & Sons, 562 p.

- Roest, W.R., and Pilkington, M., 1993, Identifying remanent magnetization effects in magnetic data: *Geophysics*, v. 58, p. 653-659.
- Roest, W.R., Verhoef, J., and Pilkington, M., 1992, Magnetic interpretation using the 3-D analytic signal: *Geophysics*, v. 57, p. 116-125.
- Rowland, J.V., baker, E., Ebinger, C.J., Keir, D., Kidane, T., Biggs, J., Hayward, N., and Wright, T.J., 2007, Fault growth at a nascent slow-spreading ridge: 2005 Dabbahu rifting episode, Afar: *Geophysical Journal International*, v. 171, p. 1226-1246.
- Salem, A., Ravat, D., Gamey, T.J., and Ushijima, K., 2002, Analytic signal approach and its applicability in environmental magnetic investigations: *Journal of Applied Geophysics*, v. 49, p. 231-244.
- Salem, A., Williams, S., Fairhead, J.D., Ravat, D., and Smith, R., 2007, Tilt-depth method: a simple depth estimation method using first-order magnetic derivatives: *The Leading Edge*, p. 1502-1505.
- Salem, A., Williams, S., Fairhead, J.D., Smith, R., and Ravat, D., 2008, Interpretation of magnetic data using tilt-angle derivatives: *Geophysics*, v. 73, p. L1-L10.
- Schaefer, H.-U., 1975, Investigations on crustal spreading in southern and central Afar (Ethiopia), *in* Pilger, A., and Rosler, A., eds., *Afar Depression of Ethiopia, Proceedings of an International Symposium on the Afar Region and Related Rift Problems*, Bad Bergzabern, Germany, 1974, Volume 1: Stuttgart, Germany, E. Schweizerbart'sche Verlagbuchhandlung, p. 289-296.
- Sharma, P.V., 1966, Rapid computation of magnetic anomalies and demagnetization effects caused by bodies of arbitrary shape: *Pure and Applied Geophysics*, v. 64, p. 89-109.
- Shearer, S.E., 2005, Three-dimensional inversion of magnetic data in the presence of remanent magnetization: Golden, CO, USA, Colorado School of Mines.
- Shearer, S.E., and Li, Y., 2004, 3D inversion of magnetic total gradient data in the presence of remanent magnetization, 74th Annual Meeting, SEG, Technical Program Expanded Abstracts, Volume 23, SEG, p. 774-777.
- Sigmundsson, F., 1992, Tectonic implications of the 1989 Afar earthquake sequence.: *Geophysical Research Letters*, v. 19, p. 877-880.
- Simkin, T., and Siebert, L., 1994, *Volcanoes of the World*: Tucson, AZ, USA, Geoscience Press, 349 p.
- Singh, B., and Guptasarma, D., 2001, New method for the fast computation of gravity and magnetic anomalies from arbitrary polyhedra: *Geophysics*, v. 66, p. 521-52.

- Smith, G.M., and Banerjee, S.K., 1986, The magnetic structure of the upper kilometer of the Marine crust: *Journal of Geophysical Research*, v. 91, p. 10337-10354.
- Souriot, T., and Brun, J.P., 1992, Faulting and block rotation in the Afar triangle, East Africa; the Danakil "crank-arm" model: *Geology*, v. 20, p. 911-914.
- Stavrev, P., and Gerovska, D., 2000, Magnetic field transforms with low sensitivity to the direction of source magnetization and high centrality: *Geophysical Prospecting*, v. 48, p. 317-340.
- Symons, D.T., A, Stupavsky, M., and Gravenor, C.P., 1980, Remanence resetting by shock-induced thixotropy in the Seminary Till, Scarborough, Ontario, Canada: *Geological Society of America Bulletin*, v. 91, p. 593-598.
- Talwani, M., and Heirtzler, J.R., 1964, Computation of magnetic anomalies caused by two dimensional structures of arbitrary shape, *in* Parks, G.A., ed., *Computers in the Mineral Industries*, School of Earth Sciences, Stanford University, p. 464-480.
- Tapponnier, P., Armijo, R., Manighetti, I., and Courtillot, V., 1990, Bookshelf faulting and horizontal block rotations between overlapping rifts in Southern Afar: *Geophysical Research Letters*, v. 17, p. 1-4.
- Tazieff, H., Varet, J., Barberi, F., and Giglia, G., 1972, Tectonic significance of the Afar (or Danakil) depression: *Nature*, v. 235, p. 144-147.
- Tivey, M., Rona, P., and Schhouten, H., 1993, Reduced crustal magnetization beneath the active sulfide mound, TAG hydrothermal field, Mid-Atlantic Ridge at 26°N: *Earth and Planetary Science Letters*, v. 115, p. 101-115.
- Tefera, M., Chernet, T., and Haro, W., 1996, Explanation of the geological map of Ethiopia, Volume 3: Addis Ababa, Ethiopia, Ethiopian Institute of Geological Surveys, p. 79.
- Telford, W.M., Geldart, L.P., and Sheriff, R.E., 1990, *Applied Geophysics*: Cambridge, UK, Cambridge University Press, 770 p.
- Thurmond, A.K., Abdelsalam, M.G., and Thurmond, J.B., 2006, Optical-radar-DEM remote sensing data integration for geological mapping in the Afar Depression, Ethiopia: *Journal of African Earth Sciences*, v. 44, p. 119-134.
- Varet, J., 1978, *Geology of central and southern Afar (Ethiopia and Djibouti Republic)*: Paris, France, CNRS, 124 p.
- Vellutini, P.J., 1990, The Manda-Inakir Rift, Republic of Djibouti: a comparison with the Asal Rift and its geodynamic interpretation: *Tectonophysics*, v. 172, p. 141-153.

- Verduzco, B., Fairhead, J.D., Green, C.M., and Mackenzie, C., 2004, New insights into magnetic derivatives for structural mapping: *The Leading Edge*, p. 116-119.
- Verosub, K., 1999, Paleomagnetic dating, *in* Noller, J.S., Sowers, J.M., and Lettis, W.R., eds., *Quaternary Geochronology. Methods and Applications*: Washington, D.C., American Geophysical Union, p. 339-356.
- Vidal, P., Deniel, C., Vellutini, P.J., Piguet, P., Coulon, C., Vincent, J., and Audin, J., 1991, Changes of mantle sources in the course of a rift evolution: The Afar case: *Journal of Geophysical Research*, v. 18, p. 1913-1916.
- Vine, F.J., 1963, Spreading of the ocean floor: new evidence: *Science*, v. 154, p. 1405-1415.
- , 1966, Spreading of the ocean floor: new evidence: *Science*, v. 154, p. 1405-1415.
- Vine, F.J., and Matthews, D.H., 1963, Magnetic anomalies over oceanic ridges: *Nature*, v. 199, p. 947-949.
- Webring, M., 1985, SAKI: Fortran program for the generalized linear inversion of gravity and magnetic profiles, Open-File Report, U.S. Geological Survey, p. 29.
- Wessel, P., and Smith, W.H., F., 1991, Free software helps map and display data, Volume 72: *EOS Transactions of the American Geophysical Union, AGU*, p. 441.
- Wright, T.J., Ebinger, C., Biggs, J., Ayele, A., Yirgu, G., Keir, D., and Stork, A., 2006, Magma-maintained rift segmentation at continental rupture in the 2005 Afar dyking episode: *Nature*, v. 442, p. 291-294.

VITA

David Lee Bridges was born in Meridian, Mississippi on June 28, 1975, the son of Ronnie Lee Bridges and Lette Huelskamp. He completed high school at Poplar Bluff Senior High in 1993 and continued his studies at Three Rivers Community College, graduating in 1998 with an A.A. degree. In 1999, he transferred to Southeast Missouri State University and completed his BS Geosciences and BGS General Studies degrees in 2002. He married Mirasol Layug Garcia in 2001 and has two children, Carl Justine Garcia (born 1996) and David Lee Bridges (born 2001). In 2004, he enrolled as a M.Sc. Student at Kansas State University in the department of Geology and Geophysics and studied under Dr. Stephan S. Gao. After graduating with his M.Sc. in 2006, he started his Ph.D. work at Missouri University of Science & Technology at Rolla, Missouri and studied under the supervision of Dr. Mohamed G. Abdelsalam. He earned his Ph.D. in 2011 and currently conducting research at Missouri S&T as a post-doctoral researcher.